QCD

Jan M. Pawlowski[1] and Tilman Plehn[1]

[1] *Institut für Theoretische Physik, Universität Heidelberg*

These lecture notes are the ambitious attempt to combine the two QCDs of the two lecturers into one coherent document. It includes many aspects of perturbative and non-perturbative QCD, including the basic theoretical concepts we need to compute observables at hadron colliders.

CONTENTS

I. BASICS

The theory of strong interactions, quantum chromodynamics (QCD), has been developed on the basis of scattering experiments that showed an internal $SU(3)$-symmetry and related charges much the same way quantum-electrodynamics (QED) shows the $U(1)$-symmetry related to the electric charge. The corresponding gauge theory, $SU(3)$ Yang-Mills theory, is non-Abelian and hence self-interacting, i.e. the (quantized) pure gauge theory is already non-trivial, in contrast to the $U(1)$-based QED.

A. Yang-Mills theory

We start by constructing the pure gauge part or Yang-Mills part of QCD as an $SU(3)$ gauge theory, fixing our conventions and repeating the main features known from the QFT II lecture. The weak $SU(2)$-theory turns out to have the same qualitative features as QCD (asymptotic freedom and confinement), but is technically simpler. On the other hand, the $SU(2)$ gauge bosons in the Standard Model are massive, leading to a major modification of this theory. Instead, we will assume massless gauge bosons throughout this lecture. As for QED, the classical action of QCD can be derived from the gauge-invariant (minimal) extension of the action of a free spin-one particle. The requirement of invariance of physics under local $SU(N_c)$ or color rotations with $\mathcal{U} \in SU(N_c)$, combined with a minimal coupling, leads us from partial to covariant derivatives,

$$\partial_\mu \to D_\mu(A) = \partial_\mu - i\, g\, A_\mu \,. \tag{I.1}$$

The gauge field A_μ in the adjoint representation is Lie-algebra–valued,

$$A_\mu = A_\mu^a\, t^a \,, \qquad \text{with} \qquad a = 1, ..., N_c^2 - 1 \,. \tag{I.2}$$

The matrices t^a are the generators of $SU(N_c)$. In physical QCD the gauge group has eight generators, $a = 1, ..., 8$, the Gell-Mann matrices. They are defined through

$$[t^a, t^b] = i\, f^{abc} t^c \,, \qquad\qquad \mathrm{tr_f}(t^a t^b) = \frac{1}{2}\delta^{ab} \,, \tag{I.3}$$

where the coefficients f^{abc} are the structure constants of the Lie algebra. and $\mathrm{tr_f}$ is the trace in the fundamental representation. The covariant derivative (I.1) does not carry any indices. In the adjoint representation it links to $SU(N_c)$ indices and reads

$$D_\mu^{ab}(A) = \partial_\mu \delta^{ab} - g\, f^{abc} A_\mu^c \,. \qquad \text{with} \qquad (t_{\rm ad}^c)^{ab} = -i\, f^{abc}. \tag{I.4}$$

The covariant derivative D_μ with its two color indices then has to transform as a tensor under gauge transformations,

$$D_\mu(A) \to D_\mu(A^{\mathcal{U}}) = \mathcal{U}\, D_\mu\, \mathcal{U}^\dagger \,, \qquad \text{with} \qquad \mathcal{U} = e^{i\omega} \in SU(N_c) \,, \tag{I.5}$$

where $\omega \in su(N_c)$ is the corresponding Lie algebra element. The covariance of D under gauge transformations in (I.5) implies

$$A_\mu \to A_\mu^{\mathcal{U}} = \frac{i}{g} U\, (D_\mu U^\dagger) = \mathcal{U}\, A_\mu\, \mathcal{U}^\dagger + \frac{i}{g} \mathcal{U}\, (\partial_\mu \mathcal{U}^\dagger) \,. \tag{I.6}$$

From the first term we confirm that in a non-Abelian gauge theory the gauge boson A_μ carries the corresponding color charge. There are various notations on the market leading to factors i and $-$ in the Lie algebra relations above. In the present lecture notes we have chosen hermitian generators which leads to the factor $+1/2$ for the trace in (I.3). It also entails real structure constants f^{abc} in the Lie-algebra in (I.3).

In analogy to QED the field strength tensor is defined through the commutator of covariant derivatives, it is the curvature tensor of the gauge theory. Based on the definitions in (I.1) and (I.3) we find

$$F_{\mu\nu} = \frac{i}{g}[D_\mu \,,\, D_\nu] = F_{\mu\nu}^a t^a \qquad \text{with} \qquad F_{\mu\nu}^a = \partial_\mu A_\nu^a - \partial_\nu A_\mu^a + g\, f^{abc} A_\mu^b\, A_\nu^c. \tag{I.7}$$

Defined as in (I.7) the field strength $F_{\mu\nu}$ also transforms covariantly (as a tensor) under gauge transformations,

$$\begin{aligned} F_{\mu\nu}(A^{\mathcal{U}}) &= \frac{i}{g}\,[D_\mu(A^{\mathcal{U}}), D_\nu(A^{\mathcal{U}})] \\ &= \frac{i}{g}\,\mathcal{U}\,[D_\mu(A_\mu), D_\nu(A_\nu)]\,\mathcal{U}^\dagger = \mathcal{U}\,F_{\mu\nu}(A)\,\mathcal{U}^\dagger\,. \end{aligned} \tag{I.8}$$

This allows us to define a gauge-invariant Yang-Mills (YM) action,

$$S_{\rm YM}[A] = \frac{1}{2}\int_x \mathrm{tr_f}\;(F_{\mu\nu}\,F_{\mu\nu}) = \frac{1}{4}\int_x F^a_{\mu\nu}\,F^a_{\mu\nu}\,, \tag{I.9}$$

with $\int_x = \int d^dx$. Its gauge invariance follows from (I.8),

$$S_{\rm YM}[A^{\mathcal{U}}] = \frac{1}{2}\int_x \mathrm{tr_f}\;\left(\mathcal{U}\,F_{\mu\nu}(A)F_{\mu\nu}(A)\,\mathcal{U}^\dagger\right) = S_{\rm YM}[A]\,, \tag{I.10}$$

where the last equality holds due to cyclicity of the trace in color space. Clearly, the action (I.9) with the field strength (I.7) is a self-interacting theory with coupling constant g. It has a quadratic kinetic term and three-gluon and four-gluon vertices. This is illustrated diagrammatically as

$S_{\rm YM}[A] \propto$ 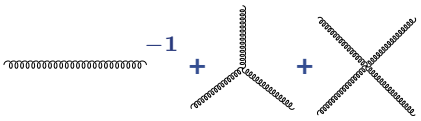

This allows us to read off the Feynman rules for the purely gluonic vertices. The full Feynman rules of QCD in the general covariant gauge are summarized in Fig. 25 in Appendix A. As in QED we can identify color-electric and color-magnetic fields as the components in the field strength tensor,

$$\begin{aligned} E^a_i &= F^a_{0i} \\ B^a_i &= \frac{1}{2}\epsilon_{ijk}F^a_{jk}. \end{aligned} \tag{I.11}$$

In contrast to QED these color-electric and magnetic fields are no observables, they change under gauge transformations. Only $\mathrm{tr}\,\vec{E}^2, \mathrm{tr}\,\vec{B}^2$ are observables.

A Yang-Mills theory can most easily be quantized through the path integral. Naively, the generating functional of pure YM-theory would read

$$Z[J] = \int dA\;\exp\left(-S_{\rm YM}[A] + \int_x J^a_\mu\,A^a_\mu\right). \tag{I.12}$$

The fundamental problem is that it contains redundant integrations due to gauge invariance of the action, see (I.10). These redundant integrations are usually removed by introducing a gauge fixing condition

$$\mathcal{F}[A_{\rm gf}] = 0 \tag{I.13}$$

Commonly used gauge fixings are

$$\begin{aligned} \partial_\mu A_\mu &= 0\,, \qquad \text{covariant or Lorenz gauge}\,, \\ \partial_i A_i &= 0\,, \qquad \text{Coulomb gauge}\,, \\ n_\mu A_\mu &= 0\,, \qquad \text{axial gauge}\,. \end{aligned} \tag{I.14}$$

The general covariant gauge has the technical advantage that it does not single out a space-time direction. This property reduces the possible tensor structure of correlation functions and hence simplifies computations. The Coulomb gauge and the axial gauge single out specific frames. At finite temperature (and density) this might be useful as the temperature singles out the thermal rest frame. In that case the Coulomb gauge and the temporal or Weyl gauge

($n_\mu = \delta_{\mu 0}$) are used often.

Gauge fields that are connected by gauge transformations are physically equivalent, i.e. their actions agree. They lie in so-called gauge orbits, $\{A^{\mathcal{U}}, \mathcal{U} \in SU(N)\}$, and fixing a gauge is equivalent to choosing a representative of such an orbit $A \to A_{\rm gf}$, up to potential (Gribov) copies. The occurrence of Gribov copies and how to handle them is discussed in Appendix B. To keep things simple we ignore them for the time being and continue with the construction of the QCD Lagrangian.

The path integral measure $\mathrm{d}A$ introduced in (I.12) can be split into an integration over physically inequivalent configurations $A_{\rm gf}$ and the gauge transformations $\mathcal{U}$,

$$\mathrm{d}A = J\,\mathrm{d}A_{\rm gf}\,\mathrm{d}\mathcal{U} \tag{I.15}$$

In (I.15) J denotes the Jacobian of the transformation $A \to (A_{\rm gf}, \mathcal{U})$, and we include $\mathrm{d}\mathcal{U}$ as the Haar measure of the gauge group, see e.g. [1]. The coordinate transformation (I.15) and the computation of the Jacobian J are done using the Faddeev-Popov quantization, [2]. To separate the integral (I.12) into the two parts shown in (I.15) we insert a very convoluted unity into the path integral,

$$1 = \int \mathrm{d}\mathcal{U}\,\delta\left[\mathcal{F}[A^{\mathcal{U}}]\right]\,\Delta_{\mathcal{F}}[A] = \Delta_{\mathcal{F}}[A]\int \mathrm{d}\mathcal{U}\,\delta\left[\mathcal{F}[A^{\mathcal{U}}]\right] \quad \Leftrightarrow \quad \Delta_{\mathcal{F}}[A] = \left(\int \mathrm{d}\mathcal{U}\,\delta\left[\mathcal{F}[A^{\mathcal{U}}]\right]\right)^{-1}, \tag{I.16}$$

where $\Delta_{\mathcal{F}}[A]$ is gauge-invariant due to the property $\mathrm{d}(\mathcal{U}\mathcal{V}) = \mathrm{d}\mathcal{U}$ of the Haar measure. For the path integral this gives us

$$\int \mathrm{d}A\; e^{-S_{\rm YM}[A]} = \int \mathrm{d}A\;\mathrm{d}\mathcal{U}\,\delta\left[\mathcal{F}[A^{\mathcal{U}}]\right]\,\Delta_{\mathcal{F}}[A]\; e^{-S_{\rm YM}[A]}\,. \tag{I.17}$$

Let us now consider a general observable $\mathcal{O}$, like *e.g.* $\mathrm{tr}F^2(x)\,\mathrm{tr}F^2(0)$. Observables are necessarily gauge invariant and local. The expectation value of $\mathcal{O}$ is defined as

$$\langle\mathcal{O}\rangle = \frac{\int \mathrm{d}A\,\mathcal{O}[A]\,e^{-S_{\rm YM}[A]}}{\int \mathrm{d}A\; e^{-S_{\rm YM}[A]}} = \frac{\int \mathrm{d}A\,\mathrm{d}\mathcal{U}\,\delta\left[\mathcal{F}[A^{\mathcal{U}}]\right]\,\Delta_{\mathcal{F}}[A]\,\mathcal{O}[A]\,e^{-S_{\rm YM}[A]}}{\int \mathrm{d}A\,\mathrm{d}\mathcal{U}\,\delta\left[\mathcal{F}[A^{\mathcal{U}}]\right]\,\Delta_{\mathcal{F}}[A]\,e^{-S_{\rm YM}[A]}}\,, \tag{I.18}$$

where we have simply inserted (I.16) into the path integral. In (I.18) all terms are gauge invariant except for the δ-function. Hence we can absorb the $\mathcal{U}$-dependence via $A \to A^{\mathcal{U}^\dagger}$. Then the (infinite) integral over the Haar measure decouples in numerator and denominator, and we arrive at

$$\langle\mathcal{O}\rangle = \frac{\int \mathrm{d}A\,\delta\left[\mathcal{F}[A]\right]\,\Delta_{\mathcal{F}}[A]\,\mathcal{O}[A]\,e^{-S_{\rm YM}[A_{\rm gf}]}}{\int \mathrm{d}A\,\delta\left[\mathcal{F}[A]\right]\,\Delta_{\mathcal{F}}[A]\,e^{-S_{\rm YM}[A_{\rm gf}]}}\,.$$

To compute the Jacobian $\Delta_{\mathcal{F}}[A]$ we apply a coordinate transformation to the δ-distribution

$$\delta[\mathcal{F}[A^{\mathcal{U}}]] = \frac{\delta[\omega-\omega_1]}{|\det\frac{\delta\mathcal{F}}{\delta\omega}|} \equiv \frac{\delta[\omega-\omega_1]}{|\det\mathcal{M}_{\mathcal{F}}[A]|} \quad \text{with} \quad \mathcal{U} = e^{i\omega}\,, \tag{I.19}$$

combined with a gauge fixing condition in the form (I.13)

$$\mathcal{F}[A_{\rm gf} = A^{\mathcal{U}(\omega_1)}] = 0\,. \tag{I.20}$$

Using the definition (I.16) this leads to

$$\Delta_{\mathcal{F}}[A] = |\det\mathcal{M}_{\mathcal{F}}[A_{\rm gf}]| \qquad \text{with} \qquad \mathcal{M}_{\mathcal{F}}[A] = \left.\frac{\delta\mathcal{F}}{\delta\omega}\right|_{\omega=0}[A]\,. \tag{I.21}$$

Here $A_{\rm gf}$ is the solution with the minimal distance to $A=0$. The inverse Jacobian $\det\mathcal{M}_{\mathcal{F}}$ of the ansatz (I.15) is called the Faddeev-Popov determinant. For its computation we consider an infinitesimal gauge transformation $\mathcal{U} = 1 + i\,g\,\omega$ where we have rescaled the transformation with the strong coupling g for convenience. Such a rescaling gives global factors of powers of $1/g$ that drop out in normalized expectation values. Then, the infinitesimal variation of the

covariant gauge $\partial_\mu A_\mu = 0$ follows as

$$\mathcal{F}[A^{\mathcal{U}}] = \partial_\mu A^{\mathcal{U}}_\mu = \partial_\mu A_\mu - \partial_\mu D_\mu \omega + O(\omega^2) \stackrel{!}{=} 0\,. \tag{I.22}$$

This gives us the Faddeev-Popov matrix

$$\mathcal{M}_{\mathcal{F}}[A] = -\frac{\delta \partial_\mu D_\mu \omega}{\delta \omega} = -\partial_\mu D_\mu \, \frac{\delta \omega}{\delta \omega} = -\partial_\mu D_\mu \mathbb{1}. \tag{I.23}$$

We assume that $-\partial^\mu D_\mu$ is a positive definite operator and we arrive at

$$\Delta_{\mathcal{F}}[A] = \det \mathcal{M}[A] = \det\left(-\partial_\mu D_\mu\right)\,. \tag{I.24}$$

A useful observation is that determinants can be represented by a Gaussian integral. In regular space such a Gaussian integral reads

$$\int_x e^{-\frac{1}{2}x^T M x} = \frac{(2\pi)^n}{\sqrt{\det M}}\,. \tag{I.25}$$

We want to use this relation to replace the Faddeev-Popov determinant (I.24) in the Lagrangian. It turns out that the usual form does not give a useful action or Lagrangian. However, we can instead use two anti-commuting Grassmann fields C and switch the sign in the exponent to

$$\det \mathcal{M}_{\mathcal{F}}[A] = \int \mathrm{d}c\,\mathrm{d}\bar{c}\, \exp\left\{\int d^dx\, d^dy\, \bar{c}^a(x) \mathcal{M}^{ab}_{\mathcal{F}}(x,y) c^b(y)\right\}\,. \tag{I.26}$$

Finally we slightly modify the gauge by introducing a Gaußian average over the gauges

$$\delta[\mathcal{F}[A^{\mathcal{U}}]] \to \int \mathrm{d}\mathcal{C}\, \delta[\mathcal{F}[A^{\mathcal{U}} - \mathcal{C}]] \exp\left\{-\frac{1}{2\xi}\int_x \mathcal{C}^a \mathcal{C}^a\right\}\,. \tag{I.27}$$

In summary, and restricting ourselves to the covariant gauge we then arrive at the generating functional for our Yang-Mills theory

$$Z[J_A, J_c, \bar{J}_c] = \int \mathrm{d}A\,\mathrm{d}c\,\mathrm{d}\bar{c}\, e^{-S_A[A,c,\bar{c}] + \int_x \left(J_A\cdot A + \bar{J}_c \cdot c - \bar{c}\cdot J_c\right)}\,. \tag{I.28}$$

The action including a general gauge fixing term and the Faddeev-Popov ghosts c^a is

$$S_A[A,c,\bar{c}] = \frac{1}{4}\int_x F^a_{\mu\nu} F^a_{\mu\nu} + \frac{1}{2\xi}\int_x \left(\partial_\mu A^a_\mu\right)^2 + \int_x \bar{c}^a \partial_\mu D^{ab}_\mu c^b\,, \tag{I.29}$$

where $\int_x = \int d^dx$ and the Landau gauge is achieved for $\xi = 0$. Note that the ghost action implies a negative dispersion for the ghost, related to the determinant of the positive operator $\mathcal{M}_{\mathcal{F}} = -\partial_\mu D_\mu$. However, this is a matter of convention, we might as well use a positive dispersion, the minus sign drops out for all correlation functions which do not involve ghosts, and only those are related to scattering amplitudes. The source term with all indices reads

$$\int_x \left(J_A \cdot A + \bar{J}_c \cdot c - \bar{c}\cdot J_c\right) \equiv \int_x \left(J^a_{A,\mu} A^a_\mu + \bar{J}^a_c c^a - \bar{c}^a J^a_c\right)\,. \tag{I.30}$$

The Feynman rules derived from (I.29) are summarized in Appendix A.

B. QCD

After briefly sketching the gauge part of QCD we now add fermionic matter fields. As before we start with the classical action, now given by the Dirac action of a quark doublet,

$$S_{\mathrm{Dirac}}[\psi, \bar{\psi}, A] = i\int_x \bar{\psi}\ \left(\not{D} + m_\psi + \mu\gamma_0\right)\ \psi\,, \tag{I.31}$$

where the Dirac matrices are defined through

$$\{\gamma_\mu\,,\,\gamma_\nu\} = 2\,\delta_{\mu\nu} \tag{I.32}$$

In (I.31), the fermions carry a Dirac index defining the 4-component spinor, gauge group indices in the fundamental representation of $SU(3)$, as well flavor indices. The latter we will ignore as long as we only talk about QCD and neglect the doublet nature of the matter fields in the Standard Model. The Dirac operator $\not{D}$ is diagonal in the flavor space as is the chemical potential term. The mass term depends on the current quark masses related to spontaneous symmetry breaking of the Higgs sector of the Standard Model. The up and down current quark masses are of the order $2-5$ MeV whereas the current quark mass of the strange quark is of the order 10^2 MeV. The other quark masses are of order $1-200$ GeV. In low energy QCD this has to be compared with the scale of strong chiral symmetry breaking $\Delta m \approx 300$ MeV. This mass scales are summarized in Table I.

Generation	first	second	third	Charge
Mass [MeV]	1.5-4	1150-1350	170×10^3	
Quark	u	c	t	$\frac{2}{3}$
Quark	d	s	b	$-\frac{1}{3}$
Mass [MeV]	4-8	80-130	$(4.1\text{-}4.4)\times10^3$	

TABLE I: Quark masses and charges. The scale of strong chiral symmetry breaking is $\Delta m \approx 300$ MeV as is $\Lambda_{\rm QCD}$. This entails that only $2+1$ flavours have to be considered for most applications to the phase diagram of QCD.

Evidently, for most applications of the QCD phase diagram we only have to consider the three lightest quark flavors, that is up, down and strange quark, to be dynamical. The current quark masses of up and down quarks are two order of magnitude smaller than all QCD infrared scales related to $\Lambda_{\rm QCD}$. Hence, the up and down quarks can be considered to be massless. This leads to the important observation that the physical masses of neutrons and protons — and hence the masses of the world around us — comes about from strong chiral symmetry breaking and has nothing to do with the Higgs sector.

In turn, the mass of the strange quark is of the order of $\Lambda_{\rm QCD}$ and has to be considered heavy for application in low energy QCD. The three heavier flavors, charm, bottom and top, are essentially static they do not contribute to the QCD dynamics relevant for its phase structure even though in particular the c-quark properties and bound states are much influenced by the infrared dynamics of QCD. In summary we will consider the $N_f = 2$ and $N_f = 2+1$ flavor cases for the phase structure of QCD, while for LHC physics all flavors are relevant.

Again in analogy to the Yang-Mills action we describe the quantized theory using its generating functional. The full generating functional of QCD is the straightforward extension of the Yang-Mills version in (I.28). The quark fields are Grassmann fields because of their fermionic nature and we are led to the generating functional

$$Z[J] = \int \mathrm{d}\Phi\, e^{-S_{\rm QCD}[\Phi]+\int_x\, J\cdot\phi}\,, \tag{I.33}$$

As a notation we have introduced super-fields and super-currents

$$\begin{aligned} \Phi &= (A, c, \bar c, \psi, \bar\psi) & J &= (J_A, J_c, \bar J_c, J_\psi, \bar J_\psi) \\ \mathrm{d}\Phi &= \int \mathrm{d}A\,\mathrm{d}c\,\mathrm{d}\bar c\,\mathrm{d}\psi\,\mathrm{d}\bar\psi & J\cdot\Phi &= J_A\cdot A + \bar J_c\cdot c - \bar c\cdot J_c + \bar J_\psi\cdot\psi - \bar\psi\cdot J_\psi\,. \end{aligned} \tag{I.34}$$

The gauge-fixed action $S_{\rm QCD}$ in (I.33) in the Landau gauge is given by

$$S_{\rm QCD}[\Phi] = \frac{1}{4}\int_x F^a_{\mu\nu}F^a_{\mu\nu} + \frac{1}{2\xi}\int_x \left(\partial_\mu A^a_\mu\right)^2 + \int_x \bar c^a \partial_\mu D^{ab}_\mu c^b + i\int_x \bar\psi\left(\not{D} + m_\psi + \mu\gamma_0\right)\psi\,. \tag{I.35}$$

The action in (I.35) is illustrated diagrammatically as
For physical observables the gauge dependence entering through the last two graphs in the first line, the ghost terms, is cancelled by the hidden gauge fixing dependence of the inverse gluon propagator. The Feynman rules are summarized in Appendix A.

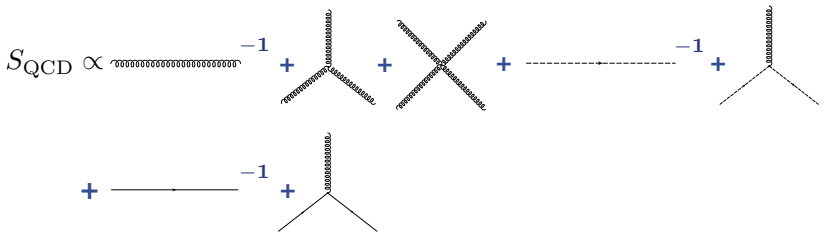

FIG. 1: Diagrammatical form of the QCD action.

II. PHYSICS OF DIVERGENCES

Now that we know the quantized action of QCD we can compute all kinds of processes to leading order in the strong couplings and beyond. From general field theory we know that when we are interested for example in cross section prediction with higher precision we need to compute further terms in its perturbative series in α_s. This computation will lead to ultraviolet divergences which can be absorbed into counter terms for any parameter in the Lagrangian. The crucial feature is that for a renormalizable theory like our Standard Model the number of counter terms is finite, which means once we know all parameters including their counter terms our theory becomes predictive.

We will see that in QCD processes we also encounter another kind of divergences. They arise from the infrared momentum regime. To understand their effects in LHC physics it is instructive to see what happens to the much better understood ultraviolet divergences. First, we will review how such ultraviolet divergences arise and how they are removed. Next, we will remind ourselves how running parameters appear in this procedure, *i.e.* how scale dependence is linked to the appearance of divergences. Finally, we need to interpret the use of running parameters physically and see that in perturbation theory they resum classes of logarithms to all orders in perturbation theory. For the infrared divergences we will follow exactly the same steps and develop some crucial features of hadron collider physics.

A. Ultraviolet divergences

Renormalization as the proper treatment of ultraviolet divergences is one of the most important things to understand about field theories; you can find more detailed discussions in any book on advanced field theory. The particular aspect of renormalization which will guide us through this section is the appearance of the renormalization scale.

In perturbation theory, scales automatically arise from the regularization of infrared or ultraviolet divergences. We can see this by writing down a simple scalar loop integral, with to two virtual scalar propagators with masses $m_{1,2}$ and an external momentum p flowing through a diagram

$$B(p^2; m_1, m_2) \equiv \int \frac{d^4q}{16\pi^2} \, \frac{1}{q^2 - m_1^2} \frac{1}{(q+p)^2 - m_2^2} \, . \tag{II.1}$$

Such two-point functions appear for example in the gluon self energy with virtual gluons, with massless ghost scalars, with a Dirac trace in the numerator for quarks, and with massive scalars for supersymmetric scalar quarks. In those cases the two masses are identical $m_1 = m_2$. The integration measure $1/(16\pi^2)$ is dictated by the Feynman rule for the integration over loop momenta. Counting powers of q in Eq.(II.1) we see that the integrand is not suppressed by powers of $1/q$ in the ultraviolet, so it is logarithmically divergent and we have to regularize it. Regularizing means expressing the divergence in a well–defined manner or scheme, allowing us to get rid of it by renormalization.

One regularization scheme is to introduce a cutoff into the momentum integral Λ, for example through the so-called Pauli—Villars regularization. Because the ultraviolet behavior of the integrand or integral cannot depend on any parameter living at a small energy scales, the parameterization of the ultraviolet divergence in Eq.(II.1) cannot involve the mass m or the external momentum p^2. The scalar two-point function has mass dimension zero, so its divergence has to be proportional to $\log(\Lambda/\mu_R)$ with a dimensionless prefactor and some scale μ_R^2 which is an artifact of the regularization of such a Feynman diagram.

A more elegant regularization scheme is dimensional regularization. It is designed not to break gauge invariance and naively seems to not introduce a mass scale μ_R. When we shift the momentum integration from 4 to $4 - 2\epsilon$ dimensions and use analytic continuation in the number of space–time dimensions to renormalize the theory, a

renormalization scale μ_R nevertheless appears once we ensure the two-point function and with it observables like cross sections keep their correct mass dimension

$$\int \frac{d^4q}{16\pi^2} \cdots \longrightarrow \mu_R^{2\epsilon} \int \frac{d^{4-2\epsilon}q}{16\pi^2} \cdots = \frac{i\mu_R^{2\epsilon}}{(4\pi)^2} \left[\frac{C_{-1}}{\epsilon} + C_0 + C_1\,\epsilon + \mathcal{O}(\epsilon^2) \right] . \tag{II.2}$$

At the end, the scale μ_R might become irrelevant and drop out after renormalization and analytic continuation, but to be on the safe side we keep it. The constants C_i in the series in $1/\epsilon$ depend on the loop integral we are considering. To regularize the ultraviolet divergence we assume $\epsilon > 0$ and find mathematically well defined poles $1/\epsilon$. Defining scalar integrals with the integration measure $1/(i\pi^2)$ will make for example C_{-1} come out as of the order $\mathcal{O}(1)$. This is the reason we usually find factors $1/(4\pi)^2 = \pi^2/(2\pi)^4$ in front of the loop integrals.

The poles in $1/\epsilon$ will cancel with the universal counter terms once we renormalize the theory. Counter terms we include by shifting parameters in the Lagrangian and the leading order matrix element. They cancel the poles in the combined leading order and virtual one-loop prediction

$$\begin{aligned} |\mathcal{M}_{\text{LO}}(g) + \mathcal{M}_{\text{virt}}|^2 &= |\mathcal{M}_{\text{LO}}(g)|^2 + 2\,\text{Re}\,\mathcal{M}_{\text{LO}}(g)\mathcal{M}_{\text{virt}} + \cdots \\ &\to |\mathcal{M}_{\text{LO}}(g+\delta g)|^2 + 2\,\text{Re}\,\mathcal{M}_{\text{LO}}(g)\mathcal{M}_{\text{virt}} + \cdots \\ \text{with} \qquad g \to g^{\text{bare}} &= g + \delta g \qquad \text{and} \quad \delta g \propto \alpha_s/\epsilon\,. \end{aligned} \tag{II.3}$$

The dots indicate higher orders in α_s, for example absorbing the δg corrections in the leading order and virtual interference. As we can see in Eq.(II.3) the counter terms do not come with a factor $\mu_R^{2\epsilon}$ in front. Therefore, while the poles $1/\epsilon$ cancel just fine, the scale factor $\mu_R^{2\epsilon}$ will not be matched between the actual ultraviolet divergence and the counter term.

We can keep track of the renormalization scale best by expanding the prefactor of the regularized but not yet renormalized integral in Eq.(II.2) in a Taylor series in ϵ, no question asked about convergence radii

$$\begin{aligned} \mu_R^{2\epsilon} \left[\frac{C_{-1}}{\epsilon} + C_0 + \mathcal{O}(\epsilon) \right] &= e^{2\epsilon \log \mu_R} \left[\frac{C_{-1}}{\epsilon} + C_0 + \mathcal{O}(\epsilon) \right] \\ &= \left[1 + 2\epsilon \log \mu_R + \mathcal{O}(\epsilon^2) \right] \left[\frac{C_{-1}}{\epsilon} + C_0 + \mathcal{O}(\epsilon) \right] \\ &= \frac{C_{-1}}{\epsilon} + C_0 + C_{-1}\,\log \mu_R^2 + \mathcal{O}(\epsilon) \\ &\to \frac{C_{-1}}{\epsilon} + C_0 + C_{-1}\,\log \frac{\mu_R^2}{M^2} + \mathcal{O}(\epsilon)\,. \end{aligned} \tag{II.4}$$

In the last step we correct by hand for the fact that $\log \mu_R^2$ with a mass dimension inside the logarithm cannot appear in our calculations. From somewhere else in our calculation the logarithm will be matched with a $\log M^2$ where M^2 is the typical mass or energy scale in our process. This little argument shows that also in dimensional regularization we introduce a mass scale μ_R which appears as $\log(\mu_R^2/M^2)$ in the renormalized expression for our observables. There is no way of removing ultraviolet divergences without introducing some kind of renormalization scale.

In Eq.(II.4) there appear two contributions to a given observable, the expected C_0 and the renormalization–induced C_{-1}. Because the factors C_{-1} are linked to the counter terms in the theory we can often guess them without actually computing the loop integral, which is very useful in cases where they numerically dominate.

Counter terms as they schematically appear in Eq.(II.3) are not uniquely defined. They need to include a given divergence to return finite observables, but we are free to add any finite contribution we want. This opens many ways to define a counter term for example based on physical processes where counter terms do not only cancel the pole but also finite contributions at a given order in perturbation theory. Needless to say, such schemes do not automatically work universally. An example for such a physical renormalization scheme is the on–shell scheme for masses, where we define a counter term such that external on–shell particles do not receive any corrections to their masses. For the top mass this means that we replace the leading order mass with the bare mass, for which we then insert the expression

in terms of the renormalized mass and the counter term

$$\begin{aligned} m_t^{\text{bare}} &= m_t + \delta m_t \\ &= m_t + m_t \frac{\alpha_s C_F}{4\pi} \left(3 \left(-\frac{1}{\epsilon} + \gamma_E - \log(4\pi) - \log \frac{\mu_R^2}{M^2} \right) - 4 + 3 \log \frac{m_t^2}{M^2} \right) \\ &\equiv m_t + m_t \frac{\alpha_s C_F}{4\pi} \left(-\frac{3}{\tilde{\epsilon}} - 4 + 3 \log \frac{m_t^2}{M^2} \right) \qquad \Leftrightarrow \qquad \frac{1}{\tilde{\epsilon}\left(\frac{\mu_R^2}{M^2}\right)} \equiv \frac{1}{\epsilon} - \gamma_E + \log \frac{4\pi\mu_R^2}{M^2} \,, \end{aligned} \tag{II.5}$$

with the color factor $C_F = (N^2-1)/(2N)$. The convenient scale dependent pole $1/\tilde{\epsilon}$ includes the universal additional terms like the Euler gamma function and the scaling logarithm. This logarithm is the big problem in this universality argument, since we need to introduce the at this stage arbitrary energy scale M to separate the universal logarithm of the renormalization scale and the parameter-dependent logarithm of the physical process.

A theoretical problem with this on–shell renormalization scheme is that it is not gauge invariant. On the other hand, it describes for example the kinematic features of top pair production at hadron colliders in a stable perturbation series. This means that once we define a more appropriate scheme for heavy particle masses in collider production mechanisms it better be numerically close to the pole mass. For the computation of total cross sections at hadron colliders or the production thresholds at e^+e^- colliders the pole mass is not well suited at all, but as we will see later this is not where we expect to measure particle masses at the LHC, so we should do fine with something very similar to the pole mass.

Another example for a process dependent renormalization scheme is the mixing of γ and Z propagators. There we choose the counter term of the weak mixing angle such that an on–shell Z boson cannot oscillate into a photon, and vice versa. We can generalize this scheme for mixing scalars as they for example appear in supersymmetry, but it is not gauge invariant with respect to the weak gauge symmetries of the Standard Model either. For QCD corrections, on the other hand, it is the most convenient scheme keeping all exchange symmetries of the two scalars.

To finalize this discussion of process dependent mass renormalization we quote the result for a scalar supersymmetric quark, a squark, where in the on–shell scheme we find

$$\begin{aligned} m_{\tilde{q}}^{\text{bare}} &= m_{\tilde{q}} + \delta m_{\tilde{q}} \\ &= m_{\tilde{q}} + m_{\tilde{q}} \frac{\alpha_s C_F}{4\pi} \left(-\frac{2r}{\tilde{\epsilon}} - 1 - 3r - (1-2r) \log r - (1-r)^2 \log \left| \frac{1}{r} - 1 \right| - 2r \log \frac{m_{\tilde{q}}^2}{M^2} \right) \,. \end{aligned} \tag{II.6}$$

with $r = m_{\tilde{g}}^2/m_{\tilde{q}}^2$. The interesting aspect of this squark mass counter term is that it also depends on the gluino mass, not just the squark mass itself. The reason why QCD counter terms tend to depend only on the renormalized quantity itself is that the gluon is massless. In the limit of vanishing gluino contribution the squark mass counter term is again only proportional to the squark mass itself

$$m_{\tilde{q}}^{\text{bare}} \Big|_{m_{\tilde{g}}=0} = m_{\tilde{q}} + \delta m_{\tilde{q}} = m_{\tilde{q}} + m_{\tilde{q}} \frac{\alpha_s C_F}{4\pi} \left(-\frac{1}{\tilde{\epsilon}} - 3 + \log \frac{m_{\tilde{q}}^2}{M^2} \right) \,. \tag{II.7}$$

Taking the limit of Eq.(II.6) to derive Eq.(II.7) is computationally not trivial, though.

One common feature of all mass counter terms listed above is $\delta m \propto m$, which means that we actually encounter a multiplicative renormalization

$$m^{\text{bare}} = Z_m \, m = (1 + \delta Z_m) \, m = \left(1 + \frac{\delta m}{m} \right) m = m + \delta m \,, \tag{II.8}$$

with $\delta Z_m = \delta m/m$ linking the two ways of writing the mass counter term. This form implies that particles with zero mass will not obtain a finite mass through renormalization. If we remember that chiral symmetry protects a Lagrangian from acquiring fermion masses this means that on–shell renormalization does not break this symmetry. A massless theory cannot become massive by mass renormalization. Regularization and renormalization schemes which do not break symmetries of the Lagrangian are ideal.

When we introduce counter terms in general field theory we usually choose a slightly more model independent

scheme — we define a renormalization point. This is the energy scale at which the counter terms cancels all higher order contributions, divergent as well as finite. The best known example is the electric charge which we renormalize in the Thomson limit of zero momentum transfer through the photon propagator

$$e \to e^{\text{bare}} = e + \delta e \; . \tag{II.9}$$

Looking back at δm_t as defined in Eq.(II.5) we also see a way to define a completely general counter term: if dimensional regularization, *i.e.* the introduction of $4 - 2\epsilon$ dimensions does not break any of the symmetries of our Lagrangian, like Lorentz symmetry or gauge symmetries, we can simply subtract the ultraviolet pole and nothing else. The only question is: do we subtract $1/\epsilon$ in the MS scheme or do we subtract $1/\tilde{\epsilon}$ in the $\overline{\text{MS}}$ scheme. In the $\overline{\text{MS}}$ scheme the counter term is then scale dependent.

Carefully counting, there are three scales present in such a scheme. First, there is the physical scale in the process. In our case of a top self energy this is for example the top mass m_t appearing in the matrix element for the process $pp \to t\bar{t}$. Next, there is the renormalization scale μ_R, a reference scale which is part of the definition of any counter term. And last but not least, there is the scale M separating the counter term from the process dependent result, which we can choose however we want, but which as we will see implies a running of the counter term. The role of this scale M will become clear when we go through the example of the running strong coupling α_s. Of course, we would prefer to choose all three scales the same, but in a complex physical process this might not always be possible. For example, any massive $(2 \to 3)$ production process naturally involves several external physical scales.

Just a side remark for completeness: a one loop integral which has no intrinsic mass scale is the two-point function with zero mass in the loop and zero momentum flowing through the integral: $B(p^2 = 0; 0, 0)$. It appears for example in the self energy corrections of external quarks and gluons. Based on dimensional arguments this integral has to vanish altogether. On the other hand, we know that like any massive two-point function it has to be ultraviolet divergent $B \sim 1/\epsilon_{\text{UV}}$ because setting all internal and external mass scales to zero is nothing special from an ultraviolet point of view. This can only work if the scalar integral also has an infrared divergence appearing in dimensional regularization. We can then write the entire massless two-point function as

$$B(p^2 = 0; 0, 0) = \int \frac{d^4q}{16\pi^2} \, \frac{1}{q^2} \frac{1}{(q+p)^2} = \frac{i\pi^2}{16\pi^2} \left(\frac{1}{\epsilon_{\text{UV}}} - \frac{1}{\epsilon_{\text{IR}}} \right) \; , \tag{II.10}$$

keeping track of the divergent contributions from the infrared and the ultraviolet regimes. For this particular integral they precisely cancel, so the result for $B(0; 0, 0)$ is zero, but setting it to zero too early will spoil any ultraviolet and infrared finiteness test. Treating the two divergences strictly separately and dealing with them one after the other also ensures that for ultraviolet divergences we can choose $\epsilon > 0$ while for infrared divergences we require $\epsilon < 0$.

To get an idea what these different scales which appear in the process of renormalization mean let us compute such a scale dependent parameter, namely the running strong coupling $\alpha_s(\mu_R^2)$. The Drell–Yan process is one of the very few relevant processes at hadron colliders where the strong coupling does not appear at tree level, so we cannot use it as our toy process this time. Another simple process where we can study this coupling is bottom pair production at the LHC, where at some energy range we will be dominated by valence quarks: $q\bar{q} \to b\bar{b}$. The only Feynman diagram is an s-channel off–shell gluon with a momentum flow $p^2 \equiv s$. At next–to–leading order this gluon propagator will be corrected by self energy loops, where the gluon splits into two quarks or gluons and re-combines before it produces the two final–state bottoms. Let us for now assume that all quarks are massless. The Feynman diagrams for the gluon self energy include a quark look, a gluon loop, and the ghost loop which removes the unphysical degrees of freedom of the gluon inside the loop. The gluon self energy correction or vacuum polarization, as propagator corrections to gauge bosons are usually labelled, will be a scalar. This way, all fermion lines close in the Feynman diagram and the Dirac trace is computed inside the loop. In color space the self energy will (hopefully) be diagonal, just like the gluon propagator itself, so we can ignore the color indices for now. In unitary gauge the gluon propagator is proportional to the transverse tensor $T^{\mu\nu} = g^{\mu\nu} - p^\nu p^\mu / p^2$. As mentioned in the context of the effective gluon–Higgs coupling, the same should be true for the gluon self energy, which we therefore write as $\Pi^{\mu\nu} \equiv \Pi \, T^{\mu\nu}$. We find the simple relations

$$\begin{aligned} T^{\mu\nu} g^\rho_\nu &= \left(g^{\mu\nu} - \frac{p^\mu p^\nu}{p^2} \right) g^\rho_\nu = T^{\mu\rho} \\ T^{\mu\nu} T^\rho_\nu &= \left(g^{\mu\nu} - \frac{p^\mu p^\nu}{p^2} \right) \left(g^\rho_\nu - \frac{p_\nu p^\rho}{p^2} \right) = g^{\mu\rho} - 2\frac{p^\mu p^\rho}{p^2} + p^2 \frac{p^\mu p^\rho}{p^4} = T^{\mu\rho} \; . \end{aligned} \tag{II.11}$$

Including the gluon, quark, and ghost loops the regularized gluon self energy with a momentum flow p^2 through the propagator reads

$$\begin{aligned} -\frac{1}{p^2}\,\Pi\left(\frac{\mu_R^2}{p^2}\right) &= \frac{\alpha_s}{4\pi}\,\left(-\frac{1}{\tilde\epsilon(\mu_R^2/M^2)}+\log\frac{p^2}{M^2}\right)\,\left(\frac{13}{6}N_c-\frac{2}{3}n_f\right)+\mathcal{O}(\log m_t^2) \\ &\equiv \alpha_s\,\left(-\frac{1}{\tilde\epsilon(\mu_R^2/M^2)}+\log\frac{p^2}{M^2}\right)\,b_0+\mathcal{O}(\log m_t^2) \\ \text{with}\qquad &\boxed{b_0=\frac{1}{4\pi}\left(\frac{11}{3}N_c-\frac{2}{3}n_f\right)\overset{\text{SM}}{>}0}\,. \end{aligned} \tag{II.12}$$

The minus sign arises from the factors i in the propagators. The number of fermions coupling to the gluons is n_f. From the comments on $B(p^2;0,0)$ we could guess that the loop integrals will only give a logarithm $\log p^2$ which is then matched by the logarithm $\log M^2$ implicitly included in the definition of $\tilde\epsilon$.

The factor b_0 arises from one-loop corrections, *i.e.* from diagrams which include one additional power of α_s. Strictly speaking, it gives the first term in a perturbative series in the strong coupling $\alpha_s = g_s^2/(4\pi)$. Later on, we will indicate where additional higher order corrections would enter.

In the second step of Eq.(II.12) we have sneaked in additional contributions to the renormalization of the strong coupling from the other one-loop diagrams in the process, replacing the factor 13/6 by a factor 11/3. This is related to the fact that there are actually three types of divergent virtual gluon diagrams in the physical process $q\bar q \to b\bar b$: the external quark self energies with renormalization factors $Z_f^{1/2}$, the internal gluon self energy Z_A, and the vertex corrections Z_{Aff}. The only physical parameters we can renormalize in this process are the strong coupling and, if finite, the bottom mass. Wave function renormalization constants are not physical, but vertex renormalization terms are. The entire divergence in our $q\bar q \to b\bar b$ process which needs to be absorbed in the strong coupling through Z_g is given by the combination

$$Z_{Aff} = Z_g Z_A^{1/2} Z_f \qquad\qquad \Leftrightarrow \qquad\qquad \frac{Z_{Aff}}{Z_A^{1/2}Z_f} \equiv Z_g\,. \tag{II.13}$$

We can check this definition of Z_g by comparing all vertices in which the strong coupling g_s appears, namely the gluon coupling to quarks, ghosts as well as the triple and quartic gluon vertex. All of them need to have the same divergence structure

$$\frac{Z_{Aff}}{Z_A^{1/2}Z_f} \overset{!}{=} \frac{Z_{A\eta\eta}}{Z_A^{1/2}Z_\eta} \overset{!}{=} \frac{Z_{3A}}{Z_A^{3/2}} \overset{!}{=} \sqrt{\frac{Z_{4A}}{Z_A^2}}\,. \tag{II.14}$$

If we had done the same calculation in QED and looked for a running electric charge, we would have found that the vacuum polarization diagrams for the photon do account for the entire counter term of the electric charge. The other two renormalization constants Z_{Aff} and Z_f cancel because of gauge invariance.

In contrast to QED, the strong coupling diverges in the Thomson limit because QCD is confined towards large distances and weakly coupled at small distances. Lacking a well enough motivated reference point we are lead to renormalize α_s in the $\overline{\text{MS}}$ scheme. From Eq.(II.12) we know that the ultraviolet pole which needs to be cancelled by the counter term is proportional to the function b_0

$$\begin{aligned} & g_s^{\text{bare}} = Z_g g_s = (1+\delta Z_g)\,g_s = \left(1+\frac{\delta g_s}{g_s}\right) g_s \\ \Rightarrow\qquad & (g_s^2)^{\text{bare}} = (Z_g g_s)^2 = \left(1+\frac{\delta g_s}{g_s}\right)^2 g_s^2 = \left(1+2\frac{\delta g_s}{g_s}\right) g_s^2 = \left(1+\frac{\delta g_s^2}{g_s^2}\right) g_s^2 \\ \Rightarrow\qquad & \alpha_s^{\text{bare}} = \left(1+\frac{\delta\alpha_s}{\alpha_s}\right)\alpha_s \overset{!}{=} \left(1-\frac{\Pi}{p^2}\bigg|_{\text{pole}}\right)\alpha_s(M^2) \overset{\text{Eq.(II.12)}}{=} \left(1-\frac{\alpha_s}{\tilde\epsilon\left(\frac{\mu_R}{M}\right)}\,b_0\right)\alpha_s(M^2)\,. \end{aligned} \tag{II.15}$$

Only in the last step we have explicitly included the scale dependence of the counter term. Because the bare coupling does not depend on any scales, this means that α_s depends on the artifical external scale M. Similar to the top mass renormalization scheme we can switch to a more physical scheme for the strong coupling as well: we can absorb

also the finite contributions of $\Pi(\mu_R^2/p^2)$ into the strong coupling by simply identifying $M^2 = p^2$. Based again on Eq.(II.12) this implies

$$\alpha_s^{\text{bare}} = \alpha_s(p^2)\left(1 - \frac{\alpha_s(p^2) b_0}{\tilde{\epsilon}(\mu_R^2/M^2)} + \alpha_s(p^2) b_0 \log\frac{p^2}{M^2}\right) . \tag{II.16}$$

On the right hand side α_s is consistently evaluated as a function of the physical scale p^2. The lograrithm just shifts the argument of $\tilde{\epsilon}$ from M^2 to p^2. This formula defines a running coupling $\alpha_s(p^2)$, because the definition of the coupling now has to account for a possible shift between the original argument p^2 and the scale M^2 coming out of the $\overline{\text{MS}}$ scheme. Since according to Eqs.(II.15) and (II.16) the bare strong coupling can be expressed in terms of $\alpha_s(M^2)$ as well as in terms of $\alpha_s(p^2)$ we can link the two scales through

$$\begin{aligned}
&\alpha_s(M^2) = \alpha_s(p^2) + \alpha_s^2(p^2) b_0 \log\frac{p^2}{M^2} = \alpha_s(p^2)\left(1 + \alpha_s(p^2) b_0 \log\frac{p^2}{M^2}\right) \\
\Leftrightarrow \qquad &\alpha_s(p^2) = \frac{\alpha_s(M^2)}{1 + \alpha_s(p^2) b_0 \log\frac{p^2}{M^2}} \\
\Leftrightarrow \qquad &\frac{d\alpha_s(p^2)}{d\log p^2} = -\alpha_s^2(p^2) b_0 + \mathcal{O}(\alpha_s^3) .
\end{aligned} \tag{II.17}$$

To the given loop order the argument of the strong coupling squared in this formula can be neglected — its effect is of higher order. We nevertheless keep the argument as a higher order effect and remember the additional terms neglected above to later distinguish different approaches to the running coupling. From Eq.(II.12) we know that $b_0 > 0$, which means that towards larger scales the strong coupling has a negative slope. The ultraviolet limit of the strong coupling is zero. This makes QCD an asymptotically free theory. We can compute the function b_0 in general models by simply adding all contributions of strongly interacting particles in this loop

$$b_0 = -\frac{1}{12\pi} \sum_{\text{colored states}} D_j \, T_{R,j} , \tag{II.18}$$

where we need to know some kind of counting factor D_j which is -11 for a vector boson (gluon), +4 for a Dirac fermion (quark), +2 for a Majorana fermion (gluino), +1 for a complex scalar (squark) and +1/2 for a real scalar. Note that this sign is not given by the fermionic or bosonic nature of the particle in the loop. The color charges are $T_R = 1/2$ for the fundamental representation of $SU(3)$ and $C_A = N_c$ for the adjoint representation. The masses of the loop particles are not relevant in this approximation because we are only interested in the ultraviolet regime of QCD where all particles can be regarded massless. This is a fundamental problem when we work with a running strong coupling constant: it is not an observable, which means that it does not have to ensure the decoupling of heavy states. On the other hand, if we treat it like an observable we need to modify it by hand, so it does not ruin the automatic decoupling of heavy particles. When we really model the running of α_s we need to take into account threshold effects of heavy particles at their respective masses. When we really model the running of α_s we need to take into account threshold effects of heavy particles at their respective masses.

We can do even better than this fixed order in perturbation theory: while the correction to α_s in Eq.(II.16) is perturbatively suppressed by the usual factor $\alpha_s/(4\pi)$ it includes a logarithm of a ratio of scales which does not need to be small. Instead of simply including these gluon self energy corrections at a given order in perturbation theory we can instead include chains of one-loop diagrams with Π appearing many times in the off–shell gluon propagator. It means we replace the off–shell gluon propagator by

$$\begin{aligned}
\frac{T^{\mu\nu}}{p^2} \to &\frac{T^{\mu\nu}}{p^2} + \left(\frac{T}{p^2}\cdot(-T\,\Pi)\cdot\frac{T}{p^2}\right)^{\mu\nu} \\
&+ \left(\frac{T}{p^2}\cdot(-T\,\Pi)\cdot\frac{T}{p^2}\cdot(-T\,\Pi)\cdot\frac{T}{p^2}\right)^{\mu\nu} + \cdots \\
= &\frac{T^{\mu\nu}}{p^2}\sum_{j=0}^{\infty}\left(-\frac{\Pi}{p^2}\right)^j = \frac{T^{\mu\nu}}{p^2}\,\frac{1}{1+\Pi/p^2} ,
\end{aligned} \tag{II.19}$$

schematically written without the factors i. To avoid indices we abbreviate $T^{\mu\nu}T^{\rho}_{\nu} = T\cdot T$ which make sense because

of $(T\cdot T\cdot T)^{\mu\nu} = T^{\mu\rho}T^{\sigma}_{\rho}T^{\nu}_{\sigma} = T^{\mu\nu}$. This resummation of the logarithm which appears in the next–to–leading order corrections to α_s moves the finite shift in α_s shown in Eqs.(II.12) and (II.16) into the denominator, while we assume that the pole will be properly taken care off in any of the schemes we discuss

$$\alpha_s^{\rm bare} = \alpha_s(M^2) - \frac{\alpha_s^2 b_0}{\tilde{\epsilon}(\mu_R^2/M^2)} \equiv \frac{\alpha_s(p^2)}{1-\alpha_s(p^2)\; b_0\; \log\dfrac{p^2}{M^2}} - \frac{\alpha_s^2 b_0}{\tilde{\epsilon}(\mu_R^2/M^2)}\;. \tag{II.20}$$

Just as in the case without resummation, we can use this complete formula to relate the values of α_s at two reference points, *i.e.* we consider it a renormalization group equation (RGE) which evolves physical parameters from one scale to another in analogy to the fixed order version in Eq.(II.17)

$$\frac{1}{\alpha_s(M^2)} = \frac{1}{\alpha_s(p^2)}\left(1-\alpha_s(p^2)\; b_0\; \log\frac{p^2}{M^2}\right) = \frac{1}{\alpha_s(p^2)} - b_0\; \log\frac{p^2}{M^2}\;. \tag{II.21}$$

The factor α_s inside the parentheses we can again evaluate at either of the two scales, the difference is a higher order effect. If we keep it at p^2 we see that the expression in Eq.(II.21) is different from the un-resummed version in Eq.(II.16). If we ignore this higher order effect the two formulas become equivalent after switching p^2 and M^2. Resumming the vacuum expectation bubbles only differs from the un-resummed result once we include some next–to–leading order contribution. When we differentiate $\alpha_s(p^2)$ with respect to the momentum transfer p^2 we find, using the relation $d/dx(1/\alpha_s) = -1/\alpha_s^2\; d\alpha_s/dx$

$$\frac{1}{\alpha_s(p^2)}\;\frac{d\alpha_s(p^2)}{d\log p^2} = -\alpha_s(p^2)\;\frac{d}{d\log p^2}\;\frac{1}{\alpha_s(p^2)} = -\alpha_s(p^2)\,b_0 \qquad \text{or} \qquad \boxed{p^2\frac{d\alpha_s}{dp^2} \equiv \frac{d\alpha_s}{d\log p^2} = \beta = -\alpha_s^2\sum_{n=0} b_n\alpha_s^n}\;. \tag{II.22}$$

In the second form we replace the one-loop running b_0 by its full perturbative series. This is the famous running of the strong coupling constant including all higher order terms b_n.

In the running of the strong coupling constant we relate the different values of α_s through multiplicative factors of the kind

$$\left(1 \pm \alpha_s(p^2) b_0 \log\frac{p^2}{M^2}\right)\;. \tag{II.23}$$

Such factors appear in the un-resummed computation of Eq.(II.17) as well as in Eq.(II.20) after resummation. Because they are multiplicative, these factors can move into the denominator, where we need to ensure that they do not vanish. Dependent on the sign of b_0 this becomes a problem for large scale ratios $|\alpha_s \log p^2/M^2| > 1$, where it leads to the Landau pole. For the strong coupling with $b_0 > 0$ and large coupling values at small scales $p^2 \ll M^2$ the combination $(1+\alpha_s b_0 \log p^2/M^2)$ can indeed vanish and become a problem.

It is customary to replace the renormalization point of α_s in Eq.(II.20) with a reference scale defined by the Landau pole. At one loop order this reads

$$\begin{aligned}
1+\alpha_s\; b_0\; \log\frac{\Lambda_{\rm QCD}^2}{M^2} &\stackrel{!}{=} 0 \qquad \Leftrightarrow \qquad \log\frac{\Lambda_{\rm QCD}^2}{M^2} = -\frac{1}{\alpha_s(M^2)b_0} \qquad \Leftrightarrow \qquad \log\frac{p^2}{M^2} = \log\frac{p^2}{\Lambda_{\rm QCD}^2} - \frac{1}{\alpha_s(M^2)b_0} \\
\frac{1}{\alpha_s(p^2)} &\stackrel{\text{Eq.(II.21)}}{=} \frac{1}{\alpha_s(M^2)} + b_0\; \log\frac{p^2}{M^2} \\
&= \frac{1}{\alpha_s(M^2)} + b_0 \log\frac{p^2}{\Lambda_{\rm QCD}^2} - \frac{1}{\alpha_s(M^2)} = b_0\log\frac{p^2}{\Lambda_{\rm QCD}^2} \qquad \Leftrightarrow \qquad \boxed{\alpha_s(p^2) = \frac{1}{b_0\log\dfrac{p^2}{\Lambda_{\rm QCD}^2}}}\;.
\end{aligned} \tag{II.24}$$

This scheme can be generalized to any order in perturbative QCD and is not that different from the Thomson limit renormalization scheme of QED, except that with the introduction of $\Lambda_{\rm QCD}$ we are choosing a reference point which is particularly hard to compute perturbatively. One thing that is interesting in the way we introduce $\Lambda_{\rm QCD}$ is the fact that we introduce a scale into our theory without ever setting it. All we did was renormalize a coupling which becomes strong at large energies and search for the mass scale of this strong interaction. This trick is called

dimensional transmutation.

In terms of language, there is a little bit of confusion between field theorists and phenomenologists: up to now we have introduced the renormalization scale μ_R as the renormalization point, for example of the strong coupling constant. In the $\overline{\text{MS}}$ scheme, the subtraction of $1/\tilde{\epsilon}$ shifts the scale dependence of the strong coupling to M^2 and moves the logarithm $\log M^2/\Lambda^2_{\text{QCD}}$ into the definition of the renormalized parameter. This is what we will from now on call the renormalization scale in the phenomenological sense, *i.e.* the argument we evaluate α_s at. Throughout this section we will keep the symbol M for this renormalization scale in the $\overline{\text{MS}}$ scheme, but from Section II C on we will shift back to μ_R instead of M as the argument of the running coupling, to be consistent with the literature.

B. Scaling logarithms

In the last section we have introduced the running strong coupling in a fairly abstract manner. For example, we did not link the resummation of diagrams and the running of α_s in Eqs.(II.17) and (II.22) to physics. In what way does the resummation of the one-loop diagrams for the s-channel gluon improve our prediction of an observable? To illustrate this we best look at a simple observable which depends on just one energy scale p^2. The first observable coming to mind is again the Drell–Yan cross section $\sigma(q\bar{q} \to \mu^+\mu^-)$, but since we are not really sure what to do with the parton densities which are included in the actual hadronic observable, we better use an observable at an e^+e^- collider. Something that will work and includes α_s at least in the one-loop corrections is the R parameter

$$R = \frac{\sigma(e^+e^- \to \text{hadrons})}{\sigma(e^+e^- \to \mu^+\mu^-)} = N_c \sum_{\text{quarks}} Q_q^2 = \frac{11 N_c}{9} \; . \tag{II.25}$$

The numerical value at leading order assumes five quarks. Including higher order corrections we can express the result in a power series in the renormalized strong coupling α_s. In the $\overline{\text{MS}}$ scheme we subtract $1/\tilde{\epsilon}(\mu_R^2/M^2)$ and in general include a scale dependence on M in the individual prefactors r_n

$$R\left(\frac{p^2}{M^2}, \alpha_s\right) = \sum_{n=0} r_n\left(\frac{p^2}{M^2}\right) \alpha_s^n(M^2) \qquad\qquad r_0 = \frac{11 N_c}{9} \; . \tag{II.26}$$

The r_n we can assume to be dimensionless — if they are not, we can scale R appropriately using p^2. This implies that the r_n only depend on ratios of two scales, the externally fixed p^2 on the one hand and the artificial M^2 on the other.

At the same time we know that R is an observable, which means that including all orders in perturbation theory it cannot depend on any artificial scale choice M. Writing this dependence as a total derivative and setting it to zero we find an equation which would be called a Callan–Symanzik equation if instead of the running coupling we had included a running mass

$$\begin{aligned}
0 \stackrel{!}{=} M^2 \frac{d}{dM^2} R\left(\frac{p^2}{M^2}, \alpha_s(M^2)\right) &= M^2 \left[\frac{\partial}{\partial M^2} + \frac{\partial \alpha_s}{\partial M^2}\frac{\partial}{\partial \alpha_s}\right] R\left(\frac{p^2}{M^2}, \alpha_s\right) \\
&= \left[M^2 \frac{\partial}{\partial M^2} + \beta \frac{\partial}{\partial \alpha_s}\right] \sum_{n=0} r_n\left(\frac{p^2}{M^2}\right) \alpha_s^n \\
&= \sum_{n=1} M^2 \frac{\partial r_n}{\partial M^2} \alpha_s^n + \sum_{n=1} \beta\, r_n\, n \alpha_s^{n-1} \qquad \text{with} \quad r_0 = \frac{11 N_c}{9} = \text{const} \\
&= M^2 \sum_{n=1} \frac{\partial r_n}{\partial M^2} \alpha_s^n - \sum_{n=1} \sum_{m=0} n r_n \alpha_s^{n+m+1} b_m \qquad \text{with} \quad \beta = -\alpha_s^2 \sum_{m=0} b_m \alpha_s^m \\
&= M^2 \frac{\partial r_1}{\partial M^2} \alpha_s + \left(M^2 \frac{\partial r_2}{\partial M^2} - r_1 b_0\right) \alpha_s^2 + \left(M^2 \frac{\partial r_3}{\partial M^2} - 2 r_2 b_0 - r_1 b_1\right) \alpha_s^3 + \mathcal{O}(\alpha_s^4) \; .
\end{aligned} \tag{II.27}$$

In the second line we have to remember that the M dependence of α_s is already included in the appearance of β, so α_s should be considered a variable by itself. This perturbative series in α_s has to vanish in each order of perturbation theory. The non–trivial structure, namely the mix of r_n derivatives and the perturbative terms in the β function we can read off the α_s^3 term in Eq.(II.27): first, we have the appropriate NNNLO corrections r_3. Next, we have one loop

in the gluon propagator b_0 and two loops for example in the vertex r_2. And finally, we need the two-loop diagram for the gluon propagator b_1 and a one-loop vertex correction r_1. The kind–of–Callan–Symanzik equation Eq.(II.27) requires

$$\begin{aligned}
\frac{\partial r_1}{\partial \log M^2/p^2} &= 0 \\
\frac{\partial r_2}{\partial \log M^2/p^2} &= r_1 b_0 \\
\frac{\partial r_3}{\partial \log M^2/p^2} &= r_1 b_1 + 2 r_2(M^2) b_0 \\
&\dots
\end{aligned} \tag{II.28}$$

The dependence on the argument M^2 vanishes for r_0 and r_1. Keeping in mind that there will be integration constants c_n and that another, in our case, unique momentum scale p^2 has to cancel the mass units inside $\log M^2$ we find

$$\begin{aligned}
r_0 &= c_0 = \frac{11 N_c}{9} \\
r_1 &= c_1 \\
r_2 &= c_2 + r_1 b_0 \log \frac{M^2}{p^2} = c_2 + c_1 b_0 \log \frac{M^2}{p^2} \\
r_3 &= \int d \log \frac{M'^2}{p^2} \left(c_1 b_1 + 2 \left(c_2 + c_1 b_0 \log \frac{M'^2}{p^2} \right) b_0 \right) \\
&= c_3 + (c_1 b_1 + 2 c_2 b_0) \log \frac{M^2}{p^2} + c_1 b_0^2 \log^2 \frac{M^2}{p^2} \\
&\dots
\end{aligned} \tag{II.29}$$

This chain of r_n values looks like we should interpret the apparent fixed-order perturbative series for R in Eq.(II.26) as a series which implicitly includes terms of the order $\log^{n-1} M^2/p^2$ in each r_n. They can become problematic if this logarithm becomes large enough to spoil the fast convergence in terms of $\alpha_s \sim 0.1$, evaluating the observable R at scales far away from the scale choice for the strong coupling constant M.

Instead of the series in r_n we can use the conditions in Eq.(II.29) to express R in terms of the c_n and collect the logarithms appearing with each c_n. The geometric series we then resum to

$$\begin{aligned}
R = \sum_n r_n \left(\frac{p^2}{M^2} \right) \alpha_s^n(M^2) &= c_0 + c_1 \left(1 + \alpha_s(M^2) b_0 \log \frac{M^2}{p^2} + \alpha_s^2(M^2) b_0^2 \log^2 \frac{M^2}{p^2} + \dots \right) \alpha_s(M^2) \\
&\quad + c_2 \left(1 + 2 \alpha_s(M^2) b_0 \log \frac{M^2}{p^2} + \dots \right) \alpha_s^2(M^2) + \dots \\
&= c_0 + c_1 \frac{\alpha_s(M^2)}{1 - \alpha_s(M^2) b_0 \log \frac{M^2}{p^2}} + c_2 \left(\frac{\alpha_s(M^2)}{1 - \alpha_s(M^2) b_0 \log \frac{M^2}{p^2}} \right)^2 + \dots \\
&\equiv \sum c_n \, \alpha_s^n(p^2) \, .
\end{aligned} \tag{II.30}$$

In the original ansatz α_s is always evaluated at the scale M^2. In the last step we use Eq.(II.21) with flipped arguments p^2 and M^2, derived from the resummation of the vacuum polarization bubbles. In contrast to the r_n integration constants the c_n are by definition independent of p^2/M^2 and therefore more suitable as a perturbative series in the presence of potentially large logarithms. Note that the un-resummed version of the running coupling in Eq.(II.16) would not give the correct result, so Eq.(II.30) only holds for resummed vacuum polarization bubbles.

This re-organization of the perturbation series for R can be interpreted as resumming all logarithms of the kind $\log M^2/p^2$ in the new organization of the perturbative series and absorbing them into the running strong coupling evaluated at the scale p^2. All scale dependence in the perturbative series for the dimensionless observable R is moved

into α_s, so possibly large logarithms $\log M^2/p^2$ have disappeared. In Eq.(II.30) we also see that this series in c_n will never lead to a scale-invariant result when we include a finite order in perturbation theory. Some higher–order factors c_n are known, for example inserting $N_c = 3$ and five quark flavors just as we assume in Eq.(II.25)

$$R = \frac{11}{3}\left(1 + \frac{\alpha_s(p^2)}{\pi} + 1.4\left(\frac{\alpha_s(p^2)}{\pi}\right)^2 - 12\left(\frac{\alpha_s(p^2)}{\pi}\right)^3 + \mathcal{O}\left(\frac{\alpha_s(p^2)}{\pi}\right)^4\right) . \tag{II.31}$$

This alternating series with increasing perturbative prefactors seems to indicate the asymptotic instead of convergent behavior of perturbative QCD. At the bottom mass scale the relevant coupling factor is only $\alpha_s(m_b^2)/\pi \sim 1/14$, so a further increase of the c_n would become dangerous. However, a detailed look into the calculation shows that the dominant contributions to c_n arise from the analytic continuation of logarithms, which are large finite terms for example from $\text{Re}(\log^2(-E^2)) = \log^2 E^2 + \pi^2$. In the literature such π^2 terms arising from the analytic continuation of loop integrals are often phrased in terms of $\zeta_2 = \pi^2/6$.

Before moving on we collect the logic of the argument given in this section: when we regularize an ultraviolet divergence we automatically introduce a reference scale μ_R. Naively, this could be an ultraviolet cutoff scale, but even the seemingly scale invariant dimensional regularization in the conformal limit of our field theory cannot avoid the introduction of a scale. There are several ways of dealing with such a scale: first, we can renormalize our parameter at a reference point. Secondly, we can define a running parameter and this way absorb the scale logarithm into the $\overline{\text{MS}}$ counter term. In that case introducing Λ_{QCD} leaves us with a compact form of the running coupling $\alpha_s(M^2; \Lambda_{\text{QCD}})$.

Strictly speaking, at each order in perturbation theory the scale dependence should vanish together with the ultraviolet poles, as long as there is only one scale affecting a given observable. However, defining the running strong coupling we sum one-loop vacuum polarization graphs. Even when we compute an observable at a given loop order, we implicitly include higher order contributions. They lead to a dependence of our perturbative result on the artificial scale M^2, which phenomenologists refer to as renormalization scale dependence.

Using the R ratio we see what our definition of the running coupling means in terms of resumming logarithms: reorganizing our perturbative series to get rid of the ultraviolet divergence $\alpha_s(p^2)$ resums the scale logarithms $\log p^2/M^2$ to all orders in perturbation theory. We will need this picture once we introduce infrared divergences in the following section.

C. Infrared divergences

After our brief discussion into ultraviolet divergences and renormalization we move to LHC processes, like the Drell–Yan process $q\bar{q} \to \mu^+\mu^-$, in perturbative QCD. We know that the partons inside the proton are described by parton distributions (pdfs), which at this stage are only probability functions in terms of the collinear momentum fraction of the partons inside the proton. The question we need to ask for a quantum-level description of $\mu^+\mu^-$ production at the LHC is: what happens if together with the two leptons we produce additional jets which for one reason or another we do not observe in the detector. Such jets could for example come from the radiation of a gluon from the initial–state quarks. We will first study the kinematics of radiating such jets and specify the infrared divergences this leads to. Next we will show that these divergences have a generic structure and can be absorbed into a re-definition of the parton densities, similar to an ultraviolet renormalization of a Lagrangian parameter. Finally, we will follow the example of the ultraviolet divergences and see what absorbing these divergences means in terms logarithms appearing in QCD calculations.

Let us get back to the radiation of additional partons in the Drell–Yan process. We can start for example by computing the cross section for the partonic process $q\bar{q} \to Zg$. However, this partonic process involves renormalization of ultraviolet divergences as well as loop diagrams which we have to include before we can say anything reasonable. Instead, we look at the crossed process

It should behave similar to any other $(2 \to 2)$ jet radiation, except that it has a different incoming state than the leading order Drell–Yan process and hence does not involve virtual corrections. This means we do not have to deal with ultraviolet divergences and renormalization, and can concentrate on parton or jet radiation from the initial state. Moreover, let us go back to Z production instead of a photon, to avoid confusion with additional massless particles in the final state.

The amplitude for this $(2 \to 2)$ process is — modulo charges and averaging factors, but including all Mandelstam

variables

$$|\mathcal{M}|^2 \sim -\frac{t}{s} - \frac{s^2 - 2m_Z^2(s+t-m_Z^2)}{st} \; . \tag{II.32}$$

The Mandelstam variable t for one massless final–state particle can be expressed as $t = -s(1-\tau)y$ in terms of the rescaled gluon emission angle $y = (1-\cos\theta)/2$ and $\tau = m_Z^2/s$. Similarly, we obtain $u = -s(1-\tau)(1-y)$, so as a first check we can confirm that $t + u = -s(1-\tau) = -s + m_Z^2$. The collinear limit when the gluon is radiated in the beam direction is given by $y \to 0$, corresponding to negative $t \to 0$ with finite $u = -s + m_Z^2$. In this limit the matrix element can also be written as

$$|\mathcal{M}|^2 \sim \frac{s^2 - 2sm_Z^2 + 2m_Z^4}{s(s-m_Z^2)} \; \frac{1}{y} + \mathcal{O}(y^0) \; . \tag{II.33}$$

This expression is divergent for collinear gluon radiation or gluon splitting, *i.e.* for small angles y. We can translate this $1/y$ divergence for example into the transverse momentum of the gluon or Z

$$sp_T^2 = tu = s^2(1-\tau)^2 \; y(1-y) = (s-m_Z^2)^2 y + \mathcal{O}(y^2) \tag{II.34}$$

In the collinear limit our matrix element squared in Eq.(II.33) becomes

$$\boxed{|\mathcal{M}|^2 \sim \frac{s^2 - 2sm_Z^2 + 2m_Z^4}{s^2} \; \frac{s-m_Z^2}{p_T^2} + \mathcal{O}(p_T^0)} \; . \tag{II.35}$$

The matrix element for the tree level process $qg \to Zq$ has a leading divergence proportional to $1/p_T^2$. To compute the total cross section for this process we need to integrate the matrix element over the entire two-particle phase space. Using the appropriate Jacobian this integration can be written in terms of the reduced angle y. Approximating the matrix element as C'/y or C/p_T^2, we then integrate

$$\int_{y^{\min}}^{y^{\max}} dy \frac{C'}{y} = \int_{p_T^{\min}}^{p_T^{\max}} dp_T^2 \frac{C}{p_T^2} = \; 2 \int_{p_T^{\min}}^{p_T^{\max}} dp_T \; p_T \; \frac{C}{p_T^2} \simeq 2C \int_{p_T^{\min}}^{p_T^{\max}} dp_T \frac{1}{p_T} = 2C \; \log \frac{p_T^{\max}}{p_T^{\min}} \tag{II.36}$$

The form C/p_T^2 for the matrix element is of course only valid in the collinear limit; in the non–collinear phase space C is not a constant. However, Eq.(II.36) describes well the collinear divergence arising from quark radiation at the LHC.

We now follow the same strategy as for the ultraviolet divergence. First, we regularize the divergence for example using dimensional regularization. Then, we find a well–defined way to get rid of it. Dimensional regularization means writing the two-particle phase space in $n = 4 - 2\epsilon$ dimensions. Just for reference, the complete formula in terms of the angular variable y then reads

$$s \; \frac{d\sigma}{dy} = \frac{\pi (4\pi)^{-2+\epsilon}}{\Gamma(1-\epsilon)} \; \left(\frac{\mu_F^2}{m_Z^2}\right)^\epsilon \; \frac{\tau^\epsilon (1-\tau)^{1-2\epsilon}}{y^\epsilon (1-y)^\epsilon} \, |\mathcal{M}|^2 \sim \left(\frac{\mu_F^2}{m_Z^2}\right)^\epsilon \; \frac{|\mathcal{M}|^2}{y^\epsilon (1-y)^\epsilon} \; . \tag{II.37}$$

In the second step we only keep the factors we are interested in. The additional factor $1/y^\epsilon$ regularizes the integral at $y \to 0$, as long as $\epsilon < 0$ by slightly increasing the suppression of the integrand in the infrared regime. This means that for infrared divergences we can as well choose $n = 4 + 2\epsilon$ space–time dimensions with $\epsilon > 0$. After integrating the leading collinear divergence $1/y^{1+\epsilon}$ we are left with a pole $1/(-\epsilon)$. This regularization procedure is symmetric in $y \leftrightarrow (1-y)$. What is important to notice is again the appearance of a scale $\mu_F^{2\epsilon}$ with the n-dimensional integral. This scale arises from the infrared regularization of the phase space integral and is referred to as factorization scale. The actual removal of the infrared pole — corresponding to the renormalization in the ultraviolet case — is called mass factorization and works exactly the same way as renormalizing a parameter: in a well–defined scheme we simply subtract the pole from the fixed-order matrix element squared.

From the discussion of the process $qg \to Zq$ we can at least hope that after taking care of all other infrared and ultraviolet divergences the collinear structure of the process $q\bar{q} \to Zg$ will be similar. In this section we will show that we can indeed write all collinear divergences in a universal form, independent of the hard process which we choose as the Drell–Yan process. In the collinear limit, the radiation of additional partons or the splitting into additional

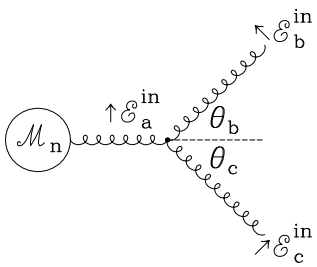

FIG. 2: Splitting of one gluon into two gluons. Figure from Ref. [3].

partons will be described by universal splitting functions.

Infrared divergences occur for massless particles in the initial or final state, so we need to go through all ways incoming or outgoing gluons and quark can split into each other. The description of the factorized phase space, with which we will start, is common to all these different channels. The first and at the LHC most important case is the splitting of one gluon into two, shown in Figure 2. The two daughter gluons are close to mass shell while the mother has to have a finite positive invariant mass $p_a^2 \gg p_b^2, p_c^2$. We again assign the direction of the momenta as $p_a = -p_b - p_c$, which means we have to take care of minus signs in the particle energies. The kinematics of this approximately collinear process we can describe in terms of the energy fractions z and $1-z$ defined as

$$z = \frac{|E_b|}{|E_a|} = 1 - \frac{|E_c|}{|E_a|} \qquad p_a^2 = (-p_b - p_c)^2 = 2(p_b p_c) = 2z(1-z)(1-\cos\theta)E_a^2 = z(1-z)E_a^2\theta^2 + \mathcal{O}(\theta^4)$$

$$\Leftrightarrow \qquad \theta \equiv \theta_b + \theta_c \simeq \frac{1}{|E_a|}\sqrt{\frac{p_a^2}{z(1-z)}}\,, \tag{II.38}$$

in the collinear limit and in terms of the opening angle θ between $\vec{p}_b$ and $\vec{p}_c$. Because $p_a^2 > 0$ we call this final–state splitting configuration time–like branching. For this configuration we can write down the so-called Sudakov decomposition of the four-momenta

$$-p_a = p_b + p_c = (-zp_a + \beta n + p_T) \;+\; (-(1-z)p_a - \beta n - p_T)\;. \tag{II.39}$$

It defines an arbitrary unit four-vector n, a p_T component orthogonal to the mother momentum p_a and to n, $(p_a p_T) = 0 = (np_T)$, and a free factor β. This way, we can specify n such that it defines the direction of the p_b–p_c decay plane. In this decomposition we can set only one invariant mass to zero, for example that of a radiated gluon $p_c^2 = 0$. The second final state will have a finite invariant mass $p_b^2 \neq 0$.

As specific choice for the three reference four-vectors is

$$p_a = \begin{pmatrix} |E_a| \\ 0 \\ 0 \\ p_{a,3} \end{pmatrix} = |E_a| \begin{pmatrix} 1 \\ 0 \\ 0 \\ 1+\mathcal{O}(\theta) \end{pmatrix} \qquad n = \begin{pmatrix} 1 \\ 0 \\ 0 \\ -1 \end{pmatrix} \qquad p_T = \begin{pmatrix} 0 \\ p_{T,1} \\ p_{T,2} \\ 0 \end{pmatrix}\;. \tag{II.40}$$

Relative to $\vec{p}_a$ we can split the opening angle θ for massless partons according to Figure 2

$$\theta = \theta_b + \theta_c \qquad \text{and} \qquad \frac{\theta_b}{\theta_c} = \frac{p_T}{|E_b|}\left(\frac{p_T}{|E_c|}\right)^{-1} = \frac{1-z}{z} \qquad \Leftrightarrow \qquad \theta = \frac{\theta_b}{1-z} = \frac{\theta_c}{z}\;. \tag{II.41}$$

The momentum choice in Eq.(II.40) has the additional feature that $n^2 = 0$, which allows us to extract β from the

momentum parameterization shown in Eq.(II.39) and the additional condition that $p_c^2 = 0$

$$\begin{aligned} p_c^2 &= (-(1-z)p_a - \beta n - p_T)^2 \\ &= (1-z)^2 p_a^2 + p_T^2 + 2\beta(1-z)(np_a) \\ &= (1-z)^2 p_a^2 + p_T^2 + 4\beta(1-z)|E_a|(1+\mathcal{O}(\theta)) \stackrel{!}{=} 0 \qquad \Leftrightarrow \qquad \beta \simeq -\frac{p_T^2 + (1-z)^2 p_a^2}{4(1-z)|E_a|} \,. \end{aligned} \tag{II.42}$$

Using this specific phase space parameterization we can divide an $(n+1)$-particle process into an n-particle process and a splitting process of quarks and gluons. First, this requires us to split the $(n+1)$-particle phase space into an n-particle phase space and the collinear splitting. The general $(n+1)$-particle phase space separating off the n-particle contribution

$$\begin{aligned} d\Phi_{n+1} &= \cdots \frac{d^3\vec{p}_b}{2(2\pi)^3|E_b|} \frac{d^3\vec{p}_c}{2(2\pi)^3|E_c|} = \cdots \frac{d^3\vec{p}_a}{2(2\pi)^3|E_a|} \frac{d^3\vec{p}_c}{2(2\pi)^3|E_c|} \frac{|E_a|}{|E_b|} \qquad \text{at fixed } p_a \\ &= d\Phi_n \frac{dp_{c,3} dp_T p_T d\phi}{2(2\pi)^3|E_c|} \frac{1}{z} \\ &= d\Phi_n \frac{dp_{c,3} dp_T^2 d\phi}{4(2\pi)^3|E_c|} \frac{1}{z} \end{aligned} \tag{II.43}$$

is best expressed in terms of the energy fraction z and the azimuthal angle ϕ. In other words, separating the $(n+1)$-particle space into an n-particle phase space and a $(1 \to 2)$ splitting phase space is possible without any approximation, and all we have to take care of is the correct prefactors in the new parameterization.

Our next task is to translate the phase space parameters $p_{c,3}$ and p_T^2 appearing in Eq.(II.43) into z and p_a^2. Starting from Eq.(II.39) for $p_{c,3}$ with the third components of p_a and p_T given by Eq.(II.40) we insert β from Eq.(II.42) and obtain

$$\begin{aligned} \frac{dp_{c,3}}{dz} &= \frac{d}{dz}\left[-(1-z)|E_a|(1+\mathcal{O}(\theta)) + \beta\right] = \frac{d}{dz}\left[-(1-z)|E_a|(1+\mathcal{O}(\theta)) - \frac{p_T^2 + (1-z)^2 p_a^2}{4(1-z)|E_a|}\right] \\ &= |E_a|(1+\mathcal{O}(\theta)) - \frac{p_T^2}{4(1-z)^2 E_a} + \frac{p_a^2}{4|E_a|} \\ &= \frac{|E_c|}{1-z}(1+\mathcal{O}(\theta)) - \frac{\theta^2 z^2 E_c^2}{4(1-z)^2 E_a} + \frac{z(1-z)E_a^2\theta^2 + \mathcal{O}(\theta^4)}{4|E_a|} \qquad \text{using Eq.(II.38) and Eq.(II.41)} \\ &= \frac{|E_c|}{1-z} + \mathcal{O}(\theta) \qquad \Leftrightarrow \qquad \frac{dp_{c,3}}{|E_c|} \simeq \frac{dz}{1-z} \,. \end{aligned} \tag{II.44}$$

In addition to substituting $dp_{c,3}$ by dz in Eq.(II.43) we also replace dp_T^2 with dp_a^2 according to

$$\frac{p_T^2}{p_a^2} = \frac{E_b^2\theta_b^2}{z(1-z)E_a^2\theta^2} = \frac{z^2E_a^2(1-z)^2\theta^2}{z(1-z)E_a^2\theta^2} = z(1-z) \quad \Leftrightarrow \quad dp_T^2 = z(1-z)dp_a^2 \,. \tag{II.45}$$

This gives us the final result for the separated collinear phase space

$$\boxed{d\Phi_{n+1} = d\Phi_n \frac{dz\, dp_a^2\, d\phi}{4(2\pi)^3} = d\Phi_n \frac{dz\, dp_a^2}{4(2\pi)^2}} \,, \tag{II.46}$$

where in the second step we assume an azimuthal symmetry.

Adding the matrix element to this factorization of the phase space and ignoring the initial–state flux factor which

is common to both processes we can now postulate a full factorization for one collinear emission in the collinear limit

$$\begin{aligned} d\sigma_{n+1} &= \overline{|\mathcal{M}_{n+1}|^2}\; d\Phi_{n+1} \\ &= \overline{|\mathcal{M}_{n+1}|^2}\; d\Phi_n \frac{dp_a^2\, dz}{4(2\pi)^2}\; (1+\mathcal{O}(\theta)) \\ &\simeq \frac{2g_s^2}{p_a^2}\; \hat{P}(z)\; \overline{|\mathcal{M}_n|^2}\; d\Phi_n \frac{dp_a^2\, dz}{16\pi^2} \qquad \text{assuming} \quad \overline{|\mathcal{M}_{n+1}|^2} \simeq \frac{2g_s^2}{p_a^2}\; \hat{P}(z)\; \overline{|\mathcal{M}_n|^2}\; . \end{aligned} \tag{II.47}$$

Using $d\sigma_n \sim \overline{|\mathcal{M}_n|^2}\; d\Phi_n$ and $g_s^2 = 4\pi\alpha_s$ we can write this relation in its most common form

$$\boxed{\sigma_{n+1} \simeq \int \sigma_n\; \frac{dp_a^2}{p_a^2} dz\; \frac{\alpha_s}{2\pi}\; \hat{P}(z)} \; . \tag{II.48}$$

We can show the assumption of factorizing matrix elements step by step, constructing the appropriate splitting kernels $\hat{P}(z)$ for all different quark and gluon configurations. If Eq.(II.48) really holds true this means that we can compute the $(n+1)$ particle amplitude squared from the n-particle case convoluted with appropriate universal splitting kernels.

As the first parton splitting in QCD we study a gluon splitting into two gluons

$$g(p_a) \to g(p_b) + g(p_c)\; , \tag{II.49}$$

also shown in Figure 2. We can compute it in the collinear configuration given in Eq.(II.38) and find

$$\begin{aligned} \overline{|\mathcal{M}_{n+1}|^2} &= \frac{2g_s^2}{p_a^2}\; \frac{N_c}{2}\; 2\left[\frac{z}{1-z} + z(1-z) + \frac{1-z}{z}\right]\; \overline{|\mathcal{M}_n|^2} \\ &\equiv \frac{2g_s^2}{p_a^2}\; \hat{P}_{g\leftarrow g}(z)\; \overline{|\mathcal{M}_n|^2} \qquad \Leftrightarrow \qquad \hat{P}_{g\leftarrow g}(z) = C_A\left[\frac{z}{1-z} + \frac{1-z}{z} + z(1-z)\right]\; , \end{aligned} \tag{II.50}$$

using $C_A = N_c$. The form of the splitting kernel is symmetric when we exchange the two gluons z and $(1-z)$. It diverges if either of the gluons become soft. The notation $\hat{P}_{i\leftarrow j} \sim \hat{P}_{ij}$ is inspired by a matrix notation which we can use to multiply the splitting matrix from the right with the incoming parton vector to get the final parton vector. Following the logic described above, with this calculation we prove that the factorized form of the $(n+1)$-particle matrix element squared in Eq.(II.47) holds in a Yang-Mills theory.

The same kind of splitting kernel we can compute for the splitting of a gluon into two quarks

$$g(p_a) \to q(p_b) + \bar{q}(p_c)\; . \tag{II.51}$$

In complete analogy to the gluon splitting into two gluons, we can factorize the $(n+1)$-particle matrix element into

$$\begin{aligned} \overline{|\mathcal{M}_{n+1}|^2} &= \frac{g_s^2}{p_a^2}\; T_R \frac{N_c^2-1}{N_c^2-1}\; \left[(1-2z)^2+1\right]\; \overline{|\mathcal{M}_n|^2} \qquad\qquad \text{with } \mathrm{tr} T^a T^b = T_R \delta^{ab} \text{ and } N_a = 2 \\ &= \frac{2g_s^2}{p_a^2}\; T_R\; \left[z^2 + (1-z)^2\right]\; \overline{|\mathcal{M}_n|^2} \\ &\equiv \frac{2g_s^2}{p_a^2} \hat{P}_{q\leftarrow g}(z)\; \overline{|\mathcal{M}_n|^2} \qquad \Leftrightarrow \qquad \hat{P}_{q\leftarrow g}(z) = T_R\left[z^2 + (1-z)^2\right]\; , \end{aligned} \tag{II.52}$$

with $T_R = 1/2$. This splitting kernel is again symmetric in z and $(1-z)$ because QCD does not distinguish between the outgoing quark and the outgoing antiquark.

The third splitting we compute is the splitting of a quark into a quark and a gluon

$$q(p_a) \to q(p_b) + g(p_c)\; . \tag{II.53}$$

It involves the same quark–quark–gluon vertex as the gluon splitting into two quarks. The factorized matrix element

for this channel has the same form as Eq.(II.52), except for the color averaging factor of the now incoming quark,

$$\begin{aligned}\overline{|\mathcal{M}_{n+1}|^2} &= \frac{g_s^2}{p_a^2}\,\frac{N_c^2-1}{2N_c}\,\frac{(1+z)^2+(1-z)^2}{1-z}\,\overline{|\mathcal{M}_n|^2} \\ &= \frac{2g_s^2}{p_a^2}\,C_F\,\frac{1+z^2}{1-z}\,\overline{|\mathcal{M}_n|^2} \\ &\equiv \frac{2g_s^2}{p_a^2}\hat{P}_{q\leftarrow g}(z)\,\overline{|\mathcal{M}_n|^2} \qquad \Leftrightarrow \qquad \hat{P}_{q\leftarrow q}(z) = C_F\frac{1+z^2}{1-z}\;. \end{aligned} \tag{II.54}$$

The color factor for gluon radiation off a quark is $C_F = (N^2-1)/(2N)$. The averaging factor $1/N_a = 2$ now is the number of quark spins in the intermediate state. Just switching $z \leftrightarrow (1-z)$ we can finally read off the kernel for a quark splitting written in terms of the final–state gluon

$$\hat{P}_{g\leftarrow q}(z) = C_F\frac{1+(1-z)^2}{z}\;. \tag{II.55}$$

This result finalizes our calculation of all QCD splitting kernels $\hat{P}_{i\leftarrow j}(z)$ between quarks and gluons . As alluded to earlier, similar to ultraviolet divergences which get removed by counter terms these splitting kernels are universal. They do not depend on the hard n-particle matrix element which is part of the original $(n+1)$-particle process. Based on our four results in Eqs.(II.50), (II.52), (II.54), and (II.55) we have by construction of the kernels $\hat{P}$ shown that the collinear factorization Eq.(II.48) holds at this level in perturbation theory.

Before using this splitting property to describe QCD effects at the LHC we need to look at the splitting of partons in the initial state, meaning $|p_a^2|, p_c^2 \ll |p_b^2|$ where p_b is the momentum entering the hard interaction. The difference to the final–state splitting is that now we can consider the split parton momentum $p_b = p_a - p_c$ as a t-channel diagram, so we already know $p_b^2 = t < 0$ from our usual Mandelstam variables argument. This space–like splitting version of Eq.(II.39) for p_b^2 gives us

$$\begin{aligned} t \equiv p_b^2 &= (-zp_a + \beta n + p_T)^2 \\ &= p_T^2 - 2z\beta(p_a n) \qquad\qquad \text{with } p_a^2 = n^2 = (p_a p_T) = (n p_T) = 0 \\ &= p_T^2 + \frac{p_T^2 z}{1-z} \qquad\qquad \text{using Eq.(II.42)} \\ &= \frac{p_T^2}{1-z} = -\frac{p_{T,1}^2 + p_{T,2}^2}{1-z} < 0\;. \end{aligned} \tag{II.56}$$

The calculation of the splitting kernels and matrix elements is the same as for the time–like case, with the one exception that for splitting in the initial state the flow factor has to be evaluated at the reduced partonic energy $E_b = zE_a$ and that the energy fraction entering the parton density needs to be replaced by $x_b \to zx_b$. The factorized matrix element for initial–state splitting then reads just like Eq.(II.48)

$$\sigma_{n+1} = \int \sigma_n\,\frac{dt}{t}dz\,\frac{\alpha_s}{2\pi}\,\hat{P}(z)\;. \tag{II.57}$$

How to use this property to make statements about the quark and gluon content in the proton will be the focus of the next section.

D. DGLAP equation

Before we include the quantum effects from parton splitting in LHC computations, let us briefly review the classical, statisitical picture of parton densities. At hadron colliders the energy distribution of incoming quarks as parts of the colliding protons has to be taken into account. We first assume that quarks move collinearly with the surrounding proton such that at the LHC incoming partons have zero p_T. Under that condition we can define a probability distribution for finding a parton just depending on the respective fraction of the proton's momentum. For this momentum fraction $x = 0\cdots 1$ the parton density function (pdf) is written as $f_i(x)$, where i denotes the different partons in the proton, for our purposes u, d, c, s, g and, depending on the details, b. All incoming partons we assume to be massless.

In contrast to so-called structure functions a pdf is not an observable. It is a distribution in the mathematical sense, which means it has to produce reasonable results when we integrate it together with a test function. Different parton densities have very different behavior — for the valence quarks (uud) they peak somewhere around $x \lesssim 1/3$, while the gluon pdf is small at $x \sim 1$ and grows very rapidly towards small x. For some typical part of the relevant parameter space ($x = 10^{-3} \cdots 10^{-1}$) the gluon density roughly scales like $f_g(x) \propto x^{-2}$. Towards smaller x values it becomes even steeper. This steep gluon distribution was initially not expected and means that for small enough x LHC processes will dominantly be gluon fusion processes.

While we cannot actually compute parton distribution functions $f_i(x)$ as a function of the momentum fraction x there are a few predictions we can make based on symmetries and properties of the hadrons. Such arguments for example lead to sum rules:

The parton distributions inside an antiproton are linked to those inside a proton through the CP symmetry, which is an exact symmetry of QCD. Therefore, we know that

$$f_q^{\bar{p}}(x) = f_{\bar{q}}(x) \qquad f_{\bar{q}}^{\bar{p}}(x) = f_q(x) \qquad f_g^{\bar{p}}(x) = f_g(x) \tag{II.58}$$

for all values of x. If the proton consists of three valence quarks uud, plus quantum fluctuations from the vacuum which can either involve gluons or quark–antiquark pairs, the contribution from the sea quarks has to be symmetric in quarks and antiquarks. The expectation values for the signed numbers of up and down quarks inside a proton have to fulfill

$$\langle N_u \rangle = \int_0^1 dx \ (f_u(x) - f_{\bar{u}}(x)) = 2 \qquad \langle N_d \rangle = \int_0^1 dx \ (f_d(x) - f_{\bar{d}}(x)) = 1 \ . \tag{II.59}$$

Similarly, the total momentum of the proton has to consist of sum of all parton momenta. We can write this as the expectation value of $\sum x_i$

$$\langle \sum x_i \rangle = \int_0^1 dx \ x \ \left(\sum_q f_q(x) + \sum_{\bar{q}} f_{\bar{q}}(x) + f_g(x) \right) = 1 \tag{II.60}$$

What makes this prediction interesting is that we can compute the same sum only taking into account the measured quark and antiquark parton densities. We find that this modified momentum sum rule only comes to 1/2. Half of the proton momentum is then carried by gluons.

We can use everything we now know about collinear parton splitting to describe incoming partons at hadron colliders. For example in $pp \to Z$ production incoming partons inside the protons transform into each other via collinear splitting until they enter the Z production process as quarks. Taking Eq.(II.57) seriously, a parton density should depend on two parameters, the final energy fraction and the virtuality,

$$f(x, -t) \ . \tag{II.61}$$

The second parameter t is new compared to the purely probabilistic picture described above. To study the parton density as a function of these two parameters, we start with a quark inside the proton with an energy fraction x_0, as it enters the hadronic phase space integral. Since this quark is confined inside the proton it can only have small transverse momentum, which means its four-momentum squared t_0 is negative and its absolute value $|t_0|$ is small. For incoming partons which on–shell have $p^2 = 0$ it gives the distance to the mass shell. Let us simplify our kinematic argument by assuming that there exists only one type of splitting, namely successive gluon radiation off an incoming quark, where the outgoing gluons are not relevant In that case each collinear gluon radiation will decrease the quark energy $x_{j+1} < x_j$ and increase its virtuality $|t_{j+1}| = -t_{j+1} > -t_j = |t_j|$ through its recoil.

From the last section we know what the successive splitting means in terms of splitting probabilities. We can describe how the parton density $f(x, -t)$ evolves in the $(x - t)$ plane as depicted in Figure 3. The starting point (x_0, t_0) is at least probabilistically given by the energy and kind of the hadron, for example the proton. For a given small virtuality $|t_0|$ we start at some kind of fixed x_0 distribution. We then interpret each branching as a step strictly downward in $x_j \to x_{j+1}$ where the t value we assign to this step is the ever increasing virtuality $|t_{j+1}|$ after the branching. Each splitting means a synchronous shift in x and t, so the actual path in the $(x - t)$ plane really consists

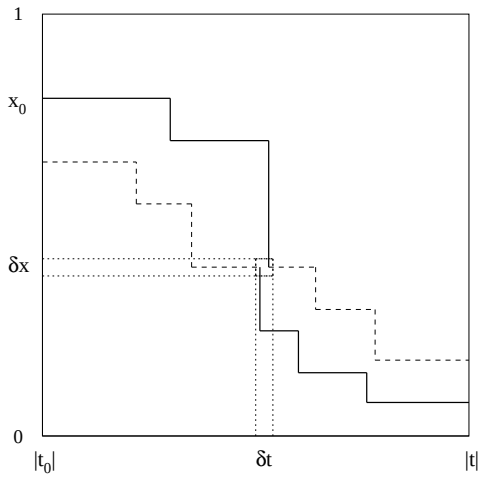

FIG. 3: Path of an incoming parton in the $(x-t)$ plane. Because we define t as a negative number its axis is labelled $|t|$.

of discrete points. The probability of such a splitting to occur is given by $\hat{P}_{q\leftarrow q}(z) \equiv \hat{P}(z)$ as it appears in Eq.(II.57)

$$\frac{\alpha_s}{2\pi}\,\hat{P}(z)\,\frac{dt}{t}\,dz\;. \tag{II.62}$$

In this picture we consider this probability a smooth function in t and z. At the end of the path we will probe this evolved parton density, where x_n and t_n enter the hard scattering process and its energy–momentum conservation.

When we convert a partonic into a hadronic cross section numerically we need to specify the probability of the parton density $f(x,-t)$ residing in an infinitesimal square $[x_j, x_j+\delta x]$ and, if this second parameter has anything to do with physics, $[|t_j|, |t_j|+\delta t]$. Using our (x,t) plane we compute the flows into this square and out of this square, which together define the net shift in f in the sense of a differential equation, similar to the derivation of Gauss' theorem for vector fields inside a surface

$$\delta f_{\text{in}} - \delta f_{\text{out}} = \delta f(x,-t)\;. \tag{II.63}$$

We compute the incoming and outgoing flows from the history of the (x,t) evolution. At this stage our picture becomes a little subtle; the way we define the path between two splittings in Figure 3 it can enter and leave the square either vertically or horizontally. Because we do not consider the movement in the (x,t) plane continuous we can choose this direction as vertical or horizontal. Because we want to arrive at a differential equation in t we choose the vertical drop, such that the area the incoming and outgoing flows see is given by δt. If we define a splitting as such a vertical drop in x at the target value t_{j+1} an incoming path hitting the square at some value t can come from any x value above the square. Using this convention and following the fat solid lines in Figure 3 the vertical flow into the square (x,t) square is proportional to δt and has the form

$$\begin{aligned}
\delta f_{\text{in}}(-t) &= \frac{\delta t}{t}\int_x^1 \frac{dz}{z}\,\frac{\alpha_s}{2\pi}\,\hat{P}(z) f\left(\frac{x}{z},-t\right) \\
&= \frac{\delta t}{t}\int_0^1 \frac{dz}{z}\,\frac{\alpha_s}{2\pi}\,\hat{P}(z) f\left(\frac{x}{z},-t\right) \qquad \text{assuming } f(x',-t)=0 \text{ for } x'>1 \\
&\equiv \delta t\,\left(\frac{\alpha_s \hat{P}}{2\pi t}\otimes f\right)(x,-t)\;.
\end{aligned} \tag{II.64}$$

In the last step we use the definition of a convolution

$$(f\otimes g)(x) = \int_0^1 dx_1 dx_2 f(x_1) g(x_2)\,\delta(x-x_1x_2) = \int_0^1 \frac{dx_1}{x_1} f(x_1) g\left(\frac{x}{x_1}\right) = \int_0^1 \frac{dx_2}{x_2} f\left(\frac{x}{x_2}\right) g(x_2)\;. \tag{II.65}$$

The outgoing flow we define in complete analogy, again leaving the infinitesimal square vertically. Following the fat solid line in Figure 3 it is also proportional to δt

$$\delta f_{\text{out}}(-t) = \delta t \int_0^1 dy \frac{\alpha_s \hat{P}(y)}{2\pi t} f(x,-t) = \frac{\delta t}{t} f(x,-t) \int_0^1 dy \, \frac{\alpha_s}{2\pi} \hat{P}(y) \, . \tag{II.66}$$

The corresponding y integration, unlike the z integration for the incoming flow is not a convolution. This integration appears because we do not know the normalization of $\hat{P}(z)$ distribution which we interpret as a probability. The reason why it is not a convolution is that for the outgoing flow we know the starting condition and integrate over the final configurations; this aspect will become important later. Combining Eq.(II.64) and Eq.(II.66) we can compute the net change in the parton density of the quarks as

$$\begin{aligned}
\delta f(x,-t) &= \frac{\delta t}{t} \left[\int_0^1 \frac{dz}{z} \frac{\alpha_s}{2\pi} \hat{P}(z) \, f\left(\frac{x}{z},-t\right) - \int_0^1 dy \, \frac{\alpha_s}{2\pi} \hat{P}(y) \, f(x,-t) \right] \\
&= \frac{\delta t}{t} \int_0^1 \frac{dz}{z} \frac{\alpha_s}{2\pi} \left[\hat{P}(z) - \delta(1-z) \int_0^1 dy \hat{P}(y) \right] f\left(\frac{x}{z},-t\right) \equiv \frac{\delta t}{t} \int_x^1 \frac{dz}{z} \frac{\alpha_s}{2\pi} \hat{P}(z)_+ \, f\left(\frac{x}{z},-t\right) \\
\Leftrightarrow \qquad \frac{\delta f(x,-t)}{\delta(-t)} &= \frac{1}{(-t)} \int_x^1 \frac{dz}{z} \frac{\alpha_s}{2\pi} \hat{P}(z)_+ \, f\left(\frac{x}{z},-t\right) \, ,
\end{aligned} \tag{II.67}$$

again assuming $f(x) = 0$ for $x > 1$, strictly speaking requiring α_s to only depend on t but not on z, and using the specifically defined plus subtraction

$$\boxed{F(z)_+ \equiv F(z) - \delta(1-z) \int_0^1 dy \, F(y)} \qquad \text{or} \qquad \int_0^1 dz \, \frac{f(z)}{(1-z)_+} = \int_0^1 dz \, \left(\frac{f(z)}{1-z} - \frac{f(1)}{1-z} \right) . \tag{II.68}$$

For the second form above we choose $F(z) = 1/(1-z)$, multiply it with an arbitrary test function $f(z)$ and integrate over z. In contrast to the original z integral the plus–subtracted integral is by definition finite in the limit $z \to 1$, where some of the splitting kernels diverge. For example, the quark splitting kernel including the plus prescription becomes $C_F((1+z^2)/(1-z))_+$. At this stage the plus prescription is simply a convenient way of writing a complicated combination of splitting kernels, but we will see that it also has a physics meaning.

Next, we check that the plus prescription indeed acts as a regularization technique for the parton densities. Obviously, the integral over $f(z)/(1-z)$ is divergent at the boundary $z \to 1$, which we know we can cure using dimensional regularization. The special case $f(z) = 1$ illustrates how dimensional regularization of infrared divergences in the phase space integration Eq.(II.37) works

$$\int_0^1 dz \, \frac{1}{(1-z)^{1-\epsilon}} = \int_0^1 dz \, \frac{1}{z^{1-\epsilon}} = \frac{z^\epsilon}{\epsilon} \bigg|_0^1 = \frac{1}{\epsilon} \qquad \text{with } \epsilon > 0 \, , \tag{II.69}$$

for $4 + 2\epsilon$ dimensions. This change in sign avoids the analytic continuation of the usual value $n = 4 - 2\epsilon$ to $\epsilon < 0$. The dimensionally regularized integral in analogy to Eq.(II.68) we can write as

$$\begin{aligned}
\int_0^1 dz \, \frac{f(z)}{(1-z)^{1-\epsilon}} &= \int_0^1 dz \, \frac{f(z)-f(1)}{(1-z)^{1-\epsilon}} + f(1) \int_0^1 dz \, \frac{1}{(1-z)^{1-\epsilon}} \\
&= \int_0^1 dz \, \frac{f(z)-f(1)}{1-z} \left(1 + \mathcal{O}(\epsilon)\right) + \frac{f(1)}{\epsilon} \\
&= \int_0^1 dz \, \frac{f(z)}{(1-z)_+} \left(1 + \mathcal{O}(\epsilon)\right) + \frac{f(1)}{\epsilon} \qquad \text{by definition} \\
\Leftrightarrow \qquad \int_0^1 dz \, \frac{f(z)}{(1-z)^{1-\epsilon}} - \frac{f(1)}{\epsilon} &= \int_0^1 dz \, \frac{f(z)}{(1-z)_+} \left(1 + \mathcal{O}(\epsilon)\right) \, .
\end{aligned} \tag{II.70}$$

The dimensionally regularized integral minus the pole, *i.e.* the finite part of the dimensionally regularized integral, is the same as the plus–subtracted integral modulo terms of the order ϵ. The third line in Eq.(II.70) shows that the difference between a dimensionally regularized splitting kernel and a plus–subtracted splitting kernel manifests itself

as terms proportional to $\delta(1-z)$. Physically, they represent contributions to a soft–radiation phase space integral.

Before we move on introducing a gluon density we can slightly reformulate the splitting kernel $\hat{P}_{q\leftarrow q}$ in Eq.(II.54). If the plus prescription regularizes the pole at $z \to 1$, what happens when we include the numerator of the regularized function, *e.g.* the quark splitting kernel? The finite difference between these results is

$$\begin{aligned}\left(\frac{1+z^2}{1-z}\right)_+ - (1+z^2)\,\left(\frac{1}{1-z}\right)_+ &= \frac{1+z^2}{1-z} - \delta(1-z)\int_0^1 dy\,\frac{1+y^2}{1-y} - \frac{1+z^2}{1-z} + \delta(1-z)\int_0^1 dy\,\frac{1+z^2}{1-y} \\ &= -\delta(1-z)\int_0^1 dy\,\left(\frac{1+y^2}{1-y} - \frac{2}{1-y}\right) \\ &= \delta(1-z)\int_0^1 dy\,\frac{y^2-1}{y-1} = \delta(1-z)\int_0^1 dy\,(y+1) = \frac{3}{2}\delta(1-z)\,. \end{aligned} \tag{II.71}$$

We can therefore write the quark's splitting kernel in two equivalent ways

$$\boxed{P_{q\leftarrow q}(z) = C_F\left(\frac{1+z^2}{1-z}\right)_+ = C_F\left[\frac{1+z^2}{(1-z)_+} + \frac{3}{2}\delta(1-z)\right]}\,. \tag{II.72}$$

Going back to our evolution in (x,t) space, the infinitesimal version of Eq.(II.67) is the Dokshitzer–Gribov–Lipatov–Altarelli–Parisi or DGLAP integro-differential equation which describes the scale dependence of the quark parton density. As we already know quarks do not only appear in $q \to q$ splitting, but also in gluon splitting. Therefore, we generalize Eq.(II.67) to include the full set of QCD partons, *i.e.* quarks and gluons. This generalization involves a sum over all allowed splittings and the plus–subtracted splitting kernels. For the quark density on the left hand side it is

$$\boxed{\frac{df_q(x,-t)}{d\log(-t)} = -t\,\frac{df_q(x,-t)}{d(-t)} = \sum_{j=q,g}\int_x^1 \frac{dz}{z}\,\frac{\alpha_s}{2\pi}\,P_{q\leftarrow j}(z)\,f_j\left(\frac{x}{z},-t\right)} \qquad \text{with} \quad P_{q\leftarrow j}(z) \equiv \hat{P}_{q\leftarrow j}(z)_+\,. \tag{II.73}$$

Expanding Eq.(II.67) beyond just gluon radiation off hard quarks, we add all relevant parton indices and splittings which lead to a quark density. Including the splitting from gluon to quark we arrive at

$$\begin{aligned}\delta f_q(x,-t) = \frac{\delta t}{t}\,\Bigg[&\int_0^1 \frac{dz}{z}\,\frac{\alpha_s}{2\pi}\,\hat{P}_{q\leftarrow q}(z)\,f_q\left(\frac{x}{z},-t\right) + \int_0^1 \frac{dz}{z}\,\frac{\alpha_s}{2\pi}\,\hat{P}_{q\leftarrow g}(z)\,f_g\left(\frac{x}{z},-t\right) \\ &- \int_0^1 dy\,\frac{\alpha_s}{2\pi}\,\hat{P}_{q\leftarrow q}(y)\,f_q(x,-t)\Bigg]\,. \end{aligned} \tag{II.74}$$

Of the three terms on the right hand side the first and the third together define the plus–subtracted splitting kernel $P_{q\leftarrow q}(z)$, just following the argument above. The second term is a proper convolution and the only term proportional to the gluon parton density. Quarks can be produced in gluon splitting but cannot vanish into it. Therefore, we have to identify the last term in Eq.(II.74) with $P_{q\leftarrow g}$, without adding a plus–regulator

$$\boxed{P_{q\leftarrow g}(z) \equiv \hat{P}_{q\leftarrow g}(z) = T_R\left[z^2 + (1-z)^2\right]}\,. \tag{II.75}$$

In principle, the splitting kernel $\hat{P}_{g\leftarrow q}$ also generates a quark, in addition to the final–state gluon. However, comparing this to the terms proportional to $\hat{P}_{q\leftarrow q}$ they both arise from the same splitting, namely a quark density leaving the infinitesimal square in the $(x-t)$ plane via the splitting $q \to qg$. Including the additional $\hat{P}_{g\leftarrow q}(y)$ would be double counting and should not appear, as the notation $g \leftarrow q$ already suggests.

The second QCD parton density we have to study is the gluon density. The incoming contribution to the infinites-

imal square is given by the sum of four splitting scenarios each leading to a gluon with virtuality $-t_{j+1}$

$$\begin{aligned}\delta f_{\rm in}(-t) &= \frac{\delta t}{t}\int_0^1 \frac{dz}{z}\,\frac{\alpha_s}{2\pi}\,\left[\hat{P}_{g\leftarrow g}(z)\left(f_g\left(\frac{x}{z},-t\right)+f_g\left(\frac{x}{1-z},-t\right)\right)+\hat{P}_{g\leftarrow q}(z)\left(f_q\left(\frac{x}{z},-t\right)+f_{\bar q}\left(\frac{x}{z},-t\right)\right)\right] \\ &= \frac{\delta t}{t}\int_0^1 \frac{dz}{z}\,\frac{\alpha_s}{2\pi}\,\left[2\hat{P}_{g\leftarrow g}(z) f_g\left(\frac{x}{z},-t\right)+\hat{P}_{g\leftarrow q}(z)\left(f_q\left(\frac{x}{z},-t\right)+f_{\bar q}\left(\frac{x}{z},-t\right)\right)\right]\,, \end{aligned} \tag{II.76}$$

using $P_{g\leftarrow\bar q}=P_{g\leftarrow q}$ in the first line and $P_{g\leftarrow g}(1-z)=P_{g\leftarrow g}(z)$ in the second. To leave the volume element in the (x,t) space a gluon can either split into two gluons or radiate one of n_f light-quark flavors. Combining the incoming and outgoing flows we find

$$\begin{aligned}\delta f_g(x,-t) =& \frac{\delta t}{t}\int_0^1 \frac{dz}{z}\,\frac{\alpha_s}{2\pi}\,\left[2\hat{P}_{g\leftarrow g}(z) f_g\left(\frac{x}{z},-t\right)+\hat{P}_{g\leftarrow q}(z)\left(f_q\left(\frac{x}{z},-t\right)+f_{\bar q}\left(\frac{x}{z},-t\right)\right)\right] \\ & -\frac{\delta t}{t}\int_0^1 dy\,\frac{\alpha_s}{2\pi}\,\left[\hat{P}_{g\leftarrow g}(y)+n_f\hat{P}_{q\leftarrow g}(y)\right] f_g(x,-t)\end{aligned} \tag{II.77}$$

We have to evaluate the four terms in this expression one after the other. Unlike in the quark case they do not immediately correspond to regularizing the diagonal splitting kernel using the plus prescription.

First, there exists a contribution to $\delta f_{\rm in}$ proportional to f_q or $f_{\bar q}$ which is not matched by the outgoing flow. From the quark case we already know how to deal with it. For the corresponding splitting kernel there is no regularization through the plus prescription needed, so we define

$$\boxed{P_{g\leftarrow q}(z)\equiv\hat{P}_{g\leftarrow q}(z)=C_F\frac{1+(1-z)^2}{z}}\,. \tag{II.78}$$

This ensures that the off-diagonal contribution to the gluon density is taken into account when we extend Eq.(II.73) to a combined quark/antiquark and gluon form. The structure of the DGLAP equation implies that the two off-diagonal splitting kernels do not include any plus prescription $\hat{P}_{i\leftarrow j}=P_{i\leftarrow j}$. We could have expected this, because off-diagonal kernels are finite in the soft limit, $z\to 1$. Applying a plus prescription would only have modified the splitting kernels at the isolated (zero-measure) point $y=1$ which for a finite value of the integrand does not affect the integral on the right hand side of the DGLAP equation.

Second, the y integral describing the gluon splitting into a quark pair we can compute directly,

$$\begin{aligned}-\int_0^1 dy\,\frac{\alpha_s}{2\pi}\,n_f\,\hat{P}_{q\leftarrow g}(y) &= -\frac{\alpha_s}{2\pi}\,n_f\,T_R\int_0^1 dy\,\left[1-2y+2y^2\right] \qquad\qquad \text{using Eq.(II.75)} \\ &= -\frac{\alpha_s}{2\pi}\,n_f\,T_R\left[y-y^2+\frac{2y^3}{3}\right]_0^1 \\ &= -\frac{2}{3}\,\frac{\alpha_s}{2\pi}\,n_f\,T_R\,.\end{aligned} \tag{II.79}$$

Finally, the terms proportional to the purely gluonic splitting $P_{g\leftarrow g}$ appearing in Eq.(II.77) require some more work. The y integral coming from the outgoing flow has to consist of a finite term and a term we can use to define

the plus prescription for $\hat{P}_{g\leftarrow g}$. We can compute the integral as

$$\begin{aligned}
-\int_0^1 dy\ \frac{\alpha_s}{2\pi}\ \hat{P}_{g\leftarrow g}(y) &= -\frac{\alpha_s}{2\pi}\ C_A\ \int_0^1 dy\ \left[\frac{y}{1-y}+\frac{1-y}{y}+y(1-y)\right] \qquad \text{using Eq.(II.50)} \\
&= -\frac{\alpha_s}{2\pi}\ C_A\ \int_0^1 dy\ \left[\frac{2y}{1-y}+y(1-y)\right] \\
&= -\frac{\alpha_s}{2\pi}\ C_A\ \int_0^1 dy\ \left[\frac{2(y-1)}{1-y}+y(1-y)\right] - \frac{\alpha_s}{2\pi}\ C_A\ \int_0^1 dy\ \frac{2}{1-y} \\
&= -\frac{\alpha_s}{2\pi}\ C_A\ \int_0^1 dy\ \left[-2+y-y^2\right] - \frac{\alpha_s}{2\pi}\ 2C_A\ \int_0^1 dz\ \frac{1}{1-z} \\
&= -\frac{\alpha_s}{2\pi}\ C_A\ \left[-2+\frac{1}{2}-\frac{1}{3}\right] - \frac{\alpha_s}{2\pi}\ 2C_A\ \int_0^1 dz\ \frac{1}{1-z} \\
&= \frac{\alpha_s}{2\pi}\ \frac{11}{6}\ C_A\ - \frac{\alpha_s}{2\pi}\ 2C_A\ \int_0^1 dz\ \frac{1}{1-z}\ . \qquad \text{(II.80)}
\end{aligned}$$

The second term in this result is what we need to replace the first term in the splitting kernel of Eq.(II.50) proportional to $1/(1-z)$ by $1/(1-z)_+$. We can see this using $f(z)=z$ and correspondingly $f(1)=1$ in Eq.(II.68). The two finite terms in Eq.(II.79) and Eq.(II.80) we have to include in the definition of $\hat{P}_{g\leftarrow g}$ ad hoc. Because the regularized splitting kernel appear inside a convolution the two finite terms require an additional term $\delta(1-z)$. Collecting all of them we arrive at

$$\boxed{P_{g\leftarrow g}(z) = 2C_A\ \left(\frac{z}{(1-z)_+}+\frac{1-z}{z}+z(1-z)\right)+\frac{11}{6}\ C_A\ \delta(1-z)-\frac{2}{3}\ n_f\ T_R\ \delta(1-z)}\ . \qquad \text{(II.81)}$$

This result concludes our computation of all four regularized splitting functions which appear in the DGLAP equation Eq.(II.73).

Before discussing and solving the DGLAP equation, let us briefly recapitulate: for the full quark and gluon particle content of QCD we have derived the DGLAP equation which describes a factorization scale dependence of the quark and gluon parton densities. The universality of the splitting kernels is obvious from the way we derive them — no information on the n-particle process ever enters the derivation.

The DGLAP equation is formulated in terms of four splitting kernels of gluons and quarks which are linked to the splitting probabilities, but which for the DGLAP equation have to be regularized. With the help of a plus–subtraction all kernels $P_{i\leftarrow j}(z)$ become finite, including in the soft limit $z\to 1$. However, splitting kernels are only regularized when needed, so the finite off-diagonal quark–gluon and gluon–quark splittings are unchanged. This means the plus prescription really acts as an infrared renormalization, moving universal infrared divergences into the definition of the parton densities. The original collinear divergence has vanished as well.

The only approximation we make in the computation of the splitting kernels is that in the y integrals we implicitly assume that the running coupling α_s does not depend on the momentum fraction. In its standard form and in terms of the factorization scale $\mu_F^2 \equiv -t$ the DGLAP equation reads

$$\boxed{\frac{df_i(x,\mu_F)}{d\log\mu_F^2} = \sum_j \int_x^1 \frac{dz}{z}\ \frac{\alpha_s}{2\pi}\ P_{i\leftarrow j}(z)\ f_j\left(\frac{x}{z},\mu_F\right) = \frac{\alpha_s}{2\pi}\ \sum_j\ \left(P_{i\leftarrow j}\otimes f_j\right)(x,\mu_F)}\ . \qquad \text{(II.82)}$$

E. Collinear logarithms

Solving the integro-differential DGLAP equation Eq.(II.82) for the parton densities is clearly beyond the scope of this writeup. Nevertheless, we will sketch how we would approach this. This will give us some information on the structure of its solutions which we need to understand the physics of the DGLAP equation.

One simplification we can make is to postulate eigenvalues in parton space and solve the equation for them. This gets rid of the sum over partons on the right hand side. One such parton density is the non–singlet parton density,

defined as the difference

$$f_q^{\rm NS} = f_u - f_{\bar u} \; . \tag{II.83}$$

Since gluons cannot distinguish between massless quarks and antiquarks, the gluon contribution to their evolution cancels. This will be true at arbitrary loop order, since flavor symmetries commute with the QCD gauge group. The corresponding DGLAP equation with leading order splitting kernels now reads

$$\frac{df_q^{\rm NS}(x,\mu_F)}{d\log\mu_F^2} = \int_x^1 \frac{dz}{z}\,\frac{\alpha_s}{2\pi}\,P_{q\leftarrow q}(z)\,f_q^{\rm NS}\left(\frac{x}{z},\mu_F\right) = \frac{\alpha_s}{2\pi}\,\left(P_{q\leftarrow q}\otimes f_q^{\rm NS}\right)(x,\mu_F)\;. \tag{II.84}$$

To solve it we need a transformation which simplifies a convolution, leading us to the Mellin transform. Starting from a function $f(x)$ of a real variable x we define the Mellin transform into moment space m

$$\boxed{\mathcal{M}[f](m) \equiv \int_0^1 dx\, x^{m-1} f(x)} \qquad\qquad f(x) = \frac{1}{2\pi i}\int_{c-i\infty}^{c-i\infty} dm\;\frac{\mathcal{M}[f](m)}{x^m}\;, \tag{II.85}$$

where for the back transformation we choose an arbitrary appropriate constant $c > 0$, such that the integration contour for the inverse transformation lies to the right of all singularities of the analytic continuation of $\mathcal{M}[f](m)$. The Mellin transform of a convolution is the product of the two Mellin transforms, which gives us the transformed DGLAP equation

$$\begin{aligned}
&\mathcal{M}[P_{q\leftarrow q}\otimes f_q^{\rm NS}](m) = \mathcal{M}\left[\int_0^1 \frac{dz}{z} P_{q\leftarrow q}\left(\frac{x}{z}\right) f_q^{\rm NS}(z)\right](m) = \mathcal{M}[P_{q\leftarrow q}](m)\;\mathcal{M}[f_q^{\rm NS}](m,\mu_F) \\
\Rightarrow \qquad &\frac{d\mathcal{M}[f_q^{\rm NS}](m,\mu_F)}{d\log\mu_F^2} = \frac{\alpha_s}{2\pi}\,\mathcal{M}[P_{q\leftarrow q}](m) \quad \mathcal{M}[f_q^{\rm NS}](m,\mu_F)\;.
\end{aligned} \tag{II.86}$$

This simple linear, first-order differential equation has the solution

$$\begin{aligned}
\mathcal{M}[f_q^{\rm NS}](m,\mu_F) &= \mathcal{M}[f_q^{\rm NS}](m,\mu_{F,0})\;\exp\left(\frac{\alpha_s}{2\pi}\,\mathcal{M}[P_{q\leftarrow q}](m)\log\frac{\mu_F^2}{\mu_{F,0}^2}\right) \\
&= \mathcal{M}[f_q^{\rm NS}](m,\mu_{F,0})\;\left(\frac{\mu_F^2}{\mu_{F,0}^2}\right)^{\frac{\alpha_s}{2\pi}\mathcal{M}[P_{q\leftarrow q}](m)} \\
&\equiv \mathcal{M}[f_q^{\rm NS}](m,\mu_{F,0})\;\left(\frac{\mu_F^2}{\mu_{F,0}^2}\right)^{\frac{\alpha_s}{2\pi}\gamma(m)}\;,
\end{aligned} \tag{II.87}$$

defining $\gamma(m) = \mathcal{M}[P](m)$.

The solution given by Eq.(II.87) still has the complication that it includes μ_F and α_s as two free parameters. To simplify our result we can include $\alpha_s(\mu_R^2)$ in the running of the DGLAP equation and identify the renormalization scale μ_R of the strong coupling with the factorization scale $\mu_F = \mu_R \equiv \mu$. This allows us to replace $\log\mu^2$ in the DGLAP equation by α_s, including the leading order Jacobian. This is clearly correct for all one-scale problems where we have no freedom to choose either of the two scales. We find

$$\frac{d}{d\log\mu^2} = \frac{d\log\alpha_s}{d\log\mu^2}\,\frac{d}{d\log\alpha_s} = \frac{1}{\alpha_s}\,\frac{d\alpha_s}{d\log\mu^2}\,\frac{d}{d\log\alpha_s} = -\alpha_s b_0\,\frac{d}{d\log\alpha_s}\;. \tag{II.88}$$

This additional factor of α_s on the left hand side will cancel the factor α_s on the right hand side of the DGLAP

equation Eq.(II.86)

$$\begin{aligned}
\frac{d\mathcal{M}[f_q^{\rm NS}](m,\mu)}{d\log\alpha_s} &= -\frac{1}{2\pi b_0}\gamma(m)\ \mathcal{M}[f_q^{\rm NS}](m,\mu) \\
\Rightarrow \qquad \mathcal{M}[f_q^{\rm NS}](m,\mu) &= \mathcal{M}[f_q^{\rm NS}](m,\mu_0)\ \exp\left(-\frac{1}{2\pi b_0}\ \gamma(m)\log\frac{\alpha_s(\mu^2)}{\alpha_s(\mu_0^2)}\right) \\
&= \mathcal{M}[f_q^{\rm NS}](m,\mu_{F,0})\ \left(\frac{\alpha_s(\mu_0^2)}{\alpha_s(\mu^2)}\right)^{\frac{\gamma(m)}{2\pi b_0}} \ . \qquad \text{(II.89)}
\end{aligned}$$

Among other things, in this derivation we neglect that some splitting functions have singularities and therefore the Mellin transform is not obviously well defined. Our convolution is not really a convolution either, because we cut it off at Q_0^2 etc; but the final structure in Eq.(II.89) really holds.

Because we will need it in the next section we emphasize that the same kind of solution appears in pure Yang–Mills theory, *i.e.* in QCD without quarks. Looking at the different color factors in QCD this limit can also be derived as the leading terms in N_c. In that case there also exists only one splitting kernel defining an anomalous dimension γ. We find in complete analogy to Eq.(II.89)

$$\boxed{\mathcal{M}[f_g](m,\mu) = \mathcal{M}[f_g](m,\mu_0)\ \left(\frac{\alpha_s(\mu_0^2)}{\alpha_s(\mu^2)}\right)^{\frac{\gamma(m)}{2\pi b_0}}} \ . \qquad \text{(II.90)}$$

To remind ourselves that in this derivation we unify the renormalization and factorization scales we denote them just as μ. This solution to the DGLAP equation is not completely determined: as a solution to a differential equation it also includes an integration constant which we express in terms of μ_0. The DGLAP equation therefore does not determine parton densities, it only describes their evolution from one scale μ_F to another, just like a renormalization group equation in the ultraviolet.

Remembering how we arrive at the DGLAP equation we notice an analogy to the case of ultraviolet divergences and the running coupling. We start from universal infrared divergences. We describe them in terms of splitting functions which we regularize using the plus prescription. The DGLAP equation plays the role of a renormalization group equation for example for the running coupling. It links parton densities evaluated at different scales μ_F.

In analogy to the scaling logarithms considered in Section II B we now test if we can point to a type of logarithm the DGLAP equation resums by reorganizing our perturbative series of parton splitting. To identify these resummed logarithms we build a physical model based on collinear splitting, but without using the DGLAP equation. We start from the basic equation defining the physical picture of parton splitting in Eq.(II.48). Only taking into account gluons in pure Yang–Mills theory it precisely corresponds to the starting point of our discussion leading to the DGLAP equation, schematically written as

$$\sigma_{n+1} = \int \sigma_n\ \frac{dt}{t} dz\ \frac{\alpha_s}{2\pi}\ \hat{P}_{g\leftarrow g}(z)\ . \qquad \text{(II.91)}$$

This form of collinear factorization does not include parton densities and only applies to final state splittings. To include initial state splittings we need a definition of the virtuality variable t. If we remember that $t = p_b^2 < 0$ we can follow Eq.(II.56) and introduce a positive transverse momentum variable $\vec{p}_T^{\,2}$ in the usual Sudakov decomposition, such that

$$-t = -\frac{p_T^2}{1-z} = \frac{\vec{p}_T^{\,2}}{1-z} > 0 \qquad\qquad \Rightarrow \quad \frac{dt}{t} = \frac{dp_T^2}{p_T^2} = \frac{d\vec{p}_T^{\,2}}{\vec{p}_T^{\,2}}\ . \qquad \text{(II.92)}$$

From the definition of p_T in Eq.(II.39) we see that $\vec{p}_T^{\,2}$ is really the transverse three-momentum of of the parton pair after splitting.

Extending the single parton radiation we consider a ladder of successive splittings of one gluon into two. For a moment, we forget about the actual parton densities and assume that they are part of the hadronic cross section σ_n. In the collinear limit the appropriate convolution gives us

$$\sigma_{n+1}(x,\mu_F) = \int_{x_0}^1 \frac{dx_n}{x_n}\ \hat{P}_{g\leftarrow g}\left(\frac{x}{x_n}\right)\sigma_n(x_n,\mu_0)\int_{\mu_0^2}^{\mu_F^2}\frac{d\vec{p}_{T,n}^{\,2}}{\vec{p}_{T,n}^{\,2}}\frac{\alpha_s(\mu_R^2)}{2\pi}\ . \qquad \text{(II.93)}$$

The dz in Eq.(II.91) we replace by the proper convolution $\hat{P} \otimes \sigma_n$, evaluated at the momentum fraction x. Because the splitting kernel is infrared divergent we cut off the convolution integral at x_0. Similarly, the transverse momentum integral is bounded by an infrared cutoff μ_0 and the physical external scale μ_F. This is the range in which an additional collinear radiation is included in σ_{n+1}.

For splitting the two integrals in Eq.(II.93) it is crucial that μ_0 is the only scale the matrix element σ_n depends on. The other integration variable, the transverse momentum, does not feature in σ_n because collinear factorization is defined in the limit $\vec{p}_T^{\,2} \to 0$. For α_s we will see in the next step how μ_R can depend on the transverse momentum. All through the argument of this subsection we should keep in mind that we are looking for assumptions which allow us to solve Eq.(II.93) and compare the result to the solution of the DGLAP equation. In other words, these assumptions we will turn into a physics picture of the DGLAP equation and its solutions.

Making μ_F the global upper boundary of the transverse momentum integration for collinear splitting is our first assumption. We can then apply the recursion formula in Eq.(II.93) iteratively

$$\begin{aligned}\sigma_{n+1}(x,\mu_F) \sim & \int_{x_0}^1 \frac{dx_n}{x_n}\, \hat{P}_{g\leftarrow g}\left(\frac{x}{x_n}\right) \cdots \int_{x_0}^1 \frac{dx_1}{x_1}\, \hat{P}_{g\leftarrow g}\left(\frac{x_2}{x_1}\right)\, \sigma_1(x_1,\mu_0) \\ & \times \int_{\mu_0}^{\mu_F} \frac{d\vec{p}_{T,n}^{\,2}}{\vec{p}_{T,n}^{\,2}} \frac{\alpha_s(\mu_R^2)}{2\pi} \cdots \int_{\mu_0} \frac{d\vec{p}_{T,1}^{\,2}}{\vec{p}_{T,1}^{\,2}} \frac{\alpha_s(\mu_R^2)}{2\pi}\,. \end{aligned} \tag{II.94}$$

The two sets of integrals in this equation we will solve one by one, starting with the $\vec{p}_T$ integrals.

To be able to make sense of the $\vec{p}_T^{\,2}$ integration in Eq.(II.94) and solve it we have to make two more assumptions in our multiple-splitting model. First, we identify the scale of the strong coupling α_s with the transverse momentum scale of the splitting $\mu_R^2 = \vec{p}_T^{\,2}$. This way we can fully integrate the integrand $\alpha_s/(2\pi)$ and link the final result to the global boundary μ_F.

In addition, we assume strongly ordered splittings in terms of the transverse momentum. If the ordering of the splitting is fixed externally by the chain of momentum fractions x_j, the first splitting, integrated over $\vec{p}_{T,1}^{\,2}$, is now bounded from above by the next external scale $\vec{p}_{T,2}^{\,2}$, which is then bounded by $\vec{p}_{T,3}^{\,2}$, etc. For the n-fold $\vec{p}_T^{\,2}$ integration this means

$$\mu_0^2 < \vec{p}_{T,1}^{\,2} < \vec{p}_{T,2}^{\,2} < \cdots < \mu_F^2 \tag{II.95}$$

At this point this is simply an *ad hoc* assumption which we need to motivate eventually.

Under these three assumptions the transverse momentum integrals in Eq.(II.94) become

$$\begin{aligned} & \int_{\mu_0}^{\mu_F} \frac{d\vec{p}_{T,n}^{\,2}}{\vec{p}_{T,n}^{\,2}} \frac{\alpha_s(\vec{p}_{T,n}^{\,2})}{2\pi} \cdots \int_{\mu_0}^{p_{T,3}} \frac{d\vec{p}_{T,2}^{\,2}}{\vec{p}_{T,2}^{\,2}} \frac{\alpha_s(\vec{p}_{T,2}^{\,2})}{2\pi} \int_{\mu_0}^{p_{T,2}} \frac{d\vec{p}_{T,1}^{\,2}}{\vec{p}_{T,1}^{\,2}} \frac{\alpha_s(\vec{p}_{T,1}^{\,2})}{2\pi} \cdots \\ = & \int_{\mu_0}^{\mu_F} \frac{d\vec{p}_{T,n}^{\,2}}{\vec{p}_{T,n}^{\,2}} \frac{1}{2\pi b_0 \log \dfrac{\vec{p}_{T,n}^{\,2}}{\Lambda^2_{\rm QCD}}} \cdots \int_{\mu_0}^{p_{T,3}} \frac{d\vec{p}_{T,2}^{\,2}}{\vec{p}_{T,2}^{\,2}} \frac{1}{2\pi b_0 \log \dfrac{\vec{p}_{T,2}^{\,2}}{\Lambda^2_{\rm QCD}}} \int_{\mu_0}^{p_{T,2}} \frac{d\vec{p}_{T,1}^{\,2}}{\vec{p}_{T,1}^{\,2}} \frac{1}{2\pi b_0 \log \dfrac{\vec{p}_{T,1}^{\,2}}{\Lambda^2_{\rm QCD}}} \cdots \\ = & \frac{1}{(2\pi b_0)^n} \int_{\mu_0}^{\mu_F} \frac{d\vec{p}_{T,n}^{\,2}}{\vec{p}_{T,n}^{\,2}} \frac{1}{\log \dfrac{\vec{p}_{T,n}^{\,2}}{\Lambda^2_{\rm QCD}}} \cdots \int_{\mu_0}^{p_{T,3}} \frac{d\vec{p}_{T,2}^{\,2}}{\vec{p}_{T,2}^{\,2}} \frac{1}{\log \dfrac{\vec{p}_{T,2}^{\,2}}{\Lambda^2_{\rm QCD}}} \int_{\mu_0}^{p_{T,2}} \frac{d\vec{p}_{T,1}^{\,2}}{\vec{p}_{T,1}^{\,2}} \frac{1}{\log \dfrac{\vec{p}_{T,1}^{\,2}}{\Lambda^2_{\rm QCD}}} \cdots . \end{aligned} \tag{II.96}$$

We can solve the individual integrals by switching variables, for example in the last integral

$$\begin{aligned}\int_{\mu_0}^{p_{T,2}} \frac{d\vec{p}_{T,1}^2}{\vec{p}_{T,1}^2} \frac{1}{\log \frac{\vec{p}_{T,1}^2}{\Lambda^2_{\rm QCD}}} &= \int_{\log\log \mu_0^2/\Lambda^2}^{\log\log p_{T,2}^2/\Lambda^2} d\log\log \frac{\vec{p}_{T,1}^2}{\Lambda^2_{\rm QCD}} \qquad \text{with} \qquad \frac{d(ax)}{(ax)\log x} = d\log\log x \\ &= \int_0^{\log\log p_{T,2}^2/\Lambda^2 - \log\log \mu_0^2/\Lambda^2} d\left(\log\log \frac{\vec{p}_{T,1}^2}{\Lambda^2_{\rm QCD}} - \log\log \frac{\mu_0^2}{\Lambda^2_{\rm QCD}}\right) \\ &= \log \frac{\log \vec{p}_{T,1}^2/\Lambda^2_{\rm QCD}}{\log \mu_0^2/\Lambda^2_{\rm QCD}}\bigg|_0^{\vec{p}_{T,1}^2 \equiv \vec{p}_{T,2}^2} = \log \frac{\log \vec{p}_{T,2}^2/\Lambda^2_{\rm QCD}}{\log \mu_0^2/\Lambda^2_{\rm QCD}} \,. \end{aligned} \tag{II.97}$$

This gives us for the chain of transverse momentum integrals

$$\begin{aligned}&\int_0^{p_{T,n}\equiv\mu_F} d\log \frac{\log \vec{p}_{T,n}^2/\Lambda^2_{\rm QCD}}{\log \mu_0^2/\Lambda^2_{\rm QCD}} \cdots \int_0^{p_{T,2}\equiv p_{T,3}} d\log \frac{\log \vec{p}_{T,2}^2/\Lambda^2_{\rm QCD}}{\log \mu_0^2/\Lambda^2_{\rm QCD}} \int_0^{p_{T,1}\equiv p_{T,2}} d\log \frac{\log \vec{p}_{T,1}^2/\Lambda^2_{\rm QCD}}{\log \mu_0^2/\Lambda^2_{\rm QCD}} \\ &= \int_0^{p_{T,n}\equiv\mu_F} d\log \frac{\log \vec{p}_{T,n}^2/\Lambda^2_{\rm QCD}}{\log \mu_0^2/\Lambda^2_{\rm QCD}} \cdots \int_0^{p_{T,2}\equiv p_{T,3}} d\log \frac{\log \vec{p}_{T,2}^2/\Lambda^2_{\rm QCD}}{\log \mu_0^2/\Lambda^2_{\rm QCD}} \left(\log \frac{\log \vec{p}_{T,2}^2/\Lambda^2_{\rm QCD}}{\log \mu_0^2/\Lambda^2_{\rm QCD}}\right) \\ &= \int_0^{p_{T,n}\equiv\mu_F} d\log \frac{\log \vec{p}_{T,n}^2/\Lambda^2_{\rm QCD}}{\log \mu_0^2/\Lambda^2_{\rm QCD}} \cdots \frac{1}{2}\left(\log \frac{\log \vec{p}_{T,3}^2/\Lambda^2_{\rm QCD}}{\log \mu_0^2/\Lambda^2_{\rm QCD}}\right)^2 \\ &= \int_0^{p_{T,n}\equiv\mu_F} d\log \frac{\log \vec{p}_{T,n}^2/\Lambda^2_{\rm QCD}}{\log \mu_0^2/\Lambda^2_{\rm QCD}} \left(\frac{1}{2}\cdots\frac{1}{n-1}\right)\left(\log \frac{\log \vec{p}_{T,n}^2/\Lambda^2_{\rm QCD}}{\log \mu_0^2/\Lambda^2_{\rm QCD}}\right)^{n-1} \\ &= \frac{1}{n!}\left(\log \frac{\log \mu_F^2/\Lambda^2_{\rm QCD}}{\log \mu_0^2/\Lambda^2_{\rm QCD}}\right)^n = \frac{1}{n!}\left(\log \frac{\alpha_s(\mu_0^2)}{\alpha_s(\mu_F^2)}\right)^n \,. \end{aligned} \tag{II.98}$$

This is the final result for the chain of transverse momentum integrals in Eq.(II.94). By assumption, the strong coupling is evaluated at the factorization scale μ_F, which means we identify $\mu_R \equiv \mu_F$.

To compute the convolution integrals over the momentum fractions in Eq.(II.94),

$$\sigma_{n+1}(x,\mu) \sim \frac{1}{n!}\left(\frac{1}{2\pi b_0}\log\frac{\alpha_s(\mu_0^2)}{\alpha_s(\mu^2)}\right)^n \int_{x_0}^1 \frac{dx_n}{x_n}\,\hat{P}_{g\leftarrow g}\left(\frac{x}{x_n}\right) \cdots \int_{x_0}^1 \frac{dx_1}{x_1}\,\hat{P}_{g\leftarrow g}\left(\frac{x_2}{x_1}\right)\,\sigma_1(x_1,\mu_0)\,, \tag{II.99}$$

we again Mellin transform the equation including the transverse momentum integrals in Eq.(II.98) into moment space

$$\begin{aligned}\mathcal{M}[\sigma_{n+1}](m,\mu) \sim& \frac{1}{n!}\left(\frac{1}{2\pi b_0}\log\frac{\alpha_s(\mu_0^2)}{\alpha_s(\mu^2)}\right)^n \mathcal{M}\left[\int_{x_0}^1 \frac{dx_n}{x_n}\,\hat{P}_{g\leftarrow g}\left(\frac{x}{x_n}\right) \cdots \int_{x_0}^1 \frac{dx_1}{x_1}\,\hat{P}_{g\leftarrow g}\left(\frac{x_2}{x_1}\right)\,\sigma_1(x_1,\mu_0)\right](m) \\ =& \frac{1}{n!}\left(\frac{1}{2\pi b_0}\log\frac{\alpha_s(\mu_0^2)}{\alpha_s(\mu^2)}\right)^n \gamma(m)^n\,\mathcal{M}[\sigma_1](m,\mu_0) \qquad \text{using } \gamma(m) \equiv \mathcal{M}[P](m) \\ =& \frac{1}{n!}\left(\frac{1}{2\pi b_0}\log\frac{\alpha_s(\mu_0^2)}{\alpha_s(\mu^2)}\,\gamma(m)\right)^n \mathcal{M}[\sigma_1](m,\mu_0)\,. \end{aligned} \tag{II.100}$$

We can now sum the production cross sections for n collinear jets and obtain

$$\begin{aligned}\sum_{n=0}^\infty \mathcal{M}[\sigma_{n+1}](m,\mu) =& \mathcal{M}[\sigma_1](m,\mu_0)\,\sum_n \frac{1}{n!}\left(\frac{1}{2\pi b_0}\log\frac{\alpha_s(\mu_0^2)}{\alpha_s(\mu^2)}\,\gamma(m)\right)^n \\ =& \mathcal{M}[\sigma_1](m,\mu_0)\,\exp\left(\frac{\gamma(m)}{2\pi b_0}\,\log\frac{\alpha_s(\mu_0^2)}{\alpha_s(\mu^2)}\right)\,. \end{aligned} \tag{II.101}$$

This way we can write the Mellin transform of the $(n+1)$ particle production rate as the product of the n-particle

	renormalization scale μ_R	factorization scale μ_F
source	ultraviolet divergence	collinear (infrared) divergence
poles cancelled	counter terms (renormalization)	parton densities (mass factorization)
summation	resum self energy bubbles	resum parton splittings
parameter	running coupling $\alpha_s(\mu_R^2)$	running parton density $f_j(x,\mu_F)$
evolution	RGE for α_s	DGLAP equation
large scales	decrease of σ_{tot}	increase of σ_{tot} for gluons/sea quarks
theory background	renormalizability	factorization
	proven for gauge theories	proven all orders for DIS
		proven order-by-order DY...

TABLE II: Comparison of renormalization and factorization scales appearing in LHC cross sections.

rate times a ratio of the strong coupling at two scales

$$\boxed{\sum_{n=0}^{\infty} \mathcal{M}[\sigma_{n+1}](m,\mu) = \mathcal{M}[\sigma_1](m,\mu_0) \left(\frac{\alpha_s(\mu_0^2)}{\alpha_s(\mu^2)}\right)^{\frac{\gamma(m)}{2\pi b_0}}} \,. \tag{II.102}$$

This is the same structure as the DGLAP equation's solution in Eq.(II.90). It means that we should be able to understand the physics of the DGLAP equation using our model calculation of a gluon ladder emission.

We should remind ourselves of the three assumptions we need to make to arrive at this form. There are two assumptions which concern the transverse momenta of the successive radiation: first, the global upper limit on all transverse momenta should be the factorization scale μ_F, with a strong ordering in the transverse momenta. This gives us a physical picture of the successive splittings as well as a physical interpretation of the factorization scale. Second, the strong coupling should be evaluated at the transverse momentum or factorization scale, so all scales are unified, in accordance with the derivation of the DGLAP equation.

Bending the rules of pure Yang–Mills QCD we can come back to the hard process σ_1 as the Drell–Yan process $q\bar{q} \to Z$. Each step in n means an additional parton in the final state, so σ_{n+1} is Z production with n collinear partons On the left hand side of Eq.(II.102) we have the sum over any number of additional collinear partons; on the right hand side we see fixed order Drell–Yan production without any additional partons, but with an exponentiated correction factor. Comparing this to the running parton densities we can draw the analogy that any process computed with a scale dependent parton density where the scale dependence is governed by the DGLAP equation includes any number of collinear partons.

We can also identify the logarithms which are resummed by scale dependent parton densities. Going back to Eq.(II.36) reminds us that we start from the divergent collinear logarithms $\log p_T^{\max}/p_T^{\min}$ arising from the collinear phase space integration. In our model for successive splitting we replace the upper boundary by μ_F. The collinear logarithm of successive initial–state parton splitting diverges for $\mu_0 \to 0$, but it gets absorbed into the parton densities and determines the structure of the DGLAP equation and its solutions. The upper boundary μ_F tells us to what extent we assume incoming quarks and gluons to be a coupled system of splitting partons and what the maximum momentum scale of these splittings is. Transverse momenta $p_T > \mu_F$ generated by hard parton splitting are not covered by the DGLAP equation and hence not a feature of the incoming partons anymore. They belong to the hard process and have to be consistently simulated. While this scale can be chosen freely we have to make sure that it does not become too large, because at some point the collinear approximation $C \simeq$ constant in Eq.(II.36) ceases to hold and with it our entire argument. Only if we do everything correctly, the DGLAP equation resums logarithms of the maximal transverse momentum size of the incoming gluon. They are universal and arise from simple kinematics.

Looking back at Sections II A and II C we introduce the factorization and renormalization scales step by step completely in parallel: first, computing perturbative higher order contributions to scattering amplitudes we encounter ultraviolet and infrared divergences. We regularize both of them using dimensional regularization with $n = 4 - 2\epsilon < 4$ for ultraviolet and $n > 4$ for infrared divergences, linked by analytic continuation. Both kinds of divergences are universal, which means that they are not process or observable dependent. This allows us to absorb ultraviolet and infrared divergences into a re-definition of the strong coupling and the parton density. This nominally infinite shift of parameters we refer to as renormalization for example of the strong coupling or as mass factorization absorbing

infrared divergences into the parton distributions.

After renormalization as well as after mass factorization we are left with a scale artifact. Scales arise as part of a the pole subtraction: together with the pole $1/\epsilon$ we have a choice of finite contributions which we subtract with this pole. Logarithms of the renormalization and factorization scales will always be part of these finite terms. Moreover, in both cases the re-definition of parameters is not based on fixed order perturbation theory. Instead, it involves summing logarithms which otherwise can become large and spoil the convergence of our perturbative series in α_s. The only special feature of infrared divergences as compared to ultraviolet divergences is that to identify the resummed logarithms we have to unify both scales to one.

The hadronic production cross section for the Drell–Yan process or other LHC production channels, now including both scales, reads

$$\sigma_{\text{tot}}(\mu_F,\mu_R) = \int_0^1 dx_1 \int_0^1 dx_2 \sum_{ij} f_i(x_1,\mu_F)\, f_j(x_2,\mu_F)\, \hat{\sigma}_{ij}(x_1x_2S,\alpha_s(\mu_R^2),\mu_F,\mu_R)\,. \tag{II.103}$$

The Drell–Yan process has the particular feature that at leading order $\hat{\sigma}_{q\bar{q}}$ only involves weak couplings, it does not include α_s with its implicit renormalization scale dependence at leading order. Strictly speaking, in Eq.(II.103) the parton densities also depend on the renormalization scale because in their extraction we identify both scales. Carefully following their extraction we can separate the two scales if we need to. Lepton pair production and Higgs production in weak boson fusion are the two prominent electroweak production processes at the LHC.

The evolution of all running parameters from one renormalization/factorization scale to another is described either by renormalization group equation in terms of a beta function in the case of renormalization or by the DGLAP equation in the case of mass factorization. Our renormalization group equation for α_s is a single equation, but in general they are sets of coupled differential equations for all relevant parameters, which again makes them more similar to the DGLAP equation.

There is one formal difference between these two otherwise very similar approaches. The fact that we can absorb ultraviolet divergences into process–independent, universal counter terms is called renormalizability and has been proven to all orders for the kind of gauge theories we are dealing with. The universality of infrared splitting kernels has not (yet) in general been proven, but on the other hand we have never seen an example where is fails for sufficiently inclusive observables like production rates. For a while we thought there might be a problem with factorization in supersymmetric theories using the $\overline{\text{MS}}$ scheme, but this issue has been resolved. A summary of the properties of the two relevant scales for LHC physics we show in Table II.

The way we introduce factorization and renormalization scales clearly labels them as an artifact of perturbation theories with divergences. What actually happens if we include all orders in perturbation theory? For example, the resummation of the self energy bubbles simply deals with one class of diagrams which have to be included, either order-by-order or rearranged into a resummation. Once we include all orders in perturbation theory it does not matter according to which combination of couplings and logarithms we order it. An LHC production rate will then not depend on arbitrarily chosen renormalization or factorization scales μ.

Practically, in Eq.(II.103) we evaluate the renormalized parameters and the parton densities at some scale. This scale dependence will only cancel once we include all implicit and explicit appearances of the scales at all orders. Whatever scale we choose for the strong coupling or parton densities will eventually be compensated by explicit scale logarithms. In the ideal case, these logarithms are small and do not spoil perturbation theory. In a process with one distinct external scale, like the Z mass, we know that all scale logarithms should have the form $\log(\mu/m_Z)$. This logarithm vanishes if we evaluate everything at the 'correct' external energy scale, namely m_Z. In that sense we can think of the running coupling as a proper running observable which depends on the external energy of the process. This dependence on the external energy is not a perturbative artifact, because a cross section even to all orders does depend on the energy. The problem in particular for LHC analyses is that after analysis cuts every process will have more than one external energy scale.

We can turn around the argument of vanishing scale dependence to all orders in perturbation theory. This gives us an estimate of the minimum theoretical error on a rate prediction set by the scale dependence. The appropriate interval of what we consider reasonable scale choices depends on the process and the taste of the people doing this analysis. This error estimate is not at all conservative; for example the renormalization scale dependence of the Drell–Yan production rate or Higgs production in weak boson fusion is zero because α_s only enters are next–to–leading order. At the same time we know that the next–to–leading order correction to the Drell–Yan cross section is of the order of 30%, which far exceeds the factorization scale dependence. Moreover, the different scaling behavior of a hadronic cross section shown in Table II implies that for example gluon–induced processes at typical x values around

10^{-2} show a cancellation of the factorization and renormalization scale variation. Estimating theoretical uncertainties from scale dependence therefore requires a good understanding of the individual process and the way it is affected by the two scales.

Guessing the right scale choice for a process is hard, often impossible. For example in Drell–Yan production at leading order there exists only one scale, m_Z. If we set $\mu = m_Z$ all scale logarithms vanish. In reality, LHC observables include several different scales. Some of them appear in the hard process, for example in the production of two or three particles with different masses. Others enter through the QCD environment where at the LHC we only consider final–state jets above a certain minimal transverse momentum. Even others appear though background rejection cuts in a specific analysis, for example when we only consider the Drell–Yan background for $m_{\mu\mu} > 1$ TeV to Kaluza–Klein graviton production. Using likelihood methods does not improve the situation because the phase space regions dominated by the signal will introduce specific energy scales which affect the perturbative prediction of the backgrounds. This is one of the reasons why an automatic comparison of LHC events with signal or background predictions is bound to fail once it requires an estimate of the theoretical uncertainty on the background simulation.

All that means that in practice there is no way to define a 'correct' scale. On the other hand, there are definitely poor scale choices. For example, using $1000 \times m_Z$ as a typical scale in the Drell–Yan process will if nothing else lead to logarithms of the size $\log 1000$ whenever a scale logarithm appears. These logarithms eventually have to be cancelled to all orders in perturbation theory, inducing unreasonably large higher order corrections.

When describing jet radiation, we usually introduce a phase space dependent renormalization scale, evaluating the strong coupling at the transverse momentum of the radiated jet $\alpha_s(\vec{p}^{\,2}_{T,j})$. This choice gives the best kinematic distributions for the additional partons because in Section II E we have shown that it resums large collinear logarithms.

The transverse momentum of a final–state particle is one of scale choices allowed by factorization; in addition to poor scale choices there also exist wrong scale choices, *i.e.* scale choices violating physical properties we need. Factorization or the Kinoshita–Lee–Nauenberg theorem which ensures that soft divergences cancel between real and virtual emission diagrams are such properties we should not violate — in QED the same property is called the Bloch–Nordsieck cancellation. Imagine picking a factorization scale defined by the partonic initial state, for example the partonic center–of–mass energy $s = x_1 x_2 S$. We know that this definition is not unique: for any final state it corresponds to the well defined sum of all momenta squared. However, virtual and real gluon emission generate different multiplicities in the final state, which means that the two sources of soft divergences only cancel until we multiply each of them with numerically different parton densities. Only scales which are uniquely defined in the final state can serve as factorization scales. For the Drell–Yan process such a scale could be m_Z, or the mass of heavy new-physics states in their production process. So while there is no such thing as a correct scale choice, there are more or less smart choices, and there are definitely very poor choices, which usually lead to an unstable perturbative behavior.

F. Parton shower

In LHC phenomenology we are usually less interested in fixed-order perturbation theory than in logarithmically enhanced QCD effects, for example collinear jet radiation. After introducing the kernels $\hat{P}_{i\leftarrow j}(z)$ as something like splitting probabilities we never applied a probabilistic approach to parton splitting. The basis of such an interpretation are Sudakov factors describing the splitting of a parton i into any of the partons j based on the factorized form Eq.(II.48)

$$\boxed{\Delta_i(t) \equiv \Delta_i(t,t_0) = \exp\left(-\sum_j \int_{t_0}^t \frac{dt'}{t'} \int_0^1 dy\ \frac{\alpha_s}{2\pi} \hat{P}_{j\leftarrow i}(y)\right)} \,. \tag{II.104}$$

We can express all Sudakov factors in terms of splitting functions Γ_j,

$$\begin{aligned} \Delta_q(t) &= \exp\left(-\int_{t_0}^t dt'\ \Gamma_{q\leftarrow q}(t,t')\right) \\ \Delta_g(t) &= \exp\left(-\int_{t_0}^t dt'\ \left[\Gamma_{g\leftarrow g}(t,t') + \Gamma_{q\leftarrow g}(t')\right]\right) \,, \end{aligned} \tag{II.105}$$

which to leading logarithm in $\log(t/t')$ read

$$\begin{aligned}\Gamma_{q\leftarrow q}(t,t') &= \frac{C_F}{2\pi}\,\frac{\alpha_s(t')}{t'}\left(\log\frac{t}{t'}-\frac{3}{2}\right)\\ \Gamma_{g\leftarrow g}(t,t') &= \frac{C_A}{2\pi}\,\frac{\alpha_s(t')}{t'}\left(\log\frac{t}{t'}-\frac{11}{6}\right)\\ \Gamma_{q\leftarrow g}(t') &= \frac{n_f}{6\pi}\,\frac{\alpha_s(t')}{t'}\;. \end{aligned} \tag{II.106}$$

These formulas have a slight problem: terms arising from next–to–leading logarithms spoil the limit $t' \to t$, where a splitting probability should vanish. Technically, we can deal with the finite terms in the Sudakov factors by requiring them to be positive semi–definite, *i.e.* by replacing $\Gamma(t,t') < 0$ with zero. For the general argument this problem with the analytic expressions for the splitting functions is irrelevant. In practice, many modern parton showers do not use these approximate formulas and instead integrate the full splitting kernels.

Instead of going in the details of Sudakov factors we only sketch how such exponentials appear in probabilistic arguments. Using Poisson statistics for something expected to occur $\langle n\rangle$ times, the probability of observing it n times is given by

$$\mathcal{P}(n;\langle n\rangle) = \frac{\langle n\rangle^n\, e^{-\langle n\rangle}}{n!} \qquad\qquad \mathcal{P}(0;\langle n\rangle) = e^{-\langle n\rangle}\;. \tag{II.107}$$

If the exponent in the Sudakov factor describes the integrated splitting probability of a parton i this means that the Sudakov itself describes a non–splitting probability of the parton i into any final state j. In other words, we can use splitting probabilities to describe initial state radiation and final state radiation, including a well-defined probability of no radiation at all.

While the Sudakov factors and splitting probabilities allow us to describe for example the emission of gluons off a hard quark line, there is a crucial piece missing from our collinear resummation argument: multiple gluon emission has to be ordered, and there cannot be interference terms between different emission stages. Such interference diagrams contributing to the full amplitude squared are called non–planar diagrams. There are three reasons to neglect them, even though none of them gives exactly zero for soft and collinear splittings. On the other hand, in combination they make for a very good reason.

First, an arguments for a strongly ordered gluon emission comes from the divergence structure of soft and collinear gluon emission. We start with the kinematical setup for gluon radiation off a massless or massive hard quark leg

The original massive quark leg with momentum $p+k$ and mass m could be attached to some hard process as a splitting final state. It splits into a hard quark p and a soft gluon k. The general matrix element without any approximation reads

$$\begin{aligned}\mathcal{M}_{n+1} &= g_s T^a\,\epsilon^*_\mu(k)\,\bar u(p)\gamma^\mu\frac{\not p+\not k+m}{(p+k)^2-m^2}\,\mathcal{M}_n\\ &= g_s T^a\,\epsilon^*_\mu(k)\,\bar u(p)\left[-\not p\gamma^\mu+2p^\mu+m\gamma^\mu+\gamma^\mu\not k\right]\,\frac{1}{2(pk)+k^2}\,\mathcal{M}_n\\ &= g_s T^a\,\epsilon^*_\mu(k)\,\bar u(p)\frac{2p^\mu+\gamma^\mu\not k}{2(pk)+k^2}\,\mathcal{M}_n\;, \end{aligned} \tag{II.108}$$

using the Dirac equation $\bar u(p)(\not p - m) = 0$. At this level, a further simplification requires for example the soft gluon limit. In the presence of only hard momenta, except for the gluon, we can define it for example as $k^\mu = \lambda p^\mu$, where p^μ is an arbitrary four-vector combination of the surrounding hard momenta. The small parameter λ then characterizes the soft limit. For the invariant mass of the gluon we assume $k^2 = \mathcal{O}(\lambda^2)$, allowing for a slightly off–shell gluon. We find the leading contribution

$$\mathcal{M}_{n+1} \sim g_s T^a\,\epsilon^*_\mu(k)\,\frac{p^\mu}{(pk)}\,\bar u(p)\,\mathcal{M}_n\;. \tag{II.109}$$

To allow for other color states we defines a color operator $\hat T^a_j$ which we insert into the matrix element of Eq.(II.109) and which assumes values of $+T^a_{ij}$ for radiation off a quark, $-T^a_{ji}$ for radiation off an antiquark and $-if_{abc}$ for radiation off a gluon. For a color neutral process like our favorite Drell–Yan process adding an additional soft gluon $q\bar q \to Zg$ we find for the sum of all possible soft emissions $\sum_j \hat T_j = 0$.

Radiating two radiated gluons instead of one look like Each soft splitting comes with a term $(\epsilon^* p)(pk)$, so the two Feynman diagrams give us the combined kinetic terms

$$\begin{aligned}
&\frac{(\epsilon_1 p)}{(p+k_1+k_2)^2-m^2}\frac{(\epsilon_2 p)}{(p+k_2)^2-m^2}+\frac{(\epsilon_2 p)}{(p+k_1+k_2)^2-m^2}\frac{(\epsilon_1 p)}{(p+k_1)^2-m^2}\\
&\quad=\frac{(\epsilon_1 p)}{2(pk_1)+2(pk_2)+(k_1+k_2)^2}\frac{(\epsilon_2 p)}{2(pk_2)}+\frac{(\epsilon_2 p)}{2(pk_1)+2(pk_2)+(k_1+k_2)^2}\frac{(\epsilon_1 p)}{2(pk_1)} \qquad k_1^2=0=k_2^2\\
&\quad\simeq\frac{(\epsilon_1 p)}{2\max_j(pk_j)}\frac{(\epsilon_2 p)}{2(pk_2)}+\frac{(\epsilon_2 p)}{2\max_j(pk_j)}\frac{(\epsilon_1 p)}{2(pk_1)} \qquad (pk_j)\text{ strongly ordered}\\
&\quad\simeq\begin{cases}\dfrac{(\epsilon_1 p)(\epsilon_2 p)}{2\max_j(pk_j)}\,\dfrac{1}{2(pk_2)} & (pk_2)\ll(pk_1)\ \ k_2\text{ softer}\\[2ex] \dfrac{(\epsilon_1 p)(\epsilon_2 p)}{2\max_j(pk_j)}\,\dfrac{1}{2(pk_1)} & (pk_1)\ll(pk_2)\ \ k_1\text{ softer}\,.\end{cases}
\end{aligned}\tag{II.110}$$

For the two Feynman diagrams this means that once one of the gluons is significantly softer than the other the Feynman diagrams with the later soft emission dominates. This argument can be generalized to multiple gluon emission by recognizing that the kinematics will always be dominated by the more divergent propagators towards the final state quark with momentum p. Note, however, that it is based on an ordering of the scalar products (pk_j) interpreted as the softness of the gluons, and we already know that a small value of (pk_j) can as well point to a collinear divergence.

Second, we can derive ordered multiple gluon emission from the phase space integration in the soft limit. For this we need to square this matrix element of Eq.(II.109). It includes a polarization sum and will therefore depend on the gauge. We choose the general axial gauge for massless gauge bosons

$$\sum_{\text{pol}}\epsilon_\mu^*(k)\epsilon_\nu(k)=-g_{\mu\nu}+\frac{k_\mu n_\nu+n_\mu k_\nu}{(nk)}-n^2\frac{k_\mu k_\nu}{(nk)^2}=-g_{\mu\nu}+\frac{k_\mu n_\nu+n_\mu k_\nu}{(nk)}\,,\tag{II.111}$$

with a light-like reference vector n obeying $n^2=0$. The matrix element squared then reads

$$\begin{aligned}
\overline{|\mathcal{M}_{n+1}|^2}&=g_s^2\,\left(-g_{\mu\nu}+\frac{k_\mu n_\nu+n_\mu k_\nu}{(nk)}\right)\left(\sum_j\hat{T}_j^a\frac{p_j^\mu}{(p_jk)}\right)^\dagger\left(\sum_j\hat{T}_j^a\frac{p_j^\nu}{(p_jk)}\right)\,\overline{|\mathcal{M}_n|^2}\\
&=g_s^2\,\left(-\left(\sum_j\hat{T}_j^a\frac{p_j^\mu}{(p_jk)}\right)^\dagger\left(\sum_j\hat{T}_j^a\frac{p_{j\mu}}{(p_jk)}\right)+\frac{2}{(nk)}\left(\sum_j\hat{T}_j^a\right)^\dagger\left(\sum_j\hat{T}_j^a\frac{(p_jn)}{(p_jk)}\right)\right)\overline{|\mathcal{M}_n|^2}\\
&=-g_s^2\,\left(\sum_j\hat{T}_j^a\frac{p_j^\mu}{(p_jk)}\right)^\dagger\left(\sum_j\hat{T}_j^a\frac{p_{j\mu}}{(p_jk)}\right)\,\overline{|\mathcal{M}_n|^2}\,.
\end{aligned}\tag{II.112}$$

The insertion operator in the matrix element has the form of an insertion current multiplied by its hermitian conjugate. This current describes the universal form of soft gluon radiation off an n-particle process

$$\boxed{\overline{|\mathcal{M}_{n+1}|^2}\equiv-g_s^2\,(J^\dagger\cdot J)\,\overline{|\mathcal{M}_n|^2}}\qquad\text{with}\quad J^{a\mu}(k,\{p_j\}=\sum_j\hat{T}_j^a\,\frac{p_j^\mu}{(p_jk)}\,.\tag{II.113}$$

We can further simplify the squared current to

$$
\begin{aligned}
(J^\dagger \cdot J) &= \sum_j \hat{T}_j^a \hat{T}_j^a \; \frac{p_j^2}{(p_j k)^2} + 2 \sum_{i<j} \hat{T}_i^a \hat{T}_j^a \; \frac{(p_i p_j)}{(p_i k)(p_j k)} \\
&= \sum_j \hat{T}_j^a \left(- \sum_{i \neq j} \hat{T}_i^a \right) \frac{p_j^2}{(p_j k)^2} + 2 \sum_{i<j} \hat{T}_i^a \hat{T}_j^a \; \frac{(p_i p_j)}{(p_i k)(p_j k)} \\
&= - \left(\sum_{i<j} + \sum_{i>j} \right) \hat{T}_i^a \hat{T}_j^a \frac{p_j^2}{(p_j k)^2} + 2 \sum_{i<j} \hat{T}_i^a \hat{T}_j^a \; \frac{(p_i p_j)}{(p_i k)(p_j k)} \\
&= 2 \sum_{i<j} \hat{T}_i^a \hat{T}_j^a \; \left(\frac{(p_i p_j)}{(p_i k)(p_j k)} - \frac{p_i^2}{2(p_i k)^2} - \frac{p_j^2}{2(p_j k)^2} \right) \qquad \text{in the general massive case} \\
&= 2 \sum_{i<j} \hat{T}_i^a \hat{T}_j^a \; \frac{(p_i p_j)}{(p_i k)(p_j k)} \qquad \text{for massless partons .}
\end{aligned}
\tag{II.114}
$$

A simple process which will illustrate the relevant point for multiple gluon emission is We first symmetrize the leading soft radiation term with respect to the two hard momenta in a particular way,

$$
\begin{aligned}
(J^\dagger \cdot J)_{12} &= \frac{(p_1 p_2)}{(p_1 k)(p_2 k)} \\
&= \frac{1}{k_0^2} \frac{1 - \cos\theta_{12}}{(1 - \cos\theta_{1k})(1 - \cos\theta_{2k})} \qquad \text{in terms of opening angles } \theta \\
&= \frac{1}{2k_0^2} \left(\frac{1 - \cos\theta_{12}}{(1 - \cos\theta_{1k})(1 - \cos\theta_{2k})} + \frac{1}{1 - \cos\theta_{1k}} - \frac{1}{1 - \cos\theta_{2k}} \right) + (1 \leftrightarrow 2) \\
&\equiv \frac{W_{12}^{[1]} + W_{12}^{[2]}}{k_0^2} \; .
\end{aligned}
\tag{II.115}
$$

The last term is an implicit definition of the two terms $W_{12}^{[1]}$. The pre-factor $1/k_0^2$ is given by the leading soft divergence. The original form of $(J^\dagger J)$ is symmetric in the two indices, which means that both hard partons can take the role of the hard parton and the interference partner. In the new form the symmetry in each of the two terms is broken. Each of the two terms we need to integrate over the gluon's phase space, including the azimuthal angle ϕ_{1k}.

To compute the actual integral we express the three parton vectors in polar coordinates where the initial parton p_1 propagates into the x direction, the interference partner p_2 in the $(x-y)$ plane, and the soft gluon in the full three-dimensional space described by polar coordinates,

$$
\begin{aligned}
\hat{p}_1 &= (1, 0, 0) && \text{hard parton} \\
\hat{p}_2 &= (\cos\theta_{12}, \sin\theta_{12}, 0) && \text{interference partner} \\
\hat{k} &= (\cos\theta_{1k}, \sin\theta_{1k}\cos\phi_{1k}, \sin\theta_{1k}\sin\phi_{1k}) && \text{soft gluon} \\
\Rightarrow \qquad \cos\theta_{2k} &\equiv (\hat{p}_2 \hat{k}) = \cos\theta_{12}\cos\theta_{1k} + \sin\theta_{12}\sin\theta_{1k}\cos\phi_{1k} \; .
\end{aligned}
\tag{II.116}
$$

From the scalar product between these four-vectors we see that of the terms appearing in Eq.(VIII.15) only the opening angle θ_{2k} includes ϕ_{1k}, which for the azimuthal angle integration means

$$
\begin{aligned}
\int_0^{2\pi} d\phi_{1k} \, W_{12}^{[1]} &= \frac{1}{2} \int_0^{2\pi} d\phi_{1k} \; \left(\frac{1 - \cos\theta_{12}}{(1 - \cos\theta_{1k})(1 - \cos\theta_{2k})} + \frac{1}{1 - \cos\theta_{1k}} - \frac{1}{1 - \cos\theta_{2k}} \right) \; . \\
&= \frac{1}{2} \; \frac{1}{1 - \cos\theta_{1k}} \int_0^{2\pi} d\phi_{1k} \; \left(\frac{1 - \cos\theta_{12}}{1 - \cos\theta_{2k}} + 1 - \frac{1 - \cos\theta_{1k}}{1 - \cos\theta_{2k}} \right) \\
&= \frac{1}{2} \; \frac{1}{1 - \cos\theta_{1k}} \left(2\pi + (\cos\theta_{1k} - \cos\theta_{12}) \int_0^{2\pi} d\phi_{1k} \; \frac{1}{1 - \cos\theta_{2k}} \right) \; .
\end{aligned}
\tag{II.117}
$$

The azimuthal angle integral in this expression for $W_{12}^{[i]}$ we can solve

$$\begin{aligned}
\int_0^{2\pi} d\phi_{1k} \frac{1}{1-\cos\theta_{2k}} &= \int_0^{2\pi} d\phi_{1k} \frac{1}{1-\cos\theta_{12}\cos\theta_{1k} - \sin\theta_{12}\sin\theta_{1k}\cos\phi_{1k}} \\
&= \int_0^{2\pi} d\phi_{1k} \frac{1}{a - b\cos\phi_{1k}} \\
&= \oint_{\text{unit circle}} dz\, \frac{1}{iz} \frac{1}{a - b\dfrac{z+1/z}{2}} \qquad \text{with} \quad z = e^{i\phi_{1k}},\ \cos\phi_{1k} = \frac{z+1/z}{2} \\
&= \frac{2}{i} \oint dz\, \frac{1}{2az - b - bz^2} \\
&= \frac{2i}{b} \oint \frac{dz}{(z-z_-)(z-z_+)} \qquad \text{with} \quad z_\pm = \frac{a}{b} \pm \sqrt{\frac{a^2}{b^2} - 1}\,. \qquad \text{(II.118)}
\end{aligned}$$

This integral is related to the sum of all residues of poles inside the closed integration contour. Of the two poles z_- is the one which typically lies within the unit circle, so we find

$$\begin{aligned}
\int_0^{2\pi} d\phi_{1k} \frac{1}{1-\cos\theta_{2k}} &= \frac{2i}{b}\, 2\pi i \frac{1}{z_- - z_+} = \frac{2\pi}{\sqrt{a^2-b^2}} \\
&= \frac{2\pi}{\sqrt{(\cos\theta_{1k} - \cos\theta_{12})^2}} = \frac{2\pi}{|\cos\theta_{1k} - \cos\theta_{12}|}\,. \qquad \text{(II.119)}
\end{aligned}$$

The entire integral in Eq.(VIII.17) then becomes

$$\begin{aligned}
\int_0^{2\pi} d\phi_{1k}\, W_{12}^{[1]} &= \frac{1}{2}\, \frac{1}{1-\cos\theta_{1k}} \left(2\pi + (\cos\theta_{1k} - \cos\theta_{12})\ \frac{2\pi}{|\cos\theta_{1k} - \cos\theta_{12}|} \right) \\
&= \frac{\pi}{1-\cos\theta_{1k}} \left(1 + \text{sign}(\cos\theta_{1k} - \cos\theta_{12})\right) \\
&= \begin{cases} \dfrac{2\pi}{1-\cos\theta_{1k}} & \text{if} \quad \theta_{1k} < \theta_{12} \\ 0 & \text{else}\,. \end{cases} \qquad \text{(II.120)}
\end{aligned}$$

The soft gluon is only radiated at angles between zero and the opening angle of the initial parton p_1 and its hard interference partner or spectator p_2. The same integral over $W_{12}^{[2]}$ gives the same result, with switched roles of p_1 and p_2. Combining the two permutations this means that the soft gluon is always radiated within a cone centered around one of the hard partons and with a radius given by the distance between the two hard partons. The coherent sum of diagrams reduces to an incoherent sum. This derivation angular ordering is exact in the soft limit.

There is a simple physical argument for this suppressed radiation outside a cone defined by the radiating legs. Part of the deviation is that the over–all process is color–neutral. This means that once the gluon is far enough from the two quark legs it will not resolve their individual charges but only feel the combined charge. This screening leads to an additional suppression factor of the kind $\theta_{12}^2/\theta_{1k}^2$. This effect is called coherence.

The third argument for ordered emission comes from color factors. Crossed successive splittings or interference terms between different orderings are color suppressed. For example in the squared diagram for three jet production in e^+e^- collisions the additional gluon contributes a color factor

$$\text{tr}(T^a T^a) = \frac{N_c^2 - 1}{2} = N_c C_F \qquad \text{(II.121)}$$

When we consider the successive radiation of two gluons the ordering matters. As long as the gluon legs do not cross

each other we find the color factor

$$\begin{aligned}
\mathrm{tr}(T^a T^a T^b T^b) &= (T^a T^a)_{il} (T^b T^b)_{li} \\
&= \frac{1}{4}\left(\delta_{il}\delta_{jj} - \frac{\delta_{ij}\delta_{jl}}{N_c}\right)\left(\delta_{il}\delta_{jj} - \frac{\delta_{ij}\delta_{jl}}{N_c}\right) \qquad \text{using} \quad T^a_{ij} T^a_{kl} = \frac{1}{2}\left(\delta_{il}\delta_{jk} - \frac{\delta_{ij}\delta_{kl}}{N_c}\right) \\
&= \frac{1}{4}\left(\delta_{il} N_c - \frac{\delta_{il}}{N_c}\right)\left(\delta_{il} N_c - \frac{\delta_{il}}{N_c}\right) \\
&= N_c \left(\frac{N_c^2 - 1}{2N_c}\right)^2 = N_c C_F^2 = \frac{16}{3}
\end{aligned} \tag{II.122}$$

Similarly, we can compute the color factor when the two gluon lines cross. We find

$$\mathrm{tr}(T^a T^b T^a T^b) = -\frac{N_c^2 - 1}{4N_c} = -\frac{C_F}{2} = -\frac{2}{3}\,. \tag{II.123}$$

Numerically, this color factor is suppressed compared to 16/3. This kind of behavior is usually quoted in powers of N_c where we assume N_c to be large. In those terms non–planar diagrams are suppressed by a factor $1/N_c^2$ compared to the planar diagrams.

Once we also include the triple gluon vertex we can radiate two gluons off a quark leg with the color factor

$$\mathrm{tr}(T^a T^b)\; f^{acd} f^{bcd} = \frac{\delta^{ab}}{2}\; N_c \delta^{ab} = \frac{N_c(N_c^2 - 1)}{2} = N_c^2 C_F = \frac{36}{3}\,. \tag{II.124}$$

This is not suppressed compared to successive planar gluon emission, neither in actual numbers not in the large-N_c limit.

We can try the same argument for a purely gluonic theory, *i.e.* radiating gluons off two hard gluons in the final state. The color factor for single gluon emission after squaring is

$$f^{abc} f^{abc} = N_c \delta^{aa} = N_c(N_c^2 - 1) \sim N_c^3\,, \tag{II.125}$$

using the large-N_c limit in the last step. For planar double gluon emission with the exchanged gluon indices b and f we find

$$f^{abd} f^{abe} f^{dfg} f^{efg} = N_c \delta^{de}\; N_c \delta^{de} \sim N_c^4\,. \tag{II.126}$$

Splitting one radiated gluon into two gives

$$f^{abc}\; f^{cef} f^{def}\; f^{abd} = N_c \delta^{cd}\; N_c \delta^{cd} \sim N_c^4\,. \tag{II.127}$$

This means that planar emission of two gluons and successive splitting of one into two gluons cannot be separated based on the color factor. We can use the color factor argument only for abelian splittings to justify ordered gluon emission.

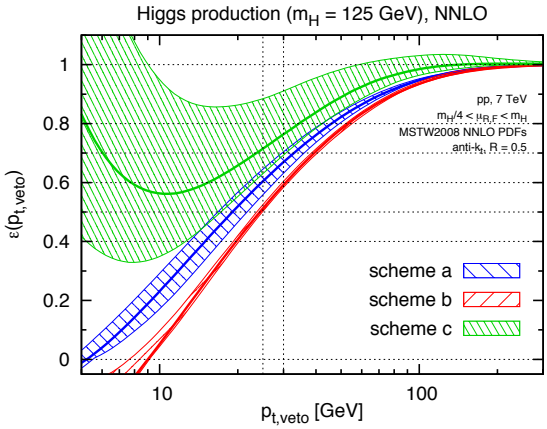

FIG. 4: Different predictions for the jet veto survival probability P_{pass} as a function of the maximum allowed $p_{T,j}$. The example process chosen is Higgs production in gluon fusion. The shaded regions indicate the independent variation of the factorization and renormalization scales within $[m_H/4, m_H]$ requiring μ_R/μ_F to lie within $[0.5, 2]$. The figure and the corresponding physics argument are taken from Ref. [**?**].

III. JETS

Until now we have described QCD in terms of its fundamental constituents, the quarks and the gluons. This framework is the same for all applications of QCD, including collider physics. On the other hand, from the running of the strong coupling we already know that a perturbative theory of quarks and gluons will at some point hit its self-consistency conditions. At colliders this defines the transition from partons to jets, where jets are defined as a spray of particles coming from a highly energetic produced parton. In this chapter we will start from quarks and gluons and slowly transition to jets at the LHC and some very recent developments in this direction.

A. Jet counting

In Higgs physics and other QCD applications the number of jets radiated from the initial (and final) state is an important observable which separates signals from backgrounds. From our discussion of collinear divergences we know that any perturbative calculation for a hadron collider by definition includes any number of collinear jets from initial state splittings. This means that the number of jets in an event in perturbatively very hard to compute: on the one hand, for a given hard process the number of jets is defined through the process; on the other hand, any number of collinear jets is always included, but only in the collinear and hence unobservable phase space configuration.

Experimentally, we can assign a probability pattern to the radiation of jets from the core process. As an example we assume NNLO or two-loop precision for an LHC production rate

$$\sigma = \sigma_0 + \alpha_s \sigma_1 + \alpha_s^2 \sigma_2 \; , \tag{III.1}$$

where we omit the over–all power of α_s in σ_0. Consequently, we define the cross section passing a cut on the number of jets or a jet veto as

$$\sigma^{(\text{pass})} \equiv P_{\text{pass}} \; \sigma = \sum_j \alpha_s^j \sigma_j^{(\text{pass})} \; . \tag{III.2}$$

This relation defines a survival probability P_{pass} of a jet veto. If we assume that the leading order prediction only includes a Higgs or a lepton pair in the final state, we know that $\sigma_0^{(\text{pass})} = \sigma_0$. Perturbatively we can compute the jet veto survival probability as

$$P_{\text{pass}}^{(\text{a})} = \frac{\sigma^{(\text{pass})}}{\sigma} = \frac{\sigma_0 + \alpha_s \sigma_1^{(\text{pass})} + \alpha_s^2 \sigma_2^{(\text{pass})}}{\sigma_0 + \alpha_s \sigma_1 + \alpha_s^2 \sigma_2} \; , \tag{III.3}$$

The result as a function of the maximum allowed $p_{T,j}$ is shown as 'scheme a' in Figure 24. The shaded region is an estimate of the theoretical uncertainty of this prediction.

Alternatively, we can argue that the proper perturbative observable is the fraction of vetoed events $(1 - P_{\text{pass}})$. Indeed, for small values of α_s the jet radiation probability vanishes and with it $(1 - P_{\text{pass}}) \sim \alpha_s \to 0$. This vetoed event fraction we can compute as $\sigma_j - \sigma_j^{(\text{pass})}$ for $j \geq 0$. However, we need to keep in mind that in the presence of an additional hard jet the NNLO rate prediction reduces to NLO accuracy of the inclusive process, so we include only the two leading terms in the numerator and denominator,

$$\begin{aligned} 1 - P_{\text{pass}}^{(\text{b})} &= \alpha_s \, \frac{\sigma_1 - \sigma_1^{(\text{pass})} + \alpha_s(\sigma_2 - \sigma_2^{(\text{pass})})}{\sigma_0 + \alpha_s \sigma_1} \\ P_{\text{pass}}^{(\text{b})} &= 1 - \alpha_s \, \frac{\sigma_1 - \sigma_1^{(\text{pass})} + \alpha_s(\sigma_2 - \sigma_2^{(\text{pass})})}{\sigma_0 + \alpha_s \sigma_1} = \frac{\sigma_0 + \alpha_s \sigma_1^{(\text{pass})} + \alpha_s^2 \sigma_2^{(\text{pass})} - \alpha_s^2 \sigma_2}{\sigma_0 + \alpha_s \sigma_1} \, . \end{aligned} \tag{III.4}$$

This defines 'scheme b' in Figure 24. Obviously, in Eq.(VIII.4) we can move the term $-\alpha_s^2 \sigma_2$ into the denominator and arrive at Eq.(VIII.3) within the uncertainty defined by the unknown α_s^3 terms.

Finally, we can consistently expand the definition of P_{pass} as the ratio given in Eq.(VIII.3). The two leading derivatives of a ratio read

$$\begin{aligned} \left(\frac{f}{g}\right)' &= \frac{f'g - fg'}{g^2} \overset{f=g}{=} \frac{f' - g'}{g} \\ \left(\frac{f}{g}\right)'' &= \left(\frac{f'g}{g^2} - \frac{fg'}{g^2}\right)' = \frac{(f'g)'g^2 - f'g2gg'}{g^4} - \frac{(fg')'g^2 - fg'2gg'}{g^4} \\ &= \frac{(f'g)' - 2f'g'}{g^2} - \frac{(fg')'g - 2fg'g'}{g^3} = \frac{f''g - f'g'}{g^2} - \frac{fg''g - fg'g'}{g^3} \overset{f=g}{=} \frac{f'' - g''}{g} - \frac{g'(f' - g')}{g^2} \end{aligned} \tag{III.5}$$

In the last steps we assume $f = g$ at the point where we evaluate the Taylor expansion. Applied to the perturbative QCD series for $(1 - P_{\text{pass}})$ around the zero-coupling limit this gives us

$$\begin{aligned} 1 - P_{\text{pass}}^{(\text{c})} &= 1 - \frac{\sigma_0 + \alpha_s \sigma_1^{(\text{pass})} + \alpha_s^2 \sigma_2^{(\text{pass})} + \cdots}{\sigma_0 + \alpha_s \sigma_1 + \alpha_s^2 \sigma_2 + \cdots} \\ P_{\text{pass}}^{(\text{c})} &= 1 + \alpha_s \, \frac{\sigma_1^{(\text{pass})} - \sigma_1}{\sigma_0} + \alpha_s^2 \, \frac{\sigma_2^{(\text{pass})} - \sigma_2}{\sigma_0} - \alpha_s^2 \, \frac{\sigma_1(\sigma_1^{(\text{pass})} - \sigma_1)}{\sigma_0^2} \, , \end{aligned} \tag{III.6}$$

defining 'scheme c' in Figure 24. The numerical results indicate that the three schemes are inconsistent within their theoretical uncertainties, and that the most consistent Taylor expansion around perfect veto survival probabilities is doing particularly poorly. Towards small $p_{T,j}$ veto ranges the fixed order perturbative approach clearly fails.

A first, non-perturbative ansatz for the calculation of the number of radiated jets is motivated by soft photon or gluon emission. In the eikonal approximation we know that the number of successively radiated jets is a Poisson distribution in the numbers of jets. If we assume such a Poisson distribution, the probability of observing exactly n jets given an expected $\langle n \rangle$ jets is

$$\mathcal{P}(n; \langle n \rangle) = \frac{\langle n \rangle^n e^{-\langle n \rangle}}{n!} \qquad \Rightarrow \qquad \boxed{P_{\text{pass}} \equiv \mathcal{P}(0; \langle n \rangle) = e^{-\langle n \rangle}} \, . \tag{III.7}$$

This probability links rates for exactly n jets, no at least n jets, *i.e.* it described the exclusive number of jets. A Poisson distribution is normalized to unity, once we sum over all possible jet multiplicities n. We consistently fix the expectation value in terms of the inclusive cross sections producing at least zero or at least one jet,

$$\langle n \rangle = \frac{\sigma_1(p_T^{\text{min}})}{\sigma_0} \, . \tag{III.8}$$

We include an infra-red cut-off p_T^{min}, defining a cross section in the presence of soft and collinear divergences. The inclusive jet ratio σ_1/σ_0 is reproduced by the ratio of the corresponding Poisson distributions. Including this expectation value $\langle n \rangle$ into Eq.(III.7) returns a veto survival probability of $\exp(-\sigma_1/\sigma_0)$.

A second ansatz comes from UA1 and UA2 data, 'phenomenologically' assuming a constant probability of radiating

a jet. In terms of the inclusive cross sections σ_n, *i.e.* the production rate for the radiation of at least n jets, this implies

$$\frac{\sigma_{n+1}(p_T^{\min})}{\sigma_n(p_T^{\min})} = R^{(\text{incl})}_{(n+1)/n}(p_T^{\min}) \; . \tag{III.9}$$

The expected number of jets is then given by

$$\begin{aligned}\langle n\rangle &= \frac{1}{\sigma_0}\sum_{j=1} j(\sigma_j - \sigma_{j+1}) = \frac{1}{\sigma_0}\left(\sum_{j=1} j\sigma_j - \sum_{j=2}(j-1)\sigma_j\right) = \frac{1}{\sigma_0}\sum_{j=1}\sigma_j \\ &= \frac{\sigma_1}{\sigma_0}\sum_{j=0}(R^{(\text{incl})}_{(n+1)/n})^j = \frac{R^{(\text{incl})}_{(n+1)/n}}{1-R^{(\text{incl})}_{(n+1)/n}} \; ,\end{aligned} \tag{III.10}$$

if $R^{(\text{incl})}_{(n+1)/n}$ is a constant. Radiating jets with such a constant probability has been observed at many experiments, including most recently the LHC, and is in the context of W+jets referred to as staircase scaling. The defining property of staircase scaling is that ratios of the $(n+1)$-jet rate to the n-jet rate for inclusive and exclusive jet rates are identical,

$$\begin{aligned}R^{(\text{incl})}_{(n+1)/n} &= \frac{\sigma_{n+1}}{\sigma_n} = \frac{\sum_{j=n+1}^{\infty}\sigma_j^{(\text{excl})}}{\sigma_n^{(\text{excl})} + \sum_{j=n+1}^{\infty}\sigma_j^{(\text{excl})}} \\ &= \frac{\sigma_{n+1}^{(\text{excl})}\sum_{j=0}^{\infty} R^j_{(n+1)/n}}{\sigma_n^{(\text{excl})} + \sigma_{n+1}^{(\text{excl})}\sum_{j=0}^{\infty} R^j_{(n+1)/n}} \qquad \text{with} \quad R_{(n+1)/n} = \frac{\sigma_{n+1}^{(\text{excl})}}{\sigma_n^{(\text{excl})}} \\ &= \frac{\dfrac{R_{(n+1)/n}\sigma_n^{(\text{excl})}}{1-R_{(n+1)/n}}}{\sigma_n^{(\text{excl})} + \dfrac{R_{(n+1)/n}\sigma_n^{(\text{excl})}}{1-R_{(n+1)/n}}} = \frac{R_{(n+1)/n}}{1-R_{(n+1)/n}+R_{(n+1)/n}} \\ &= R_{(n+1)/n} \; .\end{aligned} \tag{III.11}$$

For the Poisson distribution and the staircase distribution we can summarize the main properties of the n-jet rates in terms of the upper incomplete gamma function $\Gamma(n,\langle n\rangle)$:

	staircase scaling	Poisson scaling
$\sigma_n^{(\text{excl})}$	$\sigma_0^{(\text{excl})}\; e^{-bn}$	$\sigma_0\; \dfrac{e^{-\langle n\rangle}\langle n\rangle^n}{n!}$
$R_{(n+1)/n} = \dfrac{\sigma_{n+1}^{(\text{excl})}}{\sigma_n^{(\text{excl})}}$	e^{-b}	$\dfrac{\langle n\rangle}{n+1}$
$R^{(\text{incl})}_{(n+1)/n} = \dfrac{\sigma_{n+1}}{\sigma_n}$	e^{-b}	$\left(\dfrac{(n+1)\,e^{-\langle n\rangle}\,\langle n\rangle^{-(n+1)}}{\Gamma(n+1)-n\Gamma(n,\langle n\rangle)}+1\right)^{-1}$
$\langle n\rangle$	$\dfrac{1}{2}\dfrac{1}{\cosh b - 1}$	$\langle n\rangle$
P_{pass}	$1-e^{-b}$	$e^{-\langle n\rangle}$

B. Generating functional

A crucial question is if we can derive the Poisson and staircase scaling patterns from QCD. From our discussion of parton splittings we know that the number of radiated jets is well defined after a simple resummation. So-called

generating functionals for the jet multiplicity allow us to calculate resummed jet quantities from first principles in QCD. We construct a generating functional in an arbitrary parameter u by demanding that repeated differentiation at $u = 0$ gives exclusive multiplicity distributions $P_n \equiv \sigma_n/\sigma_{\text{tot}}$,

$$\boxed{\Phi = \sum_{n=1}^{\infty} u^n P_{n-1}} \qquad \text{with} \quad P_{n-1} = \frac{\sigma_{n-1}}{\sigma_{\text{tot}}} = \frac{1}{n!}\frac{d^n}{du^n}\Phi\bigg|_{u=0} . \tag{III.12}$$

For Φ we will suppress the argument u. In the application to gluon emission the explicit factor $1/n!$ corresponds to the phase space factor for identical bosons. Because in P_n we only count radiated jets, our definition uses P_{n-1} where other conventions use P_n. A second observable we can extract from Φ is the average jet multiplicity,

$$\frac{d\Phi}{du}\bigg|_{u=1} = \sum_{n=1}^{\infty} n\, u^{n-1}\, \frac{\sigma_{n-1}}{\sigma_{\text{tot}}}\bigg|_{u=1} = 1 + \frac{1}{\sigma_{\text{tot}}}\sum_{n=1}^{\infty}(n-1)\,\sigma_{n-1} . \tag{III.13}$$

In analogy to the DGLAP equation we can derive an evolution equation for Φ. We start by quoting the fact that for the parton densities and the Sudakov factors defined in Eq.(II.104) the there exists an evolution equation

$$f_i(x,t) = \Delta_i(t,t_0) f_i(x,t_0) + \int_{t_0}^{t}\frac{dt'}{t'}\,\Delta_i(t,t')\sum_j \int_0^{1-\epsilon}\frac{dz}{z}\,\frac{\alpha_s}{2\pi}\,\hat{P}_{i\leftarrow j}(z)\, f_j\left(\frac{x}{z},t'\right) . \tag{III.14}$$

This form reflects our interpretaion of the Sudakov factor as a non-splitting probability. We can motivate the corresponding equation for the generating functional Φ by remembering our probabilistic picture of parton splittings $i \to jk$ in the final state. The splitting particles are then described by generating functionals $\Phi(t)$ instead of parton densities $f(x,t)$, giving us

$$\boxed{\Phi_i(t) = \Delta_i(t,t_0)\Phi_i(t_0) \; + \int_{t_0}^{t}\frac{dt'}{t'}\Delta_i(t,t')\sum_{i\to j,k}\int_0^1 dz\,\frac{\alpha_s}{2\pi}\,\hat{P}_{i\to jk}(z)\,\Phi_j(z^2t')\Phi_k((1-z)^2t')}\,. \tag{III.15}$$

The difference to the DGLAP equation is that the generating functionals just count jets. Unlike for the parton densities the evolution equation does not include a convolution, but instead two generating functionals under the integral. The argument of the strong coupling we assume, without any further motivation, as $\alpha_s(z^2(1-z)^2t')$. It will become clear during our computation that this scale choice is appropriate.

The argument in this section will go two ways: first, we write down a proper differential evolution equation for $\Phi_q(t)$. Then, we solve this equation for quarks, only including the abelian splitting $q \to qg$. To start with, we insert the unregularized splitting kernel from Eq.(II.54) into the evolution equation,

$$\begin{aligned}
\Phi_q(t) &= \Delta_q(t,t_0)\Phi_q(t_0) \; + \int_{t_0}^{t}\frac{dt'}{t'}\Delta_q(t,t')\int_0^1 dz\,\frac{\alpha_s}{2\pi}\,C_F\frac{1+z^2}{1-z}\,\Phi_q(z^2t')\Phi_g((1-z)^2t') \\
&= \Delta_q(t,t_0)\Phi_q(t_0) \; + \int_{t_0}^{t}\frac{dt'}{t'}\Delta_q(t,t')\int_0^1 dz\,\frac{\alpha_s C_F}{2\pi}\,\frac{-(1-z)(1+z)+2}{1-z}\,\Phi_q(z^2t')\Phi_g((1-z)^2t') \\
&= \Delta_q(t,t_0)\Phi_q(t_0) \; + \int_{t_0}^{t}\frac{dt'}{t'}\Delta_q(t,t')\int_0^1 dz\,\frac{\alpha_s C_F}{2\pi}\,\left(\frac{2}{1-z}-1-z\right)\,\Phi_q(z^2t')\Phi_g((1-z)^2t') .
\end{aligned} \tag{III.16}$$

We can simplify the divergent part of Eq.(III.16) using the new integration parameter $t'' = (1-z)^2t'$. This gives us the Jacobian

$$\frac{dt''}{dz} = \frac{d}{dz}(1-z)^2t' = 2(1-z)(-1)t' = -2\frac{t''}{1-z} \qquad \Leftrightarrow \qquad \frac{dz}{1-z} = -\frac{1}{2}\,\frac{dt''}{t''} . \tag{III.17}$$

In addition, we approximate $z \to 1$ wherever possible in the divergent term and cut off all t integrations at the infrared

resolution scale t_0. This will give us the leading logarithm in t space,

$$\int_0^1 dz\ \frac{\alpha_s(z^2(1-z)^2t')C_F}{2\pi}\ \frac{2}{1-z}\ \Phi_q(z^2t')\Phi_g((1-z)^2t') = \Phi_q(t')\int_{t_0}^{t'} dt''\ \frac{\alpha_s(t'')C_F}{2\pi}\frac{1}{t''}\Phi_g(t'')\ . \tag{III.18}$$

For the finite part in Eq.(III.16) we neglect the logarithmic z dependence of all functions and integrate the leading power dependence $1+z$ to 3/2,

$$-\int_0^1 dz\ \frac{\alpha_s(z^2(1-z)^2t')C_F}{2\pi}\ (1+z)\ \Phi_q(z^2t')\Phi_g((1-z)^2t') \simeq -\frac{\alpha_s(t')C_F}{2\pi}\ \frac{3}{2}\ \Phi_q(t')\Phi_g(t')\ . \tag{III.19}$$

Strictly speaking, the strong coupling as well as the two generating functionals could be evaluated at any typical scale covered by the z integral, considering that the prefactor $1+z$ grows towards $z\to 1$; we assume that their change with varying z is small compared to the leading logarithm. After these two simplifying steps Eq.(III.16) reads

$$\begin{aligned}\Phi_q(t) &= \Delta_q(t,t_0)\Phi_q(t_0) + \frac{C_F}{2\pi}\int_{t_0}^t \frac{dt'}{t'}\ \Delta_q(t,t')\left(\int_{t_0}^{t'} dt''\ \frac{\alpha_s(t'')}{t''}\Phi_q(t')\Phi_g(t'') - \frac{3}{2}\alpha_s(t')\Phi_q(t')\Phi_g(t')\right) \\ &= \Delta_q(t,t_0)\Phi_q(t_0) + \frac{C_F}{2\pi}\Delta_q(t,t_0)\int_{t_0}^t \frac{dt'}{t'}\ \frac{1}{\Delta_q(t',t_0)}\ \Phi_q(t')\left(\int_{t_0}^{t'} dt''\ \frac{\alpha_s(t'')}{t''}\Phi_g(t'') - \frac{3}{2}\alpha_s(t')\Phi_g(t')\right)\ .\end{aligned} \tag{III.20}$$

The original Sudakov factor $\Delta_q(t,t')$ is split into a ratio of two Sudakov factors. This allows us to differentiate both sides with respect to t,

$$\begin{aligned}\frac{d}{dt}\Phi_q(t) &= \frac{d\Delta_q(t,t_0)}{dt}\Phi_q(t_0) + \frac{C_F}{2\pi}\frac{d\Delta_q(t,t_0)}{dt}\int_{t_0}^t \frac{dt'}{t'}\frac{1}{\Delta_q(t',t_0)}\Phi_q(t')\left(\int_{t_0}^{t'} dt''\frac{\alpha_s(t'')}{t''}\Phi_g(t'') - \frac{3}{2}\alpha_s(t')\Phi_g(t')\right) \\ &\qquad + \frac{C_F}{2\pi}\ \Delta_q(t,t_0)\frac{1}{t}\frac{1}{\Delta_q(t,t_0)}\Phi_q(t)\left(\int_{t_0}^t dt''\ \frac{\alpha_s(t'')}{t''}\Phi_g(t'') - \frac{3}{2}\alpha_s(t)\Phi_g(t)\right) \\ &= \frac{d\Delta_q(t,t_0)}{dt}\left[\Phi_q(t_0) + \frac{C_F}{2\pi}\int_{t_0}^t \frac{dt'}{t'}\frac{1}{\Delta_q(t',t_0)}\Phi_q(t')\left(\int_{t_0}^{t'} dt''\frac{\alpha_s(t'')}{t''}\Phi_g(t'') - \frac{3}{2}\alpha_s(t')\Phi_g(t')\right)\right] \\ &\qquad + \frac{C_F}{2\pi}\ \frac{1}{t}\ \Phi_q(t)\ \left(\int_{t_0}^t dt''\ \frac{\alpha_s(t'')}{t''}\Phi_g(t'') - \frac{3}{2}\alpha_s(t)\Phi_g(t)\right) \\ &= \frac{1}{\Delta_q(t,t_0)}\ \frac{d\Delta_q(t,t_0)}{dt}\ \Phi_q(t) + \Phi_q(t)\frac{C_F}{2\pi}\ \frac{1}{t}\left(\int_{t_0}^t dt''\ \frac{\alpha_s(t'')}{t''}\Phi_g(t') - \frac{3}{2}\alpha_s(t)\Phi_g(t)\right)\ .\end{aligned} \tag{III.21}$$

In the last step we use the definition in Eq.(III.20). This simplified equation has a solution which we can write in a closed form, namely

$$\begin{aligned}\Phi_q(t) &= \Phi_q(t_0)\ \Delta_q(t,t_0)\ \exp\left[\frac{C_F}{2\pi}\ \int_{t_0}^t dt'\ \frac{\alpha_s(t')}{t'}\left(\log\frac{t}{t'} - \frac{3}{2}\right)\Phi_g(t')\right] \\ &= \Phi_q(t_0)\ \exp\left[-\int_{t_0}^t dt'\ \Gamma_{q\leftarrow q}(t,t')\right]\ \exp\left[\int_{t_0}^t dt'\ \Gamma_{q\leftarrow q}(t,t')\Phi_g(t')\right] \\ &= \Phi_q(t_0)\ \exp\left[\int_{t_0}^t dt'\ \Gamma_{q\leftarrow q}(t,t')\left(\Phi_g(t')-1\right)\right]\ .\end{aligned} \tag{III.22}$$

We can prove this by straightforward differentiation of the first line in Eq.(III.22),

$$\begin{aligned}
\frac{d\Phi_q(t)}{dt} &= \Phi_q(t_0)\,\frac{d\Delta_q(t,t_0)}{dt}\,\exp\left[\frac{C_F}{2\pi}\int_{t_0}^{t}dt'\,\frac{\alpha_s(t')}{t'}\left(\log\frac{t}{t'}-\frac{3}{2}\right)\Phi_g(t')\right] \\
&\quad + \Phi_q(t)\frac{d}{dt}\left[\frac{C_F}{2\pi}\int_{t_0}^{t}dt'\,\frac{\alpha_s(t')}{t'}\left(\log t-\log t'-\frac{3}{2}\right)\Phi_g(t')\right] \\
&= \frac{1}{\Delta_q(t,t_0)}\,\frac{d\Delta_q(t,t_0)}{dt}\,\Phi_q(t)+\Phi_q(t)\,\frac{C_F}{2\pi}\,\frac{\alpha_s(t)}{t}\left(-\log t-\frac{3}{2}\right)\Phi_g(t) \\
&\quad + \Phi_q(t)\,\frac{C_F}{2\pi}\,\frac{1}{t}\int_{t_0}^{t}dt'\,\frac{\alpha_s(t')}{t'}\,\Phi_g(t')+\Phi_q(t)\,\frac{C_F}{2\pi}\,\log t\,\frac{\alpha_s(t)}{t}\,\Phi_g(t) \\
&= \frac{1}{\Delta_q(t,t_0)}\,\frac{d\Delta_q(t,t_0)}{dt}\,\Phi_q(t)+\Phi_q(t)\,\frac{C_F}{2\pi}\,\frac{1}{t}\left(\int_{t_0}^{t}dt'\,\frac{\alpha_s(t')}{t'}\,\Phi_g(t')-\alpha_s(t)\frac{3}{2}\Phi_g(t)\right)\,. \qquad \text{(III.23)}
\end{aligned}$$

The expression given in Eq.(III.22) indeed solves the evolution equation in Eq.(III.21). The corresponding computation for $\Phi_g(t)$ follows the same path.

By definition, the generating functional evaluated at the resolution scale t_0 describes an ensemble of jets which have had no opportunity to split. This means $\Phi_{q,g}(t_0)=u$. The quark and gluon generating functionals to next–to–leading logarithmic accuracy are

$$\begin{aligned}
\Phi_q(t) &= u\,\exp\left[\int_{t_0}^{t}dt'\,\Gamma_{q\leftarrow q}(t,t')\,(\Phi_g(t')-1)\right] \\
\Phi_g(t) &= u\,\exp\left[\int_{t_0}^{t}dt'\left(\Gamma_{g\leftarrow g}(t,t')\,(\Phi_g(t')-1)+\Gamma_{q\leftarrow g}(t')\left(\frac{\Phi_q^2(t')}{\Phi_g(t')}-1\right)\right)\right]\,. \qquad \text{(III.24)}
\end{aligned}$$

The splitting kernels are defined in Eq.(II.106); gluon splitting to quarks described by $\Gamma_{q\leftarrow g}$ is suppressed by a power of the logarithm $\log(t/t')$.

The logarithm $\log(t/t')$ combined with the coupling constant α_s included in the splitting kernels is the small parameter which we will use for the following argument. If this logarithmically enhanced term dominates the physics, the evolution equations for quark and gluons are structurally identical. In both cases, the Φ dependence of the exponent spoils an effective solution of Eq.(III.24). However, the logarithmic form of $\Gamma(t,t')$ ensures that the main contribution to the t' integral comes from the region where $t'\sim t_0$. Unless something drastic happens with the integrands in Eq.(III.24) this means that under the integral we can approximate $\Phi_{q,g}(t_0)=u$ and, if necessary, iteratively insert the solution for $\Phi(t)$ into the differential equation. The leading terms for both, quark and gluon evolution equations turn into the closed form

$$\Phi_{q,g}(t) = u\,\exp\left[\int_{t_0}^{t}dt'\,\Gamma_{q,g}(t,t')\,(u-1)\right] = u\,\exp\left[-(1-u)\int_{t_0}^{t}dt'\,\Gamma_{q,g}(t,t')\right]\,. \qquad \text{(III.25)}$$

Using the Sudakov factor defined in Eq.(II.104) the generating functional in the approximation of large logarithmically enhanced parton splitting is

$$\boxed{\Phi_{q,g}(t) = u\,\Delta_{q,g}(t)^{1-u}}\,. \qquad \text{(III.26)}$$

Its first derivative for general values of u is

$$\begin{aligned}
\frac{d}{du}\,\Phi_{q,g}(t) &= \Delta_{q,g}\frac{d}{du}ue^{-u\log\Delta_{q,g}} \\
&= \Delta_{q,g}\left[e^{-u\log\Delta_{q,g}}+u\,(-\log\Delta_{q,g})\,e^{-u\log\Delta_{q,g}}\right] \\
&= \Delta_{q,g}\,(1-u\log\Delta_{q,g})\,e^{-u\log\Delta_{q,g}}\,. \qquad \text{(III.27)}
\end{aligned}$$

The n-th derivative has the form

$$\frac{1}{n!}\,\frac{d^n}{du^n}\,\Phi_{q,g}(t) = \frac{(-\log\Delta_{q,g})^{n-1}}{n!}\,\Delta_{q,g}\;(n-u\log\Delta_{q,g})\;e^{-u\log\Delta_{q,g}}\;. \tag{III.28}$$

We can show this by induction, starting from the first derivative in Eq.(III.27),

$$\begin{aligned}
\frac{1}{n!}\,\frac{d^n}{du^n}\Phi_{q,g}(t) &= \frac{1}{n}\,\frac{d}{du}\,\left(\frac{1}{(n-1)!}\,\frac{d^{n-1}}{du^{n-1}}\Phi_{q,g}(t)\right) \\
&= \frac{1}{n}\,\frac{d}{du}\left[\frac{(-\log\Delta_{q,g})^{n-2}}{(n-1)!}\,\Delta_{q,g}\;(n-1-u\log\Delta_{q,g})\;e^{-u\log\Delta_{q,g}}\right] \qquad \text{using Eq.(III.28)} \\
&= \frac{(-\log\Delta_{q,g})^{n-2}}{n!}\,\Delta_{q,g}\left[(-\log\Delta_{q,g})\,e^{-u\log\Delta_{q,g}} + (n-1-u\log\Delta_{q,g})\,(-\log\Delta_{q,g})e^{-u\log\Delta_{q,g}}\right] \\
&= \frac{(-\log\Delta_{q,g})^{n-1}}{n!}\,\Delta_{q,g}\;[1+n-1-u\log\Delta_{q,g}]\;e^{-u\log\Delta_{q,g}}\;.
\end{aligned} \tag{III.29}$$

By definition, Eq.(III.28) gives the Poisson scaling pattern in the number of jets, namely

$$P_{n-1} = \Delta_{q,g}(t)\,\frac{|\log\Delta_{q,g}(t)|^{n-1}}{(n-1)!} \qquad \text{or} \qquad \boxed{R_{(n+1)/n} = \frac{|\log\Delta_{q,g}(t)|}{n+1}}\,. \tag{III.30}$$

In addition to the logarithmically enhanced Poisson case we can find a second, recursive solution for the generating functionals. It holds in the limit of small emission probabilities. The emission probability is governed by $\Gamma_{i\leftarrow j}(t,t')$, as defined in Eq.(II.106). We can make it small by avoiding a logarithmic enhancement, corresponding to no large scale ratios t/t_0. In addition, we would like to get rid of $\Gamma_{q\leftarrow g}$ while keeping $\Gamma_{g\leftarrow g}$. Purely theoretically this means removing the gluon splitting into two quarks and limiting ourselves to pure Yang-Mills theory. In that case the scale derivative of Eq.(III.24) reads

$$\begin{aligned}
\frac{d\Phi_g(t)}{dt} &= \Phi_g(t_0)\,\frac{d}{dt}\,\exp\left[\int_{t_0}^t dt'\,\Gamma_{g\leftarrow g}(t,t')\,(\Phi_g(t')-1)\right] \\
&= \Phi_g(t)\,\frac{C_A}{2\pi}\frac{d}{dt}\,\int_{t_0}^t dt'\,\frac{\alpha_s(t')}{t'}\left(\log t-\log t'-\frac{11}{6}\right)\,(\Phi_g(t')-1) \qquad \text{inserting Eq.(II.106)} \\
&= \Phi_g(t)\frac{C_A}{2\pi}\left[\frac{\alpha_s(t)}{t}\left(-\log t-\frac{11}{6}\right)\,(\Phi_g(t)-1)+\frac{d}{dt}\,\log t\,\int_{t_0}^t dt'\,\frac{\alpha_s(t')}{t'}\,(\Phi_g(t')-1)\right] \\
&= \Phi_g(t)\frac{C_A}{2\pi}\left[\frac{\alpha_s(t)}{t}\left(-\log t-\frac{11}{6}\right)\,(\Phi_g(t)-1)+\frac{1}{t}\int_{t_0}^t dt'\,\frac{\alpha_s(t')}{t'}\,(\Phi_g(t')-1)+\log t\,\frac{\alpha_s(t)}{t}\,(\Phi_g(t)-1)\right] \\
&= \Phi_g(t)\frac{C_A}{2\pi t}\left[-\frac{11}{6}\,\alpha_s(t)\,(\Phi_g(t)-1)+\int_{t_0}^t dt'\,\frac{\alpha_s(t')}{t'}\,(\Phi_g(t')-1)\right]\,.
\end{aligned} \tag{III.31}$$

This form is already greatly simplified, but in the combination of the integral and the running strong coupling it is not clear what the limit of small but finite $\log(t/t_0)$ would be. Integrating by parts we find a form which we can estimate systematically,

$$\begin{aligned}
\frac{d\Phi_g(t)}{dt} &= \Phi_g(t)\frac{C_A}{2\pi t}\left[-\frac{11}{6}\alpha_s(t)\,(\Phi_g(t)-1)-\int_{t_0}^t dt'\log t'\frac{d}{dt'}\,(\alpha_s(t')\,(\Phi_g(t')-1))+\log t'\alpha_s(t')\,(\Phi_g(t')-1)\,\Big|_{t_0}^t\right] \\
&= \Phi_g(t)\frac{C_A}{2\pi t}\left[-\frac{11}{6}\alpha_s(t)\,(\Phi_g(t)-1)-\int_{t_0}^t dt'\log\frac{t'}{t_0}\frac{d}{dt'}\,(\alpha_s(t')\,(\Phi_g(t')-1))+\log\frac{t'}{t_0}\alpha_s(t')\,(\Phi_g(t')-1)\,\Big|_{t_0}^t\right] \\
&= \Phi_g(t)\frac{C_A}{2\pi t}\left[\alpha_s(t)\left(\log\frac{t}{t_0}-\frac{11}{6}\right)\,(\Phi_g(t)-1)-\int_{t_0}^t dt'\,\log\frac{t'}{t_0}\,\frac{d}{dt'}\,(\alpha_s(t')\,(\Phi_g(t')-1))\right]\,.
\end{aligned} \tag{III.32}$$

We can evaluate this expression in the limit of $t=t_0+\delta$ or $t_0/t=1-\delta/t$. The two leading terms, ignoring all terms

of the order δ^2, read

$$\begin{aligned}\frac{d\Phi_g(t)}{dt} &= \Phi_g(t)\frac{C_A}{2\pi t}\left[\alpha_s(t)\left(\frac{\delta}{t_0}-\frac{11}{6}\right)(\Phi_g(t)-1)-(t-t_0)\,\frac{\delta}{t}\,\frac{d}{dt}\left(\alpha_s(t)\,(\Phi_g(t)-1)\right)\right]\\ &= \Phi_g(t)\,\frac{C_A}{2\pi}\,\frac{\alpha_s(t)}{t}\left(\frac{\delta}{t_0}-\frac{11}{6}\right)(\Phi_g(t)-1)+\mathcal{O}\left(\delta^2\right)\ . \end{aligned} \tag{III.33}$$

To leading order in δ/t the equation for the generating functional becomes

$$\frac{d\Phi_g(t)}{dt} = \Phi_g(t)\,\tilde\Gamma_{g\leftarrow g}(t,t_0)\ (\Phi_g(t)-1) \qquad \text{with} \qquad \tilde\Gamma_{g\leftarrow g}(t,t_0) = \frac{C_A}{2\pi}\,\frac{\alpha_s(t)}{t}\left(\log\frac{t}{t_0}-\frac{11}{6}\right)\ . \tag{III.34}$$

With $\tilde\Gamma$ we define a slightly modified splitting kernel, where the prefactor α_s/t is evaluated at the first argument t instead of the second argument t_0. Including the boundary condition $\Phi_g(t_0)=u$ we can solve this equation for the generating functional, again using the method of the known solution,

$$\boxed{\Phi_g(t) = \frac{1}{1+\dfrac{1-u}{u\tilde\Delta_g(t)}}} \qquad \text{with} \qquad \tilde\Delta_g(t) = \exp\left(-\int_{t_0}^t dt'\tilde\Gamma_{g\leftarrow g}(t',t_0)\right)\ . \tag{III.35}$$

The derivative of this solution is

$$\begin{aligned}\frac{d\Phi_g(t)}{t} &= \frac{d}{dt}\left(1+\frac{1-u}{u\tilde\Delta_g(t)}\right)^{-1}\\ &= -\Phi_g(t)^2\,\frac{1-u}{u}\,\frac{d}{dt}\exp\left(+\int_{t_0}^t dt'\,\tilde\Gamma_{g\leftarrow g}(t',t_0)\right)\\ &= -\Phi_g(t)^2\,\frac{1-u}{u\tilde\Delta_g(t)}\,\frac{d}{dt}\int_{t_0}^t dt'\,\tilde\Gamma_{g\leftarrow g}(t',t_0)\\ &= -\Phi_g(t)^2\,\left(\frac{1}{\Phi_g(t)}-1\right)\,\frac{d}{dt}\int_{t_0}^t dt'\,\tilde\Gamma_{g\leftarrow g}(t',t_0) = \Phi_g(t)\ (\Phi_g(t)-1)\ \tilde\Gamma_{g\leftarrow g}(t,t_0)\ , \end{aligned} \tag{III.36}$$

which is precisely the evolution equation in Eq.(III.34).

While we have suggestively defined a modified splitting kernel $\tilde\Gamma$ in Eq.(III.34) and even extended this analogy to a Sudakov-like factor in Eq.(III.35) it is not entirely clear what this object represents. In the limit of large $\log(t/t_0)\gg 1$ or $t\gg t_0$, which is not the limit we rely on for the pure Yang–Mills case, we find

$$\begin{aligned}\int_{t_0}^t dt'\,\tilde\Gamma_{g\leftarrow g}(t',t_0) - \int_{t_0}^t dt'\,\Gamma_{g\leftarrow g}(t',t_0) &= \frac{C_A}{2\pi}\,\int_{t_0}^t dt'\,\left(\frac{\alpha_s(t')}{t'}-\frac{\alpha_s(t_0)}{t_0}\right)\,\log\frac{t'}{t_0}\\ &\simeq -\frac{C_A}{2\pi}\,\alpha_s(t_0)\int_{t_0}^t\frac{dt'}{t_0}\,\log\frac{t'}{t_0}\\ &= -\frac{C_A}{2\pi}\,\alpha_s(t_0)\,\left[\frac{t'}{t_0}\log\frac{t'}{t_0}-\frac{t'}{t_0}\right]_1^{t/t_0} = -\frac{C_A}{2\pi}\,\alpha_s(t_0)\,\frac{t}{t_0}\log\frac{t}{t_0}\ . \end{aligned} \tag{III.37}$$

In the staircase limit $t\sim t_0$ and consistently neglecting $\log(t/t_0)$ the two kernels $\Gamma_{g\leftarrow g}$ and $\tilde\Gamma_{g\leftarrow g}$ become identical. In the same limit we find $\Delta_g\sim\tilde\Delta_g\sim 1$. Again using $t'=t_0+\delta$ and only keeping the leading terms in δ we can compute

the leading difference

$$\begin{aligned}
\tilde{\Gamma}_{g\leftarrow g}(t',t_0)-\Gamma_{g\leftarrow g}(t',t_0) &= \frac{C_A}{2\pi}\,\left(\frac{\alpha_s(t')}{t'}-\frac{\alpha_s(t_0)}{t_0}\right)\,\left(\frac{\delta}{t'}-\frac{11}{6}\right)\\
&= -\frac{C_A}{2\pi}\,\frac{11}{6}(t'-t_0)\,\frac{d}{dt}\frac{\alpha_s(t)}{t}\bigg|_{t_0} = -\frac{C_A}{2\pi}\,\frac{11}{6}\delta\,\left[\frac{1}{t}\,\frac{d\alpha_s(t)}{dt}-\frac{\alpha_s(t)}{t^2}\right]_{t_0}\\
&= -\frac{C_A}{2\pi}\,\frac{11}{6}\delta\,\left[-\frac{1}{t}\,\frac{\alpha_s^2(t)b_0}{t}-\frac{\alpha_s(t)}{t^2}\right]_{t_0} \qquad \text{using Eq.(II.22)}\\
&= \frac{C_A\alpha_s(t_0)}{2\pi}\,\frac{11}{6}\,\frac{\delta}{t_0^2}\,\left(1+b_0\alpha_s(t_0)\right)\\
\int_{t_0}^{t}dt'\,\tilde{\Gamma}_{g\leftarrow g}(t',t_0)-\int_{t_0}^{t}dt'\,\Gamma_{g\leftarrow g}(t',t_0) &= \frac{C_A\alpha_s(t_0)}{2\pi}\,\frac{11}{6}\,\frac{\delta^2}{t_0^2}\,\left(1+b_0\alpha_s(t_0)\right)\,. \qquad \text{(III.38)}
\end{aligned}$$

In the pure Yang–Mills theory the running of the strong coupling is described by $b_0 = 1/(4\pi)11N_c/3$. In both limits the true and the modified splitting kernels differ by the respective small parameter.

The closed form for the generating functional in Eq.(III.35) allows us to compute the number of jets in purely gluonic events. The first derivative is

$$\begin{aligned}
\frac{d}{du}\Phi_g(t) &= \frac{d}{du}\,u\left(u+\frac{1-u}{\tilde{\Delta}_g(t)}\right)^{-1}\\
&= \left(u+\frac{1-u}{\tilde{\Delta}_g}\right)^{-1}+u(-1)\left(u+\frac{1-u}{\tilde{\Delta}_g}\right)^{-2}\left(1-\frac{1}{\tilde{\Delta}_g}\right)\,. \qquad \text{(III.39)}
\end{aligned}$$

The form of the n-th derivative we can again prove by induction. Clearly, for $n=1$ the above result is identical with the general solution

$$\frac{d^n}{du^n}\Phi_g(t) = n!\left(\frac{1}{\tilde{\Delta}_g}-1\right)^{n-1}\left(u+\frac{1-u}{\tilde{\Delta}_g}\right)^{-n}\left[1+u\left(u+\frac{1-u}{\tilde{\Delta}_g}\right)^{-1}\left(\frac{1}{\tilde{\Delta}_g}-1\right)\right]\,. \qquad \text{(III.40)}$$

The induction step from $n-1$ to n is

$$\begin{aligned}
\frac{d^n}{du^n}\Phi_g(t) &= (n-1)!\left(\frac{1}{\tilde{\Delta}_g}-1\right)^{n-2}\left\{-(n-1)\left(u+\frac{1-u}{\tilde{\Delta}_g}\right)^{-n}\left(1-\frac{1}{\tilde{\Delta}_g}\right)\left[1+u\,\left(u+\frac{1-u}{\tilde{\Delta}_g}\right)^{-1}\left(\frac{1}{\tilde{\Delta}_g}-1\right)\right]\right.\\
&\qquad \left.+\left(u+\frac{1-u}{\tilde{\Delta}_g}\right)^{-n+1}\left[\left(u+\frac{1-u}{\tilde{\Delta}_g}\right)^{-1}\left(\frac{1}{\tilde{\Delta}_g}-1\right)+u\left(u+\frac{1-u}{\tilde{\Delta}_g}\right)^{-2}\left(\frac{1}{\tilde{\Delta}_g}-1\right)^2\right]\right\}\\
&= (n-1)!\left(\frac{1}{\tilde{\Delta}_g}-1\right)^{n-2}\left\{(n-1)\left(u+\frac{1-u)}{\tilde{\Delta}_g}\right)^{-n}\left(\frac{1}{\tilde{\Delta}_g}-1\right)\left[1+u\,\left(u+\frac{1-u}{\tilde{\Delta}_g}\right)^{-1}\left(\frac{1}{\tilde{\Delta}_g}-1\right)\right]\right.\\
&\qquad \left.+\left(u+\frac{1-u}{\tilde{\Delta}_g}\right)^{-n}\left(\frac{1}{\tilde{\Delta}_g}-1\right)\left[1+u\left(u+\frac{1-u}{\tilde{\Delta}_g}\right)^{-1}\left(\frac{1}{\tilde{\Delta}_g}-1\right)\right]\right\}\\
&= n!\left(\frac{1}{\tilde{\Delta}_g}-1\right)^{n-1}\left(u+\frac{1-u}{\tilde{\Delta}_g}\right)^{-n}\left[1+u\left(u+\frac{1-u}{\tilde{\Delta}_g}\right)^{-1}\left(\frac{1}{\tilde{\Delta}_g}-1\right)\right]\,. \qquad \text{(III.41)}
\end{aligned}$$

Evaluating Eq.(III.40) for $u = 0$ gives us the jet rates

$$P_{n-1} = \frac{1}{n!}\frac{d^n}{du^n}\Phi_g(t)\bigg|_{u=0} = \left(\frac{1}{\tilde{\Delta}_g} - 1\right)^{n-1} \tilde{\Delta}_g^n = \tilde{\Delta}_g \left(1 - \tilde{\Delta}_g\right)^{n-1} , \tag{III.42}$$

which predicts constant ratios

$$\boxed{R_{(n+1)/n} = 1 - \tilde{\Delta}_g(t)} . \tag{III.43}$$

Such constant ratios define a staircase pattern. It has for a long time been considered an accidental sweet spot where many QCD effects cancel each other to produce constant ratios of successive exclusive n-jet rates. Our derivation from the generating functionals suggest that staircase scaling is one of two pure jet scaling patterns:

1. in the presence of large scale differences abelian splittings generate a Poisson pattern with $R_{(n+1)/n} \propto 1/(n+1)$, as seen in Eq.(III.30).

2. for democratic scales non–abelian splittings generate a staircase pattern with constant $R_{(n+1)/n}$ shown in Eq.(III.43).

IV. STRONG CHIRAL SYMMETRY BREAKING

In the previous sections we discussed the ultraviolet renomalisation of QCD and its relation to the scale dependence of physics. This scale dependence is apparent in the momentum dependence of the strong running coupling $\alpha_s(p^2) = g^2(p^2)/(4\pi)$ defined in (II.22). Here p is the relevant momentum/energy scale of a given process. Let us briefly rehash the main properties of the running coupling: Its momentum dependence is captured by the β-function as leads to a running coupling which decreases with the momentum scale, i.e. ,

$$\beta_g = \frac{1}{2} p\partial_p \alpha_s = -b_0\alpha^2 + O(\alpha_s^3) \qquad \text{with} \qquad b_0 = \frac{\alpha_s^2}{12\pi}\,(11\,N_c + 2\,N_f)\ . \tag{IV.1}$$

Integrating the β-function (IV.1) at one loop leads to the running coup

$$\alpha_s(p) = \frac{\alpha_s(\mu)}{1 + \beta_0\alpha_s(\mu)\log\frac{p^2}{\mu^2}} + O(\alpha_s^2)\,, \tag{IV.2}$$

with some reference (momentum) scale μ^2. The running coupling in (IV.2) tends to zero logarithmically for $p \to \infty$. This property is called asymptotic freedom (Nobel prize 2004) and guarantees the existence of the the perturbative expansion of QCD. Its validity for large energies and momenta is by now impressively proven in various scattering experiments, see e.g. [4]. These experiments can also be used to define a running coupling (which is not unique beyond two loop, see e.g. [5]) and the related plot of $\alpha_s(p^2)$ in Fig. 5 has been taken from [4].

In turn, in the infrared regime of QCD at low momentum scales, perturbation theory is not applicable any more. The coupling grows and the failure of perturbation theory is finally signaled by the so-called Landau pole with $\alpha_s(\Lambda_{\rm QCD}) = \infty$. We emphasise that a large or diverging coupling does *not* imply confinement, the theory could still be QED-like showing a Coulomb-potential with a large coupling. The latter would not lead to the absence of coloured asymptotic states but rather to so-called color charge superselection sectors as in QED. There, we have asymptotic charged states and no physics process can change the charge. For more details on this see e.g. [6].

A. Spontaneous symmetry breaking and the Goldstone theorem

In the Standard Model we have two phenomena involving spontaneous symmetry breaking. The first is the spontaneous symmetry breaking in the Higgs sector (Englert-Brout-Higgs-Guralnik-Hagen-Kibble) which provides (current) masses for the quarks and leptons as well as for the W, Z vector bosons, the gauge bosons of the weak interactions. The corresponding Goldstone boson manifest itself as the third polarisation of the massive vector bosons (Higgs-Kibble dinner).

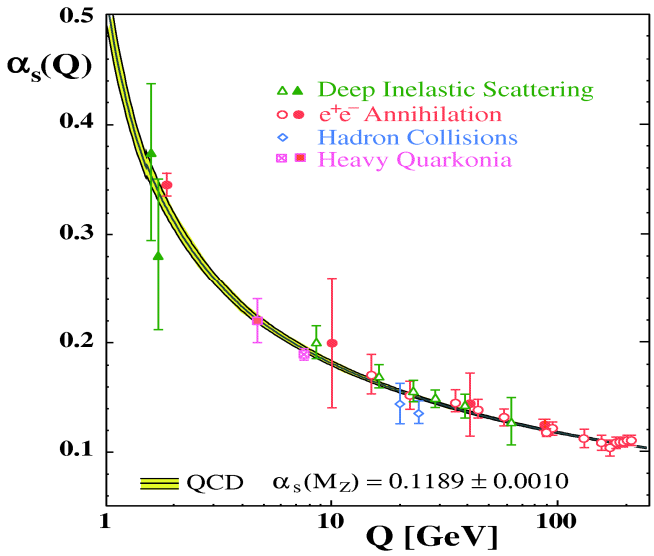

FIG. 5: Experimental tests of the running coupling, figure taken from [4].

The second phenomena is strong chiral symmetry breaking in the quark sector with a mass scale of ≈ 300 MeV. This mechanism, loosely speaking, lifts the current quark masses to constituent quark masses. For the up and down quarks the current quark mass is negligible, see Table I. The corresponding Goldstone bosons, the pions $\vec{\pi}$, are composite (quark–anti-quark) states and do not appear in the QCD action.

In the following we discuss similarities of and differences between these two phenomena. Before we come to the Standard Model, let us recall some basic facts about spontaneous symmetry breaking. Further details can be found in the literature. As a basic, but important, example we consider a simple scalar field theory with N real scalars and action

$$S[\phi] = \frac{1}{2}\int_x (\partial_\mu \phi^a)^2 + \int_x V(\rho)\,, \qquad \text{with} \qquad a = 1, ..., N\,, \qquad \text{and} \qquad \rho = \frac{1}{2}\phi^a\phi^a\,, \tag{IV.3}$$

and the ϕ^4-potential

$$V(\rho) = -\mu^2(\phi^a\phi^a) + \lambda(\phi^a\phi^a)^2\,. \tag{IV.4}$$

In the following considerations we shall not need the specific form (IV.4) but only its symmetries. Still, the simple potential (IV.4) serves as a good showcase. The action (IV.3) with the potential (IV.4) has $O(N)$-symmetry. Moreover, the potential (IV.4) has a manifold of non-trivial minima, each of which breaks $O(N)$-symmetry. This leads us to the vacuum manifold

$$V'(\rho_0) = 0\,, \qquad \text{with} \qquad \rho_0 = \frac{\mu^2}{4\lambda}\,, \tag{IV.5}$$

where the prime stands for the derivative w.r.t. ρ. In Fig. 6 the potential is depicted for the $O(2)$-case with $N = 2$.

Without loss of generality we pick a specific point on the vacuum manifold (IV.5), to wit

$$\phi_0 = \begin{pmatrix} 0 \\ \vdots \\ 0 \\ \sqrt{2\rho_0} \end{pmatrix}\,. \tag{IV.6}$$

The vacuum vector ϕ_0 in (IV.6) is invariant under the subgroup (little group) $O(N-1)$ with the generators t^a, $a = N, N+1, ...N(N-1)/2$ of $O(N)$ that acts trivially on the Nth component field ϕ^N. This subgroup rotates the first $N-1$ component fields into each other. It leaves us with $N-1$ generators t^a, $a = 1, ..., N-1$ (of the quotient $O(N)/O(N-1)$) of the $N(N-1)/2$ generators of the group $O(N)$. In turn, a rotation of the vacuum vector within

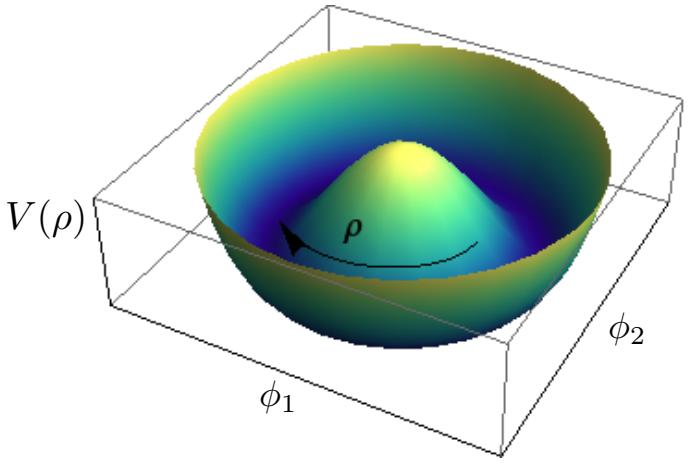

FIG. 6: Illustration of the Mexican hat potential for N = 2. The radial massive mode ρ is indicated by the arrow. The angular mode is the Goldstone mode.

this quotient generates the full vacuum manifold. Applied to a vector $\phi^a = \delta^{Na}\sqrt{2\rho}$ with length it generates all fields,

$$\phi = e^{\frac{\theta^a}{\sqrt{2\rho_0}}t^a} \begin{pmatrix} 0 \\ \vdots \\ 0 \\ \sigma \end{pmatrix} , \tag{IV.7}$$

where the denominator $1/\sqrt{2\rho_0}$ is chosen for convenience. Commonly, the Nth component field ϕ^N is expanded about the minimum $\sigma_0 = \sqrt{2\rho_0}$.

In the present lecture we choose a slightly different approach and stick to the Cartesian fields ϕ which we split into the radial mode σ and the rest, $\vec{\pi}$, i.e.

$$\phi = \begin{pmatrix} \vec{\pi} \\ \sigma \end{pmatrix} , \qquad \text{with} \qquad \phi_0 = \begin{pmatrix} 0 \\ \sigma \end{pmatrix} . \tag{IV.8}$$

Note that in an expansion about the minimum ϕ_0 in the fields $\vec{\theta}$ and $\vec{\pi}$ agree in leading order. Using the representation (IV.8) in the kinetic term in the action (IV.3) we are led to

$$S_{\text{kinetic}}[\phi] = \frac{1}{2}\int_x \left[(\partial_\mu\sigma)^2 + (\partial_\mu\vec{\pi})^2\right] . \tag{IV.9}$$

The mass term of the model is given by the quadratic term of the potential in an expansion about the minimum. It reads generally

$$\frac{1}{2}\int_x m^{2\,ab}(\phi_0)\phi^a\,\phi^b , \qquad \text{with} \qquad m^{2\,ab}(\phi_0) = \partial_{\phi^a}\partial_{\phi^b}V(\rho_0) = \delta^{ab}\,V'(\rho_0) + \phi_0^a\phi_0^b\,V''(\rho_0) . \tag{IV.10}$$

Using the expansion point (IV.6) leads to the mass matrix

$$m^{2\,ab}(\phi_0) = \delta^{ab}\,V'(\rho_0) + 2\,\delta^{Na}\delta^{Nb}\rho_0 V''(\rho_0) = 8\,\delta^{Na}\delta^{Nb}\rho_0\,\lambda . \tag{IV.11}$$

Eq.(IV.11) entails that in the symmetry-broken phase of the model we have $N-1$ massless fields, the Goldstone fields. Note that we have not used the specific form (IV.4) of the potential for this derivation.

The occurrence of the massless modes in (IV.11) is a specific case/manifestation of the Goldstone theorem. It entails in general that in the case of a spontaneous symmetry breaking of a continuous symmetry massless modes, the Goldstone modes, occur. Their number is related to the number of generators in the Quotient G/H, where G is the symmetry group and H is the subgroup (little group) which leaves the vacuum invariant.

B. Spontaneous symmetry breaking, quantum fluctuations and masses*

The classical analysis done in chapter IV A suffices to uncover the occurrence of massless modes in spontaneous symmetry breaking. However, it does not unravel the mechanism. The stability of the chosen vacuum, e.g. (IV.6), necessitates, that an infinitesimal rotation on the vacuum manifold costs an infinite amount of energy. This does only happen (for continuous symmetries) in dimensions $d > 2$. In $d \leq 2$ no spontaneous symmetry breaking of a continuous symmetry occurs, which is covered by the Mermin-Wagner theorem (Mermin-Wagner-Hohenberg-Coleman). In $d = 2$ dimensions theories with discrete symmetry can exhibit spontaneous symmetry breaking, e.g. the Ising model.

Hence, the full analysis has to be done on the quantum level. A convenient way to address these questions is the quantum analogue of the classical action, the (quantum) effective action. Formally it is defined as the Legendre transform of the Schwinger functional, $W[J] = \log Z[J]$. In the present case this is

$$\Gamma[\phi] = \sup_J \left\{ \int_x J(x)\phi(x) - \log Z[J] \right\} , \qquad \text{where} \qquad Z[J] = \int D\varphi\, e^{-S[\varphi]+\int_x J\varphi} . \tag{IV.12}$$

In the following we simply assume that (IV.12) has a maximum and is differentiable w.r.t. J. Then the definition in

(IV.12) leads to

$$\phi = \frac{1}{Z[J]}\frac{\delta Z[J]}{\delta J} = \langle\varphi\rangle\,, \qquad \text{and} \qquad J = \frac{\delta\Gamma}{\delta\phi}\,. \tag{IV.13}$$

The effective action also has a closed path integral representation in terms of a functional integro-differential equation, which we also quote for later use. For the derivation we substitute the current in (IV.12) with (IV.13) and use that $Z = \exp\{-\Gamma + \int_x J\phi\}$. This leads us to

$$e^{-\Gamma[\phi]} = \int D\varphi'\, e^{-S[\phi+\varphi']+\int_x \frac{\delta\Gamma}{\delta\phi}\varphi'}\,, \qquad \text{with} \qquad \langle\varphi'\rangle_c = 0\,, \tag{IV.14}$$

where we also shifted the integration variable $\varphi = \varphi' + \varphi$. Eq.(IV.14) leads us immediately to the quantum equations of motion in general backgrounds ϕ, the Dyson-Schwinger equations. We simply take the ϕ-derivatives on both sides and arrive at

$$\frac{\delta\Gamma}{\delta\phi} = \left\langle\frac{\delta S}{\delta\varphi}\right\rangle\,, \tag{IV.15}$$

the quantum eqautions of motion (EoM) in a given background $\phi = \langle\varphi\rangle$ triggered by the current J. Evaluated on the EoM with $J = 0$,

$$\left.\frac{\delta\Gamma}{\delta\phi}\right|_{\phi=\phi_{\rm EoM}} = 0\,, \tag{IV.16}$$

The effective action $\Gamma[\phi_{\rm EoM}] = -\log Z[0]$ it is the free energy of the theory and implies $J[\phi_{\rm EoM}] = 0$. It is also a generating functional and generates the one-particle-irreducible (1PI) diagrams of the theory. As all diagrams can be constructed from 1PI diagrams, it contains the full information about the correlation functions of the theory. In the present context, the interesting feature is its relation to the free energy. It allows us to define the effective potential

$$V_{\rm eff}[\phi_c] = \Gamma[\phi_c]/{\rm vol}_4\,, \tag{IV.17}$$

with constant fields ϕ_c and the four-volume ${\rm vol}_4 = \int d^4x$. If the effective potential shows the vacuum structure discussed above in the classical case, the theory exhibits spontaneous symmetry breaking. The Mermin-Wagner theorem simply entails that in lower dimensions the longe range nature of the quantum fluctuations washes out the non-trivial vacua.

The rôle of the effective action as the quantum analogue of the classical action is also very apparent in its relation to the propagator of the theory,

$$\langle\phi(p)\phi(-p)\rangle_c = \left.\frac{\delta^2\log Z[J]}{\delta J(p)\delta J(-P)}\right|_{J=0} = \left.\frac{1}{Z[0]}\frac{\delta^2 Z}{\delta J(p)\delta J(-P)}\right|_{J=0} - \langle\phi(p)\rangle\langle\phi(-p)\rangle\,, \qquad \text{with} \qquad \langle\phi\rangle = \frac{1}{Z[0]}\frac{\delta Z}{\delta J}\,, \tag{IV.18}$$

where the subscript $_c$ stands for connected. Now we use the relation of $\log Z$ to the effective action defined in (IV.12). We have

$$\delta(p-q) = \frac{\delta J(q)}{\delta J(p)} = \int_l \frac{\delta\phi(l)}{\delta J(p)}\cdot\frac{\delta J(q)}{\delta\phi(l)} = \int_l \frac{\delta^2\log Z}{\delta J(l)\delta J(p)}\cdot\frac{\delta^2\Gamma[\phi]}{\delta\phi(l)\delta(q)} \quad \Rightarrow \quad \langle\phi(p)\phi(q)\rangle_c = \frac{1}{\Gamma^{(2)}}(p,q)\,, \tag{IV.19}$$

with the vertices

$$\frac{\delta^n\Gamma}{\delta\phi(p_1)\cdots\phi(p_n)} = \Gamma^{(n)}(p_1,...,p_n)\,, \qquad \text{with} \qquad \langle\varphi(p_1)\cdots\varphi(p_n)\rangle_{\rm 1PI} = \Gamma^{(n)}(p_1,...,p_n)\,. \tag{IV.20}$$

The proof of the latter identity of the nth φ-derivatives with the 1PI n-point correlation functions we leave to the reader. Instead let us now come back to our simple example for spontaneous symmetry breaking. Let us assume for the moment that the full effective action resembles the classical action in (IV.3). Then the ϕ^4-potential in (IV.4) is the full quantum effective potential of the theory for $\rho \geq \rho_0$ (why is this not possible for smaller ρ?). The full

propagator of the theory is now given by

$$\langle\varphi(p)\varphi(-p)\rangle_c = \frac{1}{\Gamma^{(2)}[\phi_{\rm EoM}]}(p,-p) = \frac{1}{p^2}\left(\delta^{ab}-\delta^{aN}\delta^{bN}\right) + \frac{1}{p^2+8\rho_0\lambda}\delta^{ab}\,, \tag{IV.21}$$

which describes the massless propagation of the $N-1$ Goldstone modes, and that of one massive one, the radial field σ, with mass $m_\sigma^2 = 8\rho_0\lambda$. This links the curvature of the effective potential to the masses of the propagating modes in the theory. Note however, that this is a Euclidean concept and finally we are interested in the pole masses of the physical excitations. They are defined via the respective (inverse) screening lengths in the spatial and temporal directions. The latter are defined by

$$\lim_{\|\vec{x}-\vec{y}\|\to\infty}\langle\phi(x)\phi(y)\rangle \sim e^{-\|\vec{x}-\vec{y}\|/\xi_{\rm spat}}\,, \qquad \text{and} \qquad \lim_{|x_0-y_0|\to\infty}\langle\phi(x)\phi(y)\rangle \sim e^{-|x_0-y_0|/\xi_{\rm temp}}\,. \tag{IV.22}$$

The screening lengths $\xi_{\rm spat/temp}$ are inversely related to the pole mass $m_{\rm pol} = 1/\xi_{\rm temp}$ and screening mass $m_{\rm screen} = 1/\xi_{\rm spat}$ respectively. In the present example with the classical dispersion p^2 these masses are identical and also agree with the curvature masses $m_{\rm curv}$ derived from the effective potential. This is easily seen from (IV.21). The screening lengths and masses are derived from the Fourier transform of the propagator in momentum space and we have e.g. for the radial mode φ^N at $\vec{p}=0$

$$\lim_{|x_0-y_0|\to\infty}\int\frac{dp_0}{(2\pi)}\langle\varphi^N(p_0,0)\varphi^N(-p_0,0)\rangle_c e^{ip_0\,(x_0-y_0)} \sim e^{-|x_0-y_0|8\rho_0\lambda}\,, \tag{IV.23}$$

and hence $m_{\rm pol} = 1/\xi_{\rm temp} = m_{\rm curv}$. Here $\vec{p}=0$ has only be chosen for convenience. A similar computation can be made for the spatial screening length which agrees with the temporal one. In summary this leaves us with the definition of the pole mass as the smallest value for

$$\Gamma^{(2)}(p_0 = m_{\rm pol}, \vec{p}=0) = 0\,, \tag{IV.24}$$

related to the pole (or cut) that is closest to the Euclidean frequency axis. A similar definition holds for the screening mass.

In principle this allows for the extraction of the pole and screening masses from the Euclidean propagators. In practice this quickly runs in an accuracy problem if the propagator is only known numerically. Moreover, this problem is tightly related to reconstruction problems of analyticity properties from numerical data which is an ill-posed problem without any further knowledge.

As a last remark we add that the above identity between screening lengths, and pole, screening and curvature masses fails in the full quantum theory:

- the coincidence of curvature and screening/pole masses hinges on the classical dispersion proportional to p^2, any non-trivial momentum dependence of the propagator leads to a violation.
- The coincidence of screening and pole mass hinges on the dispersion only being a function of p^2. While this is true in the vacuum (at vanishing temperature $T=0$ and density/chemical potential $n/\mu = 0$), finite temperature and density singles out a rest frame and the dispersion depends on $\vec{p}^2$ and p_0^2 separately.

Having said this, in the following we shall first use simple approximations to the full low energy effective action of QCD for extracting the physics of chiral symmetry breaking and confinement, as well as the mechanisms behind these phenomena.

C. Little reminder on the Higgs mechanism

Now we are in the position to discuss the Higgs mechanism in the Standard Model. Again we refer to the literature for the details. The Higgs mechanisms serves as an example, at which we can discuss similarities and differences for strong chiral symmetry breaking. Moreover, it is the combination of both mechanisms of mass generation that leads to the observed world. The action of the Standard Model is given by

$$S_{\rm SM}[\Phi] = \frac{1}{4}\int_x F^a_{\mu\nu}F^a_{\mu\nu} + \frac{1}{4}\int_x W^a_{\mu\nu}W^a_{\mu\nu} + \frac{1}{4}\int_x B_{\mu\nu}B_{\mu\nu} + (D\phi)^\dagger D\phi + V_H(\phi) + \int_x \bar\psi\cdot(i\not{D} + i\,m_\psi(\phi) + i\mu\gamma_0)\cdot\psi\,, \tag{IV.25}$$

where we have introduced the electroweak gauge bosons W, B and the Higgs, a complex scalar $SU(2)$-doublet ϕ,

$$\phi = \begin{pmatrix} \phi_1 \\ \phi_2 \end{pmatrix} , \tag{IV.26}$$

with complex components ϕ_1, ϕ_2. The Higgs potential V_H is a ϕ^4-potential as (IV.4) with

$$V_H(\phi) = -\mu^2 \phi^\dagger \phi + \lambda (\phi^\dagger \phi)^2 . \tag{IV.27}$$

with non-trivial vacuum manifold

$$\rho_0 = \frac{\mu^2}{4\lambda} \qquad \text{with} \qquad \rho = \frac{1}{2}\phi^\dagger \phi . \tag{IV.28}$$

In the spirit of the discussion at the end of chapter IV A we should interpret V_H as an approximation of the full effective potential of the theory. The Higgs field couples to the electroweak gauge group with the covariant derivative

$$D_\mu \phi = (\partial_\mu - i g_W W_\mu - i g_H B_\mu)\, \phi , \tag{IV.29}$$

The mass term in (IV.25) is linear in the Higgs field and vanishes for $\phi = 0$. The left-handed fermions ψ_L in the Standard Model, leptons and quarks, couple to the weak isospin (fundamental representation) with weak isospin $\pm - 1/2$, while the right-handed fermions ψ_R do not couple (trivial representation) with weak isospin 0, that is for example

$$W_\mu \psi_R = 0 . \tag{IV.30}$$

The related covariant derivative of the fermions reads

$$D_\mu \psi = (\partial_\mu - i g A_\mu - i g_W W_\mu - i g_H B_\mu)\, \psi . \tag{IV.31}$$

The mass term $m(\phi)$ is linear in the Higgs field ϕ and hence constitues a Yukawa interaction. It relates to the Cabibbo-Kobayashi-Maskawa-Matrix (CKM) , and is not discussed in further details here. What is important in the present context, is, that a non-vanishing expectation value of the Higgs field, $\langle \phi \rangle = (0, \rho_0/\sqrt{2})$ provides mass terms for the weak gauge fields, the W, Z as well as for the (left-handed) quarks an leptons:

As in our $O(N)$-example in the previous section we expect spontaneous symmetry breaking in the scalar Higgs sector. The current masses of the leptons and quarks are then generated by the disappearance of the mass term for $\phi_0 \neq 0$. Since the structure of the full term is quite convoluted, we illustrate this at a simple example with one Dirac fermion ψ and a real scalar field σ. Then the Yukawa term reads in a mean field approximation

$$h \bar{\psi} \sigma \psi \xrightarrow{\text{mean field}} h \sigma_0\, \bar{\psi} \psi , \tag{IV.32}$$

with mass $m = h\sigma_0$ which is proportional to the vacuum expectation value of the scalar field (vacuum expectation value of the Higgs) and the Yukawa coupling h.

For the masses of the gauge field we cut a long story short and simply note that in a mean field analysis as that done above for the fermion

$$(W_\mu \phi)^\dagger (W_\mu \phi) \xrightarrow{\text{mean field}} (W_\mu \phi_0)^\dagger (W_\mu \phi_0) , \tag{IV.33}$$

leads to mass terms for the gauge fields. Since the vacuum field ϕ_0 has vanishing upper component ϕ_1 it is a combination of the generator $t^3 = \sigma_3/2$ of the weak $SU(2)$ and the generator $\mathbb{1}$ of the hypercharge $U(1)$ which remains massless: the photon. This also determines the subgroup which leaves the vacuum invariant. The superficial analysis here also reveals that the quotient involves three generators and hence we have three Goldstone bosons. In summary we hence start with three gauge bosons with two physical polarisations each together with three Goldstone bosons, which adds up to nine field degrees of freedom (dof). A convenient reparameterisation (including an appropriate gauge fixing, e.g. the unitary gauge) of the Standard Model leads us to three massive vector bosons with three polarisations each, that is again nine dofs.

D. Low energy effective theories of QCD

The Higgs mechanism in the electroweak sector of the Standard Model leads to (current) quark masses for the up and down quark of a couple of MeVs, $(m_{u/d})_{\rm cur} \approx$ 2-5 MeV, see Table I. However, the masses of the nucleons, the protons and neutrons, is about 1 GeV (proton (uud) $\approx$ 938 MeV , neutron (udd) $\approx$ 940 MeV), that is two orders of magnitude bigger. In other words, the three constituent quarks in the nucleons must have an effective mass of about $(m_{u/d})_{\rm con} \approx$ 300-4 00 MeV, the constituent quark masses. We already infer from this that there should be a further mechanism to generate this mass scale.

In low energy QCD with its mass scale $\Lambda_{\rm QCD} \approx 200 - 300\,{\rm MeV}$ the electroweak sector of the Standard Model decouples as do the heavier quarks. We are left with two light (up and down) and one heavy quark (charm), Table I. Within fully quantitative computations of the QCD dynamics at low energies the strange quark with its current mass of about 1.2 GeV is also added. Still, its dynamics is very much suppressed at momentum scales of $\Lambda_{\rm QCD}$. For the present structural analysis we first resort to two flavour QCD ($N_f = 2$) with the Euclidean action

$$S_{\rm QCD}[\Phi] = \frac{1}{4}\int_x F^a_{\mu\nu}F^a_{\mu\nu} + \int_x \bar\psi\cdot(\not D + m_\psi + i\mu\gamma_0)\cdot\psi\,, \tag{IV.34}$$

where ψ is a Dirac spinor with two flavours and Φ is the two-flavour super field, see (I.35). The physics of the matter sector at low energies and temperatures, and not too large densities is well-described by quark-hadron models, the most prominent of which is the Nambu-Jona-Lasino model. From the perturbative point of view these models are seeded in the four-fermi coupling already being generated from the propagators and couplings depicted in Fig. 1 at tree level. The related tree level diagram is depicted in Fig. 7. Its s-channel has the structure

$$g^2\left(\bar\psi\gamma_\mu t^a\psi\right)(p)\,\Pi_{\mu\nu}(p)\frac{1}{p^2}\,\left(\bar\psi\gamma_\mu t^a\psi\right)(p)\,, \tag{IV.35}$$

describing the scattering of quarks. In (IV.35) the t^a are generators of the color gauge group and the fermions are summed over the two flavours. Accordingly, (IV.35) generates a four-fermi interaction with a non-trivial momentum structure in the effective action of QCD.

The full momentum- and tensor structure is complicated even for the present simplified $N_f = 2$ case. As in the four-fermi theory (Fermi theory) for weak interactions we resort to an approximation with point-like interactions (no momentum dependence). Then (IV.35) can be rewritten in terms of an effective *local* (point-like) four-fermi interaction. Such a rewriting in terms of local four-fermi interactions holds for energies that are sufficiently low and do not resolve the large momentum structure of the scattering in (IV.35). Moreover, the coupling is dimensionful and has the canonical momentum dimension -2 (related to the $1/p^2$ term in (IV.35). In the Fermi theory of weak interactions this is the electroweak scale. In the present case it has to be related to the QCD mass gap proportional to $\Lambda_{\rm QCD}$.

We postpone the detailed analysis of this scale, and first concentrate on the tensor structure of (IV.35). This is constrained by the symmetries of the theory, for a full discussion of the symmetry pattern we refer to the literature, e.g. [7, 8] and literature therein. Since the current masses of the light quarks are nearly vanishing we first work in the chiral limit. Then, any interaction that is generated by the dynamics of QCD carries chiral symmetry: the related four-fermi interaction is chirally invariant, that is the invariance under the chiral transformations

$$\psi \to e^{i\frac{1\pm\gamma_5}{2}\alpha}\psi \quad\to\quad \bar\psi \to \bar\psi e^{i\frac{1\mp\gamma_5}{2}\alpha} \qquad \text{with} \qquad \gamma_5 = \gamma_0\gamma_1\gamma_2\gamma_3\,, \quad \text{and} \quad \{\gamma_5\,,\,\gamma_\mu\} = 0\,, \tag{IV.36}$$

which holds separately for each vector current $\psi\gamma_\mu t^a\psi$. Furthermore, in the chiral limit QCD is invariant under flavour rotations $SU(N_f)$. For example, for $N_f = 2$ with up (u) and down (d) quarks and the flavour isospin group with $SU(2)$, the transformation reads

$$\psi = \begin{pmatrix} u \\ d \end{pmatrix} \to V \begin{pmatrix} u \\ d \end{pmatrix}\,, \qquad \text{with} \qquad V = e^{i\theta^a\tau^a} \in SU(2)\,, \tag{IV.37}$$

with $a = 1, 2, 3$. For the 2+1 flavour case also considered here the respective symmetry is $SU(3)_F$. Chiral symmetry entails that the flavour rotations are a symmetry for the left- and right-handed quarks separately and the combined symmetry is $SU(2)_L \times SU(2)_R$ with symmetry transformations $V_{L/R} = e^{i\frac{1\pm\gamma_5}{2}\theta^a t^a}$. Including also the chiral $U(1)$ rotations leads us to the full symmetry group

$$G_{\rm sym} = SU(N_c) \times SU(N_f)_V \times SU(N_f)_A \times U(1)_V \times U(1)_A\,, \tag{IV.38}$$

where we have also taken into account the gauge group $SU(N_c)$. If we approximate (IV.35) by a point-like four-fermi interaction, one has to expand the tensor $\gamma_\mu \otimes \gamma_\nu$ multiplied by gauge group and flavour tensors. Then, the most general symmetric Ansatz is a combination of the tensor structures

$$\begin{aligned}(V-A) &= (\bar\psi\gamma^\mu\psi)^2 + (\bar\psi\gamma^\mu\gamma^5\psi)^2\\ (V+A) &= (\bar\psi\gamma^\mu\psi)^2 - (\bar\psi\gamma^\mu\gamma^5\psi)^2\\ (S-P) &= (\bar\psi^f\psi^g)^2 - (\bar\psi^f\gamma^5\psi^g)^2\\ (V-A)^{\rm adj} &= (\bar\psi\gamma^\mu t^a\psi)^2 + (\bar\psi\gamma^\mu\gamma^5 t^a\psi)^2\,,\end{aligned} \tag{IV.39}$$

where f, g are flavour indices and $(\bar\psi^f\psi^g)^2 \equiv \bar\psi^f\psi^g\bar\psi^g\psi^f$. While each separate term in the tensors in (IV.39) is invariant under gauge transformation, and under the flavour vector transformations, axial rotations in $SU(N_f)_A \times U(1)_A$ rotate the terms on the right hand side in (IV.39) into each other. For a related full analysis we refer to the literature. However, below we shall exemplify these computations at the relevant example of the scalar–pseudo-scalar channel

The chiral invariants (IV.39) can be rewritten using the Fierz transformations which relates different four-fermi terms on the basis of the Grassmann natures of the fermions. These transformations are explained and detailed in the literature, see e.g. [7, 8]. Here we just concentrate on the scalar–pseudo-scalar channels in physical two-flavour QCD with $N_c = 3$ and $N_f = 2$. These channels are related to the scalar σ-meson and the pseudo-scalar pions $\vec\pi$. The $(S-P)$-channel is given by

$$(S-P) = \frac{1}{2}\left[(\bar\psi\psi)^2 + (\bar\psi\vec\tau\psi)^2 - (\bar\psi\gamma^5\psi)^2 - (\bar\psi\gamma^5\vec\tau\psi)^2\right]\,, \tag{IV.40}$$

where $\vec\tau = (\sigma_1, \sigma_2, \sigma_3)$ with Pauli matrices

$$\sigma_1 = \begin{pmatrix} 0 & 1\\ 1 & 0\end{pmatrix}\,, \qquad \sigma_2 = \begin{pmatrix} 0 & -i\\ i & 0\end{pmatrix}\,, \qquad \sigma_3 = \begin{pmatrix} 1 & 0\\ 0 & -1\end{pmatrix}\,, \tag{IV.41}$$

The representation (IV.40) simplifies the identification of the scalar mode $\bar\psi\psi$ related to the scalar σ-meson, and the pseudo-scalar modes $i\bar\psi\gamma_5\vec\tau\psi$ related to the pseudo-scalar (axial-scalar) pions $\vec\pi$.

We shall use the representation (IV.40) in the following investigations of the chiral properties of low energy QCD. Hence we discuss its symmetry properties in more detail, and show explicitly its invariance under $G_{\rm sym}$. To begin with, the invariance of $(S-P)$ under gauge and flavour $U_V(1)$ transformation is apparent. The flavour $SU(2)_V$ transformations $\psi \to e^{i\theta^a\tau^a}\psi$ trivially leaves $\bar\psi\psi$ and $\bar\psi\gamma_5\psi$ invariant. For the vector and pseudo-vector bilinears we concentrate on infinitesimal transformations $e^{i\theta^a\tau^a} = 1 + i\theta^a\tau^a + O(\theta^2)$. Then the second term in (IV.40) transforms as

$$(\bar\psi\vec\tau\psi)^2 \;\longrightarrow\; (\bar\psi\vec\tau\psi)^2 + 2i\,\theta^a(\bar\psi\vec\tau\psi)(\bar\psi[\vec\tau\,,\,\tau^a]\psi) = (\bar\psi\vec\tau\psi)^2 - 2\,\theta^a\epsilon^{bac}(\bar\psi\tau^b\psi)(\bar\psi\tau^c\psi) = (\bar\psi\vec\tau\psi)^2\,. \tag{IV.42}$$

The invariance of the last term in (IV.40) under $SU(2)_V$ transformations follows analogously. Finally, axial transformations related the first two terms to the last two terms. We exemplify this property with the axial $U_A(1)$ rotations $\psi \to e^{i\gamma_5\alpha}\psi$, where we consider infinitesimal transformations with $e^{i\gamma_5\alpha} = 1\!\!1 + i\gamma_5\alpha + O(\alpha^2)$. Concentrating on the scalar and pseudo-scalar terms we have

$$(\bar\psi\psi)^2 - (\bar\psi\gamma^5\psi)^2 \;\longrightarrow\; (\bar\psi\psi)^2 - (\bar\psi\gamma^5\psi)^2 + 4i\,\alpha\Big[(\bar\psi\psi)(\bar\psi\gamma_5\psi) - (\bar\psi\gamma^5\psi)(\bar\psi\psi)\Big] = (\bar\psi\psi)^2 - (\bar\psi\gamma^5\psi)^2\,, \tag{IV.43}$$

The invariance for the full expression in (IV.40) follows analogously. It is left to study $SU(2)_A$ transformations. Now we show that (IV.40) also carries the $SU(2)_A$-invariance. To that end we consider infinitesimal $SU(2)_A$ transformations $e^{i\gamma_5\theta^a\tau^a} = 1 + i\gamma_5\theta^a\tau^a + O(\theta^2)$ of the combination $(\bar\psi\psi)^2 - (\bar\psi\gamma^5\vec\tau\psi)^2$, and use the Lie algebra identity

$$\tau^a\tau^b = \delta^{ab} + i\epsilon^{abc}\tau^c\,, \qquad \to \qquad \{\tau^a\,,\,\tau^b\} = 2\delta^{ab}\,. \tag{IV.44}$$

Then we are led to

$$(\bar\psi\psi)^2 - (\bar\psi\gamma^5\vec\tau\psi)^2 \;\longrightarrow\; (\bar\psi\psi)^2 - (\bar\psi\gamma^5\vec\tau\psi)^2 + 2i\,\theta^a\Big[(\bar\psi\psi)(\bar\psi\gamma_5\tau^a\psi) - (\bar\psi\gamma^5\tau^b\psi)\left(\bar\psi\{\tau^a\,,\,\tau^b\}\psi\right)\Big] = (\bar\psi\psi)^2 - (\bar\psi\gamma^5\psi)^2\,. \tag{IV.45}$$

The invariance of the combination $(\bar\psi\gamma_5\psi)^2 - (\bar\psi\vec\tau\psi)^2$ is shown along the same lines. Consequently (IV.40) is invariant

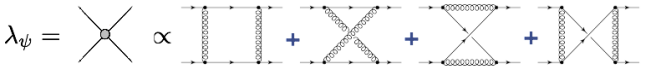

FIG. 7: One loop diagrams for the four-fermi coupling λ_ψ in QCD.

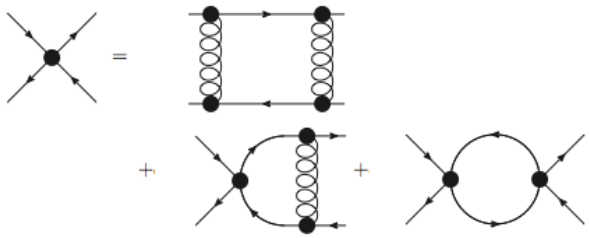

FIG. 8: One loop diagrams for the four-fermi coupling λ_ψ from the action (IV.51).

under $SU(2)_A$ transformation and hence under the full symmetry group $G_{\rm sym}$.

In QCD, we have experimental evidence for the breaking of the axial $U_A(1)$-symmetry, i.e. the pseudo-scalar η'-meson (in $N_f = 2$ the η) is anomalously heavy. This mass-difference can be nicely explained by the anomalous breaking of axial $U_A(1)$ symmetry. Consequently, giving up axial $U_A(1)$-symmetry we have to consider more four-fermi interactions as in (IV.39) (altogether 10 invariants for $N_f = 2$), in particular

$$\frac{1}{2}\left[(\bar\psi\psi)^2 - (\bar\psi\vec\tau\psi)^2 + (\bar\psi\gamma^5\psi)^2 - (\bar\psi\gamma^5\vec\tau\psi)^2\right] . \tag{IV.46}$$

It is the relative minus signs in the scalar and pseudo-scalar terms in comparison to (IV.40) that leads to the breaking of $U_A(1)$-symmetry. This is easily seen by re-doing the infinitesimal analysis (IV.43) in (IV.46). If also follows easily that the other symmetries still hold, in particular the $SU(2)_V \times SU_A(2)_A$ invariance follows as (IV.46) contains the same $SU(2)_V \times SU_A(2)_A$-invariant combinations of four-quark terms as (IV.40). Hence we conclude that the combination (IV.46) only breaks $U_A(1)$-symmetry, and adding up the two channels (IV.40) and (IV.46) leads to the $U_A(1)$-breaking combination

$$\frac{1}{2}\left[(\bar\psi\psi)^2 - (\bar\psi\gamma^5\vec\tau\psi)^2\right] . \tag{IV.47}$$

Eq.(IV.47) is invariant under the remaining symmetries $SU(N_c) \times SU(N_f)_V \times SU(N_f)_A \times U(1)_V$. This concludes our brief discussion of the global symmetries of QCD in the chiral limit.

In summary the following picture emerges: assume we perform a chain of scattering experiments of QCD/Standard Model starting at the electroweak scale ≈ 90 Gev towards the strong QCD scale $\Lambda_{\rm QCD}$. At each scale we can describe the quantum equations of motion and scattering experiments by a suitably chosen effective action $\Gamma[\phi]$. On the level of the path integral for QCD, (I.33), this is described by the Wilsonian idea of integrating out momentum modes above some momentum scale μ,

$$Z_\mu[J] = \int [{\rm d}\Phi]_{p^2\geq\mu^2}\, e^{-S_{\rm QCD}[\Phi]+\int_x J\cdot\Phi} \qquad \Rightarrow \qquad \text{Effective Action } \Gamma_\mu[\Phi]\,, \tag{IV.48}$$

where the path integral measure only contains an integration over fields Φ_μ that are non-vanishing for $p^2 \geq \mu^2$: $\Phi_\mu(p^2 < \mu^2) \equiv 0$. After Legendre transformation this leads us to an effective action $\Gamma_\mu[\Phi]$ that only contains the quantum effects of scales larger than the running (RG) scale μ and serves as a classical action for the quantum effects with momentum scales $p^2 < \mu^2$. This effective action also carries the symmetries of the fundamental QCD action, as long as these symmetries are not (anomalously broken by quantum effects.

We know already from the perturbative renormalisation programme that this amounts to adjusting the (running) coupling in the (classical) action with the sliding (experimental) momentum scale. In such a Wilsonian setting this is very apparent. The running of the coupling comes from the loop diagrams that are evaluated at the momentum scale μ. On top of this momentum adjustment of the fundamental parameters of the theory one also creates additional terms in the -effective- action. The one of importance for us is the four-fermi terms argued for above. It is created at one-loop with the box diagrams depicted in depicted in Fig. 7. This leads us finally to the following four-fermi

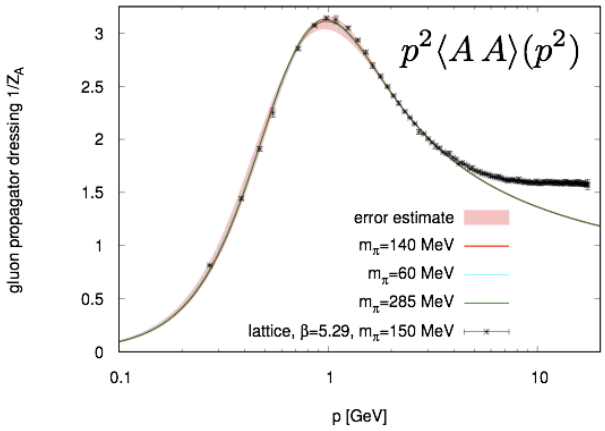

FIG. 9: Gluon propagator for $N_f = 2$ from the lattice and from non-perturbative diagrammatic methods, taken from [9].

interaction in the effective action,

$$\Gamma_{4-\text{fermi}}[\phi]|_{1-\text{loop}} = -\frac{\lambda_\psi}{4}\int\left[(\bar\psi\psi)^2 - (\bar\psi\gamma^5\vec\tau\psi)^2\right] + \cdots \qquad \text{with} \qquad \lambda_\psi \propto \alpha_s^2\,, \tag{IV.49}$$

where it is understood that the coupling λ_ψ carries the running momentum or RG scale μ introduced above. Together with the kinetic term of the quarks this is the classical action of the Nambu–Jona-Lasinio type model. Eq.(IV.49) holds for massless quarks and two flavours, $N_f = 2$. The two terms in (IV.49) carry the same quantum number as the scalar and axial-scalar excitations in low energy QCD, the sigma-meson σ and pion $\vec\pi$ respectively. The one loop diagrams generating the four-fermi coupling λ_ψ are depicted in Fig. 7. In line with the picture outlined above the four-fermi coupling λ_ψ at a given momentum scale $p = \mu$ should be computed with the loop momenta q in the box diagrams in Fig. 7 being bigger than μ. Than the related diagram is peaked at this scale and we conclude by dimensional analysis that

$$\lambda_\psi(\mu) \simeq \alpha_s^2(\mu)\frac{1}{\mu^2}\,. \tag{IV.50}$$

Note that this coupling feeds back into the loop expansion of other correlations functions such as the quark propagator and quark-gluon vertices. However, in comparison to other (one-loop) diagrams it is suppressed by additional orders of the strong coupling α_s. In turn, in the low momentum regime where α_s grows strong it gives potentially relevant contributions. Indeed, taking as a starting point for a loop analysis the sum of the QCD action (IV.34) and the four-fermi term (IV.49)

$$\Gamma[\phi] \simeq S_{\text{QCD}}[\phi] + \Gamma_{4-\text{fermi}}[\phi]\,, \tag{IV.51}$$

we get also self-interaction terms of the four-fermi coupling proportional to λ_ψ^2 as well as terms proportional to $\alpha_s\lambda_\psi$. This is depicted in Fig. 8.

The glue sector of QCD is expected to have a mass gap already present in the purely gluonic theory, related to the confinement property of Yang-Mills theory. Then this has to manifest itself in a decoupling of the gluonic contribution to the four-fermi coupling in Fig. 8. In the Landau gauge this mechanism is easily visible due to the mass gap in the gluon propagators, see Fig. 9 for lattice results and results from non-perturbative diagrammatic methods.

Note that the gluon propagator is gauge dependent, and the careful statement is that the Landau gauge facilitates the access to the related physics. One should not confuse this with a massive gluon, as the gluon is no physical particle and shows positivity violation. Moreover, the gluonic sector is certainly relevant for the confining physics and hence the decoupling discussed above only takes place in the matter sector for the specific question under investigation, the mechanism of strong chiral symmetry breaking.

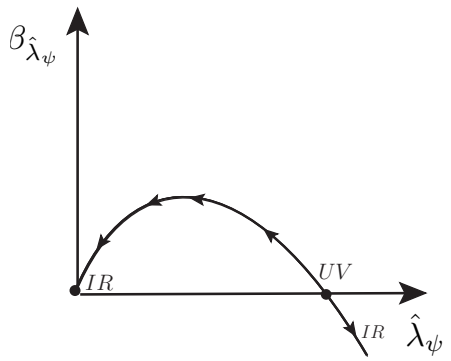

FIG. 10: Fixed point structure of λ_ψ for the four-fermi coupling in the NJL model.

E. Strong chiral symmetry breaking and quark-hadron effective theories

Assuming for the moment the gluonic decoupling we are left with a purely fermionic theory. The four-fermi term (IV.49) is the interaction part of the Nambu–Jona-Lasino model, one of the best-studied model for low energy QCD, see e.g. [7, 8, 10]. It is non-renormalisable as can be seen from the momentum dimension of the four-fermi coupling which is -2. As shown above, in QCD it is generated by fluctuations with $\lambda_\psi(p) \propto \alpha_s(p)$ and tends to zero in the UV, that is for large momenta $p \to \infty$. Its momentum dependence is best extracted from the dimensionless coupling

$$\hat\lambda_\psi = \lambda_\psi(\mu)\mu^2\,, \tag{IV.52}$$

where we have introduced the renormalisation group scale μ, here being identical with the momentum scale of the scattering process described, $\mu^2 = p^2$. The β-function of the dimensionless four-fermi coupling in (IV.52) is given by

$$\beta_{\hat\lambda_\psi} = \mu\partial_\mu\hat\lambda_\psi = 2\hat\lambda_\psi - c\,\hat\lambda^2 \qquad \text{with} \qquad c > 0\,, \tag{IV.53}$$

and is depicted in Fig. 10. The first term on the right hand side of (IV.53) encodes the trivial dimensional running of $\hat\lambda = \mu^2\lambda$. The second term on the right hand side originates in the last diagram in Fig. 8, the pure four-fermi term. In the absense of other mass scales this loop has to be proportional to μ^2 leading to a factor two in the β-function in comparison to the loop itself. The key feature relevant for the description of chiral symmetry breaking is the sign of the diagram. It is negative, $-c\hat\lambda^2$, with a positive constant c leading to (IV.53).

From the perspective of a one-loop investigation based on the classical fermionic action in (IV.51) the coupling in the loop term on the right hand side of (IV.53) is the classical one in this action. As we have done for the β-function of the strong coupling, e.g. (II.17), we can elevate this coupling to the full running coupling in terms of a one-loop RG-improvement. This accounts for a one-loop resummation of diagrams. In the present context the physics behind such an improvement is very apparent: As already indicated, the NJL-type action was derived within a successive integrating out of momentum modes, and constitutes an effective action for the UV physics with $p^2 \geq \mu^2$. Accordingly, its couplings depend on this RG-scale. In summary we end up with (IV.53) with μ-dependen couplings on the right hand side. Note that this is only a one-loop RG improvement as we have discarded the μ-dependence of the couplings in the diagram when taking the μ-derivative. The related terms are proportional to $-c/2\,\hat\lambda\,\mu\partial_\mu\hat\lambda_\psi$ and can be shuffled to the left hand side. This accounts for a further resummation leading to (IV.53) with a global factor $1/(1 + c/2\,\hat\lambda)$ on the right hand side. In the following qualitative analysis it is dropped and we strictly resort to the one-loop improvement.

The β-function of (IV.53) is depicted in Fig. 10. It divides the positive $\hat\lambda_\psi$-axis into two physically distinct regimes,

$$I_1 = [0, \hat\lambda_{\rm UV}) \qquad \text{and} \qquad I_2 = (\hat\lambda_{\rm UV}, \infty) \qquad \text{with} \qquad \beta_{\hat\lambda_\psi}(\hat\lambda_{\rm UV}) = 0 \qquad \text{with} \qquad \hat\lambda_{\rm UV} = \frac{2}{c}\,. \tag{IV.54}$$

The zeroes of the β-function are fixed points of the renormalisation group flows, and $\hat\lambda_{\rm UV} \neq 0$ is a non-trivial fixed point FP of the β-function while $\hat\lambda_{\rm Gauß} = 0$ is the trivial Gauian fixed point (related to the free Gaußian theory). Now we initiate the RG-flow at an initial ultraviolet scale $\mu_{\rm in}$ with some value of the dimensionless four-fermi coupling

$$\hat\lambda(\mu_{\rm in}) = \hat\lambda_{\rm in}\,. \tag{IV.55}$$

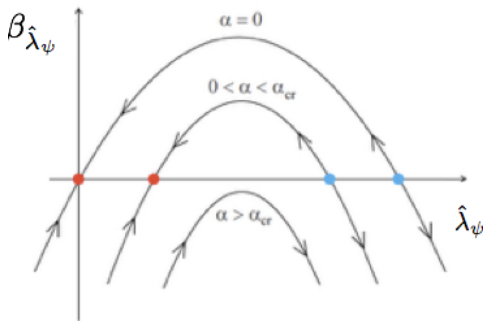

FIG. 11: Fixed point structure of λ_ψ of the full β-function

If $\hat\lambda_{\rm in} < \hat\lambda_{\rm UV}$ and we lower the running momentum scale, the RG-flow lowers the four-fermi coupling towards 0. Accordingly $\hat\lambda_\psi(\mu \to 0) = 0$. Since the regime of small couplings is governed by the linear term $2\hat\lambda_\psi$ in the β-function in (IV.53) this entails $\lambda_\psi(\mu \to 0) = \lambda_0$. Here λ_0 is some finite value which is adjusted by the input $\hat\lambda_{\rm in}$ at the initial scale $\mu_{\rm in}$.

In turn, if $\hat\lambda_{\rm in} > \hat\lambda_{\rm UV}$, the RG-flow toward smaller μ drives $\hat\lambda_\psi$ towards ∞. Then the linear term can be neglected as it is sub-leading and the RG-flow reads

$$\mu\partial_\mu\hat\lambda = -c\,\hat\lambda_\psi^2\,, \qquad \longrightarrow \qquad \hat\lambda(\mu) = \frac{\hat\lambda(\mu_0)}{1+\hat\lambda(\mu_0)c\,\log\mu/\mu_0}\,, \tag{IV.56}$$

where μ_0 is some reference scale at which the approximation in the RG-flow in (IV.56) is already valid. We conclude from (IV.56) diverges at

$$\mu = \mu_0 \exp\left\{-\frac{1}{c\,\lambda(\mu_0)}\right\}\,, \tag{IV.57}$$

which signals a resonance in the four-fermi scalar-pseudo–scalar channel.

At this scale chiral symmetry breaking occurs. To make this more apparent we resort to a further rewriting of our low energy effective theory in terms of the scalar, σ, and pseudo-scalar, $\vec\pi$, degrees of freedom. This is suggestive already for the reason that the divergence in (IV.56) entails that these resonance are relevant degrees of freedom for lower momentum scales. For the rewriting of the theory we use the Hubbard-Stratonovich transformation, see e.g. [7, 8, 10]. With this transformation we a four-fermi interaction using a scalar auxiliary field. Concentrating on the scalar part of the four-fermi interaction in (IV.49) we write at some momentum scale μ,

$$-\frac{\lambda_\psi}{4}(\bar\psi\psi)^2 = \left[\frac{h}{2}(\bar\psi\psi)\sigma + \frac{m_\varphi^2}{2}\sigma^2\right]_{{\rm EoM}(\sigma)}\,, \qquad \text{with} \qquad \lambda_\psi = \frac{h^2}{m_\varphi^2}\,. \tag{IV.58}$$

Accordingly we can extend the effective action $\Gamma[\phi]$ given in (IV.51) by the right hand side of (IV.58) while dropping the four-fermi term. For the sake of simplicity we concentrate on the σ-meson first and reduce the four-fermi term to its scalar part. Then

$$\Gamma[\phi] \to \Gamma[\phi,\sigma] = \Gamma[\phi]|_{\lambda_\psi\to 0} + \left[\frac{h}{2}(\bar\psi\psi)\sigma + \frac{m^2}{2}\sigma^2\right]_{h^2/m^2=\lambda_\psi}\,, \tag{IV.59}$$

This new effective action agrees with the original one on the equation of motion of σ and hence carries the same physics. As a side remark, note that the 1PI correlation functions of quarks and gluon derived from $\Gamma[\phi,\sigma]$ at fixed σ do not agree with the quark and gluon correlation functions derived from $\Gamma[\phi] = \Gamma[\phi,\sigma_{\rm EoM}(\phi)]$, the implicit dependences also contribute.

A similar derivation can be done for the pion part of the four-fermi interaction, and hence the whole four-fermi interaction can be bosonised. The mesonic equations of motion can be summarised in

$$\sigma_{\rm EoM} = \frac{h}{2m_\varphi^2}\,\bar\psi\psi\,, \qquad\qquad \vec\pi_{\rm EoM} = \frac{h}{2m_\varphi^2}\,\bar\psi\, i\gamma_5\vec\tau\psi\,. \tag{IV.60}$$

On the level of the generating functional of QCD, (IV.58) and its extension to pions can be implemented by a Gaußian path integral with

$$\exp\left\{\frac{\lambda_\psi}{4}\int\left[(\bar\psi\psi)^2-(\bar\psi\gamma^5\vec\tau\psi)^2\right]\right\}=\int \mathrm{d}\sigma\mathrm{d}\vec\pi\,\exp\left\{-\int_x\left(\frac{1}{2}m^2(\sigma^2+\vec\pi^2)+\frac{h}{2}\bar\psi\left[\sigma+i\gamma_5\vec\tau\vec\pi\right]\psi\right)\right\}_{h^2/m^2=\lambda_\psi}\,. \quad \text{(IV.61)}$$

We also remark that as shift in the σ-field,

$$\sigma\to-\frac{2}{h}m_\psi+\sigma\,, \quad \text{(IV.62)}$$

eliminates the quark mass term at the expense of the linear term in σ that can be interpreted as a source term. Inserting this identity in the path integral for the low energy dofs including the currents for the fundamental fields, the quarks and gluons (and ghosts) as well as current for the mesonic dofs we have the full generating functional in this setting. Performing the Legendre transformation we are immediately led to (IV.59). Kinetic terms as well as a potential for σ are generated by further quantum effects. In summary this leads us finally to a low energy effective theory with a classical action $S_{\rm eff}=\Gamma_{\rm UV}$, where $\Gamma_{\rm UV}$ is the full quantum effective action including quantum fluctuations above a given cutoff scale Λ. This also entails that $S_{\rm eff}$ carries a Λ-dependence. $S_{\rm eff}$ is given by

$$S_{\rm eff}[\psi,\bar\psi,\phi]\propto\int_x\bar\psi\cdot(\not{D}+m_\psi)\cdot\psi+\int_x\left[(\partial_\mu\sigma)^2+(\partial_\mu\vec\pi)^2\right]+\int_x\frac{h}{2}\bar\psi\left[\sigma+i\gamma_5\vec\tau\vec\pi\right]\psi+\int_x V_{\rm UV}(\rho) \quad \text{(IV.63)}$$

with $\phi=(\sigma,\vec\pi)$ and

$$V_{\rm UV}(\rho)=m_\varphi^2\rho+\frac{\lambda}{2}\rho^2\,,\qquad\text{with}\qquad\rho=\frac{1}{2}\left(\sigma^2+\vec\pi^2\right)\,. \quad \text{(IV.64)}$$

As indicated above, the quark mass term can be eliminated at the expense of a linear term in σ by the shift of σ in (IV.62). On the level of the quadratic quark-meson interaction (IV.61) this triggers a linear term $c_\sigma\sigma$ and the full potential reads

$$V_{\rm UV}(\rho)=m_\varphi^2\rho+\frac{\lambda_\varphi}{2}\rho^2-c_\sigma\,\sigma\,,\qquad\text{with}\qquad c_\sigma=\frac{2}{h}m_\varphi^2m_\psi\,. \quad \text{(IV.65)}$$

This concludes the derivation of the low energy effective theory with the action (IV.63) from QCD by *integrating-out* QCD quantum fluctuations above the validity scale of the low energy effective theory. From the gluonic decoupling scale $\Lambda_{\rm dec}\lesssim 1$ GeV one concludes that (IV.63) should be seen as a classical action for quantum fluctuations with momenta $p^2\lesssim 1$ GeV, see Fig. 9. A more detailed analysis reveals that the initial scale for low energy effective theories has to be taken far lower for quantitative computations. Nonetheless, for qualitative considerations it is sufficient, and, as a matter of fact, low energy effective theories even work well quantitatively at surprisingly large moment scale about 1 GeV.

In (IV.63) we have introduced a self-interaction of the mesonic fields proportional to ρ^2 as well as an explicit breaking term linear in σ related to the quark mass term. The question arises, is this the most general ϕ^4-term one can generate from QCD? As mentioned before, the symmetries of this low energy effective field theory (EFT) are determined by those of the action of QCD. In the chiral limit the full symmetry group is (IV.38). The axial $U_A(1)$ symmetry is anomalously broken, hence our restriction to the $U_A(1)$-breaking combination (IV.47). In its bosonised quark-meson mode version the symmetry transformations with $G_{\rm sym}$ also involve transformations of the mesonic fields. Their transformation properties can be most easily accessed in the matrix notation for the field. To that end we introduce

$$\hat\phi=\mathbb{1}\,\sigma+i\gamma_5\vec\tau\vec\pi\qquad\text{with}\qquad\hat\phi_{\rm EoM}=\frac{h}{2m_\varphi^2}\left(\mathbb{1}\,\bar\psi\psi-\gamma_5\vec\tau\,\bar\psi\gamma_5\vec\tau\psi\right)\,, \quad \text{(IV.66)}$$

where we have used (IV.60) in the second equation. Now we can read-off the symmetry transformations under $V\in SU(N_c)\times SU(N_f)_V\times SU(N_f)_A\times U(1)_V$ from (IV.66) by evoking the symmetry transformations of the quarks. One easily sees that axial $U(1)_A$-rotations do not close on σ and $\vec\pi$. For example, $\sigma_{\rm EoM}$ transforms into $\bar\psi\gamma_5\psi$. Furthermore, ϕ is invariant under vector $U_V(1)$ transformations. Similarly, σ is invariant under transformations with $e^{i\theta^a\tau^a}\in SU(2)_V$, while π is rotated, $\vec\pi\to V\vec\pi$ with $V=e^{\theta^at^a}\in O(3)$ with $(t^a)^{bc}=\epsilon^{abc}$. This follows from

$$\bar\psi\gamma_5\vec\tau\psi\;\longrightarrow\;\bar\psi\gamma_5\vec\tau\psi+i\theta^a\bar\psi\gamma_5[\vec\tau\,,\,\tau^a]\psi=\bar\psi\gamma_5\vec\tau\psi-\theta^a\epsilon^{bac}\bar\psi\gamma_5\tau^c\psi\,. \quad \text{(IV.67)}$$

Finally, transformations with $e^{i\gamma_5\theta^a\tau^a} \in SU(2)_A$ rotate $(\sigma, \vec{\pi})$ into each other. This is read-off from the infinitesimal transformations of $\hat{\phi}_{\text{EoM}}$ leading to

$$\sigma \to \sigma + 2\theta^a\pi^a\,, \qquad\qquad \pi^b \to \pi^b - \theta^b\sigma\,. \tag{IV.68}$$

Combining all the manifestations of the symmetry group we are led to an $O(4)$ invariance of our low energy effective field theory, sloppily written as

$$\psi \to V\psi \quad \text{with} \quad V \in G_{\text{sym}}/U_A(1)\,, \qquad \phi \to e^{\theta^a t^a}\phi\,, \qquad \text{with} \quad \phi = \begin{pmatrix} \vec{\pi} \\ \sigma \end{pmatrix} \quad \text{and} \quad e^{\theta^a t^a} \in O(4)\,. \tag{IV.69}$$

In conclusion chiral symmetry breaking is in one-to-one correspondence to the breaking of the $O(4)$-symmetry. Moreover, the formulation with effective mesonic σ and pion degrees of freedom now allows us to discuss strong chiral symmetry breaking in complete analogy to the Higgs mechanism that served as an introductory example. Let us first consider the fully symmetric case with $c_\sigma = 0$. The mesonic sector of (IV.63) simply is an $O(4)$-model, and the QCD four-fermi coupling are related to the Yukawa coupling and the mesonic mass parameters via the relation (IV.58) in the Hubbard-Stratonovich transformation. Accordingly, a diverging λ_ψ implies a vanishing m_φ if the Yukawa coupling is fixed. Hence, at the singularity of λ_ψ the mesonic mass parameter m_φ^2 changes sign. For $m_\varphi^2 < 0$ we are in the phase of -spontaneously- broken $O(4)$-symmetry. We choose the σ direction as our radial mode, and its expectation value is given by

$$\sigma_0 = \sqrt{\frac{-m_\varphi^2}{\lambda_\varphi}}\,, \tag{IV.70}$$

in the chiral limit. This leads to an effective quark mass term with

$$m_\psi = \frac{h}{2}\sigma_0 = \frac{h}{2}\sqrt{\frac{-m_\varphi^2}{\lambda_\varphi}}\,, \tag{IV.71}$$

which in QCD is of the order of 300 MeV.

In summary we have derivated low energy EFTs in QCD by successively integrating out momentum shells of quantum fluctuations in QCD. The first class of low energy EFTS we encountered are the *Nambu-Jona–Lasigno type four-quark models* (in short in a slight abuse of notation NJL-model), baptised after a seminal work of Nambu and Jona-Lasigno from 1961 introducing a four-fermi model for Nucleons. The NJL-model is not renormlisable and requires a ultraviolet cutoff scale Λ_{UV} that cannot be removed.

In a second step we have bosonised the resonant scalar–pseudo-scalar channels of the four-quark interaction leading us to a Yukawa-type model, the *Quark-Meson Model* (QM-model). This model is renormalisable and its UV cutoff Λ_{UV} seemingly can be removed to infinity. However, we emphasise that the two models are equivalent on the level of the respective path integrals via the Hubbard-Stratonovich transformation. In other words, if one considers all quantum fluctuations in both models the physics results are the same, as must be the necessity of a ultraviolet cutoff scale Λ_{UV}. In the QM model this necessity is encoded in a UV-instability of the model. In other words, its renormalisability is of no help if it comes to the existence of the model at large scales.

Finally, despite being low energy EFTs, these models have a complicated dynamics reflecting the strongly-correlated nature of low energy QCD. Hence, typically one resorts to approximations within these models. In the reminder of this chapter we shall discuss different approximations to the Quark-Meson model ranging from a mean-field treatment to a full non-perturbative renormalisation group study.

F. Low energy quantum fluctuations

In the last chapter we have derived the action of the QM-model by integrating out quantum fluctuations above a momentum scale $\Lambda \approx 1$ GeV. We have argued that below this scale the gluonic degrees of freedom become less important and decouple from the theory below the mass gap of QCD. Practically, this can be seen from the results for gluonic correlation functions such as the gluon propagator displayed in Fig. 9. This entails that the action (IV.63) serves as a classical action for the quantum fluctuations with momenta $p^2 \leq \Lambda^2$. More explicitly we use the definition

(IV.48) with $\mu = \Lambda$ and arrive at the path integral

$$Z \approx \int [d\phi\, d\psi d\bar{\psi}]_{p^2\leq\Lambda^2} e^{-S_{\text{eff},\Lambda}[\psi_<,\bar{\psi}_<,\phi_<]} \qquad \text{with} \qquad Z_\Lambda \simeq e^{-S_{\text{eff},\Lambda}}\,, \tag{IV.72}$$

where we have dropped the source terms. The fields $\psi_<, \bar{\psi}_<, \phi_<$ only carry low momentum modes with momenta $p^2 < \Lambda^2$. Then the full quark field $\psi = \psi_< + \psi_>$ is a sum of $\psi_< = \psi_{p^2\geq\mu^2}$ and $\psi_> = \psi_{p^2\geq\mu^2}$. Note also that the path integral of the large momentum modes in (IV.48) is performed in the presence of fields that also carry low momentum contributions,

$$Z_\Lambda[\psi_<, \bar{\psi}_<, \phi_<] = \int [\mathrm{d}\Phi]_{p^2\geq\mu^2}\, e^{-S[\phi,\Phi]}\,. \tag{IV.73}$$

where S is the QCD action with a bosonised scalar–pseudo-scalar channel. Eq.(IV.72) is approximate as we do not integrate out the low momentum gluons. Therefore low energy quantum effects with momentum scales $p^2 \leq \Lambda$ are encoded in loop diagrams with the classical action $S_{\text{eff},\Lambda} \simeq \Gamma_\Lambda$ defined in (IV.63). Here, Γ_Λ is the effective action that originates in the integrating-out of QCD fluctuations with momenta $p^2 \geq \Lambda^2$. Henceforth we drop the supscripts $_{<,>}$ for the sake of readability.

As we have seen at the end of the last chapter, the coupling parameters in the mesonic potential play a crucial rôle for chiral symmetry breaking. Here we compute the one-loop correction to the 'classical' potential V in (IV.65) as well as studying its the renormalisation group or flow equation.

1. Quark quantum fluctuations

First we note that the quark path integral in (IV.72) with the action $S_{\text{eff},\Lambda}$ in (IV.63) is Gaußian, and hence the one-loop computation is exact. This leads to the following representation of (IV.72),

$$Z \approx \int\int [d\phi]_{p^2\leq\Lambda^2} e^{-S_{\phi,\text{eff},\Lambda}[\phi]}\,, \tag{IV.74}$$

with

$$S_{\phi,\text{eff},\Lambda}[\phi] = \int_x \left[(\partial_\mu\sigma)^2 + (\partial_\mu\vec{\pi})^2\right] + \int_x V_{\text{UV}}(\rho) - \ln\left[\frac{1}{\mathcal{N}}\int [d\psi d\bar{\psi}]_{p^2\leq\Lambda^2} e^{-\int_x \bar{\psi}\cdot\left(\not{\partial} + m_\psi\right)\cdot\psi + \int_x \frac{h}{2}\bar{\psi}[\sigma + i\gamma_5\vec{\tau}\vec{\pi}]\psi}\right]\,, \tag{IV.75}$$

where $1/\mathcal{N}$ is an appropriate, field-independent normalisation specified later. The quark path integral can be rewritten as follows,

$$\frac{1}{\mathcal{N}}\int [d\psi d\bar{\psi}]_{p^2\leq\Lambda^2}\, e^{-\int_x \bar{\psi}\cdot\left(\not{\partial} + \frac{h}{2}[\sigma + i\gamma_5\vec{\tau}\vec{\pi}]\right)\cdot\psi} = \frac{1}{\mathcal{N}}\det{}_\Lambda\left(\not{\partial} + \frac{h}{2}\left[\sigma + i\gamma_5\vec{\tau}\vec{\pi}\right]\right)\,, \tag{IV.76}$$

where $\det_\Lambda$ is the determinant from momentum modes with $p^2 \leq \Lambda^2$. Expanded in powers of the field, the logarithm of (IV.76) adds to the kinetic term in (IV.75) as well as to the potential V. It also leads to terms with higher order derivatives or derivative couplings such as $Z(\rho)(\partial_\mu\phi)^2$, $(\phi\Delta\phi)^2$. As we work at low energies we drop these terms in the spirit of an expansion in p^2/m^2_{gap} where m^2_{gap} is the lowest mass scale in QCD. Evidently the pion plays a special role as is has a very small mass in comparison to the QCD mass scale Λ_{QCD} The mass scales m_{had} of all other hadronic low energy degrees of freedom in QCD satisfy $m_{\text{had}} \gtrsim \Lambda_{\text{QCD}}$. Accordingly the pion carries the quantum fluctuations in QCD for scales below Λ_{QCD}. These scale considerations are also behind the impressively successful framework of chiral perturbation theory. In summary at leading order the low energy effective action $S_{\phi,\text{eff}}$ only changes to $V_{\text{UV}} \to V_{\phi,\text{eff}}$,

$$V_{\phi,\text{eff}}(\rho) = V_{\text{UV}}(\rho) + \Delta V_q(\rho)\,, \tag{IV.77}$$

with

$$\Delta V_q(\rho) = -\mathrm{Tr}_\Lambda \ln\left(\not{\partial} + \frac{h}{2}\left[\sigma + i\gamma_5\vec{\tau}\vec{\pi}\right]\right) + \ln\mathcal{N}\,, \qquad V_{\text{UV}}(\rho) = m^2_\varphi\rho + \frac{\lambda_\varphi}{2}\rho^2\,. \tag{IV.78}$$

In (IV.78) we have used that for a given operator $\mathcal{O}$ we have $\ln\det_\Lambda\mathcal{O} = \mathrm{Tr}_\Lambda\ln\mathcal{O}$, where the trace sums over momenta with $p^2 \leq \Lambda^2$, as well as Dirac and internal indices, and the 'classical' potential V defined in (IV.64). For the present

considerations and scales the gluonic fluctuations and background are irrelevant. Thus we have dropped the gluonic fluctuations and we also put the gauge field to zero, $A_\mu = 0$. At finite temperature and density we also will consider constant temporal backgrounds $A_0 \neq 0$ which is related to so-called *statistical confinement*. Finally we introduce a convenient choice for the normalisation $\ln \mathcal{N}$: the quark determinant at vanishing background,

$$\ln \mathcal{N} = \mathrm{Tr}_\Lambda \ln \partial\!\!\!/ \,. \tag{IV.79}$$

Due to the symmetry analysis performed above the fermionic determinant can only depend on the $O(4)$-invariant combination $\rho = 1/2(\sigma^2 + \vec{\pi}^2)$, and we can simplify the computation by using $\vec{\pi} \equiv 0$. In momentum space we have

$$\begin{aligned} V_{\phi,\mathrm{eff}}(\sigma^2/2) &= V_{\mathrm{UV}}(\sigma^2/2) - N_f N_c \int \frac{d\Omega_4}{(2\pi)^4} \int_0^\Lambda dp\, p^3\, \mathrm{tr}_{\mathrm{Dirac}} \ln \frac{i\partial\!\!\!/ + \frac{h}{2}\sigma}{i\partial\!\!\!/} \\ &= V_{\mathrm{UV}}(\sigma^2/2) - \frac{6}{\pi^2} \int_0^\Lambda dp\, p^3 \ln \frac{p^2 + \frac{h^2}{4}\sigma^2}{p^2} \,, \end{aligned} \tag{IV.80}$$

where $\int d\Omega_4 = 2\pi^2$ is the four-dimensional angular integration. The prefactor $N_f N_c = 6$ in the middle part in (IV.80) comes from the trace over flavour and colour space. The Dirac trace gives a factor 4, while the momentum symmetrisation with $p \to -p$ provides a factor $1/2$. The denominators in (IV.80) come from the normalisation (IV.79). Note also that up to these prefactors (IV.80) is nothing but the Coleman-Weinberg potential of a φ^4-theory with interaction $\lambda/4!\,\varphi^2$ where we substitute $\lambda\,\varphi^2 \to h^2\,\rho$. We have an important relative minus sign due to the fermion loop and a symmetry factor $4N_f N_c = 24$ due to the number of degrees of freedom. We simply could take over this well-known result, for a detailed discussion see e.g. chapter 1.4 in the QFTII lecture.

For its importance we recall the computation here, and also discuss some particularities due to the embedding in QCD in the present low energy EFT context. The momentum integral in (IV.80) is easily performed. We also restore the full mesonic field content, $\sigma^2/2 \to \rho$, and arrive at

$$V_{\phi,\mathrm{eff}}(\rho) = V_{\mathrm{UV}}(\rho) - \frac{3}{8\pi^2} \left[2\Lambda^2 h^2 \rho + h^4 \rho^2 \left[\ln \frac{h^2\rho}{2\Lambda^2} - \ln\left(1 + \frac{h^2\rho}{2\Lambda^2}\right)\right] + 4\Lambda^4 \ln\left(1 + \frac{h^2\rho}{2\Lambda^2}\right)\right] . \tag{IV.81}$$

Up to the symmetry factor -24 this is precisely the result of the Coleman-Weinberg computation performed originally in the context of the Higgs mechanism. We note that (IV.81) seemingly depends on the momentum cutoff scale Λ. However, the potential $V_{\mathrm{UV}}(\rho)$ is the result of integrating-out quantum fluctuations up to the momentum scale Λ and hence also is Λ-dependent. Indeed, the full generating functional Z of QCD in (IV.72) cannot be Λ-dependent, to wit

$$\Lambda \frac{\partial Z}{\partial \Lambda} = 0 \,. \tag{IV.82}$$

Eq.(IV.82) is the (cutoff) RG-equation for the generating functional of QCD. In the present context it is only approximately valid as we did not include the quantum fluctuations of gluons below the cutoff scale Λ. Accordingly, (IV.82) only holds in our present EFT setting if the cutoff scale Λ is small enough. This will be aparent in the final, renormalised result, and we shall resume the discussion of the sufficient smallness of the cutoff scale there.

For the time being let us also drop the integration of the mesonic fluctuations. In this approximation $V_{\phi,\mathrm{eff}}(\rho)$ is the full effective potential of our low energy EFT. Using (IV.82) for the full effective potential (IV.80) or (IV.81), $\Lambda\partial_\Lambda V_{\mathrm{eff}} = 0$, leads us to scaling relations for the couplings in the potential V. As Λ only appears in the integration limit in (IV.80), the integrand simply is the Λ-derivative and we obtain

$$\begin{aligned} \Lambda\partial_\Lambda V_{\mathrm{UV}} &= \frac{6}{\pi^2}\Lambda^4 \ln\left(1 + \frac{h^2\rho}{2\Lambda^2}\right) \\ &= \frac{3}{\pi^2}\left(\Lambda^2 h^2 \rho - \frac{h^4}{4}\rho^2\right) + O(\rho^3/\Lambda^2) \,, \end{aligned} \tag{IV.83}$$

and

$$\Lambda\partial_\Lambda V_{\mathrm{UV}} = \Lambda \frac{\partial m_\varphi^2}{\partial \Lambda}\rho + \frac{1}{2}\Lambda \frac{\partial \lambda_\varphi}{\partial \Lambda}\rho^2 \,. \tag{IV.84}$$

The RG equation (IV.84) signifies that the present quark-meson model is indeed renormalisable: the divergences can

be absorbed in the couplings of the classical action. For the sake of completeness we also remark that In a full analysis two further logarithmic singularities occur, the wave function renormalisations of quarks and mesons which also can be absorbed by wave functions in the classical action with e.g. $\partial_\mu\phi^2 \to Z_{\phi,\Lambda}\partial_\mu\phi^2$. The scale derivatives of m_φ^2 and λ_φ define the β-functions of meson mass and self-coupling respectively,

$$\beta_{m_\varphi^2} = \Lambda\frac{\partial(m_\varphi^2/\Lambda^2)}{\partial\Lambda}\,, \qquad\qquad \beta_{\lambda_\varphi} = \Lambda\frac{\partial\lambda_\varphi}{\partial\Lambda}\,, \tag{IV.85}$$

in analogy to the β-function of the strong coupling in (IV.1) and the four-fermi coupling in (IV.53) discussed before. Now we use $\Lambda\partial_\Lambda\Lambda^2 = 2\Lambda^2$ and $\Lambda\partial_\Lambda \ln\Lambda^2/\Lambda_{\rm QCD}^2 = 2$ for integrating the RG-equation (IV.83). For the logarithmic term we have to introduce a reference scale which we choose to be the dynamical scale of QCD, $\Lambda_{\rm QCD}^2$. Practically this scale is identified with the UV cutoff scale of the low energy EFT which is proportional to $\Lambda_{\rm QCD}^2$, and is typically of the order of 1 GeV. In summary this leads us to

$$m_\varphi^2 = m_{\varphi,\rm r}^2 + \frac{3}{2\pi^2}\Lambda^2h^2\,, \qquad\qquad \lambda_\varphi = \lambda_{\varphi,\rm r} - \frac{3}{4\pi^2}h^4\ln\frac{\Lambda^2}{\Lambda_{\rm QCD}^2}\,, \tag{IV.86}$$

with the renormalised couplings $m_{\varphi,\rm r}^2, \lambda_{\varphi,\rm r}$. In the present approximation without the mesonic quantum fluctuations they directly carry the physics. The Λ-independent constant part in the subtraction is chosen such that the ρ^2-term in the effective potential has the coupling $\lambda_{\varphi,\rm r}$. It is evident from (IV.86) that a variation of the reference scale in the logarithmic term can be absorbed in an according variation of $\lambda_{\varphi,\rm r}$,

$$\Lambda_{\rm QCD}\frac{\partial\lambda_\varphi}{\partial\Lambda_{\rm QCD}} = 0 \qquad\longrightarrow\qquad \Lambda_{\rm QCD}\frac{\partial\lambda_{\varphi,\rm r}}{\partial\Lambda_{\rm QCD}} = \beta_{\lambda_\varphi}\,, \tag{IV.87}$$

where we have assumed the absense of other scales. This relation is again governed by the β-function β_{λ_φ}, and reflects the invariance observables do not depend on this choice. Inserting these results back into (IV.81) leads us to the final, Λ-independent effective potential

$$V_{\phi,\rm eff}(\rho) = m_{\varphi,\rm r}^2\rho + \frac{\lambda_{\varphi,\rm r}}{2}\rho^2 - \frac{3}{8\pi^2}h^4\rho^2\left[\ln\frac{h^2\rho}{2\Lambda_{\rm QCD}^2} - \frac{1}{2}\right]\,. \tag{IV.88}$$

As already discussed in the beginning of the derivation, (IV.88) is the Coleman-Weinberg result in disguise. Multiplying with the symmetry factor $-4N_fN_c = -24$ gives precisely the same logarithmic term in the ρ^2 contribution. The missing constant term simply originates in the different renormalisation procedure: with the present one all corrections to the relevant couplings including the constant parts are absorbed, that is $m_\varphi^2 \to m_{\varphi,\rm r}^2$ and $\lambda_\varphi \to \lambda_{\varphi,\rm r}$. As these couplings have to be fixed by appropriate infrared observables this is a convenient choice. In summary we have the following practical and consistent RG procedure:

(0) Regularisation: Sharp momentum cutoff with $p^2 \le \Lambda^2$ in all loops.

(1) Renormalisation: Remove all divergent terms in the loop contributions. For the logarithmic term substitute $\ln\Lambda^2 \to \ln\Lambda_{\rm QCD}^2$.

(2) Renormalisation scheme: we demand $\partial_\rho V_{\phi,\rm eff} = \partial_\rho V_{\phi,\rm UV} + O(\rho^2) + \ln\rho$–terms. This is arranged by the $-1/2$ in the bracket in (IV.88). It enforces that the ρ-dependent pion mass function $m_\pi(\rho) = \partial_\rho V_{\phi,\rm eff}(\rho)$ simply is $m_{\phi,\rm r}^2$ in the symmetric regime, that is for vanishing ρ. Moreover, the linear term in ρ of m_π^2 is given by the UV coupling $\lambda_{\phi,\rm r}$. This cannot be expressed within a Taylor expansion at $\rho = 0$ due to the logarithmic term.

(3) Physics: The relevant parameters $h, m_{\varphi,\rm r}, \lambda_{\varphi,\rm r}$ and the explicit symmetry breaking scale c are fixed by the pion decay constant f_π, the physical pion and σ pole masses, $m_{\pi,\rm pol}, m_{\sigma,\rm pol}$ and the constituent quark mass $m_{q,\rm const}$.

Depending on the values of $m_{\varphi,\rm r}^2, \lambda_{\varphi,\rm r}$ the effective potential in (IV.88) has non-trivial minima or describes the symmetric phase. The effect of the fermionic quantum fluctuations is most easily accessed via the scale-running of the parameters in the 'classical' potential $V(\rho)$. Concentrating on the scale-dependence of the mass parameter m_φ^2 in (IV.86) we conclude that lowering the cutoff scale Λ lowers the effective mass m_φ^2. This entails that the fermionic quantum fluctuation¡s indeed lower the mass parameter. Put differently, the quark fluctuations trigger chiral symmetry breaking.

Moreover, deep in the symmetric phase, that is for large Λ, the mesonic quantum fluctuations are suppressed in comparison to the quark fluctuations. In the vicinity of the symmetry breaking scale Λ_χ the mesonic fluctuations are

getting massless, $m_\varphi \to 0$ and the mesonic fluctuations kick in. In turn, the effective quark mass grows in the chirally broken regime with $m_\psi = h/2\sigma_0$, and eventually the quark fluctuations are switched off for Λ below the constituent quark mass. ...

2. *Mesonic quantum fluctuations*

The remaining mesonic fluctuations can be treated at one loop similarly to the fermionic computation done above. The result is a Coleman-Weinberg type potential without the relative minus sign. Accordingly, the mesonic fluctuations work against chiral symmetry breaking. Due to the different scales and coupling sizes this is a marginal effect even in the chiral limit. In the physical scale with explicit chiral symmetry breaking and a pion mass of about 140 MeV the mesonic quantum fluctuations also decouple for scales Λ below the pion mass.

It is left to integrate-out the quantum fluctuations of the mesonic degrees of freedom in (IV.74). Again concentrating on the low energy effective potential in the spirit of the lowest order of a derivative expansion we have

$$V_{\text{eff}}(\rho) = V_{\phi,\text{eff}}(\rho) + \Delta V_\phi(\rho) + c_\sigma\,\sigma \qquad \text{with} \qquad \Delta V_\phi(\rho) = \frac{1}{2}\text{Tr}_\Lambda \ln\left[-\partial_\mu^2 + m_\phi^2(\rho)\right]\,, \tag{IV.89}$$

where ΔV_ϕ is the one loop approximation to the mesonic path integral (IV.74) with the 'classical' potential $V_{\phi,\text{eff}}(\rho)$, and Tr_Λ sums over all momenta $p^2 \leq \Lambda^2$. In (IV.89) we have re-introduced the linear term in σ that triggers the explicit symmetry breaking. In the present case ΔV_ϕ boils down to

$$\Delta V_\phi(\rho) = \frac{1}{4\pi^2}\int_0^\Lambda dp\, p^3 \left[3\ln\left(p^2 + m_\pi^2(\rho)\right) + \ln\left(p^2 + m_\sigma^2(\rho)\right)\right]. \tag{IV.90}$$

For (IV.90) we have used that we can evaluate the expressions for vanishing $\vec{\pi} = 0$ as done in the quark case. Then the mass matrix is diagonal, see (IV.11), and reads for a given potential V

$$m_\pi^2(\rho) = \partial_\rho V(\rho)\,, \qquad\qquad m_\sigma^2(\rho) = \left(\partial_\rho + 2\rho\partial_\rho^2\right)V(\rho)\,. \tag{IV.91}$$

Accordingly, the factor three in front of the first term on the right hand side in (IV.90) accounts for the $N_f^2 - 1 = 3$ pions. In the present case we have $V_{\phi,\text{eff}}(\rho)$ and the mass functions read

$$\begin{aligned} m_\pi^2(\rho) &= m_{\varphi,\text{r}}^2 + \left(\lambda_{\varphi,\text{r}} - \frac{3}{4\pi^2}\,h^4 \ln\frac{h^2\rho}{2\Lambda_{\text{QCD}}^2}\right)\rho\,, \\ m_\sigma^2(\rho) &= m_{\varphi,\text{r}}^2 + 3\left(\lambda_{\varphi,\text{r}} - \frac{1}{2\pi^2} - \frac{3}{4\pi^2}\,h^4 \ln\frac{h^2\rho}{2\Lambda_{\text{QCD}}^2}\right)\rho \end{aligned} \tag{IV.92}$$

The integration in (IV.91) is the same as in the quark case and we arrive at

$$\begin{aligned} \Delta V_\phi(\rho) = &\frac{3}{16\pi^2}\left[\Lambda^2 m_\pi^2 + m_\pi^4\left[\ln\frac{m_\pi^2}{\Lambda^2} - \ln\left(1+\frac{m_\pi^2}{\Lambda^2}\right)\right] + \Lambda^4\ln\left(1+\frac{m_\pi^2}{\Lambda^2}\right)\right] \\ &+ \frac{1}{16\pi^2}\left[\Lambda^2 m_\sigma^2 + m_\sigma^4\left[\ln\frac{m_\sigma^2}{\Lambda^2} - \ln\left(1+\frac{m_\sigma^2}{\Lambda^2}\right)\right] + \Lambda^4\ln\left(1+\frac{m_\sigma^2}{\Lambda^2}\right)\right], \end{aligned} \tag{IV.93}$$

where m_π^2, m_σ^2 are the ρ-dependent masses defined in (IV.91). Seemingly (IV.93) introduces divergent terms that are neither proportional to ρ^0, ρ, ρ^2 due to ΔV_q in (IV.91). However, (IV.93) goes beyond one-loop (ΔV_q is already one-loop) and these terms are to be expected and can be removed within a consistent renormalisation procedure. Here, our simple renormalisation procedure discussed below (IV.88) pays off. Then after renormalisation (IV.93) turns into

$$\Delta V_\phi(\rho) = \frac{3}{16\pi^2}m_\pi^4\left[\ln\frac{m_\pi^2}{\Lambda_{\text{QCD}}^2} - \frac{1}{2}\right] + \frac{1}{16\pi^2}m_\sigma^4\left[\ln\frac{m_\sigma^2}{\Lambda_{\text{QCD}}^2} - \frac{1}{2}\right], \tag{IV.94}$$

where $m_\pi(\rho), m_\sigma(\rho)$ are derived from (IV.91). As described in the discussion of the renormalisation scheme described

below (IV.88), the factor $-1/2$ in the brackets arrange for

$$m^2_{\text{eff},\pi}(\rho) = \partial_\rho V_{\text{eff}}(\rho) = m^2_{\varphi,\text{r}} + \lambda_{\varphi,\text{r}}\rho - \frac{3}{8\pi^2}\rho \ln\frac{h^2\rho}{2\Lambda^2_{\text{QCD}}} + \frac{3}{8\pi^2}m^2_\pi(\partial_\rho m^2_\pi)\ln\frac{m^2_\pi}{\Lambda^2_{\text{QCD}}}\,. \tag{IV.95}$$

From (IV.94) we can proceed in several ways:

(0) We drop ΔV_ϕ completely. As in (2) the missing quantum fluctuations are partially absorbed in the couplings $m_\varphi, \lambda_\varphi$. This approximation is also called 'extended mean field' in the literature. It is very close to the mean field approximation with $V_{\text{eff}}(\rho) = V(\rho)$, where we also drop ΔV_q.

(1) As ΔV_q already is a one loop expression we drop it in the computation of (IV.94). This leads us to a consistent one-loop computation. This amounts to dropping some quantum contributions in comparison to (1). However, as in (1) we have to fix the parameters $h, m_\varphi, \lambda_\varphi$ in the effective potential with the low energy observables. This implicitly absorbes (part of the) dropped contributions in these couplings. Differences between (1) and (2) only occur due to missing contributions in (2) in the couplings $\lambda_{\varphi,n}$ of the ρ^n-terms in V_{eff} with $n \geq 3$.

(2) For the evaluation of (IV.89) with $V + \Delta V_q$ in (IV.88) and ΔV_ϕ in (IV.94) we have to take into account that already the effective potential $V + \Delta V_q$ may not be convex. In non-convex regimes its second derivatives are not positive definite: $m_\pi < 0$ for $\rho < \rho_\pi$, where ρ_π is the solution of the reduced EoM: $V'_{\text{cl}}(\rho_\pi) + \Delta V'_q(\rho_\pi) = 0$. The σ mass also gets negative for even smaller ρ.

A simple resolution of this artefact of the approximation is to continue the result from larger $\rho \geq \rho_\pi$. The more consistent way is to resolve the related renormalisation group (RG) equation for the effective potential. The RG approach is able to deal consistently with the regimes with negative curvature which are indeed flattened out by quantum fluctuations. This effect cannot be seen in perturbation theory.

In any case the result of this computation is an effective potential $V_{\text{eff}}(\rho)$ which depends on the couplings $h, m_\varphi, \lambda_\varphi$. We either compute these couplings from QCD or we fix them with low energy observables such as the meson mass, the pion decay constant and the constituent quark mass. Here we use the latter way which is described in details below.

(3) We solve the full renormalisation group equation, (IV.82), for the effective potential, that governs its scale-dependence, see (IV.96) below. Integrating the RG equation provides an iterative and fully consistent inclusion of the fluctuation effects. The RG is described in the chapter IV F 3 below, where it is also detailed how it boils down to the procedures (0)-(2) described above.

In the following we will consider all of these approximations, in particular at finite temperature and density. This allows us to evaluate the importance of the quantum (and later thermal) fluctuations as well as the stability of the results.

*3. RG equation for the effective potential**

The present considerations are but one step away from a consistent treatment of the low energy effective theory with functional renormalisation group methods. For that purpose let us reconsider the RG equation for the ultraviolet potential V_{UV} derived from (IV.82). Below (IV.82) we have discussed the renormalisation group scaling that originates in the quark quantum fluctuations. In the general case the RG-scaling of the potential comes from both quark and meson fluctuations. This leads us to

$$\Lambda\partial_\Lambda V_{\text{UV}} = -\Lambda\partial_\Lambda\left(\Delta V_q + \Delta V_\phi\right)\,. \tag{IV.96}$$

(IV.96) entails how the UV effective potential V_{UV} at a large cutoff scale Λ changes with lowering or increasing the cutoff scale. In the discussion so far we have concentrated on the UV relevant terms that scale with positive powers of the cutoff Λ. Then we ensured the cutoff independence of the full effective potential $V_{\text{eff}} = V_{\text{UV}} + \Delta V_q + \Delta V_\phi$ by an appropriate renormalisation procedure. The low energy quark and meson fluctuation are encoded in the terms $\Delta V_q + \Delta V_\phi$. Such a treatment assumes an asymptotically large cutoff scale.

Here we take a different point of view: iteratively lowering to cutoff scale Λ from large values (w.r.t. the non-perturbative infrared pyhsics) leads to shifting more and more infrared fluctuations from $\Delta V_q + \Delta V_\phi$ to V_{UV}. Indeed, at $\Lambda = 0$ we have

$$V_{\text{eff}} = V_{\Lambda=0}\,, \qquad \text{with} \qquad V_\Lambda = V_{\text{UV},\Lambda}\,, \tag{IV.97}$$

the former 'UV' effective potential is the full quantum effective potential. Evidently, if the cutoff scale is not asymptotically large, also the UV-irrelevant terms cannot be neglected in (IV.96). Note also that its right hand side has to be seen as a function of V_Λ, the one-loop computations done before indeed used V_Λ a a classical potential. Hence, it is only left to bring (IV.96) in a form that only depends on V_Λ on both sides.

To that end we consider an infinitesimal RG step with $\Lambda^2 \to \Lambda^2(1-\epsilon)$. This is governed by the path intgeral

$$Z \approx \int_{\Lambda^2(1-\epsilon)}^{\Lambda^2} [d\phi\, d\psi d\bar{\psi}] e^{-S_{\text{eff},\Lambda}[\psi,\bar{\psi},\phi]} \qquad \text{with} \qquad e^{-S_{\text{eff},\Lambda}} \simeq Z_\Lambda\,. \tag{IV.98}$$

Now we exploit that each loop in a loop expansion of (IV.98) is proportional to ϵ as it only takes into account momenta with $\Lambda^2(1-\epsilon) \leq p^2 \leq \Lambda^2$. Hence, for $\epsilon \to 0$ the one-loop contribution is leading, and the ϵ-derivative can be converted in the Λ-derivative of the momentum integration boundary of the one-loop expressions for ΔV_q and ΔV_ϕ, (IV.78) and (IV.89) respectively. This leads us to

$$\Lambda\partial_\Lambda V_\Lambda = -\frac{1}{4\pi^2}\Lambda^4 \left[3\ln\left(1+\frac{m_\pi^2(\rho)}{\Lambda^2}\right) + \ln\left(1+\frac{m_\sigma^2(\rho)}{\Lambda^2}\right)\right] + \frac{6}{\pi^2}\Lambda^4 \ln\left(1+\frac{h^2}{2}\frac{\rho}{\Lambda^2}\right)\,, \tag{IV.99}$$

where

$$m_{\pi/\sigma}^2(\rho) = \Gamma^{(2)}_{\Lambda,\pi\pi/\sigma\sigma}(\rho, p=0) = V^{(2)}_{\Lambda,\pi\pi/\sigma\sigma}(\rho)\,, \qquad \frac{h^2}{2}\rho = \Gamma^{(2)}_{\Lambda,\psi\bar{\psi}}(\rho, p=0)\,, \qquad \text{with} \qquad \Gamma^{(2)}_\Lambda = \Gamma_{\text{UV},\Lambda}\,, \tag{IV.100}$$

are the second derivatives of the scale-dependent 'UV' effective action Γ_Λ. We emphasise that the implicit Λ-dependence in $\Gamma^{(2)}$ is not hit by the ϵ-derivative.

The approximations (0)-(2) now follow from respective approximations of (IV.99): For (0) we drop the meson fluctuations, for (1) we do not feed back the RG-running of V_{UV} on the right hand side of (IV.99), for (2) we integrate out the quarks first. This is done with introducing separate cutoffs for quarks, Λ_q and mesons, Λ_ϕ and take the limit $\Lambda_q/\Lambda_\phi \to 0$.

Eq.(IV.99) is the Wegner-Houghton equation [11] for the effective potential of the current Quark-Meson Model. For the sake of completeness we also quote the full Wegner-Houghton equation for the effective action: as the derivation of (IV.99) simply follows from the RG-invariance of the generating functional Z, it also applies to the full effective action. Hence we conclude

$$\Lambda\partial_\Lambda \Gamma_\Lambda[\psi,\bar{\psi},\phi] = -\frac{1}{2}\text{Tr}_{p^2=\Lambda^2} \ln \frac{\Gamma^{(2)}_{\phi\phi}}{\Lambda^2} + \text{Tr}_{p^2=\Lambda^2} \ln \frac{\Gamma^{(2)}_{\psi\bar{\psi}}}{\Lambda^2}\,, \tag{IV.101}$$

where the trace $\text{Tr}_{p^2=\Lambda^2} = \text{Tr}\,\delta(\sqrt{p^2}-\Lambda)$ only sums over the momentum shell with $p^2 = \Lambda^2$. Eq.(V.34) is, together with the Callan-Symanzik equation [12, 13], the first of many functional renormalisation group equations for the effective action. These continuum RG equations are based on continuum version [14, 15] of the Kadanoff block spinning procedure on the lattice, [16], for the first seminal work on the RG see [17, 18]. In particular the pioneering work [17] already emphasises and details the full power of the renormalisation group, and is still very much under-appreciated by the community.

4. EFT couplings

It is left to fix the couplings parameters in our low energy effective theory with the classical action S_{eff} defined (IV.63). After integrating out the quarks and mesons we are led to the full low energy effective action Γ_{lowE} with

$$\Gamma_{\text{lowE}}[\psi,\bar{\psi},\phi] = \int_x \bar{\psi}\cdot(\not{\partial} + m_\psi)\cdot\psi + \int_x \left[(\partial_\mu\sigma)^2 + \partial_\mu\vec{\pi})^2\right] + \int_x \frac{h}{2}\bar{\psi}\left[\sigma + i\gamma_5\vec{\tau}\vec{\pi}\right]\psi + \int_x V_{\text{eff}}(\rho)\,, \tag{IV.102}$$

with the effective potential $V_{\text{eff}} = V_{\phi,\text{eff}} + \Delta V_\phi + c\sigma$ defined in (IV.89) with $V_{\phi,\text{eff}} = V_{\text{UV}} + \Delta V_q$. In the best approximation discussed here, $V_{\phi,\text{eff}}$ is given by (IV.88) and ΔV_ϕ by (IV.94). We have the fermion mass m_ψ or mesonic shift parameter c, the Yukawa coupling h, the mesonic mass parameter m_ϕ^2 and the mesonic self-coupling λ_ϕ. The fermion mass can be traded for the shift parameter c as argued before. The value of the latter determines the expectation value of the σ-field which is, in the present approximation, simply is the pion decay constant,

$$\sigma_0 = \langle\sigma\rangle = f_\pi\,, \qquad f_\pi \approx 93\,\text{MeV}\,. \tag{IV.103}$$

Observables	Value [MeV]	EFT couplings	Value
f_π	93	$\sigma_0 = f_\pi$	93 MeV
$m_{\rm con}$	300	$h = \dfrac{2m_{\rm con}}{f_\pi}$	6.45
m_π	138	m_ϕ	$m_\phi(m_\pi, m_\sigma)$
m_σ	450	λ_ϕ	$\lambda_\phi(m_\pi, m_\sigma)$
$f_{\pi,\chi}$	88	$c_\sigma = f_\pi m_\pi^2$	$1.77 * 10^6 \text{MeV}^3$

TABLE III: Low energy observables and related EFT couplings as used for the $N_f = 2$ computations. While the σ-expectation value σ_0 and the Yukawa coupling are directly related to pion decay constant and constituent quark masses in the present appoximations, the other EFT couplings depend on the approximations (0)–(3) described below (IV.95).

The latter value related to the physical f_π's $(f_\pi^\pm, f_\pi^0)$ measured in the experiment. Consequently c could be dropped, we simply evaluate the theory on this expectation value. Accordingly, h is determined by the constituent quark mass,

$$m_{\psi,\rm con} = \frac{1}{2} h \langle\sigma\rangle = \frac{1}{2} h\, f_\pi \qquad \longrightarrow \qquad h \approx 6.45 \quad \text{with} \quad m_{\psi,\rm con} \approx 300\,\text{MeV}\,. \tag{IV.104}$$

Note that the constituent quark masses of the quarks depend on the model and approximation used, typical values for up and down quark masses are $m_{\psi,\rm con} \approx 340$ MeV in full QCD. A reduced value in (IV.104) for two flavour QCD is common place in the $N_f = 2$ quark-meson model. The related observable is the chiral condensate,

$$\langle\bar\psi(x)\psi(x)\rangle = -\int \frac{d^4p}{(2\pi)^4} \text{tr}\,\langle\psi(p)\bar\psi(-p)\rangle\,, \tag{IV.105}$$

where the trace sums over Dirac and flavour indices.

Finally we have to fix λ_ϕ and m_ϕ with the Yukawa coupling and σ-expectation value σ_0 deduced above, see also Table III. Note also, that a potential further input is the value of the pion decay constant in the chiral limit,

$$f_{\pi,\chi} = f_\pi(m_\pi = 0) \approx 88\,\text{MeV}\,, \tag{IV.106}$$

which can be determined with chiral perturbation theory, functional continuum methods or from chiral extrapolations of lattice results at different finite pion masses. This leaves us with a triple of 'observables' $(m_\pi, m_\sigma, f_{\pi,\chi})$, see Table III, and a triple of EFT couplings $(m_\phi, \lambda_\phi, c_\sigma)$. Note that the inclusion of $f_{\pi,\chi}$ as an 'observable' relates to the correct chiral dynamics reflected in the curvature and four-meson interaction in the chiral limit. The pion and sigma masses are related to those found in the Particle Data Booklet (2016), [19] of the Particle Data Group (PDG). Here, the pion mass is taken between that of the charged pions $\pi^\pm$ with $m_{\pi^\pm} \approx 139.57$ MeV and the neutral pion π^0 with $m_{\pi^0} \approx 134.98$ MeV, and the mass of the sigma meson is taken to be that of the $f_0(500)$, see [20], that is $m_\sigma \approx 450\,\text{MeV}$, despite the f_0 certainly not being a simple $q\bar q$ state. The unclear nature of the value of m_σ is one of the biggest uncertainties for low energy EFTs. Typically, its values range from 400–550 MeV, see PDG, [19].

Seemingly, this leaves us with as many unknowns as physics input. However, c can be determined from the pion mass and the pion decay constant with $m_\pi^2 = \partial_\rho V_{\rm eff}(\rho_0)$ and $\rho_0 = \sigma_0^2/2 = f_\pi^2/2$. This follows from the EoM for σ,

$$\partial_\sigma V_{\rm eff}(\rho_0) = \sigma_0 m_\pi^2 = c_\sigma \qquad \longrightarrow \qquad c_\sigma = f_\pi m_\pi^2 \approx 1.77 * 10^6\,\text{MeV}^3\,. \tag{IV.107}$$

We conclude that in the current approximation to the UV effective action, the pion decay constant in the chiral limit, $f_{\pi,\chi}$, is a prediction.

Here we present a crude (mean-field) estimate of its value based on the assumption of being close to the chiral limit. It is based on the expansion of the full effective potential about the unperturbed minimum in the broken phase,

$$V_{\rm eff} = \sum_{n=2}^{\infty} \frac{\lambda_n}{n!} (\rho - \kappa)^n + c_\sigma \sigma\,, \qquad \text{with} \qquad \kappa = \frac{f_{\pi,\chi}^2}{2}\,, \quad \lambda_2 = \lambda_{\phi,\rm eff}\,. \tag{IV.108}$$

Close to the chiral limit the difference $(f_\pi - f_{\pi,\chi})/f_\pi \ll 1$ is small. In the vicinity of the unperturbed minimum κ the

full effective potential can be written as

$$V_{\rm eff} = \frac{\lambda_{\phi,\rm eff}}{2}\left(\rho-\kappa\right)^2 + c_\sigma\sigma + O\left(\left(\rho-\kappa\right)^2\right)\,. \tag{IV.109}$$

Dropping the higher terms leads us to

$$m_\pi^2 = \lambda_{\phi,\rm eff}\frac{f_\pi^2 - f_{\pi,\chi}^2}{2}\,, \qquad m_\sigma^2 = \lambda_{\phi,\rm eff}\frac{3f_\pi^2 - f_{\pi,\chi}^2}{2}\,. \tag{IV.110}$$

In this leading order, the mesonic self-coupling drops out of the relation for $f_{\pi,\chi}$ and we arrive at the estimate

$$f_{\pi,\chi} = f_\pi\sqrt{\frac{1-3\frac{m_\pi^2}{m_\sigma^2}}{1-\frac{m_\pi^2}{m_\sigma^2}}} \approx 83\,\text{MeV}\,, \qquad \text{and} \qquad \lambda_{\phi,\rm eff} = \frac{m_\sigma^2 - m_\pi^2}{f_\pi^2} \approx 21.2\,. \tag{IV.111}$$

This is a very good agreement with the theoretical prediction of $f_{\pi,\chi} \approx 88\,\text{MeV}$, in particular given the crude nature of the present estimate. Beyond the current mean field level it improves further Still, the current EFT makes a prediction for either $f_{\pi,\chi}$ or m_σ, and the question arises which of them should be taken as a physics input: we first note that $f_{\pi,\chi} \approx 88\,\text{MeV}$ is under far better theoretical control than the mass of the σ-meson. Apart from the difficulties of identifying directly the σ-mesons in the EFT's at hand with a resonance in the particle spectrum, it has a large width. Hence it cannot be assumed that the curvature mass $m_{\sigma,\rm curv}$ we use here is in good agreement with the pole mass $m_{\sigma,\rm pol}$, see the discussion at the end of chapter IV B. This is in stark contradistinction to the pion masses where the (non-trivial) identification $m_{\pi,\rm curv} \approx m_{\pi,\rm pol}$ holds true on the percent level. This suggestes to adjust m_σ such that $f_{\pi,\chi} \approx 88$ MeV. In the mean field discussion done here this leads to $m_\sigma^2 \approx 600 - 650\,\text{MeV}$. Note that with a future better determination of the curvature mass $m_{\sigma,\rm curv}$ a semi-quantitative EFT might require higher oder mesonic UV-couplings such as $\lambda_{3,\rm UV} \neq 0$ in (IV.109). This is related to the fact that the physical UV cutoff $\Lambda_{\rm UV} \approx 1$ GeV, at which the low energy EFT is initiated, is less than one order of magnitude larger than the physical scales.

This discussion completes our EFT picture of chiral symmetry breaking in QCD. In essence it also extends to the $N_f = 2+1$ flavour case and beyond, then, however, a consistent determination of the low energy couplings including the correct chiral dynamics, e.g. $f_{\pi,\chi}$ is far more intricate.

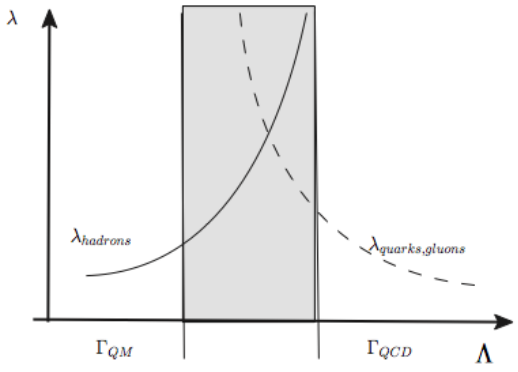

FIG. 12: Scale dependence of the effective four-fermi coupling. The shaded area is the regime where the effective field theory is triggered.

V. CHIRAL PHASE TRANSITION

In the last chapter we have learned that chiral symmetry breaking is triggered by the quark fluctuations, while the mesonic low energy fluctuations work against symmetry breaking. The symmetry breaking scale Λ_χ is of the order of 300-400 MeV.

The vacuum physics is used to fix the parameters of the low energy effective theory such as the mesonic mass function, the Yukawa coupling, and the expectation value of the radial mode, $\langle\sigma\rangle$. The related observables are the pion and sigma pole masses, the constituent quark mass as well as the pion decay constant.

In heavy ion collisions or the early universe the temperature is/has been high of the order of hundreds of MeV. In Kelvin this translates into $100\,\text{MeV}\approx 1.16 * 10^{12}$ Kelvin. It is expected that a high temperatures the system undergoes a phase transition to the chirally symmetric phase. As a rough estimate the phase transition temperature T_c is expected to be of the order of the chiral symmetry breaking scale Λ_χ which itself has been argued to be of the order of Λ_{QCD}, the only intrinsic scale in QCD.

A. Mesons at finite temperature

For a more quantitative investigation we need a thermal formulation of QCD or at least of the low energy effective theory we have derived in the previous chapter. Here we give a brief introduction to the -Euclidean- path integral at finite temperature, where we follow the introduction of the path integral in chapter 1, QFT II. We start with the partition function of a scalar theory at finite temperature

$$Z_T = \text{Tr}\, e^{-\beta\hat{H}} = \sum_n e^{-\beta E_n} \quad \text{with} \quad \beta = \frac{1}{T} \quad \text{and} \quad \hat{H}|n\rangle = E_n|n\rangle\,, \tag{V.1}$$

with the Hamiltonian operator of a scalar theory

$$\hat{H}[\hat{\phi},\hat{\pi}] = \int d^3x \left[\frac{1}{2}\hat{\pi}^2 + \frac{1}{2}(\vec{\nabla}\phi)^2 + V(\hat{\phi})\right]. \tag{V.2}$$

with field operator $\hat{\phi}$ and field momentum operator $\hat{\pi}$. In (V.1) we dropped the source term for the sake of brevity. Eq.(V.1) is the standard statistical partition function at finite temperature well known from quantum mechanics. Now we rewrite this partition function in terms of a basis in field and canonical momentum space. First we note that the trace in (V.1) can be rewritten in terms of field eigenstates with

$$\text{Tr}\, e^{-\beta\hat{H}} = \int d\phi\, \langle\phi|\, e^{-\beta\hat{H}}\, |\phi\rangle \qquad \text{with} \qquad \hat{\phi}(\vec{x})|\phi\rangle = \phi(\vec{x})|\phi\rangle\,, \tag{V.3}$$

with the eigenvalues $\phi(\vec{x})$. Moreover, the statistical operator $e^{-\beta\hat{H}}$ can be interpreted as the evolution operator $U(0,i\beta)$ in an imaginary time from the initial state $|\phi(t_{\text{i}})\rangle$ at $t_{\text{i}} = 0$ to the final state $|\phi(t_{\text{f}})\rangle$ at $t_{\text{f}} = i\beta$ with

$$U(0,i\beta) = e^{i\hat{H}(t_{\text{f}}-t_{\text{i}})} \qquad \text{and} \qquad |\phi(t_{\text{f}})\rangle = |\phi(t_{\text{i}})\rangle\,. \tag{V.4}$$

The identification of initial and final state is the trace condition in (V.3). Now we simply repeat all the steps for the derivation of the path integral of a scalar theory. Also adding a source term we arrive at

$$Z_T[J] = \int_{\phi(\beta,\vec{x})=\phi(0,\vec{x})} d\phi\, e^{-S_T[\phi]+\int_0^\beta d^4x\, J(t,\vec{x})\phi(\vec{x})}\,, \tag{V.5}$$

with the periodic fields $\phi(t+\beta,\vec{x}) = \phi(t,\vec{x})$ and the finite temperature action $S_T[\phi]$ with

$$S_T[\phi] = \int_0^\beta d^4x \left[\frac{1}{2}(\partial_\mu\phi)^2 + V(\phi)\right], \qquad \text{where} \qquad \int_0^\beta d^4x = \int_0^\beta dt \int d^3x\,. \tag{V.6}$$

Accordingly, the path integral of a finite temperature field theory is related to a Euclidean path integral with a finite time extent in imaginary time $t \in [0\,,\,\beta]$. Note that this time does *not* describe the time evolution of the system but simply the statistical nature of the thermal partition function. The real time correlation function are obtained by a Wick rotation, for more details see finite temperature quantum field theory books such as Le Bellac or Kapusta. The

correlation functions are periodic in imaginary time,

$$\langle\phi(x_1)\cdots\phi(t_i+\beta,\vec{x})\cdots\phi(x_n)\rangle = \langle\phi(x_1)\cdots\phi(t_i,\vec{x})\cdots\phi(x_n)\rangle\,. \tag{V.7}$$

Finally we want to repeat the computation of the effective potential in the last chapter section IV F at finite temperature. This is done in momentum frequency space and we would like to illustrate the differences at finite temperature at the important example of the propagator

$$G_\phi(x-y) = \langle\phi(x)\phi(y)\rangle - \langle\phi(x)\rangle\langle\phi(y)\rangle\,. \tag{V.8}$$

The propagator in spatial momentum and frequency space is given by

$$G_\phi(\omega_n,\vec{p}) = \int_0^\beta d^4x\, e^{i\,(\omega_n t+\vec{p}\vec{x})}\, G_\phi(t,\vec{x})\,, \qquad \text{where} \qquad \omega_n = 2\pi T n\,, \qquad \text{with} \quad n\in\mathbb{Z}\,. \tag{V.9}$$

The discrete frequencies ω_n are called Matsubara frequencies and originate in the finite imaginary time extent. The frequency Fourier transformation back gives

$$G_\phi(t,\vec{p}) = \sum_{n\in\mathbb{Z}} e^{-i\omega_n t} G_\phi(\omega_n,\vec{p})\,, \tag{V.10}$$

which has the necessary periodicity in imaginary time, $G(t+\beta,\vec{p}) = G(t,\vec{p})$, of a correlation function, see (V.7). In frequency and spatial momentum space the classical propagator looks the same as in the vacuum. We have

$$G_\phi(\omega_n,\vec{p}) = \frac{1}{\omega_n^2+\vec{p}^2+m^2} \qquad \text{with} \qquad m^2(\phi) = \partial_\phi^2 V(\phi)\,. \tag{V.11}$$

While the Fourier transformation w.r.t. spatial momentum is also the same as at $T=0$, that w.r.t. frequency changes. Here we discuss the Fourier transformation for $t=0$ for the mixed representation $G_\phi(t,\vec{p})$,

$$G_\phi(t=0,\vec{p}) = T\sum_{n\in\mathbb{Z}} \frac{1}{\omega_n^2+\vec{p}^2+m^2} = \frac{1}{2\epsilon_p^\phi}\coth\beta\,\epsilon_p^\phi = \frac{1}{2\epsilon_p^\phi}\left[1+2\,n_B(\epsilon_p^\phi)\right]\,, \tag{V.12}$$

with the dispersion ϵ_p^ϕ and the thermal distribution function $n_B(\omega)$ given by

$$\epsilon_p^\phi(m) = \sqrt{\vec{p}^2+m^2}\,, \qquad\qquad n_B(\omega) = \frac{1}{e^{\beta|\omega|}-1} \tag{V.13}$$

The latter is the standard Bose-Einstein distribution and clearly shows the thermal nature of the Matsubara path integral.

As a warm-up of the computation for the effective potential in the quark-meson theory at finite temperature we compute that of the scalar theory used here as an example. Its thermal part is related to the thermal pressure of the theory with potential. To that end we remind ourselves that the scalar free energy density Ω_ϕ and the pressure of the theory are given by

$$Z_T[0] = e^{-\beta\mathcal{V}\,\Omega_\phi}\,, \qquad\qquad p_\phi = -\frac{\partial\mathcal{V}\Omega_\phi}{\partial\mathcal{V}} \quad \text{with} \quad \mathcal{V} = \int d^3x\,. \tag{V.14}$$

The one-loop contribution to the free energy density and pressure are hence given by

$$\Omega_\phi \simeq \frac{1}{2\mathcal{V}} T\,\mathrm{Tr}\ln\left(-\partial_\mu^2+m^2\right) = \frac{1}{2}T\sum_{n\in\mathbb{Z}}\int\frac{d^3p}{(2\pi)^3}\,\ln\left(\omega_n^2+\vec{p}^2+m^2\right)\,, \quad p_\phi \simeq -\frac{1}{2}T\sum_{n\in\mathbb{Z}}\int\frac{d^3p}{(2\pi)^3}\,\ln\left(\omega_n^2+\vec{p}^2+m^2\right)\,, \tag{V.15}$$

where we dropped the normalisations in Ω_ϕ and p_ϕ. We also remind the reader that $m^2 = m^2(\phi)$ as introduced in (V.11). Note also that the pressure is nothing but (minus) the effective potential at finite temperature. At vanishing temperature we encountered singularities in the computation of the effective potential proportional to Λ^4, λ^2 and $\ln\Lambda$ that had to be absorbed in the bare couplings. The highest singularity proportional to Λ^4 we disregarded as the absolute value of the potential energy which cannot be measured. The expressions in (V.15) are also infinite,

showing the standard divergence of zero point functions at vanishing temperature. Similarly, we could introduce a spatial momentum cutoff Λ with $p^2 \leq \Lambda^2$ and proceed as in the last chapter. In the following we shall not make this cutoff explicit for the following reason: it is one of the cornerstones, and can be proven in thermal field theory all singularities are temperature-independent. This statement can be understood heuristically as the ultraviolet singularities are short-distance singularities. At short-distance singularities the finite extent in time-direction cannot be accessed. For detailed discussions we refer to the literature, here this fact will simply come out.

For the computation we take the mass (squared) derivative of the pressure, $\partial_{m_\phi^2} p$. This removes the logarithm from the expression and leaves us with integrals and sums that can be computed by complex analysis. The mass-derivative of the pressure is related to the momentum integral of the propagator in the mixed representation $G(0,\vec{p})$ computed in (V.12),

$$\partial_{m^2} p_\phi \simeq -\frac{1}{2}\int \frac{d^3p}{(2\pi)^3}\, G_\phi(0,\vec{p}) = -\frac{1}{4}\int \frac{d^3p}{(2\pi)^3}\frac{1}{\epsilon_p^\phi}\left[1+2\,n_B(\epsilon_p^\phi)\right]\,. \tag{V.16}$$

Eq.(V.16) entails that the mass-derivative of the pressure, and hence the pressure, only carries a temperature-independent singularity proportional to $1/\epsilon_p^\phi$. The term proportional to n_B vanishes in the zero temperature limit. Upon integration over m^2 the pressure is given by

$$p_\phi \simeq -\int \frac{d^3p}{(2\pi)^3}\left[\frac{1}{2}\epsilon_p^\phi + T\,\ln\left(1-e^{-\beta\epsilon_p^\phi}\right)\right]\,. \tag{V.17}$$

The singular, temperature-independent piece pressure in (V.17) proportional to ϵ_p^ϕ is nothing but the effective potential at vanishing temperature which we have computed for a fermionic theory in the last chapter. Its renormalisation can be performed analogously. Here we are only interested in the thermal pressure, and we subtract the pressure at vanishing temperature,

$$\begin{aligned} p_{\phi,\text{thermal}} &= p_\phi(T) - p_\phi(T=0) \\ &= -\,T\int \frac{d^3p}{(2\pi)^3}\ln\left(1-e^{-\beta\epsilon_p^\phi}\right) = -\frac{T}{2\pi^2}\int_0^\infty dp\,p^2\,\ln\left(1-e^{-\beta\epsilon_p^\phi}\right)\,. \end{aligned} \tag{V.18}$$

Eq.(V.18) is manifestly finite as for large momenta $p^2 \gg m_\phi^2, T^2$ the exponential in the logarithm decays with $\exp(-p/T$, the typical thermal decay. It is also positive as the argument in the logarithm is always smaller than one and hence the logarithm is strictly negative. With the minus sign in front of the integral this leads to a positive expression, as expected for a thermal pressure. For a given temperature (V.18) takes its maximal value for $m_\phi^2 = 0$ and decays monotonously with increasing m_ϕ^2 as the thermal part of the mass-derivative is negative, see (V.16). For $m_\phi^2 \to \infty$ the thermal pressure vanishes. Accordingly the pressure is positive for all m_ϕ^2. For large masses $m_\phi \gg T$ the pressure decays exponentially with $\exp(-m_\phi/T)$ (up to polynomial prefactors). For vanishing masses the momentum integration can be performed easily and we arrive at

$$p_{\phi,\text{thermal}}|_{m^2=0} = \frac{\pi^2 T^4}{90}\,. \tag{V.19}$$

The explicit result for vanishing mass is the Stefan-Boltzmann pressure of a free gas. It is the tree-level thermal pressure. Note also that (V.18) is the result for the thermal part of the (one-loop) effective potential of a bosonic theory, see (V.18).

Now we have collected all results for discussing the mesonic fluctuations in our $N_f = 2$ low energy effective theory. The mesonic contribution to the pressure and hence to minus the free energy density/effective potential are simply given by summing up (V.18) for the sigma and the three pions leading to

$$\left[\Omega_{\phi,T}(\phi) - \Omega_{\phi,T=0}(\phi)\right]_{\text{mes.flucs.}} \simeq \frac{T}{2\pi^2}\int_0^\infty dp\,p^2\,\ln\left(1-e^{-\beta\epsilon_p^\phi(m_\sigma)}\right) + 3\frac{T}{2\pi^2}\int_0^\infty dp\,p^2\,\ln\left(1-e^{-\beta\epsilon_p^\phi(m_\pi)}\right)\,, \tag{V.20}$$

The concentration on the thermal part of the fluctuations allows us to simply add (V.20) to the low energy effective action at valishing temperature regardless of how we have treated the mesonic fluctuations there. Note also in this contect that (V.20) is finite as it should be: in thermal field theory all UV divergences can be treated already in the $T = 0$ case and the subtractions can be chosen to be temperature-independent.

In (V.20) this comes about as it only summarises the thermal fluctuations and momentum fluctuations with $p \gg T$

are suppressed. Accordingly in the context of our low energy EFT setup (V.20) is only valid for $T/\Lambda \ll 1$. For larger temperatures already the Matsubara sum that takes account of high frequencies is at odds with the fact that $p_0^2 + \vec{p}^2 \leq \Lambda^2$.

B. Quarks at finite temperature

In summary we are but one step away from our goal of accessing the thermal chiral phase transition in QCD in the quark-meson EFT. For that task we need to translate the results above to the -free- quark path integral. The computation of the last chapter in the vacuum carries over here, we only have to discuss the fermionic Matsubara frequencies. For that end we redo the derivation of the thermal path integral for fermions again by starting from partition function Z_T as defined in the scalar case in (V.1). Everything goes as in the scalar case except one subtlety concerning the trace. Again more details can be found in the QFT II lecture notes, chapter 2. As in the case of the bosonic field we need coherent states that allow us to define $\hat{\psi}|\psi\rangle = \psi|\psi\rangle$. For the sake of the argument we restrict ourselves to one creation and annihilation operator $a, a^\dagger$ and Grassmann variable c. A coherent state is given by

$$|c\rangle = (1 - c\, a^\dagger)|0\rangle = e^{-c\, a^\dagger}|0\rangle \qquad \text{with} \qquad a|c\rangle = c\, a\, a^\dagger)|0\rangle = c|0\rangle = c(1 - c\, a^\dagger)|0\rangle = c|c\rangle\,, \tag{V.21}$$

where the latter property proves the coherence property of the state. The dual state $\langle c| = |c\rangle^\dagger$ has the property

$$\langle c|a^\dagger = -\langle c|c^*\,. \tag{V.22}$$

In consequence, instead of periodicity of the fields in time in the scalar case coming from the trace in (V.1) we have anti-periodicity,

$$\psi(t + \beta, \vec{x}) = -\psi(t, \vec{x})\,, \tag{V.23}$$

that reflects the Grassmannian nature of the fermionic field. The fermionic path integral Z_q with the Dirac action at finite temperature then reads

$$Z_{q,T}[J] = \int_{\psi(\beta,\vec{x}) = -\psi(0,\vec{x})} d\bar{\psi}\, d\psi\, e^{-S_{D,T}[\phi] + \int_0^\beta d^4x\, \bar{J}_\psi(t,\vec{x})\psi(\vec{x}) - \bar{\psi} J_\psi}\,, \qquad S_{D,T}[\psi] = \int_0^\beta d^4x\, \bar{\psi}\cdot(\not{D} + m_\psi + i\,\gamma_0\mu)\cdot\psi\,. \tag{V.24}$$

As in the scalar case we can reveal the thermal nature of correlation functions derived from the generating functional (V.24) by looking at the Dirac propagator of the quarks in the mixed representation at vanishing time, $G_q(t, \vec{p})$. To that end we first notice that the Fourier transformation of the anti-periodic fermionic fields is reflected in a shift of the Matsubara modes by πT. We have

$$\psi(x) = T\sum_{n\in\mathbb{Z}} \int \frac{d^3p}{(2\pi)^3} e^{-i(\omega_{n,f}\, t + \vec{p}\vec{x})}\psi(p_0, \vec{p})\,, \qquad \omega_{n,f} = 2\pi\left(n + \frac{1}{2}\right)\,, \tag{V.25}$$

where the additional factor $e^{i\pi T\, t}$ leads to the minus sign in the periodicity relation (V.23) with $e^{i\pi T\,(t+\beta)} = e^{i\pi} e^{i\pi T\, t} = -e^{i\pi T\, t}$. Now we perform the computation for the frequency sum of the quark propagator G_q with N_f flavours and N_c colors,

$$\frac{1}{m_\psi}\frac{1}{4N_f N_c}\,\mathrm{tr}\, G_q(t = 0, \vec{p}) = T\sum_{n\in\mathbb{Z}} \frac{1}{\omega_{n,f}^2 + \vec{p}^2 + m_\psi^2} = \frac{1}{2\epsilon_p^\psi}\tanh\beta\epsilon_p^\psi = \frac{1}{2\epsilon_p^\psi}\left[1 + 2n(\epsilon_p^\psi)\right]\,, \tag{V.26}$$

where the trace tr in (V.26) sums over flavour, color and Dirac space. The dispersion ϵ_p and the thermal distribution function $n(\omega)$ are given by

$$\epsilon_p^\psi(m_\psi) = \sqrt{\vec{p}^2 + m_\psi^2}\,, \qquad n_F(\omega) = \frac{1}{e^{\beta\omega} + 1}\,. \tag{V.27}$$

The latter is the expected Fermi-Dirac distribution. The difference to the Bose-Einstein statistics in the scalar case originates in the anti-periodicity of the fermions related to their Grassmannian nature. The free energy and pressure can be derived analogously to the scalar case. The one-loop contribution to the quark free energy density Ω_q and the

pressure are hence given by

$$\Omega_q \simeq -\frac{T}{2\mathcal{V}} \operatorname{Tr} \ln\left(-\partial_\mu^2 + m^2\right) = -2N_c N_f\, T \sum_{n\in\mathbb{Z}} \int \frac{d^3p}{(2\pi)^3}\, \ln\left(\omega_{n,f}^2 + \vec{p}^2 + m^2\right)\,,$$

$$p_q \simeq 2N_c N_f\, T \sum_{n\in\mathbb{Z}} \int \frac{d^3p}{(2\pi)^3}\, \ln\left(\omega_{n,f}^2 + \vec{p}^2 + m^2\right) = 12\, T \sum_{n\in\mathbb{Z}} \int \frac{d^3p}{(2\pi)^3}\, \ln\left(\omega_{n,f}^2 + \vec{p}^2 + m^2\right)\,, \tag{V.28}$$

where as in the scalar case we dropped the normalisations in Ω_q and p_q. For the pressure we have also inserted the $N_f = 2, N_c = 3$ case discussed here.

For a first simple computation we also use $\mu = 0$, a vanishing quark chemical potential. The prefactor -2 in comparison to the prefactor $1/2$ in the scalar case comes from the relative minus sign and factor 2 of the fermionic loop, the symmetrisation of the frequency and spatial momentum trace and the Dirac trace: $-1 * 1/2 * 4 = -2$ instead of $1/2$ in the scalar case. The factor $N_c N_f$ counts the degrees of freedom. For the computation of the thermal pressure we proceed similar to the scalar case with a m_ψ^2-derivative which maps the pressure to (V.26). We also remove the divergent vacuum contribution which is the effective potential at vanishing temperature, see (IV.88). The grand potential and thermal quark pressure in the $N_f = 2$ case is then given by

$$\Omega_{q,T}(\psi,\bar\psi,\phi) - \Omega_{q,T=0}(\psi,\bar\psi,\phi) = -\frac{12}{\pi^2} T \int_0^\infty dp\, p^2\, \ln\left(1 + e^{-\beta\epsilon_p^\psi}\right) = -p_{q,\text{thermal}}\,, \tag{V.29}$$

where

$$m_\psi^2(\phi) = \frac{1}{2} h^2 \rho\,. \tag{V.30}$$

This has to be compared with (V.20) for the mesons. Both expressions for the pressure are strictly positive which is due to

$$\mp \ln\left(1 \mp e^{-\beta\epsilon_p^{\phi/\psi}}\right) \geq 0\,, \tag{V.31}$$

with the minus signs in the bosonic case and the plus sign in the fermionic one. The global $\mp$ in (V.31) reflects the relative sign of fermionic and bosonic loops while the $\mp$ reflects the Bose-Einstein vs Fermi-Dirac quantum statistics.

The sum of (V.20) and (V.38),

$$\Omega_T(\psi,\bar\psi,\phi) - \Omega_{T=0}(\psi,\bar\psi,\phi) = \Omega_{\phi,T} + \Omega_{q,T} - \Omega_{\phi,T=0} + \Omega_{q,T=0} \tag{V.32}$$

encodes all thermal fluctuations on one loop. As in the vaccum case for $T = 0$ we have several possibilities of how to integrate out the thermal fluctuations, e.g. either in parallel or successively. Even though being relevant for the quantitative results, it is irrelevant for the access of the mechnism of chiral symmetry restauration at large temperatures: At large temperatures the quark exhibits a Matsubara gapping as the lowest lying Matsubara mode is πT in comparison to the vanishing one in the mesonic case. For higher temperatures more and more of the infrared quark fluctuations are gapped. However, the quark fluctuations triggers strong chiral symmetry breaking in the first place. Consequently at large enough temperatures chiral symmmtry breaking is melted away.

C. RG for the effective potential at finite temperature*

For quantitative statements the RG equation as in chapter IV F 3 or similar non-perturbative techniques such as Dyson-Schwinger equations or 2PI/nPI techniches (2-particle irreducible/n-particle irreducible) should be used. Here we just extend the Wegner-Houghton equation we have derived for the $T = 0$ case in chapter IV F 3. There we have the frequency and spatial momentum integration with an $O(4)$-dimensional momentum cutoff with $p^2 \geq \Lambda^2$ in the integrals.

At finite temperature the four-momentum is given by $(2\pi T)^2 n^2 + \vec{p}^2$ and the related θ-function is $\theta((2\pi T)^2 n^2 + \vec{p}^2 - \Lambda^2)$. A four dimensional cutoff leads to discontinuous flows as it jumps if we sweep over one of the Matsubara modes. In (V.34) we would have to substitute

$$\operatorname{Tr}\delta(\sqrt{p^2} - \Lambda) \to \operatorname{Tr}\delta(\sqrt{(2\pi T)^2 n^2 + \vec{p}^2} - \Lambda)\,, \tag{V.33}$$

which makes the non-analyticity apparent. Even though the spatial momentum integration smoothens the non-analyticity, it is present and hampers in particular the simple computation of the thermodynamical properties such as the pressure, see [21]. This is not a conceptual problem as these jumps have to be absorbed in the Λ-dependence of the initial condition, it hampers explicit computations.

For that reason we choose a spatial momentum cutoff $\vec{p}^2 > \Lambda^2$, leading us to the functional Wegner-Houghton equation

$$\Lambda\partial_\Lambda \Gamma_\Lambda[\psi,\bar\psi,\phi] = -\frac{1}{2}\mathrm{Tr}_{\vec{p}^2=\Lambda^2}\ln\frac{\Gamma^{(2)}_{\phi\phi}}{\Lambda^2} + \mathrm{Tr}_{\vec{p}^2=\Lambda^2}\ln\frac{\Gamma^{(2)}_{\psi\bar\psi}}{\Lambda^2}\,, \tag{V.34}$$

where the trace

$$\mathrm{Tr}_{\vec{p}^2=\Lambda^2} = T\sum_n \int \frac{d^3p}{(2\pi)^3}\delta(\sqrt{p^2}-\Lambda)\,, \tag{V.35}$$

now only sums over the spatial momentum shell with $p^2=\Lambda^2$, but over all Matsubara modes. In the line of the arguments in chapter IV F 3 this cutoff is now applied to all fluctuations and not only to the thermal ones.

Practically our computations so far allow us to read off the flow equation for the effective potential. For the meson part we start with (V.17) for a scalar mode, leading to

$$\Omega_{\phi,\Lambda} \simeq \frac{1}{2\pi^2}\int_\Lambda^{\Lambda_{\rm UV}} dp\, p^2\,\left[\frac{1}{2}\epsilon_p^\phi + T\,\ln\left(1-e^{-\beta\epsilon_p^\phi}\right)\right] + \Omega_{\phi,\Lambda_{\rm UV}}\,, \tag{V.36}$$

including the vacuum part. Hence, we simply read-off (minus) the integrand as the Λ-derivative of Ω_ϕ. Applying this immediately to the mesonic part of our EFT we arrive at

$$\Lambda\partial_\Lambda\Omega_{\phi,\Lambda}(\phi) = -\frac{\Lambda^3}{2\pi^2}\left\{\frac{1}{2}\left[\epsilon_\Lambda^\phi(m_\sigma)+\frac{3}{2}\epsilon_\Lambda^\phi(m_\pi)\right] + T\,\left[\ln\left(1-e^{-\beta\epsilon_\Lambda^\phi(m_\sigma)}\right)+\ln\left(1-e^{-\beta\epsilon_\Lambda^\phi(m_\pi)}\right)\right]\right\}\,, \tag{V.37}$$

where the spatial momentum arguments in the dispersions ϵ_p^ϕ are now taken at the cutoff scale, $p=\lambda$. The first two terms on the right hand side is the $T=0$ flow as the second term vanishes for $T=0$. It is different from its counter part in (IV.99) as (V.37) only involves a spatial momentum cutoff, reflected in the cubic power of Λ.

The derivation of the quark part of the flow proceeds similarly. We start with the expression for Ω_q or $-p_q$ after integration of the Matsubara frequency, (V.38) and restore the $T=0$ part,

$$\Omega_{q,\Lambda}(\psi,\bar\psi,\phi) = -\frac{12}{\pi^2}\int_\Lambda^{\Lambda_{\rm UV}} dp\, p^2\,\left[\epsilon_p^\psi + T\,\ln\left(1+e^{-\beta\epsilon_p^\psi}\right)\right] + \Omega_{q,\Lambda_{\rm UV}}(\psi,\bar\psi,\phi)\,, \tag{V.38}$$

leading us to the flow

$$\Lambda\partial_\Lambda\Omega_{q,\Lambda}(\psi,\bar\psi,\phi) = \frac{12\Lambda^3}{\pi^2}\left[\epsilon_\Lambda^\psi + T\,\ln\left(1+e^{-\beta\epsilon_\Lambda^\psi}\right)\right]\,. \tag{V.39}$$

As in the mesonic part, the first term on the right hand side is the $T=0$ part of the flow. It also does not match its counterpart in (IV.99) due to the different cutoffs.

In summary we are led to the full flow

$$\begin{aligned}\Lambda\partial_\Lambda\Omega_\Lambda(\psi,\bar\psi,\phi) = &-\frac{\Lambda^3}{2\pi^2}\Bigg\{\frac{1}{2}\left[\epsilon_\Lambda^\phi(m_\sigma)+\frac{3}{2}\epsilon_\Lambda^\phi(m_\pi)\right] - 12\,\epsilon_\Lambda^\psi \\ &+ T\,\left[\ln\left(1-e^{-\beta\epsilon_\Lambda^\phi(m_\sigma)}\right)+\ln\left(1-e^{-\beta\epsilon_\Lambda^\phi(m_\pi)}\right) - 24\,T\,\ln\left(1+e^{-\beta\epsilon_\Lambda^\psi}\right)\right]\Bigg\}\,,\end{aligned} \tag{V.40}$$

where the first line is the $T=0$ part of the flow, while the second line is the thermal part. Note that both parts are dependent on derivatives of Ω via the mass-functions and hence feed into each other. One cannot simply solve the $T=$-part first. For example, the thermal pressure is given by (minus) the Λ-integral of the second line on the solution of the full flow equation. If we take Λ-independent mass functions, the Λ-integral gives the one-loop expressions we have started with.

VI. CONFINEMENT

In chapter IV we have discussed the emergence of strong chiral symmetry breaking in QCD which is ultimately related to the growth of the strong coupling $\alpha_s(p^2)$ towards the infrared, $p^2 \to 0$. This growth triggers a grows in the four-quark interaction that develops a resonance at the chiral symmetry breaking (momentum) scale. It is also the simplicity of this mechanism or better its representation in terms of correlation functions that allowed us to derive a relatively simple low energy effective theory that encorporates strong chiral symmetry breaking in QCD.

In chapter V this set-up was used to explored strong chiral symmetry breaking at finite temperature. Thermal fluctuations decrease the strong coupling $\alpha_s(p^2)$ and finally melt-down chiral symmetry breaking. This is monitored in a simple way by the temperature-dependence of the chiral order parameter, the expectation value of the scalar sigma field, $\sigma_0 \propto \langle\bar\psi\psi\rangle$.

We hope for a similarly simple picture for the phenomenon of confinement in the formulation of QCD in terms of correlation functions. Indeed we shall see that while the mechanism and dynamics of confinement is rather intricate in comparison, we have simple signatures of confinement in terms of its order parameter, the potential of which can be derived from low order correlation functions of quarks and gluons. It also allows us to extend the low energy EFTs introduced and used in the last chapters to also encorporate confinement. This set-up then enables us to study the confinement-deconfinement phase transition at finite temperature as well as the full phase structure at finite temperature and density. Before we start, a word of caution is required: this fascinating area has been the subject of intense studies over the past decades and has many facets ranging from mathematical physics -and in particular topological considerations- to phenomenological applications and the relation of the confinement dynamics to hadronic properties of QCD. Here we only can scratch the surface and shall take a practical approach: the lecture aims at being self-contained for the computations discussed, other equally interesting subjects are mentioned but not detailed. A fully comprehensive study is way beyond the scope of the current lecture course.

To begin with we discuss the question of the symmetry behind confinement and the related order parameter. For having a clean setting we restrict ourselves to pure Yang-Mills theory with static quark sources. Then confinement is the phenomenon that a quark–anti-quark pair experiences a linear potential when pulled apart. The expectation value of such a state $\langle\mathcal{O}_{q\bar q}(\vec x,\vec y)\rangle$ with a static quark q at the position $\vec x$ and a static anti-quark $\bar q$ at the position $\vec y$ is related to its free energy $F_{q\bar q}$,

$$\langle\mathcal{O}_{q\bar q}(\vec x,\vec y)\rangle \propto e^{-F_{q\bar q}(r)}\,, \qquad\qquad r = \|\vec x-\vec y\|\,. \tag{VI.1}$$

In (VI.1) we have used translation invariance present in an infinite volume, and hence the free energy only depends on the distance r between the quark and the anti-quark. For small distances the strong coupling $\alpha_s(p\propto 1/r\to\infty)\to 0$ gets small and perturbation theory is applicable. Therefore we expect a Coulomb-type potential with a $1/r$ dependence for $r\to\infty$. At large distances $r\to\infty$ the strong coupling grows large and perturbation theory is not applicable anymore. In this regime confinement predicts a linear dependence of the free energy/potential on r. This leads us to

$$\lim_{r\Lambda_{\rm QCD}\to 0} F_{q\bar q}(r) \propto \frac{1}{r} \qquad \text{and} \qquad \lim_{r\Lambda_{\rm QCD}\to\infty} F_{q\bar q}(r) \propto \sigma\, r\,, \tag{VI.2}$$

where $\sigma \propto (420)\,\text{MeV})^2$ in pure Yang-Mills theory is the string tension. As remarked before there are no scales in pure Yang-Mills theory except the dynamical scale $\Lambda_{\rm QCD}$, so the explicit value above is up to our disposal, and we should rather determine a ratio of scales such as $\sqrt{\sigma}/\Lambda_{\rm QCD}$. Typically the string tension is used to gauge other observables such as the critical temperature of the confinement-deconfinement phase transition at finite temperature. We will come back to this point later.

A. Order parameters for confinement

The computation of the expectation value in (VI.1) enables us at vanishing temperature to monitor the r-dependence of the free energy of a $q\bar q$-pair. It also provides us with an order parameter for confinement: to that end we consider the limit $r\to\infty$. If confinement is present the free energy tends towards infinity in this limit and the expectation value $\langle\mathcal{O}_{q\bar q}\rangle$ vanishes. In turn, if we still had a Coulomb-type potential for large distances we get a finite value for $\langle\mathcal{O}_{q\bar q}\rangle$. This is what we expect for large temperature. As we have seen in the discussion of chiral symmetry breaking at finite temperature, increasing temperatures effectively increases the energy scale of the system. This heuristic

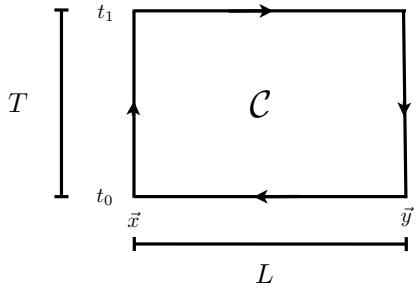

FIG. 13: e^+e^- pair.

argument is discussed in more details later. In summary we expect

$$\lim_{r\to\infty}\langle\mathcal{O}_{q\bar{q}}\rangle = \begin{cases} 0\,, & T < T_{\rm conf} \\ > 0\,, & T > T_{\rm conf} \end{cases} \quad . \tag{VI.3}$$

Accordingly, we have a clear signature for the confining phase as well as the deconfining phase. The above disucssion also makes clear why we restricted ourselves first to pure Yang-Mills theory with static quarks: in the presence of dynamical quarks quark–anti-quark pairs can be created if the potential $V_{q\bar{q}}$ between quark and anti-quark is large enough. These additional $q, \bar{q}$ can bind with the original pair into new $q\bar{q}$ pairs. This leads to a shielding of color force between the original pair and the effecitive potential levels at a finite value for $r \to \infty$.

It is left to determine the operator $\mathcal{O}_{q\bar{q}}$ as well as the underlying symmetry behind the confinement-deconfinement phase transition in pure Yang-Mills, as well as its breaking by dynamical quarks. To that end let us first consider an electron-positron pair, which is created at some initial time, pulled apart, kept at some distance L and then is annihilated, this describes a path $\mathcal{C}$ in space-time, see Fig. 13. The related free energy is described by a path integral, where the current J_μ of the worldlines of the e^+e^- pair is coupled to the photon field A_μ with

$$\int_x J_\mu A_\mu = -i\,e\left(\int_{t_0}^{t_1} d\tau\,[A_0(t,\vec{x}) - A_0(t,\vec{y})] + \int_{\vec{x}}^{\vec{y}} d\vec{z}\left[\vec{A}(t_1,\vec{x}) - \vec{A}(t_0,\vec{y})\right]\right)\,, \tag{VI.4}$$

with the worldline current

$$J_\mu(x) = -i\,e\int_{\mathcal{C}} dz_\mu \delta(z-x)\,. \tag{VI.5}$$

The global sign in the current is pure convention and is related to that in the covariant derivative, in our case we have $D_\mu = \partial_\mu - i\,g A_\mu$, see (I.1).

In conclusion the source term (or operator of such a static electron-positron pair) is given by

$$\mathcal{W}_{\mathcal{C}}[A] = e^{\int_x J_\mu A_\mu} = \underbrace{e^{-i\,e\int_{\mathcal{C}} dz_\mu\, A_\mu(z)}}_{\rm Wegner-Wilson\ Loop}. \tag{VI.6}$$

The Wegner-Wilson loop in QED has a very simple interpretation which we shall discuss briefly. Consider a closed path $\mathcal{C}$ that is the boundary of an area $\mathcal{A}$. Then the integral in the exponent can be rewritten with Stokes' theorem as

$$e\int_{\mathcal{C}=\partial\mathcal{A}} dz_\mu\, A_\mu(z) = e\frac{1}{2}\int_{\mathcal{A}} dx_\mu dy_\nu\, F_{\mu\nu}\,. \tag{VI.7}$$

Accordingly, the phase in the Wegner-Wilson loop simply is the flux through the area $\mathcal{A}$ with the boundary $\mathcal{C}$. This is an observable quantity and is gauge invariance is evident from the flux representation (VI.7). In the gauge field representation the gauge invariance of (VI.6) follows with the $U(1)$ gauge transformations $U = \exp i\omega \in U(1)$ of $A_\mu \to A_\mu + 1/e\,\partial_\mu\omega$ with,

$$\mathcal{W}_{\mathcal{C}}[A^U] = e^{-i\,e\int_{\mathcal{C}} dz_\mu\, A^U_\mu(z)} = e^{-i\,e\int_{\mathcal{C}} dz_\mu \left(A_\mu(z) + \frac{1}{e}\partial_\mu\omega\right)} = e^{-i\,e\int_{\mathcal{C}} dz_\mu\, A_\mu(z)}\,, \tag{VI.8}$$

where we have used that $\int_{\mathcal{C}} dz_\mu\,\partial_\mu\omega = 0$. Note also that an open Wilson line related to a path from the position x to

the position y is a *parallel transporter* that transports gauge transformations from the position x to y,

$$\mathcal{W}_{\mathcal{C}_{x,y}}[A] = e^{-i\,e\int_{\mathcal{C}_{x,y}} dz_\mu\, A_\mu(z)}\,, \qquad \text{with} \qquad \mathcal{W}_{\mathcal{C}_{x,y}}[A^U] = U(x)\mathcal{W}_{\mathcal{C}_{x,y}}[A]U^\dagger(y)\,, \tag{VI.9}$$

This allows to define gauge-invariant correlation functions of e.g. fermionic fields ψ such as

$$\langle\bar\psi(x)\mathcal{W}_{\mathcal{C}_{x,y}}[A]\psi(y)\rangle\,. \tag{VI.10}$$

In the case with dynamical electrons (VI.10) describes a e^+e^- pair.

The above definitions and relations extend straightforwardly to non-Abelian gauge groups. The only change comes from the fact that now the gauge field is matrix valued and the simple exponential of $i\,g\int dz_\mu\, A_\mu$ does not have the necessary transformation properties (VI.9) and the closed loop would fail to be gauge invariant. This situation is similar to that of defining the time-evolution operator in quantum mechanics and quantum field theory (S-matrix) on the basis of a Hamiltonian operator $\hat H$. There the resolution is to resort to time-ordering. In the present case we resort to path ordering which then transports the gauge transformation along the path. We define

$$U_{\mathcal{C}_{x,y}} = \mathcal{P}e^{-ig\int_{\mathcal{C}_{x,y}} dz_\mu\, A_\mu(z)}\,, \qquad \text{with} \qquad U_{\mathcal{C}_{x,y}}[A^U] = U(x)\,U_{\mathcal{C}_{x,y}}U^\dagger(y)\,, \qquad U(x)\in SU(N_c)\,. \tag{VI.11}$$

The loop $U_{\mathcal{C}}\in SU(N_c)$ is a group element and the transformation property under gauge transformation of A_μ, (I.6), originates in the path ordering defined with

$$\mathcal{P}A_{\mu_1}(x(s_1))\cdots A_{\mu_n}(x(s_n)) = A_{\mu_{\sigma(1)}}(x(s_{\sigma(1)})\cdots A_{\mu_{\sigma(n)}}(x(s_{\sigma(n)}))\,, \qquad \text{with} \qquad s_{\sigma(1)}\le s_{\sigma(2)}\le\cdots\le s_{\sigma(n)}\,. \tag{VI.12}$$

In (VI.12) $s\in[0,1]$ is an isomorphic (invertible) parameterisation $x(s)$ of the given path $C_{x,y}$ with $x(0)=x$ and $x(1)=y$. For integrals this leads to the relations well-known from the time ordering, the simplest one being that for a product of two integrals,

$$\frac{1}{2}\mathcal{P}\left[\int_x^y dz_\mu\, A_\mu(z)\int_x^y dz'_\nu A_\nu(z')\right] = \int_x^y dz_\mu\, A_\mu(z)\int_z^y dz'_\nu A_\nu(z')\,. \tag{VI.13}$$

Higher products follow similarly. Due to the path ordering derivatives of $U_{\mathcal{C}_{x,y}}$ w.r.t. x or y pull down a gauge field to the left or to the right respectively.

$$\partial^x_\mu\, U_{\mathcal{C}_{x,y}} = i\,gA_\mu(x)\,U_{\mathcal{C}_{x,y}}\,, \qquad\qquad \partial^y_\mu\, U_{\mathcal{C}_{x,y}} = U_{\mathcal{C}_{x,y}}\,(-i)\,gA_\mu(y)\,. \tag{VI.14}$$

With these properties the covariant derivative can be simply expressed as a parallel transport of the partial derivative, to wit

$$U_{\mathcal{C}_{x,y}}\partial^x_\mu\, U^\dagger_{\mathcal{C}_{x,y}} = \partial^x_\mu - igA_\mu(x)\,. \tag{VI.15}$$

The property (VI.15) can be used to get a solution of the Dirac equation in terms of a phase factor $\mathcal{W}_{\mathcal{C}}$ and the solution of the free dirac equation ψ_0. This is discussed in detail later for the static finite temperature case. In summary we conclude that the expectation value of a static quark–anti-quark pair $q\bar q$ is given by

$$W[L,T] = \frac{1}{Z}\int dA\,\mathcal{W}_{\mathcal{C}}(A)\,e^{-S_{\rm YM}[A]}\,, \qquad \text{with} \qquad \mathcal{W}_{\mathcal{C}}[A] = \mathrm{tr_f}\,U_{\mathcal{C}}\,. \tag{VI.16}$$

In the limit, where the time T tends towards infinity, the correlation function (**??**) is proportional to the exponential of the interaction energy $E(L)$ of this state (times T). All other contributions vanish exponentially fast with $(E_i - E(L))T>0$, where E_i is the energy of the related state. We have

$$\lim_{T\to\infty} W[L,T] = F(L)\,E^{-E(L)T}\,, \tag{VI.17}$$

which relates to the exponential of the free energy of a static quarkanti-quark state. The prefactor $F(L)$ relates to the overlap of the Wilson loop with the ground state. In the confining phase the Wegner-Wilson loop is given by $\mathcal{W}[T,L]\simeq e^{-F_{\bar qq}[T,L]}$ with $F_{\bar qq}[T,L]$ having a linear dependence on both L and T. The linear dependence in L we have discussed before. The linear dependence in T simply follows from the fact that in our Euclidean formulation the

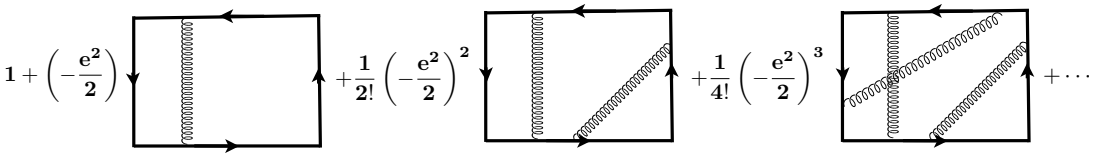

FIG. 14: Perturbative expansion of the Wilson loop expectation value for e^+e^-.

time direction is not different from the spatial ones. Hence we conclude

$$\lim_{L\,T\to\infty} W[T,L] \simeq e^{-\sigma LT}\,, \tag{VI.18}$$

with the string tension σ. Eq.(VI.18) is the area law that signals confinement as does the linear potential. it is left to discuss the symmetry behind the confinement-deconfinement phase transition. This will be discuss in chapter VI B.

For its computation let us first discuss the far simpler case of an electron-positron pair e^+e^-. Then the static potential is the standard Coulomb potential. Indeed in the static limit there is no self-interaction of the photon and the expectation value of the Wilson loop is simply given by the sum of boxes with n photon exchanges from positions x_i to y_i where one integrates over x_i and y_i on the contour $\mathcal{C}[L,T]$. This is depicted in Fig. 14.

In other words we have

$$W[L,T] = e^{-\frac{e^2}{2}\int_{\mathcal{C}[L,T]} dx_\mu \int_{\mathcal{C}[L,T]} dy_\nu \langle A_\mu(x)A_\nu(y)\rangle_{\rm sub}}\,, \tag{VI.19}$$

where we have used that $\langle A_{\mu_1}\cdots A_{\mu_{n+1}}\rangle = 0$. The subscript $\langle\cdots\rangle_{\rm sub}$ refers to the necessary subtraction of infinite selfenergies related to close loops with endpoints $x = y$. Moreover, all correlation functions decay in products of two-point functions (Wick-theorem), schematically we have $\langle A_1\cdots A_{2n}\rangle = \langle A_1A_2\rangle\cdots\langle A_{2n-1}A_{2n}\rangle + \cdots$, and there are $(2n-1)(2n-3)\cdots$ combinations. Upon contour integration all combinations give the same contribution and overall we have the nth order term in the propagator

$$\frac{(2n-1)(2n-3)\cdots}{(2n)!}2^n\left(-\frac{e^2}{2}\right)^n\left(\int_{\mathcal{C}} dx_\mu\int_{\mathcal{C}} dy_\nu\langle A_\mu(x)A_\nu(y)\rangle\right)^n = \frac{1}{n!}\left(-\frac{e^2}{2}\int_{\mathcal{C}} dx_\mu\int_{\mathcal{C}} dy_\nu\langle A_\mu(x)A_\nu(y)\rangle\right)^n\,, \tag{VI.20}$$

for a general contour $\mathcal{C}$, leading to the Gaußian expression (VI.19). This leaves us with the task of computing

$$\begin{aligned}\int_{\mathcal{C}} dx_\mu\int_{\mathcal{C}} dy_\nu\langle A_\mu(x)A_\nu(y)\rangle &= \int_{\mathcal{C}} dx_\mu\int_{\mathcal{C}} dy_\nu\int\frac{d^4p}{(2\pi)^4}\frac{1}{p^2}\left(\delta_{\mu\nu}-(1-\xi)\frac{p_\mu p_\nu}{p^2}\right)e^{ip(x-y)}\\ &= \int_{\mathcal{C}} dx_\mu\int_{\mathcal{C}} dy_\mu\int\frac{d^4p}{(2\pi)^4}\frac{1}{p^2}e^{ip(x-y)}\\ &= \int_{\mathcal{C}} dx_\mu\int_{\mathcal{C}} dy_\mu\,\frac{1}{4\pi^2}\frac{1}{(x-y)^2}\,.\end{aligned} \tag{VI.21}$$

To be explicit, we picked a covariant gauge in (VI.21). However, we have already proven that the *closed* Wilson line is gauge invariant which now is explicit as the ξ-dependent term drops out with the help of

$$\int_{\mathcal{C}} dx_\mu p_\mu e^{ipx} = -i\int_{\mathcal{C}} dx_\mu\partial^x_\mu e^{ipx} = 0\,, \tag{VI.22}$$

which eliminates all longitudinal contributions for closed loops. Note that this is not valid for open Wilson lines.

Finally we are interested in the large T-limit in (VI.17) where we have

$$\begin{aligned} V_{e^+e^-}(L) &= -\lim_{T\to\infty}\frac{1}{T}\log W[L,T] = \lim_{T\to\infty}\frac{1}{T}\frac{e^2}{2}\lim_{T\to\infty}\int_{\mathcal{C}[L,T]}dx_\mu\int_{\mathcal{C}[L,T]}dy_\mu\,\left(\frac{1}{4\pi^2}\frac{1}{(x-y)^2}\right)_{\rm sub} \\ &= -\lim_{T\to\infty}\frac{1}{T}e^2\lim_{T\to\infty}\int_{t_0}^{t_1}dx_0\int_{t_0}^{t_1}dy_0\,\left(\frac{1}{4\pi^2}\frac{1}{(x_0-y_0)^2+L^2}\right) \\ &= -\lim_{T\to\infty}\frac{1}{T}\frac{e^2}{4\pi}\lim_{T\to\infty}\int_{t_0}^{t_1}dx_0\int_{t_0-x_0}^{t_1-x_0}dy_0\,\left(\frac{1}{\pi}\frac{1}{y_0^2+L^2}\right) \\ &= -\lim_{T\to\infty}\frac{1}{T}2\frac{e^2}{4\pi}\int_0^T dx_0\,\arctan\left(\frac{x_0}{L}\right) \\ &= -\frac{e^2}{4\pi}\frac{1}{L}\,. \end{aligned} \tag{VI.23}$$

Eq.(VI.23) is the Coulomb potential as expected. The L-dependence we could have determined without any computation from dimensional arguments.

Adapting, within a bold step, the above analysis in QCD within a Gaußian approximation (no self-interaction of the gluons), we are led to the same result, up to a colour factor $\mathrm{tr}_{\rm f}t^at^a) = N_cC_F = (N_c^2-1)/2$, see (**??**). This is to be expected in perturbation theory, which is what the Gaußian approximation relies on.

In turn, relying on this approximation also in the non-perturbative confining secotr of QCD or Yang-Mills theory, the static potential has the behaviour $V_{q\bar q}\sim L$, it is linear in the distance between quark and anti-quark. This requires a gluon propagator

$$\lim_{p\to 0}\langle A_\mu(p)A_\nu(-p)\rangle \propto \frac{1}{(p^2)^2}\,, \tag{VI.24}$$

which is the limit of what is allowed in a covariant local quantum field theory. Eq.(VI.24) suggests gluon dominance (over the ghost) in the infrared. Indeed, such propagators have been computed in the Landau gauge in the Mandelstam approximation (no ghosts). However, it turns out that in the Landau gauge the gluon propagators are not infrared enhanced as (VI.24) but infrared suppressed. Moreover, any n-loop contribution (even in full propagators and vertices) to the Wilson loop expectation value does not show the required linear behaviour, it only comes about by a full resummation of all diagrams. Nonetheless these considerations show that gauge fixing should be rather seen as offering the possibility to device an appropriate parameterisation of the theory rather than a liability. For example, it can be shown that in Coulomb gauge the Gaußian approximation is working at least qualitatively.

B. Confinement-deconfinement phase transition at finite temperature

The dynamics of confinement and the confinement-deconfinement phase transition is the second cornerstone of the low energy QCD phenomenology we have to unravel. Here we aim at a treatment of this phenomenon within the continuum formulation of QCD similar to that of the chiral phase structure in chapter V. We mainly concentrate on the effective potential of the order parameter, the Polyakov loop. This observable is derived directly from the Wilson loop discussed before.

1. Polyakov loop

We consider a rectangular Wilson loop,Fig. 13, within the static situation also used in the previous chapters VI A, **??**. At finite temperature T the time is limited to $t\in[0,\beta]$ with $\beta = 1/T$, see chapter V A. Moreover, the gauge fields are periodic in time up to gauge transformations, i.e.

$$A_\mu(t+\beta,\vec x) = \frac{i}{g}T(t,\vec x)\left(D_\mu T^\dagger(t,\vec x)\right)\,,\qquad c(t+\beta,\vec x) = T(t,\vec x)\,c(t,\vec x)\,T^\dagger(t,\vec x)\,,\quad \bar c(t+\beta,\vec x) = T(t,\vec x)\,\bar c(t,\vec x)\,T^\dagger(t,\vec x) \tag{VI.25}$$

with $T(t,\vec{x}) \in SU(N)$ are the *transition functions*. It follows from (VI.25) that under gauge transformations they transform as

$$T^U(t,\vec{x}) = U(t+\beta,\vec{x})\, T(t,\vec{x})\, U^\dagger(t,\vec{x})\,, \tag{VI.26}$$

they parallel transport gauge transformations from t to $t+\beta$. The transformation property (VI.25) ensures the periodicity of gauge invariant quantitites. It is indeed possible to restrict ourselves to strictly periodic fields, $t \equiv \mathbb{1}$, even though this limits the possible gauge choice. For the time being we restrict ourselves to the periodic case and discuss the general case at the end. The state we want to construct is the one, where we desribe a static quark–anti-quark pair for all times. To that end we take a path that extends in time direction from $t=0$ to β. Then the spatial paths at fixed time $t=0$ and $t=\beta$ have to be identified (up to the orientation) due to the periodicity on the lattice, as well as the fact that we have restricted ourselves to periodic gauge fields. We conclude that the path $\mathcal{C}[L,\beta]$ splits into two loops winding around the time direction at the points $\vec{x}$ and $\vec{y}$ with $L = |\vec{x}-\vec{y}|$. The Wilson loop expectation value is then given by

$$\frac{1}{N_C^2} W[L,\beta] = \langle \mathcal{W}_{\mathcal{C}[L,\beta]}[A] \rangle = \langle L[A_0](\vec{x}) L^\dagger[A_0](\vec{y}) \rangle\,, \tag{VI.27}$$

where $L[A_0]$ is the Polyakov loop variable with

$$L = \frac{1}{N_c} \mathrm{tr_f}\, P(\beta,\vec{x})\,, \qquad \text{with} \qquad P(t,\vec{x}) = \mathcal{P} e^{-i\,g\int_0^t A_0(\tau,\vec{x}) d\tau}\,. \tag{VI.28}$$

The normalisation of the Polyakov loop is such that it is unity for a vanishing gauge field, $L[0]=1$. It lives in the fundamental representation as it is related to a creation operator of a quark. It is gauge invariant under periodic gauge transformations that keep the strict periodicity of the gauge field we have required. In general we have

$$L[A^U] = \frac{1}{N_c} \mathrm{tr_f}\, \left[U^\dagger(\beta,\vec{x}) U(0,\vec{x})\right]\, P(\beta,\vec{x})\,, \tag{VI.29}$$

where we have used the cyclicity of the trace. The combination $\left[U^\dagger(\beta,\vec{x})U(0,\vec{x})\right]$ is unity for periodic gauge transformations, which is the case we have restricted ourselves to when deriving (VI.27) from the gauge invariant Wilson loop. In the general case the two spatial parts of the path at $t=0,\beta$ only cancel up to the transition functions. Working through the derivation we get

$$L = \frac{1}{N_c} \mathrm{tr_f}\, T(0,\vec{x}) P(\beta,\vec{x})\,, \tag{VI.30}$$

which is also gauge invariant under non-periodic gauge transformations. Here we only consider $T \equiv \mathbb{1}$ but (VI.30) has to be used for example in the temporal axial gauge $A_0 \equiv 0$. Evidently, in this gauge (VI.28) simply is one. However, in order to achieve this gauge non-periodic gauge transformations (in time) have to be used. Then, the whole physics information of the Polyakov loop is stored in the transition function T instead of the gauge field. While this is not a convenient choice in continuum formulations it is a common choice on the lattice. There is is obtained by taking trivial temporal link variables $U_0 = \mathbb{1}$ for all but the last link from $t=\beta-a$ to β.

We now come back to our main line of arguments, and restrict ourselves to the fully periodic case. The Wilson loop in (VI.27) is an order parameter for confinement. More precisely in the confining phase it tends towards zero for large distances, $L\to\infty$, due to the area law,

$$\lim_{L\to\infty} W[L,\beta] \simeq \lim_{L\to\infty} e^{-\sigma\beta L} = 0\,. \tag{VI.31}$$

In turn, in the deconfined regime of the theory the quark–anti-quark potential $V_{q\bar{q}}$ is Coulomb-like, $V_{q\bar{q}} \propto 1/|\vec{x}-\vec{y}|$ and the Wilson loop follows a perimeter law, leading to

$$\lim_{L\to\infty} W[L,\beta] > 0\,. \tag{VI.32}$$

In conclusion the Wilson loop expectation value or Polyakov loop two-point correlation function for $L\to\infty$ serves as an order parameter for confinement at finite temperature. Moreover, in this limit we can use the clustering

decomposition property of a *local* quantum field theory,

$$\lim_{|\vec{x}-\vec{y}|\to\infty} \langle A(\vec{x})B(\vec{y})\rangle - \langle A(\vec{x})\rangle \langle B(\vec{y})\rangle = 0\,. \tag{VI.33}$$

for local operators A and B. Hence we conclude that

$$\lim_{L\to\infty} W[L,\beta] = \langle L[A_0](\vec{x})\rangle \langle L^\dagger[A_0](\vec{y})\rangle\,, \tag{VI.34}$$

it only depends on the temporal component of the gauge field. The Polyakov loop expectation value $\langle L[A_0]\rangle$ does not depend on the spacial variable due to translation invariance. Thus also the Polyakov loop expectation value itself serves as an order parameter for confinement,

$$\langle L[A_0]\rangle = \begin{cases} 0 & \text{confining regime} \\ \neq 0 & \text{deconfining regime} \end{cases} \tag{VI.35}$$

So far we have argued on a heuristic level which led us to (VI.35) as an order parameter, without even discussing the symmetry behind the pattern in (VI.35): we are searching for a symmetry that is preserved by the Yang-Mills action but does not keep $\langle L[A_0]\rangle$ invariant. This is the center symmetry of the gauge group. The center elements are those elements that commute with all other elements in the gauge group. In $SU(N)$ these are the Nth roots of unity in the groups. For the cases used here, the example group $SU(2)$ and the physical group $SU(3)$, the centers $\mathcal{Z}$ are

$$\mathcal{Z}_{SU(2)} = \{\mathbb{1}, -\mathbb{1}\} \simeq Z_2\,, \qquad \mathcal{Z}_{SU(3)} = \{\mathbb{1}, \mathbb{1}\, e^{\frac{2}{3}\pi i}, \mathbb{1}\, e^{\frac{4}{3}\pi i}\} \simeq Z_3\,. \tag{VI.36}$$

where the identities $\mathbb{1}$ in $SU(2)$ and $SU(3)$ are $\mathbb{1}_{2\times 2}$ and $\mathbb{1}_{3\times 3}$ respectively. The non-trivial center elements in (VI.36) are related to combinations of generators in the algebra. This relation is not unique as the eigenvalues of the combination of algebra elements is only determined up to $2\pi n$ with $n \in \mathbb{Z}$. For example, one representation is

$$SU(2): \quad -\mathbb{1} = e^{\pi i \sigma_3}\,, \qquad SU(3): \quad \mathbb{1}\, e^{\frac{2}{3}\pi i} = e^{2\pi i \frac{1}{\sqrt{3}}\lambda_8}\,, \qquad \mathbb{1}\, e^{\frac{4}{3}\pi i} = e^{2\pi i \frac{2}{\sqrt{3}}\lambda_8}\,. \tag{VI.37}$$

with the Pauli matrices in (IV.41) and the Gell-Mann matrices

$$\lambda_1 = \begin{pmatrix} 0 & 1 & 0 \\ 1 & 0 & 0 \\ 0 & 0 & 0 \end{pmatrix}, \quad \lambda_2 = \begin{pmatrix} 0 & -i & 0 \\ i & 0 & 0 \\ 0 & 0 & 0 \end{pmatrix}, \quad \lambda_3 = \begin{pmatrix} 1 & 0 & 0 \\ 0 & -1 & 0 \\ 0 & 0 & 0 \end{pmatrix}, \quad \lambda_4 = \begin{pmatrix} 0 & 0 & 1 \\ 0 & 0 & 0 \\ 1 & 0 & 0 \end{pmatrix},$$

$$\lambda_5 = \begin{pmatrix} 0 & 0 & -i \\ 0 & 0 & 0 \\ i & 0 & 0 \end{pmatrix}, \quad \lambda_6 = \begin{pmatrix} 0 & 0 & 0 \\ 0 & 0 & 1 \\ 0 & 1 & 0 \end{pmatrix}, \quad \lambda_7 = \begin{pmatrix} 0 & 0 & 0 \\ 0 & 0 & -i \\ 0 & i & 0 \end{pmatrix}, \quad \lambda_8 = \frac{1}{\sqrt{3}} \begin{pmatrix} 1 & 0 & 0 \\ 0 & 1 & 0 \\ 0 & 0 & -2 \end{pmatrix}, \tag{VI.38}$$

in the fundamental representation of $SU(3)$. The generators of the $SU(3)$ algebra are $t^a_{\text{fund}} = \lambda^a/2$. In the adjoint repesentation the generators of the algebra are given by the structure constants, see (I.4). The $SU(3)$ structure constants are given by

$$\begin{aligned} &SU(2): \quad f^{abc} = \epsilon^{abc}\,, \\ &SU(3): \quad f^{123} = 1\,, \quad f^{147} = f^{246} = f^{257} = f^{345} = \frac{1}{2}\,, \quad f^{156} = f^{367} = \frac{1}{2}\,, \quad f^{458} = f^{678} = \frac{1}{2}\,. \end{aligned} \tag{VI.39}$$

Hence, in the adjoint representation these elements are all represented by $\mathbb{1}$,

$$Z_{\text{ad}} = \mathbb{1}_{\text{ad}}\,, \qquad \text{for} \qquad Z \in \mathcal{Z}\,. \tag{VI.40}$$

In the adjoint representation every center element is mapped to the identity, $z = \mathbb{1}_{\text{ad}}, \forall z \in \mathcal{Z}$. Hence we have

$$\mathcal{Z}_{\text{ad}} = \{\mathbb{1}_{\text{ad}}\}\,. \tag{VI.41}$$

As the gauge fields and the ghosts live in the adjoint representation, the gauge-fixed Yang-Mills action is trivially invariant under center transformations. In turn, the Polyakov loop $L[A_0]$ is the trace of the Polyakov line $P(\beta, \vec{x})$ in

the *fundamental* representation, see (VI.28). It transforms with

$$P(\beta,\vec{x}) \to z\, P(\beta,\vec{x})\,, \qquad \text{with} \qquad z \in \mathcal{Z}\,. \tag{VI.42}$$

We conclude that in the center-symmetric phase of the theory the Polyakov loop expectation value (VI.35) has to vanish while in the center-broken phase it is finite. Having identified the symmetry we can envoke universality to predict the scaling of the order parameter in the vicinity of the phase transition:

For $SU(2)$ we are in the Ising universality class, the symmetry group being Z_2. If $SU(2)$-Yang-Mills exhibits a second order phase transition (and it does), it should have Ising scaling. This is indeed seen. For $SU(3)$ the symmetry group is Z_3 and we epxect a first order phase transition which is also seen. Our explicit computations later will not encorporate the full fluctuation analysis so detecting Ising scaling is out of reach here. However, we are able to see the seoncd and first order nature of the respective phase transitions. This closes our very rough symmetry discussion.

We also would like to get an intuitive understanding for the Polyakov loop expectation value. We have argued for the Wilson loop expectation value, that it is related to the expectation value of a static quark–anti-quark pair,

$$W[L,\beta] \simeq \langle \bar{q}(\vec{x})\, \mathcal{P} e^{-i\,g\int_{C_{\vec{x},\vec{y}}} A_\mu dz_\mu} q(\vec{y})\rangle\,, \tag{VI.43}$$

where the path-ordered phase ensures gauge invariance. Using -naively- the clustering decomposition property (or short declustering) for $|\vec{x}-\vec{y}| \to \infty$, we can decompose the expectation value in (VI.43) in the product of the expectation value of a quark state and and anti-quark state. Naturally the latter have to vanish as the creation of a single quark or anti-quark requires an infinite energy. However, be aware of the fact that the quark and anti-quark states do not belong to the Hilbert space of QCD and hence we cannot apply declustering that easily.

Still, the Polyakov loop expectation value is related to the heuristic situation described above. To see this more clearly let us consider a static quark. This situation can be achieved by taking the infinite quark mass limit, $m_q \to \infty$. The Dirac equation

$$(\not{D} + m_\psi)\,\psi = 0\,, \tag{VI.44}$$

then reduces to a space-independent equation as the quark cannot move, $\vec{\partial}_x \psi = 0$. Hence, the Dirac equation (VI.44) reads in the static limit

$$(\gamma_0 D_0 + m_\psi)\,\psi = 0\,. \tag{VI.45}$$

A solution to this equation is given by

$$\psi(x) = P(t,\vec{x})\psi_0(x)\,, \qquad \text{with} \qquad (\gamma_0\partial_0 + m_\psi)\,\psi_0 = 0\,. \tag{VI.46}$$

where ψ_0 solves the free Dirac equation, and $P(t,\vec{x})$ is the untraced Polyakov loop (VI.28). For proving (VI.46) we use that $(D_0 P(t,\vec{x})) = 0$ following from (VI.14). Hence, in a -vague- sense we can identify the Polyakov loop expectation value with the interaction part of a static quark.

2. Polyakov loop potential

As in the case of chiral symmetry breaking we would like to compute the effective potential of the order parameter, $V_{\rm Pol}[L]$. This turns out to be a formidable task both on the lattice and in the continuum. Note however, that the computation of the expectation value itself is simple on the lattice.

In the continuum we compute the effective potential of QCD, that is the effective action $\Gamma[\Phi]$ for constant fields. Before we embark on the explicit computation we first have to deal with the issue of gauge invariance in the gauge-fixed approach we are working in. To that end we upgrade our covariant gauge fixing to the *background gauge*: To that end we split our gauge field in a background $\bar{A}$ and a fluctuation a, to wit

$$A_\mu = \bar{A}_\mu + a_\mu\,. \tag{VI.47}$$

While the background $\bar{A}$ is kept fixed, a carries all the quantum fluctuations. In the path integral the integration over A then turns into one over a. So far nothing has been changed. Now we modify our gauge fixing,

$$\partial_\mu A_\mu = 0 \to \bar{D}_\mu a = 0\,, \qquad \text{with} \qquad \bar{D}_\mu = D_\mu(\bar{A})\,. \tag{VI.48}$$

For $\bar{A} = 0$ we regain the orginial covariant gauge fixing. For the background gauge fixing the gauge fixed classical action with ghost term reads

$$S_A[\bar{A}, a, c, \bar{c}] = S_{\rm A}[A] + \frac{1}{2\xi}\int_x (\bar{D}^{ab}_\mu a^b_\mu)^2 + \bar{c}^a \bar{D}^{ad}_\mu D^{db}_\mu c^b \,. \tag{VI.49}$$

In the presence of the background field and with the gauge fixing (VI.48) we have an additional -auxiliary- gauge symmetry: the gauge-fixed action is invariant under *background gauge transformations*

$$\bar{A}^U_\mu = \frac{i}{g} U\,(\bar{D}_\mu U^\dagger)\,, \qquad a^u = U\,a_\mu\,U^\dagger \quad \longrightarrow \quad A^U = \frac{i}{g} U\,(D_\mu U^\dagger)\,. \tag{VI.50}$$

Evidently this is true for the Yang-Mills action, it is left to show this for the gauge fixing and ghost term. The gauge fixing condition (VI.48) transforms as a tensor under (VI.50): $\bar{D}_\mu a \to U\,\bar{D}_\mu a\,U^\dagger$ and hence $\mathrm{tr}(\bar{D}_\mu a)^2$ is invariant under (VI.50). The Faddeev-Popov operator $\mathcal{M}$ in the background gauge is given by

$$\mathcal{M} = -\bar{D}_\mu D_\mu \to U\,\bar{D}_\mu D_\mu\,U^\dagger\,. \tag{VI.51}$$

It also transforms as a tensor and hence the ghost term is gauge invariant under (VI.50). However, the background gauge transformations are an auxiliary symmetry. The physical gauge transformations are those of the fluctuation field at fixed background $\bar{A}$, the *quantum gauge transformations*

$$\bar{A}^U_\mu = \bar{A}_\mu\,, \qquad a^u = U\,(D_\mu U^\dagger) \quad \longrightarrow \quad A^U = \frac{i}{g} U\,(D_\mu U^\dagger)\,. \tag{VI.52}$$

Again this can be understood by choosing the standard covariant gauge with a vanishing background. Then, (VI.52) is the only gauge transformation left, while (VI.50) leads to a non-vanishing background and hence changes the gauge fixing. The neat feature of the background field formalism is that it can be shown that both transformations are indeed related via *background independence* of the quantum equations of motion. Therefore background gauge invariance under the transformations (VI.50) carries physical gauge invariance, more details can be found in Appendix C

Still, the introduction of the background seems to complicate matters but it indeed facilitates computations and gives a more direct access to physics. Here we explore both properties. First we note that the introduction of $\bar{A}$ leads to an effective action that depends on two fields,

$$\Gamma[A] \to \Gamma[\bar{A}, a]\,. \tag{VI.53}$$

Switching of the mean value of the fluctuation field, $a = 0$ leads to a (background) gauge invariant action

$$\Gamma[A] = \Gamma[A, a = 0] \tag{VI.54}$$

As mentioned before, this is the physical gauge invariance. Moreover, one can show that the background correlation functions are directly related to S-matrix elements. In summary the effective action $\Gamma[A]$ defined in (VI.54) carries the information about the Polyakov loop potential.

Now we proceed with the explicit computation of the effective potential at one loop. For the Polyakov loop potential the only mean field of interest is the temporal component of the gauge field, and the other fields are put to zero. We will perform this computation first on the one-loop level with the classical ghost and gluon propagators. Finally we will introduce the fully non-perturbative propagators to this one-loop computation. This re-sums infinitely many diagrams and carries the essential non-perturbative computation. The explicit results are in semi-quantitative agreement with the full results obtained with functional renormalisation group methods and also show a good agreement with the lattice results.

In summary the Polyakov loop potential for constant temporal gauge fields is given by

$$V_{\rm Pol}(A_0) = \frac{1}{2}\mathrm{Tr}\,\ln G_A^{-1}(A_0) - \mathrm{Tr}\,G_c^{-1}(A_0) - \mathcal{N}\,, \tag{VI.55}$$

where the color traces in (VI.55) are in the adjoint representation and CN is the normalisation of the potential which we leave open for now. For the one-loop computation we have $G^{-1} = S^{(2)}_A$ with S_A in (VI.49) and hence

$$G_A^{-1}(A_0) = -D_\rho^2\,\delta^{\mu\nu} + \left(1 - \frac{1}{\xi}\right) D_\mu D_\nu\,, \qquad\qquad G_c^{-1}(A_0) = -D_\rho^2\,. \tag{VI.56}$$

In (VI.56) we have used that the spin one terms proportional to $F_{\mu\nu}$ drop out for a constant A_0-background. In the re-summed non-perturbative approximation we use numerical results, e.g. the Yang-Mills analog of Figure 9 at finite temperature. For constant fields we can assume the fields to lay in the Cartan subalgebra, as we can always rotate the field into the Cartan subalgebra with constant gauge transformations. We expand the Cartan-valued field A_0 in the fundamental representation in the the color eigenfunctions and eigenvalues of A_0. In the present context it always occurs in combination with temperature and coupling in Matsubara sums with $2\pi Tn + gA_0 = 2\pi T(n + \beta g/(2\pi)A_0)$, and we define the dimensionless algebra-valued field

$$\hat{\varphi} = \frac{\beta g}{2\pi} A_0 \,, \qquad\qquad L(\hat{\varphi}) = L[A_0] = \mathrm{tr}\, e^{-2\pi i\,\hat{\varphi}} \,. \tag{VI.57}$$

The eigenvalue equation of the field $\hat{\varphi}$ in the fundamental representation is given by

$$\hat{\varphi}^{\rm f}|\varphi_n^{\rm f}\rangle = \nu_n^{\rm f}|\varphi_n^{\rm f}\rangle \,, \qquad n \in 1, ..., N_c \,, \tag{VI.58}$$

where the superscript ^{f} indicates the fundamental representation. The eigenvalues for $SU(2)$ and $SU(3)$ are given by

$$SU(2):\, \nu_n^{\rm f} \in \left(\pm\frac{\varphi}{2}\right) \,, \qquad\qquad SU(3):\, \nu_n^{\rm f} \in \left(\pm\frac{\varphi_3 + \frac{1}{\sqrt{3}}\varphi_8}{2} \,, -\frac{1}{\sqrt{3}}\varphi_8\right) \,. \tag{VI.59}$$

Using (VI.58) and (VI.59) in the Polyakov loop in $SU(2)$ we arrive at

$$\hat{\varphi} = \varphi_3 \frac{\sigma^3}{2} \qquad \stackrel{\varphi=\varphi_3}{\longrightarrow} \qquad L(\varphi) = \cos\pi\varphi \,, \tag{VI.60}$$

For $SU(3)$ we have

$$\hat{\varphi} = \frac{2\pi}{\beta g}\left(\varphi_3\frac{\lambda^3}{2} + \varphi_8\frac{\lambda^8}{2}\right) \qquad \longrightarrow \qquad L(\varphi_3,\varphi_8) = \frac{1}{3}\left(e^{\frac{2\pi i\,\varphi_8}{\sqrt{3}}} + 2\cos(\pi\varphi_3)\, e^{-\frac{2\pi i\,\varphi_8}{\sqrt{3}}}\right) \,, \tag{VI.61}$$

with $\lambda^{3,8}$ given in (VI.38). As the Polyakov loop potential (for vanishing chemical potential) has minima at $\varphi_3 = 0$ we can work with the Polyakov loop variable at $\varphi_8 = 0$,

$$L(\varphi) = \frac{1}{3}\left(1 + 2\cos\pi\varphi\right) \,, \tag{VI.62}$$

with $L(\varphi) = L(\varphi_3 = \varphi, 0)$. Then, confinement is signaled by the (mean) gauge field configurations

$$\varphi = \frac{1}{2} \quad \text{for } SU(2) \,, \qquad \text{and} \qquad \varphi = \frac{2}{3} \quad \text{for } SU(3) \,. \tag{VI.63}$$

As a preparation for the full computation we go through the perturbative computation. This already reveals the main mechanism we need for the access of the confinement-deconfinement phase transition. This computation has been done independently in [22] and [23] in 1980 (published 81). The potential is often called the Weiss potential.

For the explicit computation we restrict ourselves to $SU(2)$. The result does not depend on the gauge fixing parameter ξ and we choose $\xi = 1$, Feynman gauge, in order to facilitate the computation. Then the Lorentz part of the trace in the gauge field loop can be performed immediately, leading to a factor four for the four polarisations of a vector field. We have

$$V_{\rm Pol}(A_0) \simeq 4 * \frac{1}{2}\mathrm{Tr}\,\ln(-D_\rho^2) - 2 * \frac{1}{2}\mathrm{Tr}\,\ln(-D_\rho^2) = 2\frac{1}{2}\mathrm{Tr}\,\ln(-D_\rho^2) \,, \tag{VI.64}$$

where we have made explicit the multiplicities of gluon and ghost, and we dropped the normalisation. The gluon dominates and the final result is twice that of one polarisation, which accounts for the two physical polarisations of the gluon. This is an expected property as we compute a gauge invariant potential that should reflect the fact that we only have two physical polarisations, and the gauge fixing is only a means to finally compute gauge invariant quantities. Now we use that we can diagonalise the operator D_ρ^2 in the adjoint representation in the algebra. The color eigenfunctions and eigenvalues in the adjoint representation are given by

$$\frac{g\beta}{2\pi}A_0^{\rm ad}|\varphi_n^{\rm ad}\rangle = \nu_n^{\rm ad}|\varphi_n^{\rm ad}\rangle \,, \qquad n \in 1, ..., N_c^2 - 1 \,, \tag{VI.65}$$

and

$$SU(2):\ \nu_n^{\rm ad} \in (0\,,\,\pm\varphi)\,, \qquad SU(3):\ \nu_n^{\rm ad} \in \left(0\,,\,0\,,\,\pm\varphi_3\,,\,\pm\frac{\varphi_3 \pm \sqrt{3}\varphi_8}{2}\right)\,. \tag{VI.66}$$

Note that the eigenvalues of $T^3_{\rm ad}$ are ± 1, while they are $\pm 1/2$ in the fundamental representation. The relative factor $1/2$ reflects the sensitivity to center transformations in the fundamental representation and the insensitivity in the adjoint representation. Performing the trace in (VI.64) in terms of the eigenfunctions $|\varphi_n\rangle$ and momentum modes, we arrive at

$$V_{\rm Pol}(A_0) \simeq 2\Big[V_{\rm mode}(\varphi) + V_{\rm mode}(-\varphi)\Big]\,, \tag{VI.67}$$

with $V_{\rm Pol}$ being $1/2{\rm Tr}\ln(-D^2)$, where the gauge field is substitute by one eigenmode,

$$\begin{aligned} V_{\rm mode}(\varphi) &= \frac{T}{2}\sum_{n\in\mathbb{Z}}\int\frac{d^3p}{(2\pi)^3}\left\{\ln\frac{(2\pi T)^2(n+\varphi)^2+\vec{p}^2}{(2\pi T)^2n^2+\vec{p}^2}\right\} \\ &= \frac{T}{4\pi^2}\sum_{n\in\mathbb{Z}}\int_0^\infty dp\,p^2\left\{\ln\frac{(2\pi T)^2(n+\varphi)^2+p^2}{(2\pi T)^2n^2+p^2}\right\}\,, \end{aligned} \tag{VI.68}$$

where the denominator in the logarithm in (VI.68) is a normalisation of the mode potential at vanishing φ: $V_{\rm mode}(0) = 0$. The sum in (VI.68) can be performed analytically by taking first a derivative w.r.t. p^2 and then using contour integrals. It results in

$$V_{\rm mode}(\varphi) = \frac{T}{4\pi^2}\int_0^\infty dp\,p^2\left\{\left[\sum_\pm \ln\sinh\frac{\beta p \pm 2\pi i\,\varphi}{2}\right] - 2\ln\sinh\frac{\beta p}{2}\right\}\,. \tag{VI.69}$$

Now we use that

$$\begin{aligned} \sum_\pm \ln\sinh\frac{\beta p \pm 2\pi i\,\varphi}{2} - 2\ln\sinh\frac{\beta p}{2} &= \sum_\pm \ln(1-e^{-\beta p\pm 2\pi i\,\varphi}) - 2\ln(1-e^{-\beta p}) \\ &= \sum_\pm\sum_{n=1}^\infty \frac{1}{n}\,e^{-\beta p n}\left(e^{\pm 2\pi i\,n\varphi}-1\right)\,. \end{aligned} \tag{VI.70}$$

In (VI.70) we have pulled out a factor $\ln\exp(\beta p \pm 2\pi i\varphi)/2 = (\beta p \pm 2\pi i\varphi)/2$ from the $\ln\sinh$-terms with φ, and $2\ln\exp\beta p/2 = \beta p$ from the $\ln\sinh$-term in the normalisation. These terms cancel each other and we are led to the right hand sid e of (VI.70). Then we have expanded the logarithms in a Taylor expansion in the exponentials. In summary this leads us to

$$\begin{aligned} V_{\rm mode}(\varphi) &= \frac{T}{4\pi^2}\int_0^\infty dp\,p^2\sum_\pm\sum_{n=1}^\infty \frac{1}{n}\,e^{-\beta p n}\left(e^{\pm 2\pi i\,n\varphi}-1\right) \\ &= \frac{T^4}{\pi^2}\sum_{n=1}^\infty\frac{1}{n^4}\left(\cos 2\pi n\varphi - 1\right)\,. \end{aligned} \tag{VI.71}$$

The sum in (VI.71) is gain easily performed with methods of complex analysis and we arrive at

$$\beta^4\,V_{\rm mode}(\varphi) = \frac{\pi^2}{48}\left[4\left(\tilde{\varphi}-\frac{1}{2}\right)^2-1\right]^2\,, \qquad \tilde{\varphi} = \varphi \bmod 1\,, \tag{VI.72}$$

where we have devided out the trivial dimensional thermal factor T^4. Inserting (VI.72) in (VI.67) for the Polyakov

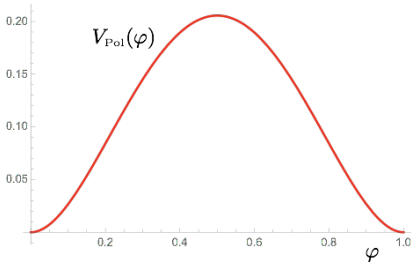

FIG. 15: One loop Polyakov loop potential for $SU(2)$.

loop potential we are led to

$$\beta^4\, V_{\rm pol}(A_0) = \frac{\pi^2}{12}\left[4\left(\tilde{\varphi}-\frac{1}{2}\right)^2-1\right]^2\,, \tag{VI.73}$$

for $SU(2)$, while for $SU(3)$ the potential is given by

$$V_{\rm pol}(A_0) = \sum_{n=1}^{8} V_{\rm mode}(\nu_n)\,, \tag{VI.74}$$

with the eigenvalues ν_n in (VI.66). We have plotted the $SU(2)$ potential in Figure 15 as it has a very simple form which carries already the relevant information. The potential has minima at $\varphi = 0, 1$ and a maximum at $\varphi = 1/2$. For the minima the Polyakov loop variable $L[A_0]$ takes the value ± 1, the maximum is the center-symmetric value $L[A_0] = 0$. This structure is also present for all $SU(N)$-theories and originates in the -necessary- center symmetry of the potential. The center transformation in $SU(2)$ is given by

$$\varphi \to 1-\varphi\,, \tag{VI.75}$$

which maps $L[\varphi = 0] = 1 \to L[\varphi = 1] = -1$ and vice versa, this comes via the multiplication of the Polyakov line $P(\vec{x})$ with the center element $-\mathbb{1}$. We conclude that in perturbation theory the potential has its minimum at the maximally center-breaking values, the theory is in the center-broken phase. At large temperatures perturbation theory is valid and quantum fluctuations are small: the fluctuating gauge field is close to $A_0 = 0$. This leads to

$$\lim_{T\to\infty} L[\langle A_0\rangle] = 1\,. \tag{VI.76}$$

In turn, for small temperatures the potential should exhibit a minimum at $\varphi = 1/2$. Interestingly, this is achieved within the one loop computation if the gluon contributions are switched off, and the ghost contribution is left.

Finally we come back to the normalisation of $V_{\rm pol}(A_0)$ in (VI.55). We have normalised it such that $V_{\rm pol}(A_0) = 0$. However, if we choose the normalisation as

$$\mathcal{N} = \left[\frac{1}{2}{\rm Tr}\,\ln G_A^{-1}(0) - {\rm Tr}\, G_c^{-1}(0)\right]_{T=0}\,, \tag{VI.77}$$

the value of the effective potential simply is the thermal pressure of the theory. The difference between (VI.77) and that chosen in (VI.68) for the mode potential is given by

$$\Delta\mathcal{N} = 2(N_c^2-1)\left[\frac{T}{2}\sum_{n\in\mathbb{Z}}\int\frac{d^3p}{(2\pi)^3}\ln\left[(2\pi T)^2n^2+\vec{p}^2\right] - \int\frac{d^4p}{(2\pi)^4}\ln p^2\right] = -p_{A,\rm SB} \quad \text{with} \quad p_{A,\rm SB} = \frac{\pi^4T^4}{45}(N_c^2-1)\,. \tag{VI.78}$$

Eq.(VI.78) is nothing but (minus) the Stefan-Boltzmann pressure of a $SU(N_c)$ gauge theory, see (V.19) for the scalar case. It is the scalar pressure times the number of physical modes: two physical transversal polarisations times the

number of color modes, (N_c^2-1), leading to $2(N_c^2-1)p_{\phi,\mathrm{SB}}$. This leads us to our final result

$$\beta^4 V_{\mathrm{pol}}(A_0) = \frac{\pi^2}{12}\left[4\left(\tilde{\varphi}-\frac{1}{2}\right)^2-1\right]^2 - \frac{\pi^4}{45}(N_c^2-1)\,. \tag{VI.79}$$

We proceed with a non-perturbative computation of the Polyakov loop potential which still keeps the analogy to the one loop computation above. Even though this is an approximation, both the numerical result as well as the conceptual structure are also present in the full computation. We again start with (VI.55). Now, instead of using the classical inverse propagators we utilise the fully non-perturbative ones. These propagators can only be computed with numerical non-perturbative approaches, either gauge fixed lattice simulations or with functional methods such as the functional renormalisation group (FRG) already used in the low energy EFT for chiral symmetry breaking or Dyson-Schwinger equations (DSEs). Instead of using the available numerical data we add another approximation in order to keep our approach semi-analytic.

From Fig. 9 we know that the gluon propagator exhibits a mass gap for low momenta. In turn, for large momenta is runs logarithmically. This behaviour is also present at finite temperature, see Fig. 17. There we plot the momentum dependence of the dressing of the chromo-magnetic gluon propagator for different temperatures. Both, results from functional methods and from gauge-fixed lattice simulations are shown. The dressing is defined as

$$\frac{1}{Z_A^{\mathrm{M}}(\vec{p}^2)} = \frac{1}{2}\,\vec{p}^2\,\langle A_i(0,\vec{p})A_i(0,-\vec{p})\rangle\,, \tag{VI.80}$$

it is the dressing of the gluon propagator perpendicular ro the heat bath. In Fig. 16 we plot the temperature-dependent mass (screening mass) of chromo-electric gluon propagator, the gluon propagator parallel to the heat bath,

$$\frac{1}{Z_A^{\mathrm{E}}(\vec{p}^2)} = \vec{p}^2\,\langle A_0(0,\vec{p})A_0(0,-\vec{p})\rangle\,. \tag{VI.81}$$

Note that the simple relations (VI.80), (VI.81) are only valid for $p_0 = 0$. For $p_0 \neq 0$ one has to use the thermal projection operators, see e.g. [24]. At large temperatures we expect them to tend towards their perturbative values. This is indeed happening, however, we need higher order thermal perturbation theory. The one-loop Debye mass is given by

$$m_D^0 = \sqrt{\frac{N}{3}}\,g_T T + \mathcal{O}(g_T^2 T)\,, \tag{VI.82}$$

and is also displayed in Fig. 16. For the comparison, the temperature-dependent coupling is fully non-perturbative and has been also taken from [24] for internal consistency, for more details see there. In [25] higher order effects have been taken into account, leading to

$$m_D = m_D^0 + \left(c_D + \frac{N}{4\pi}\ln\left(\frac{m_D^0}{g_T^2 T}\right)\right) g_T^2 T + \mathcal{O}(g_T^3 T)\,. \tag{VI.83}$$

Eq.(VI.83) already leads to a very good agreement with the full result above 600 MeV. At low temperatures, the mass settles at its $T = 0$ value, indicated by the $1/T$ behaviour of m_d/T in Fig. 16b, and the perturbative prescriptions fail even with the full non-perturbative coupling. The Debye mass itself for low temperatures is depicted in Fig. 16a, from which it is evident that a temperature-independent (or decaying) additional part $\Delta m_D(T=0) \approx 380$ MeV to m_D^0 would lead to agreement up to $\approx 150\,\mathrm{MeV}$.

In conclusion a good semi-quantitative approximation to the thermal propagator (in particular the chromo-magnetic on) is the perturbative propagator with a temperature-dependent mass term. It goes beyond the scope of the present lecture notes to present a full computation, here we simply investigate the qualitative effect of such a mass gap, first done in [29], for a full, comprehensive analysis see [30]. We revisit (VI.71) for simple massive propagators

$$G_A \propto \frac{1}{(2\pi T)^2(n+\varphi)^2 + \vec{p}^2 + m_T^2}\,, \tag{VI.84}$$

even dropping the perturbative running. While the latter is important for the correct scaling (fixing Λ_{QCD} and hence

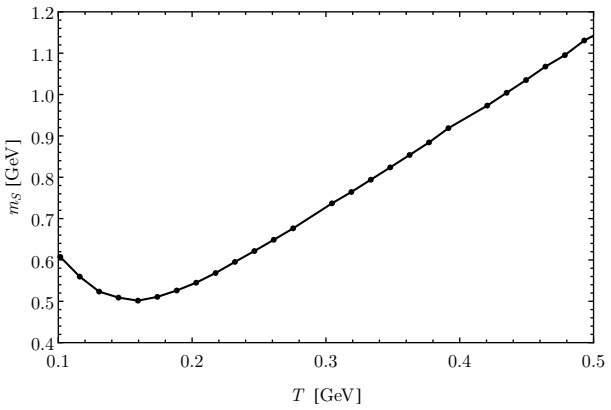

(a) Screening mass m_s in units of GeV at low temperatures. In the limit $T \to 0$ the screening mass smoothly tends towards its finite $T = 0$ value, see back curve in Fig. 17.

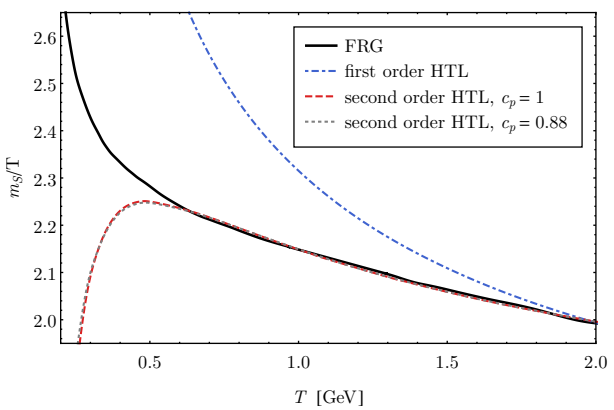

(b) Dimensionless Debye screening m_s/T mass at high temperatures in comparison with leading order perturbation theory (VI.82) and the Arnold-Yaffe prescription (VI.83) for accommodating beyond leading order effects [25].

FIG. 16: Debye screening mass m_s, plot taken from [24], for more details see there.

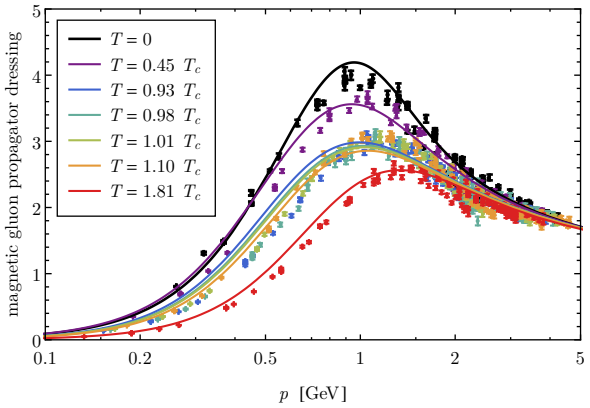

(a) Magnetic gluon dressing in $SU(2)$ from [24] in comparison with $SU(2)$ lattice results from [26, 27].

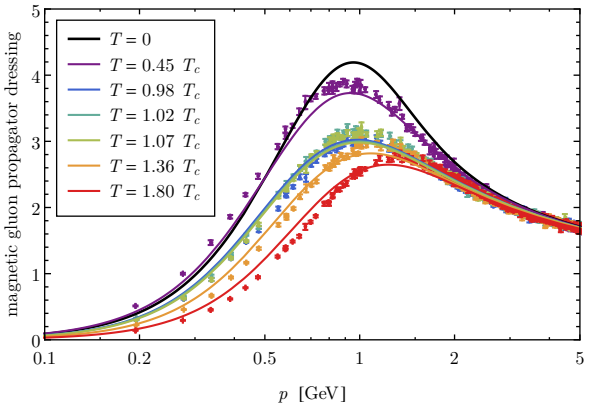

(b) Magnetic gluon dressing in $SU(2)$ from [24] in comparison with $SU(3)$ lattice results from [28].

FIG. 17: Magnetic gluon propagator dressing (VI.80).

for the correct T_c it is not important for the confining property. With the propagator (VI.84) we are led to

$$V_{\text{mode}}(\varphi, m) = \frac{T}{4\pi^2} \sum_{\pm} \sum_{n=1}^{\infty} \frac{1}{n} \left(e^{\pm 2\pi i\, n\varphi} - 1\right) \int_0^\infty dp\, p^2\, e^{-\left(\beta\sqrt{p^2+m^2}\right))n}$$

$$= \frac{T^4}{4\pi^2} \sum_{\pm} \sum_{n=1}^{\infty} \frac{1}{n} \left(e^{\pm 2\pi i\, n\varphi} - 1\right) \int_0^\infty d\bar{p}\, \bar{p}^2\, e^{-\left(\sqrt{\bar{p}^2+\beta^2 m^2}\right)n}\,. \tag{VI.85}$$

The momentum integration in (VI.86) cannot be performed analytically. However, in the zero temperature limit the terms in the sum decays with $e^{(-\beta m)n}$ up to polynomials. This is seen easily for the absolute value of the mode

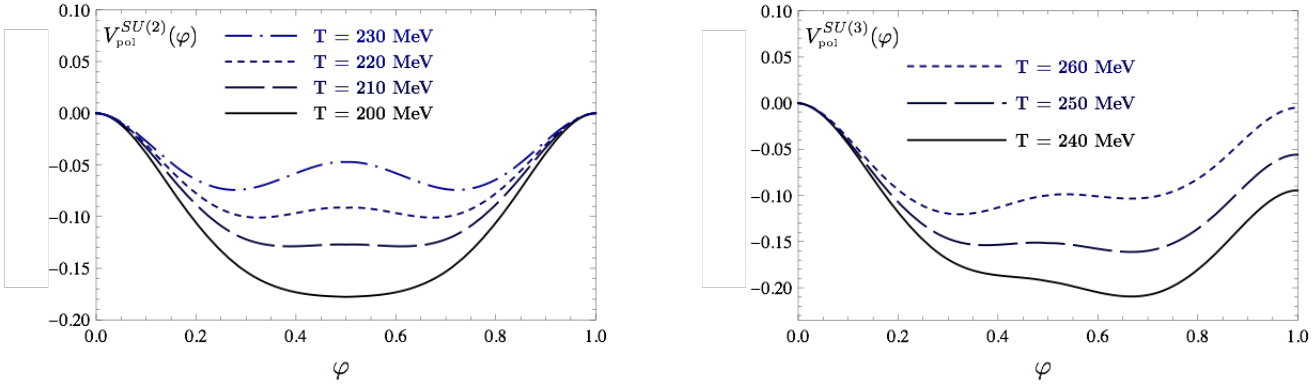

(a) $SU(2)$ Polyakov loop potential.

(b) $SU(3)$ Polyakov loop potential

FIG. 18: $SU(2)$ and $SU(3)$ Polyakov loop potential taken from [30] for different temperatures across the phase transition. The potentials exhibits the second and first order of the $SU(2)$ and $SU(3)$ transitions respectively.

potential,

$$
\begin{aligned}
|V_{\rm mode}(\varphi,m)| &\leq \frac{T^4}{4\pi^2}\sum_{n=1}^{\infty}\frac{1}{n}\int_0^\infty d\bar{p}\,\bar{p}^2\,e^{-\left(\sqrt{\bar{p}^2+\beta^2m^2}\right)n} \\
&\leq \frac{T^4}{4\pi^2}\sum_{n=1}^{\infty}\frac{1}{n}\left[\int_0^{\beta m} d\bar{p}\,\bar{p}^2\;e^{-(\beta m)n}+\int_0^{\beta m} d\bar{p}\,\bar{p}^2\,e^{-\bar{p}n}\right] \\
&\stackrel{\beta m\to\infty}{\longrightarrow} T^4\,{\rm Pol}(\beta m)\,e^{-\beta m}\,,
\end{aligned}
\tag{VI.86}
$$

with a polynomial ${\rm Pol}(\beta m)$. In summary the mode potential decays exponentially for gapped propagators. This entails that for sufficiently small temperatures the contributions of the chromo-electro and the two chromo-magnetic modes decay exponentially. The longitudinal gauge mode stays trivial and gives the contribution $2V_{\rm mode}(\varphi)$. Now we use that the ghost propagator keeps it $1/(-D^2)$ behaviour it already has perturbatively. In a covariant gauge this is already suggested from the ghost-gluon vertex which is linear in the anti-ghost momentum. Hence, all loop corrections to the inverse ghost propagator are proportional to p^2 from the onset. If no additional singularity is created from the propagators in the loops it stays this way. Since the gluon propagator is gapped this is only possible with a global non-trivial scaling.

Let us now study the case of a trivial ghost propagator and a gapped gluon propagator. In this case we conclude that

$$
\begin{aligned}
\lim_{T=0} V_{\rm Pol}(A_0) &\simeq \frac{1}{2}\lim_{T\to 0}{\rm Tr}\,\ln G_A^{-1}(A_0)-\lim_{T\to 0}{\rm Tr}\,G_c^{-1}(A_0) \\
&\simeq \frac{1}{2}{\rm Tr}\,\ln(-D_\rho^2)(A_0)-{\rm Tr}\,\ln(-D_\rho^2)(A_0) \qquad \text{(VI.87)} \\
&= -{\rm Tr}\,\ln(-D_\rho^2)(A_0)=\sum_i V_{\rm mode}(\varphi_i)\,. \qquad \text{(VI.88)}
\end{aligned}
$$

With the mode potential (VI.68), see Fig. 15 this gives confinement. The present qualitative study can be extended to a fully non-perturbative one with the help of functional methods, leading to the $SU(2)$ and $SU(3)$ potentials depicted in Fig. 18 taken from [30]. The respective Polyakov loop expectation values $L[\langle A_0\rangle]$ are shown in Fig. 19.

The above considerations also hold in full Yang-Mills theory without approximations. This allows us to formulate a confinement criterion in Yang-Mills theory with (VI.55), (VI.73) and (VI.86):

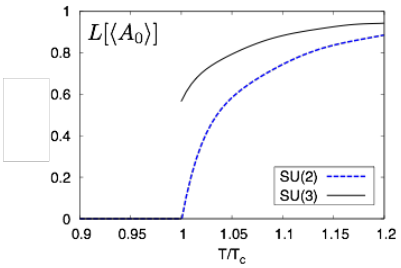

FIG. 19: Polyakov loop expectation values $L[\langle A_0\rangle]$ for $SU(2)$ and $SU(3)$ taken from [29].

Confinement criterion: *'In covariant gauges the gluon propagator has to be gapped relative to the ghost at low temperatures'*

put forward in [29]. Note that we have been led to this criterion in the one-loop resummed approximation with (VI.55). However, it can be proven in Yang-Mills theory without approximations on the basis of the functional renormalisation group, [29, 30], as well as Dyson-Schwinger equations and the two-particle irreducible (2PI) formalism [30]. It also extend beyond the covariant gauges, e.g. to the Coulomb gauge. In QCD with dynamical QCD -as expected- the quark contributions spoil the applicability of the confinement criterion as they introduce center-breaking terms to the potential, for a detailed discussion see [30].

We close this chapter with some remarks on the order parameter we introduced. We started with the Polyakov loop variable $\langle L[A_0]\rangle$, but computed the Polyakov loop potential $V_{\rm pol}[A_0]$ with the order parameter $\langle A_0\rangle$ or $L[\langle A_0\rangle]$. As both are order parameters for the same symmetry, this is not relevant for us. Still, one can investigate their relation: evidently they are not the same but only agree in a Gaußian approximation,

$$\langle L[A_0]\rangle \neq L[\langle A_0\rangle]\,, \tag{VI.89}$$

Dropping for the moment the necessary renormalisation of $\langle A_0\rangle$, they satisfy the Jensen inequality,

$$\langle L[A_0]\rangle \leq L[\langle A_0\rangle]\,, \tag{VI.90}$$

see [29]. We conclude that if $L[\langle A_0\rangle] = 0$, so is $\langle L[A_0]\rangle$. In turn, one can show that $L[\langle A_0\rangle]$ vanishes if $\langle L[A_0]\rangle$ does, see [32]. While $L[\langle A_0\rangle]$ has so far only been computed with functional methods, we have a solid results for $\langle L[A_0]\rangle$ from the lattice, both in Yang-Mills theory and in QCD. More recently, $\langle L[A_0]\rangle$ has been also computed with the FRG on the basis of $L[\langle A_0\rangle]$ in quantitative agreement with the lattice results [31], see Fig. 21. Seemingly, their relation is rather non-trivial but is has been shown in [31] that most of the difference between $\langle L[A_0]\rangle$ and $L[\langle A_0\rangle$ comes from

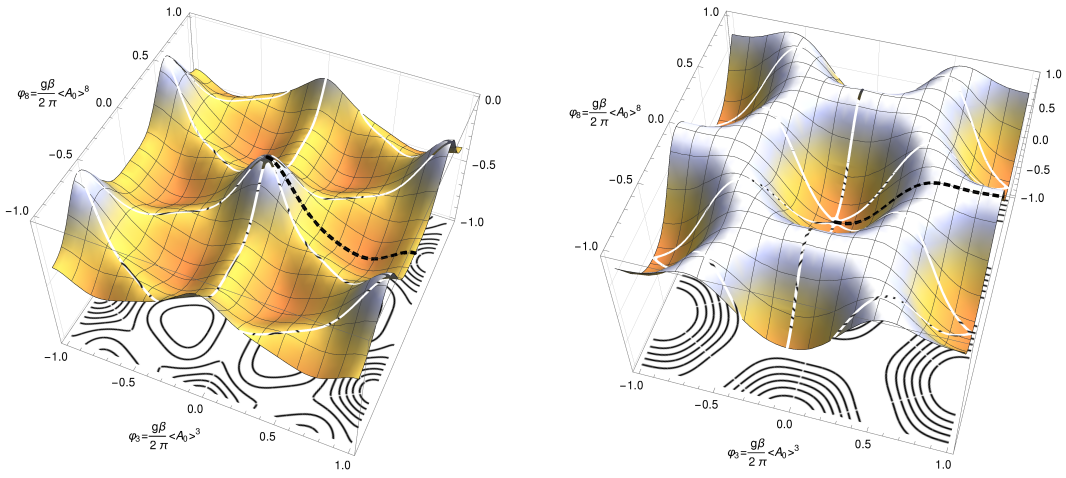

FIG. 20: The infrared glue potential, $V(\varphi_3, \varphi_8)$, is shown in the confined phase (left, $T = 236$ MeV) and in the deconfined phase (right, $T = 384$ MeV). We restrict ourselves to the line $\varphi_8 = 0$ and $\varphi_3 \geq 0$ (indicated by the black, dashed line), where one of the equivalent minima is always found, and where $L[\langle A0\rangle]$ is real and positive semi-definite.

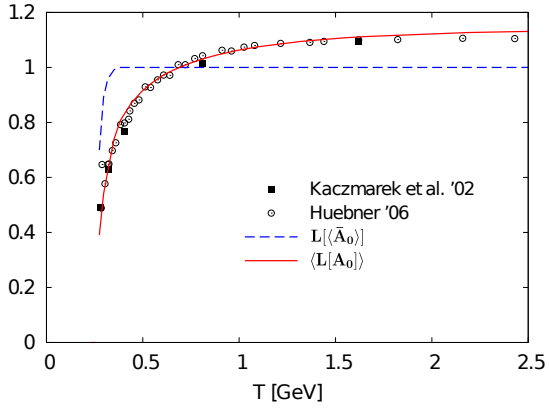

FIG. 21: Expectation value of $\langle L[A_0]\rangle$ versus $L[\langle\bar{A}_0\rangle]$ from [31]. Both observables are order parameters for the confinement-deconfinement phase transition. Moreover, $L[\langle\bar{A}_0\rangle] = 1$ entails $\langle\bar{A}_0\rangle = 0$.

a temperature dependent normalisation of the former. In any case there is a relation

$$\langle L[A_0]\rangle(\varphi) \tag{VI.91}$$

that maps $\varphi = \beta g/(2\pi)\langle A_0\rangle$ to the Polyakov loop epectation value in a given background.

VII. PHASE STRUCTURE OF QCD

In this final chapter of the low energy part of the QCD lecture notes we discuss the phase structure of QCD at finite temperature and density. Here we shall study this in a combination of the low energy model for chiral symmetry breaking discussed in the chapters IV and V and the confinement physics of the Polyakov loop potential discussed in the previous chapter VI. This class of low energy EFTs is called *Polyakov loop augmented/enhanced low energy EFTs*. They are based on the following observation that can be made already on a one-loop level (with resummed propagators). The full one loop resummed effective action of $N_f = 2$ flavour QCD including effective mesonic degrees of freedom is given by

$$\Gamma_{\rm QCD}[\Phi] = S_{\rm QCD}[\Phi] + \frac{1}{2}{\rm Tr}\,\ln\, G_A^{-1}[\Phi] - {\rm Tr}\,\ln\, G_c^{-1}[\Phi] - {\rm Tr}\,\ln\, G_q^{-1}[\Phi] + \frac{1}{2}{\rm Tr}\,\ln\, G_\phi^{-1}[\Phi]\,, \qquad \Phi = (A_\mu, c, \bar c, \psi, \bar\psi, \sigma, \vec\pi)\,, \tag{VII.1}$$

with the gluon and ghost propagators G_A, G_c carrying the physics and fluctuations of the glue sector of QCD, and the quark and meson propagators carrying the physics and fluctuations of the matter sector of QCD. Note that (VII.1) with the full propagators is a complicated non-perturbative equation where all different loops feed into each other. For example, taking the derivative of (VII.1) w.r.t. the gauge field, we get

$$\frac{\delta\Gamma - S}{\delta A_0} = \frac{1}{2}{\rm Tr}\,\Big[\Gamma^{(3)}\,G\Big]_{AA} - {\rm Tr}\,G_c^{-1}[\Phi]\,\Big[\Gamma^{(3)}\,G\Big]_{c\bar c} - {\rm Tr}\,\Big[\Gamma^{(3)}\,G\Big]_{q\bar q} + \frac{1}{2}{\rm Tr}\,\Big[\Gamma^{(3)}\,G\Big]_{\phi^*\phi}\,, \tag{VII.2}$$

where the mesonic part has been dropped and G is the full matrix propagator of all modes. This has to be compared with the A_0-DSE

$$\frac{\delta\Gamma}{\delta A_0} = \left\langle \frac{\delta S}{\delta A_0} \right\rangle\,, \tag{VII.3}$$

the QCD-version of (IV.15). It is derived analoguously from the path integral representation of the QCD effective action Γ, see (C.1), by taking an A_0-derivative. It is depicted in Fig. 22. The vertices in the DSE (VII.3) are the classical ones while in (VII.2) they are the full quantum vertices. The other difference is the two-loop term in Fig. 22 that is not present in (VII.2) but can be understood as part of the dressed vertices, see e.g. [30]. In any case, the two-loop term in the DSE is typically dropped in explicit computations for technical reasons, and modern applications often use 2PI and 3PI (three-particle irreducible) approximations that feature dressed vertices.

Note also that the Wegner-Houghton RG, or more generally functional renormalisation group equations for QCD, are one loop excact, see chapter IV F 3. Hence, they are given by a sum of gluon, ghost, quark and optionally meson diagrams, see Fig. 23. Note that the equation in Fig. 23 is exact, no two-loop or higher loop terms are missing.

1. *Glue Sector*

We conclude that (VII.1) provides a good qualitative approximation to full QCD, and the following formal arguments also go through beyond the current approximation: we are interested in the low energy limit of QCD, in which the gapped gluons do not drive the matter dynamics anymore. Since the ghost terms only couple to matter through the gluons, they also decouple even though they are massless. Hence, in a first qualitative approximation we can drop the dynamics of the glue sector. Still, the gluons, i.e. $\langle A_0\rangle$ serve as a background for the matter fluctuations. Its value is determined by the Polyakov loop potential in QCD, obtained by evaluating (VII.1) for constant A_0-background. The

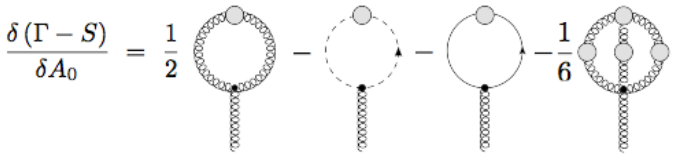

FIG. 22: Functional A_0-Dyson-Schwinger equation for QCD.

glue part of the potential,

$$V_{\rm glue}(A_0) = \frac{1}{2}{\rm Tr}\,\ln\, G_A^{-1}[A_0] - {\rm Tr}\,\ln\, G_c^{-1}[A_0]\,, \tag{VII.4}$$

The definition of $V_{\rm glue}$ is identical to that in pure Yang-Mills theory, (VI.55). In (VII.4), however, the QCD gluon and ghost propagator enter. A common procedure is now to use lattice results on the pressure and the Polyakov loop expectation value in pure Yang-Mills theory for an estimate of $V_{\rm glue}$. From the perspective of the correlation functions approaches discussed here this is justified if the Yang-Mills gluon and ghost propagators in an A_0-background are similar to those in QCD. This is indeed the case, the biggest difference coming from the RG-scaling that is reflected in the momentum-dependence at large and medium momenta $p^2 \gtrsim 2-5\,{\rm GeV}^2$. This can be made even more quantitative if simply comparing the two glue potentials (in terms of A_0) in QCD and Yang-Mills theory, see [33]. Apart from the different absolute temperature scale and the different RG-running the two potentials agree semi-quantitatively.

These results support in retrospect the low energy EFT approach with lattice-induced Polyakov loop potentials $V(L,\bar L)$. On the lattice the Polyakov loop variables

$$L = \langle L[A_0]\rangle\,, \qquad\qquad \bar L = \langle L^*[A_0]\rangle\,, \tag{VII.5}$$

are computed. At vanishing density we have $\bar L = L^*$. At non-vanishing density this relation is not valid anymore as the chemical potential leads to a complex action in the path integral, and hence $\langle L[A_0]\rangle^* \neq \langle L[A_0]^*\rangle$. The respective potential is $U_{\rm pol}(L,\bar L)$. We emphasise that the potential $V_{\rm pol}(\varphi)$ is not simply $U(L(\varphi),\bar L(\varphi))$ due to (VI.89).

These potentials are derived as follows:

(1a) Computee the Yang-Mills pressure (zero-point function) and the Polyakov loop expectation value (one-point function)

$$p_{\rm A}(T) = , \qquad L = \langle L[A_0]\rangle(T), \qquad \bar L = \langle L[A_0]\rangle(T)\,. \tag{VII.6}$$

(1b) Further correlation functions of the Polyakov loop variable are computed. At present this approach only extends to the two-point functions of the Polyakov loop, [34]. The two-point function of the Polyakov loop is nothing but its propagator at large distances, which is given by the inverse of the second derivative of the Polyakov loop potential. We write schematically

$$\begin{pmatrix} \langle LL\rangle & \langle L\bar L\rangle \\ \langle \bar L L\rangle & \langle \bar L\bar L\rangle \end{pmatrix} \propto \begin{pmatrix} \partial_L^2 U_{\rm pol} & \partial_L\partial_{\bar L} U_{\rm pol} \\ \partial_{\bar L}\partial_L U_{\rm pol} & \partial_{\bar L}^2 U_{\rm pol} \end{pmatrix}^{-1}\,. \tag{VII.7}$$

(2) Construct a potential $V_{\rm YM}(L,\bar L)$ that leads to all the observables under (1a) and potentially (1b). We have

$$p_{\rm A} = -V(L_{\rm EoM},\bar L_{\rm EoM})\,, \qquad \frac{\partial U(L,\bar L)}{\partial L}\bigg|_{\substack{L=L_{\rm EoM}\\ \bar L=\bar L_{\rm EoM}}} = 0\,, \qquad \frac{\partial U(L,\bar L)}{\partial \bar L}\bigg|_{\substack{L=L_{\rm EoM}\\ \bar L=\bar L_{\rm EoM}}} = 0\,, \tag{VII.8}$$

and (VII.7), evaluated on the equations of motion.

Here we quote the standard form of the Polyakov loop potential. It reads

$$U(L,\bar L) = \frac{1}{2}a(T)\bar L\, L + b(T)\ln\, M_H(L,\bar L) + \frac{1}{2}c(T)\,(L^3+\bar L^3) + d(T)(\bar L\, L)^2\,, \tag{VII.9}$$

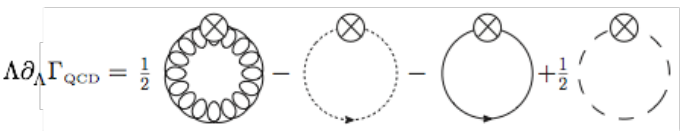

FIG. 23: Functional renormalisation group equation for QCD. In the Wegner-Houghton case the cross stands for the restriction of the loop integration to $p^2 = \Lambda^2$.

where M_H comes from the Haar measure of the gauge group

$$M_H = 1 - 6\,\bar{L}\,L + 4(L^3 + \bar{L}^3) - 3(\bar{L}\,L)^2\,. \tag{VII.10}$$

Eq.(VII.9) is a variation of a Landau-Ginsburg-type phi^4-potential commonly used for describing phase transitions. The cubic terms proportional to $c(T)$ and in M_H carry the center symmetry $L \to zL$ where the cubic roots $z \in Z_3$ has the property $z^3 = 1$. Thse terms drives the phase transition. The parameters $a(T), b(T), c(T)$ are now adjusted to the temperature-dependent observables in (1). Examples can be found e.g. in [34–36]. The latter work also contains a detailed study of various model potentials. We close this discussion we a few remarks. Firstly, as it is not possible to compute the glue potential in QCD on the lattice, we have to rely on Yang-Mills potentials on the lattice extrapolated to the glue potential. Secondly, the direct computation of the Polyakov loop potential in Yang-Mills theory proves to be very costly and has not fully been resolved yet. For that reason one has to rely on potentials that only match a few but important observables. Thirdly, the Polyakov loop potential $U_{\rm pol}$ is not the natural input in the low energy EFTs, it is $V_{\rm pol}$ and the two only agree in the Gaußian approximations.

Alternatively one computes the glue potential directly in the continuum, but at present neither $U_{\rm pol}$ nor $V_{\rm pol}$ has been computed to a quantitative satisfactory precision. This task is left for future work.

2. Matter sector

It is left to discuss the matter sector. In (VII.1) it looks identical to the low energy EFT or the DSE/FRG in QCD we have discussed in the context of strong chiral symmetry breaking. However, now we have to consider also the glue background A_0 or $L, \bar{L}$ depending on the tratment of the glue sector. Since the mesons are color-neutral, they do not couple to the gluon and hence the meson loop stays the same as before.

However, the quark loop has to be taken in an A_0 background. We recall the one-loop expression in (V.28), now in the presence of an A_0 background as well as a chemical potential μ. It reads

$$\begin{aligned}\Omega_{q,T} - \Omega_{q,T,\mu=0} &= -\,4\,T \sum_{n\in\mathbb{Z}} \int \frac{d^3p}{(2\pi)^3}\,\mathrm{tr_f}\,\ln \frac{(2\pi T)^2\left(n+\frac{1}{2}+\hat{\varphi}+i\,\mu\right)^2 + \vec{p}^2 + m_q^2}{(2\pi T)^2\left(n+\frac{1}{2}\right)^2 + \vec{p}^2 + m_q^2} - p_{q,\rm thermal} \\ &= -\,\frac{2}{\pi^2}\,T \sum_{n\in\mathbb{Z}} \int_0^\infty dp\,p^2\,\mathrm{tr_f}\left\{\ln\left(1 + Pe^{-\beta(\epsilon_p^q-\mu)}\right) + \ln\left(1 + P^\dagger e^{-\beta(\epsilon_p^q+\mu)}\right)\right\},\end{aligned} \tag{VII.11}$$

where $P(\vec{x}) = P(\beta,\vec{x})$ is the untraced Polyakov loop, see (VI.28), and we recall the quark dispersion and the thermal distribution function from (V.27)

$$\epsilon_p^q = \sqrt{\vec{p}^2 + m_q^2}\,, \qquad\qquad n_F(\omega) = \frac{1}{e^{\beta\omega}+1}\,. \tag{VII.12}$$

In the present approximation $P, P^\dagger$ are $\vec{x}$-independent. The combinations $Pe^{\beta\mu}$ and $Pe^{-\beta\mu}$ reflect the relation of L and $\bar{L}$ to the creation operator of quark and anti-quark states respectively. The final expression in (VII.11) reduces to the quark contribution of the grand potential (V.38) discussed in chapter V for $P = \mathbb{1}$. Due to the subtraction of the $T = 0$ grand potential hidden in $p_{q,\rm thermal}$ is nothing but the negative thermal pressure in a given background. On the EoM for all fields it is the physical quark pressure of the system. The color trace in (VII.11) can be rewritten as a determinant with $\mathrm{tr_f}\,\ln\mathcal{O} = \ln\det_{\rm f}\mathcal{O}$, and we are led to

$$\begin{aligned}\Omega_{q,T} - \Omega_{q,T,\mu=0} = -\,\frac{2}{\pi^2}T \int_0^\infty dp\,p^2 \Big\{&\ln\Big[1 + 3(L + \bar{L}e^{-\beta(\epsilon_p^q-\mu)})\,e^{-\beta(\epsilon_p^q-\mu)} + e^{-3\beta(\epsilon_p^q-\mu)}\Big] \\ &+ \ln\Big[1 + 3(\bar{L} + Le^{-\beta(\epsilon_p^q+\mu)})\,e^{-\beta(\epsilon_p^q+\mu)} + e^{-3\beta(\epsilon_p^q+\mu)}\Big]\Big\}.\end{aligned} \tag{VII.13}$$

For $L = \bar{L} = 1$ and $\mu = 0$ (VII.13) reduces to the one in (V.38) in chapter V. This happens for large temperatures, $T/T_{\rm conf} \to \infty$ deep in the perturbative regime. Then we simply see the thermal distribution of single quarks. Note

that (VII.13) only vanishes for $T \to 0$ if $\epsilon_p > |\mu|$ for all p. For $\mu^2 > m_q^2$ we have

$$\lim_{T\to 0} \left(\Omega_{q,T} - \Omega_{q,T,\mu=0}\right) = -\frac{6}{\pi^2} \int_0^{\sqrt{\mu^2-m_q^2}} dp\, p^2 \, \left(|\mu| - \epsilon_p^q\right) \,, \tag{VII.14}$$

reflecting the fact that for $\mu^2 > m_q^2$ the level of the Fermi sea is rising accordingly and the part of the quark fluctuations below disappear from the fluctuation spectrum. As we have subtracted the grand potential at $T = 0$ *and* $\mu = 0$, this term is left in the $T \to 0$ limit.

For $T/T_{\rm conf} \to 0$ the Polyakov loop expectation value tends towards one, $L = \bar{L} = 0$. Interestingly, for these values we have

$$\Omega_{q,T} - \Omega_{q,T,\mu=0} = -\frac{2}{\pi^2} T \int_0^\infty dp\, p^2 \left\{ \ln\left[1 + e^{-3\beta(\epsilon_p^q - \mu)}\right] + \ln\left[1 + e^{-3\beta(\epsilon_p^q + \mu)}\right]\right\}, \tag{VII.15}$$

the grand potential (or negative thermal pressure) of a gas of three-quark states, in our case the nucleons. This observation has been called *statistical confinement* as the confining value of the background Polyakov loop gives the thermal distribution of nucleons. If this property is investigated more carefully, the related distribution functions are given by

$$n_F(x, L, \bar{L}) = \frac{1 + 2\bar{L}\, e^{\beta x} + L\, e^{2\beta x}}{1 + 3\bar{L}\, e^{2\beta x} + 3L\, e^{2\beta x} + e^{3\beta x}} \,, \qquad x = \sqrt{p^2 + m_q^2} - \mu \,, \qquad \bar{x} = \sqrt{p^2 + m_q^2} + \mu \,, \tag{VII.16}$$

for the quark and $n_F(\bar{x}, \bar{L}, L)$ for the anti-quark. As for the grand potential, the Polyakov-loop enhanced themral distribution functions tend towards the quark and anti-quark distribution functions for $L, \bar{L} \to 1$. For $L, \bar{L} \to 0$ (VII.16) gives the nucleon distribution function. However, this only happens if

$$\lim_{T/T_{\rm conf}\to 0} L\, e^{2\beta x} \to 0 \,. \tag{VII.17}$$

It can be shown that the limit (VII.17) is not present in QCD, see [37]. This does not invalidate the above picture as the failure of (VII.17) orginates in mesonic contributions that indeed should be present. Moreover, the grand potential is that of nucleons.

This concludes our derivation of the low energy EFT that governs the phase structure of QCD. This specific type of low energy EFT has been constructed in [35]. On the one loop level its grand potential in $N_f = 2$ flavor QCD is given by the sum of the quark contribution (VII.13), the mesonic contribution and the Polyakov loop potential. This combination gives access to the two basic phenomena that governs the phase structure, confinement and chiral symmetry breaking.

A. RG for the phase structure*

Here we simply repeat the steps for the derivation of the Wegner-Houghton equation done in chapter V C for finite temperature at finite temperature and density. The mesonic part is the same as in (V.40) and we can just take it over here. The thermal quark part at finite density can be read off from (VII.15) while the vacuum part (at $\mu = 0$) of the integral is the same as before. In summary we get

$$\begin{aligned}
\Lambda\partial_\Lambda \Omega_\Lambda(\psi, \bar{\psi}, \phi) = &-\frac{\Lambda^3}{2\pi^2}\left\{ \frac{1}{2}\left[\epsilon_\Lambda^\phi(m_\sigma) + \frac{3}{2}\epsilon_\Lambda^\phi(m_\pi)\right] - 12\,\epsilon_\Lambda^q \right. \\
&+ T\left[\ln\left(1 - e^{-\beta\epsilon_\Lambda^\phi(m_\sigma)}\right) + \ln\left(1 - e^{-\beta\epsilon_\Lambda^\phi(m_\pi)}\right)\right] \\
&- 4\,T\left\{\ln\left[1 + 3(L + \bar{L}e^{-\beta(\epsilon_\Lambda^q - \mu)})\, e^{-\beta(\epsilon_\Lambda^q - \mu)} + e^{-3\beta(\epsilon_\Lambda^q - \mu)}\right]\right. \\
&\left.\left. + \ln\left[1 + 3(\bar{L} + Le^{-\beta(\epsilon_\Lambda^q + \mu)})\, e^{-\beta(\epsilon_\Lambda^q + \mu)} + e^{-3\beta(\epsilon_\Lambda^q + \mu)}\right]\right\}.
\end{aligned} \tag{VII.18}$$

In (VII.18) the first line is the $T, \mu = 0$ part of the flow, the second line comprises the thermal part of the meson fluctuations, while the last two lines comprise the thermal and density fluctuations of the quarks. As has been discussed

above, this term does not vanish in the limit $T \to 0$ but removes the infrared part of the vacuum fluctuations of the quark above the onset chemical potential $\mu^2 = m_q^2$, see (VII.14).

VIII. JET RADIATION

A. Jet ratios and jet veto

From the Feynman diagram for weak boson fusion we see that the diagram describing a gluon exchange between the two quark lines multiplied with the Born diagram is proportional to the color factor $\mathrm{tr}T^a \mathrm{tr}T^b \delta^{ab} = 0$. The only way to avoid this suppression is the interference of two identical final–state quarks, for example in ZZ fusion. First, this does not involve only valence quarks and second, this assumes a phase space configuration where one of the two supposedly forward jets turns around and goes backwards, so the interfering diagrams contribute in the same phase space region. This means that virtual gluon exchange in weak boson fusion is practically absent.

In Section **??** we will see that virtual gluon exchange and real gluon emission are very closely related. Radiating a gluon off any of the quarks in the weak boson fusion process will lead to a double infrared divergence, one because the gluon can be radiated at small angles and one because the gluon can be radiated with vanishing energy. The divergence at small angles is removed by redefining the quark parton densities in the proton. The soft, non–collinear divergence has to cancel between real gluon emission and virtual gluon exchange. However, if virtual gluon exchange does not appear, non–collinear soft gluon radiation cannot appear either. This means that additional QCD jet activity as part of the weak boson fusion process is limited to collinear radiation, *i.e.* radiation along the beam line or at least in the same direction as the far forward tagging jets. Gluon radiation into the central detector is suppressed by the color structure of the weak boson fusion process.

While it is not immediately clear how to quantify such a statement it is a very useful feature, for example looking at the top pair backgrounds. The $WWb\bar{b}$ final state as a background to $qqH, H \to WW$ searches includes two bottom jets which can mimic the signal's tagging jets. At the end, it turns out that it is much more likely that we will produce another jet through QCD jet radiation, *i.e.* $pp \to t\bar{t}$+jet, so only one of the two bottom jets from the top decays needs to be forward. In any case, the way to isolate the Higgs signal is to look at additional central jets.

As described above, for the signal additional jet activity is limited to small-angle radiation off the initial–state and final–state quarks. For a background like top pairs this is not the case, which means we can reduce all kinds of background by vetoing jets in the central region above $p_{T,j} \gtrsim 30$ GeV. This strategy is referred to as central jet veto or mini-jet veto. Note that it has nothing to do with rapidity gaps at HERA or pomeron exchange, it is a QCD feature completely accounted for by standard perturbative QCD.

From QCD we then need to compute the probability of not observing additional central jets for different signal and background processes. Postponing the discussion of QCD parton splitting to Section **??** we already know that for small transverse momenta the $p_{T,j}$ spectra for massless states will diverge, as shown in Eq.(**??**). Looking at some kind of n-particle final state and an additional jet radiation we can implicitly define a reference point p_T^{crit} at which the divergent rate for one jet radiation σ_{n+1} starts to exceed the original rate σ_n, whatever the relevant process might be

$$\sigma_{n+1}(p_T^{\text{crit}}) \; = \; \int_{p_T^{\text{crit}}}^{\infty} dp_{T,j} \; \frac{d\sigma_{n+1}}{dp_{T,j}} \stackrel{!}{=} \sigma_n \; . \tag{VIII.1}$$

This condition defines a point in p_T below which our perturbation theory in α_s, *i.e.* in counting the number of external partons, breaks down. For weak boson fusion Higgs production we find $p_T^{\text{crit}} \sim 10$ GeV, while for QCD processes like $t\bar{t}$ production it becomes $p_T^{\text{crit}} = 40$ GeV. In other words, jets down to p_T =10 GeV are perturbatively well defined for Higgs signatures, while for the QCD backgrounds jets below 40 GeV are much more frequent than they should be looking at the perturbative series in α_s. This fixes the p_T range where a central jet veto will be helpful to reject backgrounds

$$p_{T,j} > 30 \text{ GeV} \qquad \text{and} \qquad \eta_j^{(\text{tag } 1)} < \eta_j < \eta_j^{(\text{tag } 2)} \; . \tag{VIII.2}$$

The second condition reminds us of the fact that only central jets will be rare in weak boson fusion. The smaller the p_T threshold the more efficient the central jet veto becomes, but at some point experimental problems as well as non–perturbative QCD effects will force us to stay above 20 or 30 or even 40 GeV.

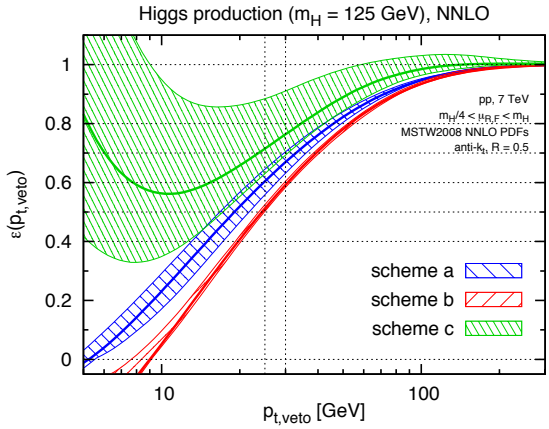

FIG. 24: Different predictions for the jet veto survival probability P_{pass} as a function of the maximum allowed $p_{T,j}$. The example process chosen is Higgs production in gluon fusion. The shaded regions indicate the independent variation of the factorization and renormalization scales within $[m_H/4, m_H]$ requiring μ_R/μ_F to lie within $[0.5, 2]$. The figure and the corresponding physics argument are taken from Ref. [**?**].

If we assign a probability pattern to the radiation of jets from the core process we can compute the survival probability P_{pass} of such a jet veto. For many years we have been told that higher orders in the perturbative QCD series for the Higgs production cross section is the key to understanding LHC rates. For multi–jet observables like a jet veto this is not necessarily true. As an example we assume NNLO or two-loop precision for the Higgs production rate $\sigma = \sigma_0 + \alpha_s\sigma_1 + \alpha_s^2\sigma_2$ where we omit the over–all factor α_s^2 in σ_0. Consequently, we define the cross section passing the jet veto $\sigma^{(\text{pass})} = P_{\text{pass}}\,\sigma = \sum_j \alpha_s^j \sigma_j^{(\text{pass})}$. Because the leading order prediction only includes a Higgs in the final state we know that $\sigma_0^{(\text{pass})} = \sigma_0$. Solving this definition for the veto survival probability we can compute

$$P_{\text{pass}}^{(\text{a})} = \frac{\sigma^{(\text{pass})}}{\sigma} = \frac{\sigma_0 + \alpha_s\sigma_1^{(\text{pass})} + \alpha_s^2\sigma_2^{(\text{pass})}}{\sigma_0 + \alpha_s\sigma_1 + \alpha_s^2\sigma_2}\,, \tag{VIII.3}$$

motivated by including the maximum number of terms (NNLO) in the numerator and denominator. The result as a function of the maximum allowed $p_{T,j}$ is shown as 'scheme a' in Figure 24. The shaded region is an estimate of the theoretical uncertainty of this prediction.

Alternatively, we can argue that the proper perturbative observable is the fraction of vetoed events $(1 - P_{\text{pass}})$. Indeed, for small values of α_s the jet radiation probability vanishes and with it $(1 - P_{\text{pass}}) \sim \alpha_s \to 0$. This vetoed event fraction we can compute as $\sigma_j - \sigma_j^{(\text{pass})}$ for $j \geq 0$. However, we need to keep in mind that in the presence of an additional jet the NNLO prediction for the inclusive Higgs production rate reduces to NLO accuracy, so we include the two leading terms in the numerator and denominator,

$$\begin{aligned} 1 - P_{\text{pass}}^{(\text{b})} &= \alpha_s\,\frac{\sigma_1 - \sigma_1^{(\text{pass})} + \alpha_s(\sigma_2 - \sigma_2^{(\text{pass})})}{\sigma_0 + \alpha_s\sigma_1} \\ P_{\text{pass}}^{(\text{b})} &= 1 - \alpha_s\,\frac{\sigma_1 - \sigma_1^{(\text{pass})} + \alpha_s(\sigma_2 - \sigma_2^{(\text{pass})})}{\sigma_0 + \alpha_s\sigma_1} = \frac{\sigma_0 + \alpha_s\sigma_1^{(\text{pass})} + \alpha_s^2\sigma_2^{(\text{pass})} - \alpha_s^2\sigma_2}{\sigma_0 + \alpha_s\sigma_1}\,. \end{aligned} \tag{VIII.4}$$

This defines 'scheme b' in Figure 24. Obviously, in Eq.(VIII.4) we can move the term $-\alpha_s^2\sigma_2$ into the denominator and arrive at Eq.(VIII.3) within the uncertainty defined by the unknown α_s^3 terms.

Finally, we can consistently Taylor expand the definition of P_{pass} as the ratio given in Eq.(VIII.3). The two leading

derivatives of a ratio read

$$\left(\frac{f}{g}\right)' = \frac{f'g - fg'}{g^2} \overset{f=g}{=} \frac{f'-g'}{g}$$
$$\left(\frac{f}{g}\right)'' = \left(\frac{f'g}{g^2} - \frac{fg'}{g^2}\right)' = \frac{(f'g)'g^2 - f'g2gg'}{g^4} - \frac{(fg')'g^2 - fg'2gg'}{g^4}$$
$$= \frac{(f'g)' - 2f'g'}{g^2} - \frac{(fg')'g - 2fg'g'}{g^3} = \frac{f''g - f'g'}{g^2} - \frac{fg''g - fg'g'}{g^3} \overset{f=g}{=} \frac{f''-g''}{g} - \frac{g'(f'-g')}{g^2} \qquad \text{(VIII.5)}$$

In the last steps we assume $f = g$ at the point where we evaluate the Taylor expansion. Applied to the perturbative QCD series for $(1 - P_{\text{pass}})$ around the zero-coupling limit this gives us

$$1 - P^{(c)}_{\text{pass}} = 1 - \frac{\sigma_0 + \alpha_s\sigma_1^{(\text{pass})} + \alpha_s^2\sigma_2^{(\text{pass})} + \cdots}{\sigma_0 + \alpha_s\sigma_1 + \alpha_s^2\sigma_2 + \cdots}$$
$$P^{(c)}_{\text{pass}} = 1 + \alpha_s \frac{\sigma_1^{(\text{pass})} - \sigma_1}{\sigma_0} + \alpha_s^2 \frac{\sigma_2^{(\text{pass})} - \sigma_2}{\sigma_0} - \alpha_s^2 \frac{\sigma_1(\sigma_1^{(\text{pass})} - \sigma_1)}{\sigma_0^2} , \qquad \text{(VIII.6)}$$

defining 'scheme c' in Figure 24. The numerical results indicate that the three schemes are inconsistent within their theoretical uncertainties, and that the most consistent Taylor expansion around perfect veto survival probabilities is doing particularly poorly. Towards small $p_{T,j}$ veto ranges the fixed order perturbative approach clearly fails. The way to improve the theoretical prediction is a re-organization of the perturbation theory for small jet transverse momenta. We introduce this approach with its leading term, the parton shower, in Section II F. For now we conclude that our theoretical approach has to go beyond a fixed number of (hard) jets and include the production of any number of jets in some kind of modified perturbative series.

One ansatz for the distribution of any number of radiated jets is motivated by soft photon emission off a hard electron. In Section **??** we derive the Poisson distribution in the numbers of jet which follows in the soft limit. If we for now assume a Poisson distribution, the probability of observing exactly n jets given an expected $\bar{n}$ jets is

$$f(n;\bar{n}) = \frac{\bar{n}^n e^{-\bar{n}}}{n!} \qquad \Rightarrow \qquad \boxed{P_{\text{pass}} \equiv f(0;\bar{n}) = e^{-\bar{n}}} . \qquad \text{(VIII.7)}$$

Note that this probability links rates for exactly n jets, no at least n jets, *i.e.* it described the exclusive number of jets. The Poisson distribution is normalized to unity, once we sum over all possible jet multiplicities n. It defines the so-called exponentiation model. We consistently fix the expectation value in terms of the inclusive cross sections producing at least zero or at least one jet,

$$\langle n \rangle \equiv \bar{n} = \frac{\sigma_1(p_T^{\min})}{\sigma_0} . \qquad \text{(VIII.8)}$$

This ensures that the inclusive jet ratio σ_1/σ_0 is reproduced by the ratio of the corresponding Poisson distributions. Including this expectation value $\bar{n}$ into Eq.(VIII.7) returns a veto survival probability of $\exp(-\sigma_1/\sigma_0)$. This comes out roughly as 88% for the weak boson fusion signal and as 24% for the $t\bar{t}$ background. For the signal–to–background ratio this implies a three-fold increase.

An alternative model starts from a constant probability of radiating a jet, which in terms of the inclusive cross sections σ_n, *i.e.* the production rate for the radiation of at least n jets, reads

$$\frac{\sigma_{n+1}(p_T^{\min})}{\sigma_n(p_T^{\min})} = R^{(\text{incl})}_{(n+1)/n}(p_T^{\min}) . \qquad \text{(VIII.9)}$$

We derive this pattern in Section **??**. The expected number of jets is then given by

$$\begin{aligned}\langle n\rangle &= \frac{1}{\sigma_0}\sum_{j=1} j(\sigma_j-\sigma_{j+1}) = \frac{1}{\sigma_0}\left(\sum_{j=1} j\sigma_j - \sum_{j=2}(j-1)\sigma_j\right) = \frac{1}{\sigma_0}\sum_{j=1}\sigma_j \\ &= \frac{\sigma_1}{\sigma_0}\sum_{j=0}(R^{(\text{incl})}_{(n+1)/n})^j = \frac{R^{(\text{incl})}_{(n+1)/n}}{1-R^{(\text{incl})}_{(n+1)/n}}\,, \end{aligned} \tag{VIII.10}$$

if $R^{(\text{incl})}_{(n+1)/n}$ is a constant. Assuming the series converges this turns into a requirement on $p_T^{\min}$. Radiating jets with such a constant probability has been observed at many experiments, including most recently the LHC, and is in the context of W+jets referred to as staircase scaling. We will derive both, the Poisson scaling and the staircase scaling from QCD in Section **??**. Even without saying anything on how to calculate exclusive processes with a fixed number of jets we can derive a particular property of the constant probability of staircase scaling: the ratios of the $(n+1)$-jet rate to the n-jet rate for inclusive and exclusive jet rates are identical. We can see this by computing the inclusive $R^{(\text{incl})}_{(n+1)/n}$ in terms of exclusive jet rates

$$\begin{aligned} R^{(\text{incl})}_{(n+1)/n} &= \frac{\sigma_{n+1}}{\sigma_n} = \frac{\sum_{j=n+1}^{\infty}\sigma_j^{(\text{excl})}}{\sigma_n^{(\text{excl})}+\sum_{j=n+1}^{\infty}\sigma_j^{(\text{excl})}} \\ &= \frac{\sigma_{n+1}^{(\text{excl})}\sum_{j=0}^{\infty}R^j_{(n+1)/n}}{\sigma_n^{(\text{excl})}+\sigma_{n+1}^{(\text{excl})}\sum_{j=0}^{\infty}R^j_{(n+1)/n}} \qquad \text{with} \quad R_{(n+1)/n} = \frac{\sigma^{(\text{excl})}_{n+1}}{\sigma^{(\text{excl})}_n} \\ &= \frac{\dfrac{R_{(n+1)/n}\sigma_n^{(\text{excl})}}{1-R_{(n+1)/n}}}{\sigma_n^{(\text{excl})}+\dfrac{R_{(n+1)/n}\sigma_n^{(\text{excl})}}{1-R_{(n+1)/n}}} = \frac{R_{(n+1)/n}}{1-R_{(n+1)/n}+R_{(n+1)/n}} \\ &= R_{(n+1)/n}\,. \end{aligned} \tag{VIII.11}$$

To show that the exponentiation model and staircase scaling are not the only assumptions we can make to compute jet rates we show yet another, but similar ansatz which tries to account for an increasing number of legs to radiate jets off. Based on

$$\frac{\sigma_{j+1}(p_T^{\min})}{\sigma_j(p_T^{\min})} = \frac{j+1}{j}\,R^{(\text{incl})}_{(n+1)/n}(p_T^{\min})\,, \tag{VIII.12}$$

the expectation for the number of jets radiated gives, again following Eq.(VIII.10)

$$\begin{aligned}\langle n\rangle &= \frac{1}{\sigma_0}\sum_{j=1} j\sigma_j = \frac{1}{\sigma_0}\,\sigma_0\sum_{j=1} j(R^{(\text{incl})}_{(n+1)/n})^j \\ &= R^{(\text{incl})}_{(n+1)/n}\sum_{j=1} j(R^{(\text{incl})}_{(n+1)/n})^{j-1} = \frac{R^{(\text{incl})}_{(n+1)/n}}{(1-R^{(\text{incl})}_{(n+1)/n})^2}\,. \end{aligned} \tag{VIII.13}$$

All of these models are more or less well motivated statistical approximations. The do not incorporate experimental effects or the non–perturbative underlying event, *i.e.* additional energy dependent but process independent jet activity in the detectors from many not entirely understood sources. For many reasons none of them is guaranteed to give us a final and universal number. However, by the time we get to Section **??** we will at least be able to more accurately describe the central jet veto in QCD.

For the Poisson distribution and the staircase distribution we can summarize the main properties of the n-jet rates in terms of the upper incomplete gamma function $\Gamma(n,\bar{n})$:

	staircase scaling	Poisson scaling
$\sigma_n^{(\text{excl})}$	$\sigma_0^{(\text{excl})}\ e^{-bn}$	$\sigma_0\ \dfrac{e^{-\bar{n}}\bar{n}^n}{n!}$
$R_{(n+1)/n} = \dfrac{\sigma_{n+1}^{(\text{excl})}}{\sigma_n^{(\text{excl})}}$	e^{-b}	$\dfrac{\bar{n}}{n+1}$
$R_{(n+1)/n}^{(\text{incl})} = \dfrac{\sigma_{n+1}}{\sigma_n}$	e^{-b}	$\left(\dfrac{(n+1)\,e^{-\bar{n}}\,\bar{n}^{-(n+1)}}{\Gamma(n+1)-n\Gamma(n,\bar{n})}+1\right)^{-1}$
$\langle n\rangle$	$\dfrac{1}{2}\dfrac{1}{\cosh b-1}$	$\bar{n}$
P_{pass}	$1-e^{-b}$	$e^{-\bar{n}}$

B. Ordered emission

From the derivation of the Catani–Seymour dipoles we know that for example the emission of a gluon off a hard quark line is governed by distinctive soft and collinear phase space regimes. In our argument for the exponentiation of gluon radiation matrix elements in Eq.(**??**) there is one piece missing: multiple gluon emission has to be ordered by some parameter, such that in squaring the multiple emission matrix element we can neglect interference terms. These interference diagrams contributing to the full amplitude squared are called non–planar diagrams. The question is if we can justify to neglect them from first principles field theory and QCD. There are three reasons to do this, even though none of them gives exactly zero for soft and collinear splittings. On the other hand, in combination they make for a very good reason.

First, an arguments for a strongly ordered gluon emission comes from the divergence structure of soft and collinear gluon emission. Two successively radiated gluons look like

According to Eq.(II.109) single gluon radiation with momentum k off a hard quark with momentum p is described by a kinematic term $(\epsilon^* p)(pk)$. For successive radiation the two Feynman diagrams give us the combined kinetic terms

$$\begin{aligned}
&\frac{(\epsilon_1 p)}{(p+k_1+k_2)^2-m^2}\frac{(\epsilon_2 p)}{(p+k_2)^2-m^2}+\frac{(\epsilon_2 p)}{(p+k_1+k_2)^2-m^2}\frac{(\epsilon_1 p)}{(p+k_1)^2-m^2}\\
&\quad=\frac{(\epsilon_1 p)}{2(pk_1)+2(pk_2)+(k_1+k_2)^2}\frac{(\epsilon_2 p)}{2(pk_2)}+\frac{(\epsilon_2 p)}{2(pk_1)+2(pk_2)+(k_1+k_2)^2}\frac{(\epsilon_1 p)}{2(pk_1)} \qquad k_1^2=0=k_2^2\\
&\quad\simeq\frac{(\epsilon_1 p)}{2\max_j(pk_j)}\frac{(\epsilon_2 p)}{2(pk_2)}+\frac{(\epsilon_2 p)}{2\max_j(pk_j)}\frac{(\epsilon_1 p)}{2(pk_1)} \qquad (pk_j)\text{ strongly ordered}\\
&\quad\simeq\begin{cases}\dfrac{(\epsilon_1 p)(\epsilon_2 p)}{2\max_j(pk_j)}\ \dfrac{1}{2(pk_2)} & (pk_2)\ll(pk_1)\ \ k_2\text{ softer}\\[2ex] \dfrac{(\epsilon_1 p)(\epsilon_2 p)}{2\max_j(pk_j)}\ \dfrac{1}{2(pk_1)} & (pk_1)\ll(pk_2)\ \ k_1\text{ softer}\,.\end{cases}
\end{aligned}\tag{VIII.14}$$

Going back to the two Feynman diagrams this means that once one of the gluons is significantly softer than the other the Feynman diagrams with the later soft emission dominates. After squaring the amplitude there will be no phase space regime where interference terms between the two diagrams are numerically relevant. The coherent sum over gluon radiation channels reduces to a incoherent sum, ordered by the softness of the gluon.

This argument can be generalized to multiple gluon emission by recognizing that the kinematics will always be dominated by the more divergent propagators towards the final state quark with momentum p. Note, however, that it is based on an ordering of the scalar products (pk_j) interpreted as the softness of the gluons. We already know that a small value of (pk_j) can as well point to a collinear divergence; every step in the argument of Eq.(VIII.14) still applies.

Second, we can derive ordered multiple gluon emission from the phase space integration in the soft or eikonal approximation. There, gluon radiation is governed by the so-called radiation dipoles given in Eq.(II.114). Because each dipole includes a sum over all radiating legs in the amplitude, the square includes a double sum over the hard legs. Diagonal terms

vanish at least for over–all color–neutral processes. Because the following argument is purely based on kinematics we will ignore all color charges and other factors.

For successive gluon radiation off a quark leg the question we are interested in is where the soft gluon k is radiated, for example in relation to the hard quark p_1 and the harder gluon p_2. The kinematics of this process is the same as soft gluon radiation of a quark–antiquark pair produced in an electroweak process. For the dipoles we let the indices i, j run over the harder quark, antiquark, and possibly gluon legs. A well–defined process with all momenta defined as outgoing is

in the approximation of abelian QCD, *i.e.* no triple gluon vertices. We start by symmetrizing the leading soft radiation dipole with respect to the two hard momenta in a particular way,

$$\begin{aligned}
(J^\dagger \cdot J)_{12} &= \frac{(p_1 p_2)}{(p_1 k)(p_2 k)} \\
&= \frac{1}{k_0^2} \frac{1-\cos\theta_{12}}{(1-\cos\theta_{1k})(1-\cos\theta_{2k})} \qquad \text{in terms of opening angles } \theta \\
&= \frac{1}{2k_0^2} \left(\frac{1-\cos\theta_{12}}{(1-\cos\theta_{1k})(1-\cos\theta_{2k})} + \frac{1}{1-\cos\theta_{1k}} - \frac{1}{1-\cos\theta_{2k}} \right) + (1 \leftrightarrow 2) \\
&\equiv \frac{W_{12}^{[1]} + W_{12}^{[2]}}{k_0^2} \; . \qquad \text{(VIII.15)}
\end{aligned}$$

The last term is an implicit definition of the two terms $W_{12}^{[1]}$. The pre-factor $1/k_0^2$ is given by the leading soft divergence. The original form of $(J^\dagger J)$ is symmetric in the two indices, which means that both hard partons can take the role of the hard parton and the interference partner. In the new form the symmetry in each of the two terms is broken. Each of the two terms we need to integrate over the gluon's phase space, including the azimuthal angle ϕ_{1k}. Note, however, that this splitting into two contributions is not the standard separation into the two diagrams. It is a specific ansatz to show the ordering patterns we will see below.

To compute the actual integral we express the three parton vectors in polar coordinates where the initial parton p_1 propagates into the x direction, the interference partner p_2 in the $(x-y)$ plane, and the soft gluon in the full three-dimensional space described by polar coordinates,

$$\begin{aligned}
\hat{p}_1 &= (1,0,0) && \text{hard parton} \\
\hat{p}_2 &= (\cos\theta_{12}, \sin\theta_{12}, 0) && \text{interference partner} \\
\hat{k} &= (\cos\theta_{1k}, \sin\theta_{1k}\cos\phi_{1k}, \sin\theta_{1k}\sin\phi_{1k}) && \text{soft gluon} \\
\Rightarrow \qquad \cos\theta_{2k} &\equiv (\hat{p}_2 \hat{k}) = \cos\theta_{12}\cos\theta_{1k} + \sin\theta_{12}\sin\theta_{1k}\cos\phi_{1k} \; . && \text{(VIII.16)}
\end{aligned}$$

From the scalar product between these four-vectors we see that of the terms appearing in Eq.(VIII.15) only the opening angle θ_{2k} includes ϕ_{1k}, which for the azimuthal angle integration means

$$\begin{aligned}
\int_0^{2\pi} d\phi_{1k}\, W_{12}^{[1]} &= \frac{1}{2} \int_0^{2\pi} d\phi_{1k} \left(\frac{1-\cos\theta_{12}}{(1-\cos\theta_{1k})(1-\cos\theta_{2k})} + \frac{1}{1-\cos\theta_{1k}} - \frac{1}{1-\cos\theta_{2k}} \right) \; . \\
&= \frac{1}{2} \frac{1}{1-\cos\theta_{1k}} \int_0^{2\pi} d\phi_{1k} \left(\frac{1-\cos\theta_{12}}{1-\cos\theta_{2k}} + 1 - \frac{1-\cos\theta_{1k}}{1-\cos\theta_{2k}} \right) \\
&= \frac{1}{2} \frac{1}{1-\cos\theta_{1k}} \left(2\pi + (\cos\theta_{1k} - \cos\theta_{12}) \int_0^{2\pi} d\phi_{1k} \frac{1}{1-\cos\theta_{2k}} \right) \; . \qquad \text{(VIII.17)}
\end{aligned}$$

The azimuthal angle integral in this expression for $W_{12}^{[i]}$ we can solve

$$\begin{aligned}
\int_0^{2\pi} d\phi_{1k} \frac{1}{1-\cos\theta_{2k}} &= \int_0^{2\pi} d\phi_{1k} \frac{1}{1-\cos\theta_{12}\cos\theta_{1k} - \sin\theta_{12}\sin\theta_{1k}\cos\phi_{1k}} \\
&= \int_0^{2\pi} d\phi_{1k} \frac{1}{a - b\cos\phi_{1k}} \\
&= \oint_{\text{unit circle}} dz\, \frac{1}{iz} \frac{1}{a - b\dfrac{z+1/z}{2}} \qquad \text{with} \quad z = e^{i\phi_{1k}},\ \cos\phi_{1k} = \frac{z+1/z}{2} \\
&= \frac{2}{i} \oint dz\, \frac{1}{2az - b - bz^2} \\
&= \frac{2i}{b} \oint \frac{dz}{(z-z_-)(z-z_+)} \qquad \text{with} \quad z_\pm = \frac{a}{b} \pm \sqrt{\frac{a^2}{b^2} - 1}\,. \qquad \text{(VIII.18)}
\end{aligned}$$

This integral is related to the sum of all residues of poles inside the closed integration contour. Of the two poles z_- is the one which typically lies within the unit circle, so we find

$$\begin{aligned}
\int_0^{2\pi} d\phi_{1k} \frac{1}{1-\cos\theta_{2k}} &= \frac{2i}{b}\, 2\pi i \frac{1}{z_- - z_+} = \frac{2\pi}{\sqrt{a^2-b^2}} \\
&= \frac{2\pi}{\sqrt{(\cos\theta_{1k} - \cos\theta_{12})^2}} = \frac{2\pi}{|\cos\theta_{1k} - \cos\theta_{12}|}\,. \qquad \text{(VIII.19)}
\end{aligned}$$

The entire integral in Eq.(VIII.17) then becomes

$$\begin{aligned}
\int_0^{2\pi} d\phi_{1k}\, W_{12}^{[1]} &= \frac{1}{2}\, \frac{1}{1-\cos\theta_{1k}} \left(2\pi + (\cos\theta_{1k} - \cos\theta_{12})\ \frac{2\pi}{|\cos\theta_{1k} - \cos\theta_{12}|} \right) \\
&= \frac{\pi}{1-\cos\theta_{1k}} \left(1 + \text{sign}(\cos\theta_{1k} - \cos\theta_{12})\right. \\
&= \begin{cases} \dfrac{2\pi}{1-\cos\theta_{1k}} & \text{if} \quad \theta_{1k} < \theta_{12} \\ 0 & \text{else}\,. \end{cases} \qquad \text{(VIII.20)}
\end{aligned}$$

The soft gluon is only radiated at angles between zero and the opening angle of the initial parton p_1 and its hard interference partner or spectator p_2. The same integral over $W_{12}^{[2]}$ gives the same result, with switched roles of p_1 and p_2. Combining the two permutations this means that the soft gluon is always radiated within a cone centered around one of the hard partons and with a radius given by the distance between the two hard partons. Again, the coherent sum of diagrams reduces to an incoherent sum. This derivation angular ordering is exact in the soft limit.

There is a simple physical argument for this suppressed radiation outside a cone defined by the radiating legs. Part of the deviation is that the over–all process is color–neutral. This means that once the gluon is far enough from the two quark legs it will not resolve their individual charges but only feel the combined charge. This screening leads to an additional suppression factor of the kind $\theta_{12}^2/\theta_{1k}^2$. This effect is called coherence.

The third argument for ordered emission comes from color factors. Crossed successive splittings or interference terms between different orderings are color suppressed. For example in the squared diagram for three jet production in e^+e^- collisions the additional gluon contributes a color factor

$$\text{tr}(T^a T^a) = \frac{N_c^2 - 1}{2} = N_c C_F \qquad \text{(VIII.21)}$$

When we consider the successive radiation of two gluons the ordering matters. As long as the gluon legs do not cross

each other we find the color factor

$$\begin{aligned}
\mathrm{tr}(T^a T^a T^b T^b) &= (T^a T^a)_{il} (T^b T^b)_{li} \\
&= \frac{1}{4} \left(\delta_{il}\delta_{jj} - \frac{\delta_{ij}\delta_{jl}}{N_c} \right) \left(\delta_{il}\delta_{jj} - \frac{\delta_{ij}\delta_{jl}}{N_c} \right) \qquad \text{using} \quad T^a_{ij} T^a_{kl} = \frac{1}{2} \left(\delta_{il}\delta_{jk} - \frac{\delta_{ij}\delta_{kl}}{N_c} \right) \\
&= \frac{1}{4} \left(\delta_{il} N_c - \frac{\delta_{il}}{N_c} \right) \left(\delta_{il} N_c - \frac{\delta_{il}}{N_c} \right) \\
&= N_c \left(\frac{N_c^2 - 1}{2N_c} \right)^2 = N_c C_F^2 = \frac{16}{3}
\end{aligned} \tag{VIII.22}$$

Similarly, we can compute the color factor when the two gluon lines cross. We find

$$\mathrm{tr}(T^a T^b T^a T^b) = -\frac{N_c^2 - 1}{4N_c} = -\frac{C_F}{2} = -\frac{2}{3} \,. \tag{VIII.23}$$

Numerically, this color factor is suppressed compared to 16/3. This kind of behavior is usually quoted in powers of N_c where we assume N_c to be large. In those terms non–planar diagrams are suppressed by a factor $1/N_c^2$ compared to the planar diagrams.

Once we also include the triple gluon vertex we can radiate two gluons off a quark leg with the color factor

$$\mathrm{tr}(T^a T^b)\; f^{acd} f^{bcd} = \frac{\delta^{ab}}{2}\; N_c \delta^{ab} = \frac{N_c (N_c^2 - 1)}{2} = N_c^2 C_F = \frac{36}{3} \,. \tag{VIII.24}$$

This is not suppressed compared to successive planar gluon emission, neither in actual numbers not in the large-N_c limit.

We can try the same argument for a purely gluonic theory, *i.e.* radiating gluons off two hard gluons in the final state. The color factor for single gluon emission after squaring is

$$f^{abc} f^{abc} = N_c \delta^{aa} = N_c (N_c^2 - 1) \sim N_c^3 \,, \tag{VIII.25}$$

using the large-N_c limit in the last step. For planar double gluon emission with the exchanged gluon indices b and f we find

$$f^{abd} f^{abe} f^{dfg} f^{efg} = N_c \delta^{de}\; N_c \delta^{de} = N_c^3 \,. \tag{VIII.26}$$

Splitting one radiated gluon into two gives

$$f^{abc}\; f^{cef} f^{def}\; f^{abd} = N_c \delta^{cd}\; N_c \delta^{cd} = N_c^3 \,. \tag{VIII.27}$$

This means that planar emission and successive splittings cannot be separated based on the color factor for either hard radiating quarks or gluons. We can use the color factor argument only for abelian splittings to justify ordered gluon emission.

Appendix A: Feynman rules for QCD in the covariant gauge

In this Appendix we depict the Feynman rules for QCD in the general covariant gauge.

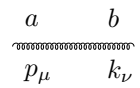

$$= \delta^{ab}\delta^{(4)}(p+k)\left(\delta_{\mu\nu} - (1-\xi)\frac{p_\mu p_\nu}{p^2}\right)\frac{1}{p^2}$$

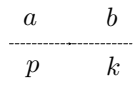

$$= -\delta^{ab}\delta^{(4)}(p+k)\frac{1}{p^2}$$

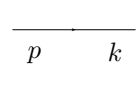

$$= \delta^{(4)}(p+k)\frac{1}{i\not{p}+m}$$

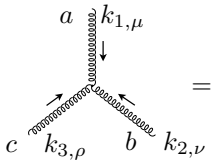

$$= i\,g f^{abc}(2\pi)^4\delta^{(4)}(k_1+k_2+k_3)\Big[(k_2-k_1)_\rho\,\delta_{\mu\nu} + (k_1-k_3)_\nu\,\delta_{\mu\rho} + (k_3-k_2)_\mu\,\delta_{\nu\rho}\Big]$$

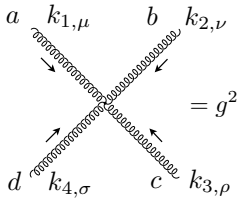

$$= g^2(2\pi)^4\delta^{(4)}\left(\sum_{i=1}^{4}k_i\right)\Big[f^{iab}f^{icd}\left(\delta_{\mu\rho}\delta_{\nu\sigma}-\delta_{\mu\sigma}\delta_{\nu\rho}\right) + f^{iac}f^{ibd}\left(\delta_{\mu\nu}\delta_{\rho\sigma}-\delta_{\mu\sigma}\delta_{\nu\rho}\right) + f^{iad}f^{ibc}\left(\delta_{\mu\nu}\delta_{\rho\sigma}-\delta_{\mu\rho}\delta_{\nu\sigma}\right)\Big]$$

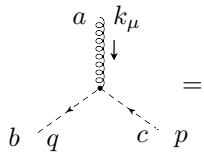

$$= -i\,g f^{abc}p_\mu(2\pi)^4\delta^{(4)}(p-q-k)$$

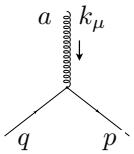

$$= -i\,g\gamma_\mu T^a\,(2\pi)^4\,\delta^{(4)}(p-q-k)$$

FIG. 25: Feynman rules.

Appendix B: Gribov copies

In Chapter I A we have derived the gauge-fixed path integral under the assumption that there is only one representative of the gauge orbit that satisfies the gauge fixing condition. However, there might be several (Gribov) copies, i.e. several physically equivalent solutions to the gauge fixing condition that are related by gauge transformations not yet fixed by the gauge fixing condition $\mathcal{F}=0$. Indeed, any sufficiently smooth gauge exhibits (infinite many) Gribov copies, $\sum_{\text{Gribov copies}} = \#_{\text{Gr}}$. As for the integration over the gauge group, $\#_{\text{Gr}}$ occurs in the numerator as well as the denominator in (I.18) and hence cancels. It is left to compute the Jacobian $J[A] = \Delta_{\mathcal{F}}[A]$. To that end we use the

representation of the Dirac δ-function

$$\delta[\mathcal{F}[A^{\mathcal{U}}]] = \sum_{i=1}^{\#_{\rm Gr}} \frac{1}{|\det\frac{\delta\mathcal{F}}{\delta\omega}|}\delta[\omega-\omega_i] \quad \text{with} \quad \mathcal{U}=e^{i\omega}. \tag{B.1}$$

which leads to

$$\Delta_{\mathcal{F}}[A] = \left(\sum_{i=1}^{\#_{\rm Gr}} \frac{1}{\big|\det\mathcal{M}_{\mathcal{F}}[A^{e^{i\omega_i}}]\big|}\right)^{-1} \qquad \text{with} \qquad \mathcal{M}_{\mathcal{F}}[A] = \left.\frac{\delta\mathcal{F}}{\delta\omega}\right|_{\omega=0}[A^{e^{i\omega}}]\,. \tag{B.2}$$

In the QFTII lecture notes in chapter IV, Appendix A the occurance of the Gribov copies in gauge field reparameterisations due to gauge fixings is elucidated at the simple example of the reparameterisation of a two-dimensional intergal.

Appendix C: Some important fact of the background field approach

In the background field approach the effective action has the following integro-differential path integral representation which facilitates the access to important properties,

$$e^{-\Gamma[\bar{A},a]} = \int D\hat{a}\,\Delta_{\mathcal{F}}[\bar{A},\hat{a}+a]\,\delta[\bar{D}_\mu(\hat{a}_\mu+a)]\,e^{-S_{\rm YM}[A+\hat{a}]+\int_x\frac{\delta\Gamma[\bar{A},a]}{\delta a_\mu}\hat{a}_\mu}\,, \qquad J=\frac{\delta\Gamma[\bar{A},a]}{\delta a} \quad a=\langle\hat{a}\rangle\,. \tag{C.1}$$

where $\hat{A}=\bar{A}+\hat{a}$, $\bar{D}=D(\bar{A})$, $D=D(A)$ and we restricted ourselves to *Landau-deWitt gauge* ($\xi=0$) with the background gauge fixing condition

$$\bar{D}_\mu\hat{a}_\mu=0\,, \qquad \longrightarrow \qquad \mathcal{M}[\bar{A},\hat{a}+a]=-\bar{D}_\mu D_\mu\,, \qquad \Delta_{\mathcal{F}}[\bar{A},\hat{a}+a]=\det\mathcal{M}[\bar{A},\hat{a}+a]\,. \tag{C.2}$$

see (VI.48). Inserting the relation between the a-derivative of Γ and the current J in (C.1) as well as using $\Gamma=\int_x J_\mu a_\mu-\log Z$ we arrive at the standard path integral expression for $Z[J]$ in the gauge (C.2). First we note that the effective action, evaluated on the equation of motion for the fluctuation field a,

$$\left.\frac{\delta\Gamma[\bar{A},a]}{\delta a_\mu}\right|_{a=a_{\rm EoM}}=0 \tag{C.3}$$

does not depend on the background field: the effective action $\Gamma[\bar{A},a_{\rm EoM}]$ is given by (C.1) without the source term. Then the path integral in (C.1) reduces to

$$e^{-\Gamma[\bar{A},a_{\rm EoM}]}=\int D\hat{a}_{\rm gf}\,e^{-S_{\rm YM}[A+\hat{a}_{\rm gf}]}\,. \tag{C.4}$$

Even though the measure depends on the background field via the gauge fixing, the intergration leads to $\bar{A}$-independent result as the action $S_{\rm YM}$ is gauge invariant. Accordingly we have

$$\frac{\delta\Gamma[\bar{A},a_{\rm EoM}]}{\delta\bar{A}}=\left.\frac{\delta}{\delta\bar{A}}\right|_{a_{\rm EoM}}\Gamma[\bar{A},a_{\rm EoM}]]=0\,. \tag{C.5}$$

The first relation in (C.5) follows with (C.3), the second from the $\bar{A}$-independence of the integration in (C.4). In conclusion, a solution to the EoM of a also is one of $\bar{A}$. Eq.(C.4) also entails that

$$\Gamma[\bar{A},a_{\rm EoM}(\bar{A})]=\Gamma[\bar{A}+a_{\rm EoM}(\bar{A})]\,, \tag{C.6}$$

it only depends on the full gauge field A.

---

[1] W. Tung, *Group Theory in Physics* (World Scientific, 1985).

[2] L. Faddeev and V. Popov, Phys.Lett. **B25**, 29 (1967).
[3] R. K. Ellis, W. J. Stirling, and B. R. Webber, Camb. Monogr. Part. Phys. Nucl. Phys. Cosmol. **8**, 1 (1996).
[4] S. Bethke, Progress in Particle and Nuclear Physics **58**, 351 (2007), arXiv:hep-ex/0606035.
[5] J. C. Collins, (1984).
[6] R. Alkofer and L. von Smekal, Phys. Rept. **353**, 281 (2001), hep-ph/0007355.
[7] M. Buballa, Phys.Rept. **407**, 205 (2005), hep-ph/0402234.
[8] J. Braun, (2011), 1108.4449.
[9] A. K. Cyrol, M. Mitter, J. M. Pawlowski, and N. Strodthoff, (2017), 1706.06326.
[10] S. Klevansky, Rev.Mod.Phys. **64**, 649 (1992).
[11] F. J. Wegner and A. Houghton, Phys. Rev. **A8**, 401 (1973).
[12] K. Symanzik, Commun. Math. Phys. **18**, 227 (1970).
[13] C. G. Callan, Phys. Rev. D **2**, 1541 (1970).
[14] K. G. Wilson, Phys.Rev. **B4**, 3184 (1971).
[15] K. G. Wilson, Phys.Rev. **B4**, 3174 (1971).
[16] L. P. Kadanoff, Physics **2**, 263 (1966).
[17] E. C. G. Stueckelberg and A. Petermann, Helv. Phys. Acta **26**, 499 (1953).
[18] M. Gell-Mann and F. E. Low, Phys. Rev. **95**, 1300 (1954).
[19] Particle Data Group, C. Patrignani *et al.*, Chin. Phys. **C40**, 100001 (2016).
[20] J. R. Pelaez, Phys. Rept. **658**, 1 (2016), 1510.00653.
[21] L. Fister and J. M. Pawlowski, Phys. Rev. **D92**, 076009 (2015), 1504.05166.
[22] D. J. Gross, R. D. Pisarski, and L. G. Yaffe, Rev.Mod.Phys. **53**, 43 (1981).
[23] N. Weiss, Phys.Rev. **D24**, 475 (1981).
[24] A. K. Cyrol, M. Mitter, J. M. Pawlowski, and N. Strodthoff, (2017), 1708.03482.
[25] P. B. Arnold and L. G. Yaffe, Phys. Rev. **D52**, 7208 (1995), hep-ph/9508280.
[26] A. Maas, J. M. Pawlowski, L. von Smekal, and D. Spielmann, Phys.Rev. **D85**, 034037 (2012), 1110.6340.
[27] A. Maas, private communication.
[28] P. J. Silva, O. Oliveira, P. Bicudo, and N. Cardoso, Phys. Rev. **D89**, 074503 (2014), 1310.5629.
[29] J. Braun, H. Gies, and J. M. Pawlowski, Phys.Lett. **B684**, 262 (2010), 0708.2413.
[30] L. Fister and J. M. Pawlowski, (2013), 1302.1373.
[31] T. K. Herbst, J. Luecker, and J. M. Pawlowski, (2015), 1510.03830.
[32] F. Marhauser and J. M. Pawlowski, (2008), 0812.1144.
[33] L. M. Haas, R. Stiele, J. Braun, J. M. Pawlowski, and J. Schaffner-Bielich, (2013), 1302.1993.
[34] P. M. Lo, B. Friman, O. Kaczmarek, K. Redlich, and C. Sasaki, Phys. Rev. **D88**, 074502 (2013), 1307.5958.
[35] B.-J. Schaefer, J. M. Pawlowski, and J. Wambach, Phys.Rev. **D76**, 074023 (2007), 0704.3234.
[36] B.-J. Schaefer, M. Wagner, and J. Wambach, Phys.Rev. **D81**, 074013 (2010), 0910.5628.
[37] W.-j. Fu and J. M. Pawlowski, Phys. Rev. **D92**, 116006 (2015), 1508.06504.